CORA Cork Open Research Archive
Cartlann Taighde Oscailte Chorcaí

Title	Exploring co-milling as a strategy to improve the dissolution of poorly water-soluble drugs
Authors	Pätzmann, Nicolas
Publication date	2025-11-30
Original Citation	Pätzmann, N. 2025. Exploring co-milling as a strategy to improve the dissolution of poorly water-soluble drugs. PhD Thesis, University College Cork.
Type of publication	Doctoral thesis
Rights	© 2025, Nicolas Pätzmann. - https://creativecommons.org/licenses/by/4.0/
Download date	2026-11-12 06:13:18
Item downloaded from	https://hdl.handle.net/10468/18863

UCC
University College Cork, Ireland
Coláiste na hOllscoile Corcaigh

Ollscoil na hÉireann
National University of Ireland
Coláiste na hOllscoile Corcaigh
University College Cork
School of Pharmacy



Exploring Co-milling as a strategy to improve the dissolution of poorly water-soluble drugs

Thesis Presented by

Nicolas Pätzmann

In fulfilment of the requirements for the degree of

Doctor of Philosophy

under the supervision of

Prof. Dr. Brendan T. Griffin (University College Cork, Ireland)

and

Dr. Josef Beránek (Zentiva, k.s, Czechia)

and

Prof. Dr. Martin Kuentz (FHNW, Switzerland)

and

Dr. Patrick O´Dwyer (University College Cork, Ireland)

Head of School:

Prof. Dr. Brendan Griffin

November 2025







Table of Contents

Acknowledgements **6**

Research Funding **8**

Declaration **9**

First author publications **10**

Concomitant Peer Reviewed Publication **10**

Conference presentations **11**

Abstract **13**

Abbreviations **15**

Thesis overview **0**

Chapter 1: Introduction and Literature review **0**

1.1 Limitations of oral drug absorption 0

1.1.1 Assessments of oral drug absorption: From BCS to rDCS 0

1.2 Formulation strategies to overcome dissolution rate and solubility limited drug absorption 6

1.3 Application of milling to improve oral drug absorption 7

1.3.1 Mechanisms of milling induced disorder 11

1.3.2 Co-milling of poorly water-soluble drugs 13

1.3.3 Co-milling with hydrophilic polymers 14

1.3.4 Mechanically activated “co-amorphous” drug formulations 15

1.3.5 Inclusion complexation by Co-milling 16

1.3.6 Co-milling with pharmaceutical silicates 17

1.3.7 Co-milling with Surfactants 17

1.3.8 Co-milling with sugar alcohols 19

1.3.9 Co-milling with proteins 20

1.3.10 Co-milling to produce Co-crystals 20

1.4 Integration of Artificial Intelligence methods in computational pharmaceutics 21

1.4.1 Machine Learning algorithms 23

1.4.2 Applications of Machine Learning in drug formulation development 26

1.5 Aims of the thesis 28

***Chapter 2: Predictive computational models for assessing the impact of co-milling on drug dissolution* 29**

2.1 Graphical abstract 30

2.2 Abstract 31

2.3 Introduction 32

2.4 Materials and Methods 34

2.4.1 Materials 34

2.4.2 Compound selection and characteristics 34

2.4.3 Preparation of COM, PM and milled drugs 37

2.4.4 Dissolution medium preparation 37

2.4.5 Dissolution tests and apparent solubility measurements 37

2.4.6 Particle size distribution 38

2.4.7 X-Ray powder diffraction (XRPD) 38

2.4.8 Calculation of Co-Milling Dissolution Ratios 39

2.4.9 Statistics and model development 39

2.5 Results and discussion 41

2.5.1 Dissolution profiles 41

2.5.2 Influence of co-milling on solid state properties of drug substances 46

2.5.3 Prediction of Co-Milling Dissolution Ratios 47

2.6 Conclusion 57

***Chapter 3: Co-milling of glass forming ability class III drugs: Comparing the impact of low and high glass transition temperatures* 58**

3.1 Graphical abstract 59

3.2 Abstract 60

3.3 Introduction 61

3.4 Materials and Methods 64

3.4.1 Materials 64

3.4.2 Sample preparation by ball milling and blending 64

3.4.3 Dissolution medium preparation 64

3.4.4 Biorelevant dissolution Testing 65

3.4.5 Particle size distribution determination 65

3.4.6 Specific surface area measurements 66

3.4.7 X-ray powder diffraction (XRPD) 66

3.4.8 Differential scanning calorimetry (DSC) 66
3.5 Results 67
3.5.1 Impact of milling and co-milling on the drug crystallinity assessed by X-Ray powder diffraction 67
3.5.2 Glass forming ability class determination of fenofibrate and apremilast 69
3.5.3 In vitro Dissolution profiles of apremilast and fenofibrate in different formulations 70
3.5.4 Relationship between surface area of co-milled mixtures and drug dissolution 72
3.5.5 Melting point depression of co-milled drugs and its correlation with the in vitro dissolution c_{max} of the high-T_g glass former apremilast 73
3.5.6 Stability study of co-milled drugs based on the melting point depression approach 75
3.6 Discussion 76
3.7 Conclusion 79
Chapter 4: Exploring co-milling of poorly water-soluble drugs with swellable polymers to enhance the dissolution rate **80**
4.1 Graphical Abstract 81
4.2 Abstract 82
4.3 Introduction 83
4.3 Materials and Methods 85
4.3.1 Materials 85
4.3.2 Preparation of milled drugs, physical blends and co-milled mixtures 85
4.3.3 Biorelevant Dissolution testing and intrinsic dissolution rate determination 86
4.3.4 X-Ray powder diffraction 87
4.3.5 Particle size determination 87
4.3.6 Specific surface area measurements 88
4.3.7 Thermal analysis via differential scanning calorimetry 89
4.3.8 Descriptor variables calculation and statistical analysis 90
4.3.9 Analysis based on the refined Developability Classification System 90
4.4 Results and discussion 91
4.4.1 Influence of co-milling on the dissolution of poorly water-soluble drugs 91

4.4.2 Influence of superdisintegrant selection on the initial drug release from co-milled formulations 98
4.4.3 Statistical analysis to identify relationships between drug properties and Co-milling-induced Intrinsic Dissolution Rate enhancement 102
4.4.4 Using the refined Developability Classification System to assess the impact of co-milling on dissolution rate limited absorption 105
4.5 Conclusion 109
Chapter 5: Impact of Co-milling on Drug Particle Size Reduction and Crystal Lattice Disorder **110**
5.1 Introduction 110
5.2 Materials and Methods 112
5.2.1 Materials 112
5.2.2 Milling conditions 112
5.2.3 X-Ray powder diffraction analysis 113
5.2.4 Drug particle size determination 113
5.2.5 Thermal analysis 114
5.2.6 Statistical analysis 114
5.3 Results 115
5.3.1 Influence of Co-milling with PVP on drug Particle Size and Distribution Compared to Conventional Milling 115
5.3.2 Influence of Physicochemical and Structural Properties on Milling Induced Crystallinity Loss 120
5.4 Discussion 124
5.5 Conclusion 125
Chapter 6: Thesis discussion **126**
6.1 Overview and Summary 126
6.2 Identification of suitable drug candidates for co-milling 127
6.3 Excipient selection in pharmaceutical co-milling 130
6.4 The relationship between the drug's glass transition temperature (T_g) and the co-milling temperature 134
6.5 The role of melting point depression for supersaturating co-milled drug formulations 137

6.6 Mechanisms of particle aggregation inhibition and size reduction of Co-milling with Polyvinylpyrrolidone 141
6.7 Perspectives for the Upscaling of Co-milling 142
7 Conclusions **144**
8 Future perspectives **145**
9 References **146**
10 Supplementary materials **169**
10.1 Appendix Chapter 2 169
10.1.1 Apparent solubility values of investigated compounds in FaSSIF 169
10.1.2 Measured median particle sizes (D50) of drug powders 170
10.1.3 Co-Milling Dissolution Ratios, 15 min timepoint 171
10.1.4 Co-Milling Dissolution Ratios, 60 min timepoint 172
10.1.5 Multicollinearity diagnosis of multiple linear regression equations 173
10.1.6 Powder X-ray diffractograms of screened drug compounds in co-milled and physical mixtures 173
10.1.7 Powder X-ray diffractograms of unprocessed drug powder and milled drug powder 188
10.1.8 Polymorphs of investigated compounds 203
10.1.9 Variables importance in Projection plots 204
10.2 Appendix Chapter 3 206
10.21 Particle sizes of drug powders 206
10.22 Specific surface areas of co-milled mixtures 206
10.23 Thermograms of apremilast mixtures freshly after preparation and 3 months stability testing 207
10.24 Thermograms of fenofibrate mixtures freshly after preparation and 3 months stability testing 223
10.3 Appendix Chapter 5 247
10.3.1 Particle size measurement validation 247

Acknowledgements

Firstly, I would like to thank my supervisors Dr. Josef Beránek, Dr. Patrick O'Dwyer, Prof. Martin Kuentz and Prof. Brendan Griffin. Thank you, Josef, for the warm welcome in Prague and your consistent support at every stage of the PhD. Thank you, Patrick, for always being there as my first advisor to discuss science as well as all the other challenges that come with doing a PhD. Thank you, Martin, for the wonderful time in your laboratory in Basel and for all our discussions (in front of the campus) where we shared our genuine passion for science. Thank you, Brendan, for your constant effort to be a great supervisor. Your guidance, support, and dedication have truly made a difference and I am thankful for the fantastic opportunity to spend the final period of the PhD in Cork. I truly admire how you all balance professionalism as scientists with empathy and humanity as supervisors. I have learned so much from each of you, not only how to become a scientist, but also how to grow personally and become the person I am today.

Moreover, I want to thank my colleagues in Zentiva, in particular Marek, Tereza, Lukas, David, Shaida and Ondrej who trained me in all the new techniques and always had a minute to talk about problem-solving solutions. A special thanks to David Blanco for sharing so many memorable moments with me throughout this journey.

My biggest thanks to Andreas, Jitka, and Andrea for making my time in Basel more enriching and enjoyable than I could have ever imagined.

Thank you, Theo, Andrew, Lianne, Jack, Callum, and all the other PhD students at UCC for making my time in Cork such a truly enjoyable and memorable experience.

I would like to express my sincere thanks to the InPharma consortium for the opportunity to participate in the research and training program. I am grateful to have been part of such an outstanding team, which provided an excellent environment for developing new skills and fostering my professional growth.

Thanks to my friends Nils, Felix, Enno, Simon, Johannes, Jonas, Carl, David, Steffen, Dustin, Niklas, Niklas, Marcel, Dominic, Lea, Alicia, Pamela, Marek and Michael. Words cannot capture how much you mean to me.

A heartfelt thank you to Hami for your unwavering trust, understanding, love and for always being there to listen. Your support was invaluable, I could not have completed this thesis without you.

Finally, I would not be where I am today without my family. Thank you, Mom and Dad, for your endless support and unwavering love. To my sister Anna, thank you for always being a steady light through every phase of this journey. The constant presence of each of you, your patience, and your strength have meant more to me than words can ever express. I am endlessly grateful.

Research Funding

This project has received funding from the European Union`s Horizon 2020 research and innovation programme under the Marie Curie Sklodowska-Curie grant agreement No. 955756.

Declaration

This thesis has not been previously submitted, in part or in whole, to this or any other university for any degree and is, except where noted and acknowledged, the original work of the author.

Signature:  Date: 28th August 2025

First author publications

1. Nicolas Pätzmann, Patrick J. O´Dwyer, Josef Beránek, Martin Kuentz, Brendan T. Griffin.
   Predictive computational models for assessing the impact of co-milling on drug dissolution.
   Published in European Journal of Pharmaceutical Sciences, Volume 198, 1st July 2024.
   DOI: 10.1016/j.ejps.2024.106780
2. Nicolas Pätzmann, Josef Beránek, Brendan T. Griffin, Martin Kuentz, Patrick J. O´Dwyer.
   Co-milling of glass forming ability class III drugs: Comparing the impact of low and high glass transition temperatures.
   Published in European Journal of Pharmaceutical Sciences, Volume 209, 1st June 2025.
   DOI: 10.1016/j.ejps.2025.107081
3. Nicolas Pätzmann, Josef Beránek, Brendan T. Griffin, Martin Kuentz, Patrick J. O´Dwyer.
   Exploring co-milling of poorly water-soluble drugs with swellable polymers to enhance the dissolution rate.
   Published in AAPS PharmSciTech, Volume 27, 14th November 2025.
   DOI: 10.1208/s12249-025-03270-w
4. Nicolas Pätzmann, Patrick J. O´Dwyer, Josef Beránek, Martin Kuentz, Brendan T. Griffin.
   Predictive Insights into Co-Milling-Induced Changes in Drug Particle Size and Crystal Lattice Disorder
   In Preparation for submission as a technical note to The AAPS Journal.

Concomitant Peer Reviewed Publication

David Blanco, Nicolas Pätzmann, Pablo García-Triñanes
Microdynamic Flowability for Early API Characterisation: A Case Study on Palbociclib

Published in Pharmaceutical Science Advances, Volume 3, December 2025, 100069

DOI: 10.1016/j.pscia.2025.100069

Conference presentations

1. Nicolas Pätzmann.
   Computational tools to predict the dissolution rate enhancement of co-milling approaches.
   Oral presentation at the Symposium of the Pharmaceutical Applied Research Center, Prague, Czech Republic, 16th June 2022.
2. Nicolas Pätzmann.
   Computational tools to predict dissolution rate enhancement of Co-Milling to overcome dissolution rate limited absorption
   Oral presentation at the InPharma Annual Meeting 2022, Cork, Ireland: 22nd June 2022
3. Nicolas Pätzmann.
   Computational tools to predict Dissolution rate enhancement of Co-milling approaches.
   Oral presentation at the InPharma monthly Meeting, Online, 6th December 2022.
4. Nicolas Pätzmann.
   Computational tools to predict dissolution rate gains after co-milling
   Oral presentation at the InPharma Annual Meeting 2023, Athens, Greece: 13th June 2023
5. Nicolas Pätzmann, Patrick J. O´Dwyer, Josef Beránek, Martin Kuentz, Brendan T. Griffin.
   Computational Prediction of Initial Dissolution Performance after Co-milling with PVP.
   Poster presented at the AAPS Annual Meeting PharmSci 360, Orlando, USA, 22nd – 25th October 2023.
6. Nicolas Pätzmann, Patrick J. O´Dwyer, Brendan T. Griffin, Martin Kuentz, Josef Beránek.
   Influence of co-milling conditions on drugs of different glass forming ability classes.
   Poster presented at the 14th World Meeting on Pharmaceutics, Biopharmaceutics and Pharmaceutical Technology 2024, Vienna, Austria, 18th – 21st March 2024.
7. Nicolas Pätzmann, Patrick J. O´Dwyer, Brendan T. Griffin, Martin Kuentz, Josef Beránek.
   Melting Point Depression and Dissolution Enhancement in Co-Milled Formulations of Apremilast.
   Poster presented and awarded at the Annual Meeting of the European Federation for Pharmaceutical Sciences (EUFEPS), Debrecen, Hungary, 23rd – 25th May 2024.

8. Nicolas Pätzmann.
   Co-milling of thermodynamically good glass formers with Tgs above and below processing temperature.
   Oral presentation at the InPharma Annual Meeting 2024, Odense, Denmark: 10th June 2024.
9. Nicolas Pätzmann, Patrick J. O´Dwyer, Brendan T. Griffin, Martin Kuentz, Josef Beránek.
   Co-milling of thermodynamically good glass former with T_gs above and below processing temperature.
   Poster presented at the Joint Nordic POP & InPharma International Symposium, Odense, Denmark, 11th and 12th June 2024.
10. Nicolas Pätzmann.
    Predictive computational models for assessing the impact of co-milling on drug dissolution.
    Oral presentation at the Joint Nordic POP & InPharma International Symposium, Odense, Denmark, 12th June 2024.
11. Michal Romański, Nicolas Pätzmann, Patrick J. O´Dwyer, Josef Beránek, Martin Kuentz, Brendan T. Griffin, Dorota Danielak.
    Effect of superdisintegrant co-milling on the relative bioavailability of poorly soluble drugs evaluated by pharmacokinetics simulations in the COMPASS software.
    Poster presented at the Annual Meeting of the European Federation for Pharmaceutical Sciences (EUFEPS), Vienna, Austria, 19th – 21st February 2025.

Abstract

Poor dissolution in gastrointestinal fluids remains a critical limitation to the oral absorption of many poorly water-soluble drugs. Co-milling offers a solvent-free and industrially scalable technology to overcome dissolution rate limited absorption. However, its broader application has been constrained by the complexity of mechanochemical transformations, particularly in the presence of excipients, and the limited predictive understanding of these processes. Therefore, this thesis aimed to establish a data-driven framework to enhance both the mechanistic understanding and predictability of co-milling outcomes for poorly water-soluble drugs.

A series of experimental co-milling studies was carried out using a diverse selection of drugs and excipients. These investigations incorporated biorelevant dissolution testing, multivariate data modelling, solid-state and thermal analyses, as well as particle size characterization.

The first major finding of this thesis was the development of a predictive model to quantify the dissolution enhancement achievable through co-milling. Using data from 29 crystalline drugs co-milled with PVP K25, key molecular and physicochemical properties, such as particle size, logD6.5, molecular complexity (Kappa 3) and apparent solubility, were identified as reliable predictors of the co-milling induced dissolution improvement. The models achieved high predictive accuracy, offering a practical computational tool to support early formulation development.

Secondly, the influence of the drug glass transition temperature (T_g) on co-milling performance was examined. A distinct difference was observed between low T_g (fenofibrate) and high T_g (apremilast) drugs. Apremilast, milled below its T_g, exhibited progressive amorphization and supersaturation during dissolution testing. A strong linear correlation between melting point depression and maximum drug concentration (c_{max}) in vitro ($R^2 > 0.98$) highlighted melting point depression as a promising critical quality attribute to anticipate drug

supersaturation and for stability purposes. Fenofibrate, in contrast, retained its crystallinity and showed signs of recrystallisation upon storage, emphasising the central role of T_g in predicting both performance and stability.

Thirdly, the role of tablet disintegrants in co-milling performance and biopharmaceutical relevance was investigated. Thirteen drugs were co-milled with three widely used crosslinked excipients: croscarmellose sodium, sodium starch glycolate, and crospovidone. All 39 co-milled formulations showed increased intrinsic dissolution rates (IDR), with molecular descriptors such as polar surface area and size correlating positively with enhancement. Excipient performance varied with drug type, with sodium starch glycolate more effective for acidic drugs and croscarmellose sodium for neutral or basic compounds. Co-milling with tablet disintegrants successfully addressed dissolution rate limitations in all rDCS class IIa drugs, confirming its utility as a biopharmaceutically meaningful formulation approach.

Lastly, the issue of process variability in particle size reduction was addressed. Milling without excipients often led to particle aggregation and inconsistent size distributions. In contrast, co-milling with PVP yielded significantly improved and highly reproducible particle size reduction across all tested drugs. Notably, the extent of size reduction was accurately predicted based solely on the initial particle size. These findings underscore the suitability of PVP based co-milling as a robust and scalable approach for early-stage drug formulation.

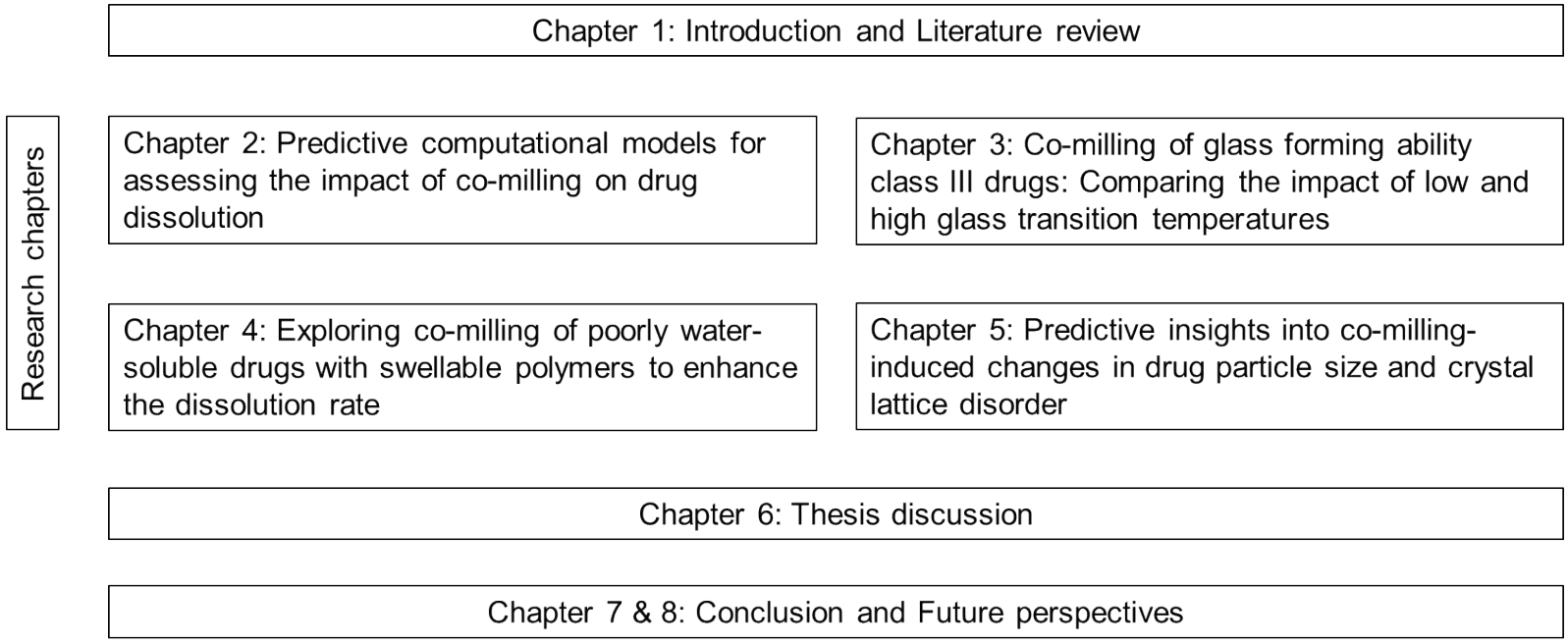
In conclusion, this thesis demonstrates that co-milling can be transformed from an empirical technique into a scientifically grounded and predictable formulation strategy. The models and mechanistic insights developed here offer practical guidance for the rational design of oral dosage forms and support the advancement of more sustainable pharmaceutical development.

Abbreviations

ADME	Absorption, Distribution, Metabolism, and Excretion
AI	Artificial intelligence
AUC	Area under the dissolution curve
BCS	Biopharmaceutics Classification System
BDDCS	Biopharmaceutics Drug Disposition Classification System
clogD$_{6.5}$	Calculated decadic logarithm of the distribution coefficient (Octanol/water) at pH 6.5
c_{max}	Highest dissolved drug concentration during in vitro dissolution testing
COM	Co-milled mixture
COMDR$_{15\ min}$	Co-Milling Dissolution Ratio after 15 min
COMDR$_{60\ min}$	Co-Milling Dissolution Ratio after 60 min
D50	Median particle size
DCS	Developability Classification System
DSC	Differential Scanning Calorimetry
FASSIF	Fasted State Simulated Intestinal Fluid
g	Grams
GFA	Glass forming ability
HBA	Number of hydrogen bond acceptors
HBD	Number of hydrogen bond donors
HPMC	Hydroxypropyl Methylcellulose
IDR	Intrinsic dissolution rate
IDRR	Intrinsic dissolution rate ratio
Kg	Kilograms
L	Liters
Min	minutes
mL	Milliliters
ML	Machine learning
MLR	Multiple linear regression
MW	Molecular Weight
PBPK	Physiologically based pharmacokinetic modeling
PCA	Principal Component Analysis

pH	Negative decadic logarithm of the H_3O^+ concentration
PLS-DA	Partial least squares discriminant analysis
PM	Physically blended mixtures
PSA	Polar surface area
PVP	Polyvinylpyrrolidone K25
QSPR	Quantitative structure property relationships
RAMEB	Randomly methylated β-cyclodextrin
RBC	Rotatable bond count
rDCS	Refined Developability Classification System
RMSE	Root mean square error
$RMSE_{cv}$	Root mean square error of cross validation
rpm	Revolutions per minute
s	Seconds
SLS	Sodium lauryl sulfate
SMILES	Simplified Molecular Input Line Entry System
SSA	Specific surface area
T_RDmtr	Relative topological diameter of the hydrogen-suppressed molecular graph
T_g	Glass transition temperature
T_m	Melting point
VIP	Variables Importance in Projection
XRPD	X-ray Powder Diffraction
µg	Microgram
µL	Microliters
µm	Micrometers

Thesis overview



Chapter 1: Introduction and Literature review

1.1 Limitations of oral drug absorption

Oral administration of drugs provides a patient-friendly delivery route that supports treatment adherence and enables the cost-effective, scalable production of oral dosage forms, ultimately improving global access to medicines (Dressman et al., 1984). However, the majority of newly discovered and potentially highly effective drug candidates in the development pipeline exhibit limited absorption following oral administration (Sugano and Terada, 2015). A widely recognized reason for this limited oral absorption is the insufficient dissolution of small molecule drugs in gastric and intestinal fluids, which is a prerequisite for the drug to be absorbed and reach its target receptors via systemic circulation (Levy and Hollister, 1965). Newly discovered drug molecules with high receptor affinity for target proteins often display high hydrophobicity and lipophilicity, which typically result in these slow dissolution rates and poor solubility in gastrointestinal fluids (Ditzinger et al., 2019).

1.1.1 Assessments of oral drug absorption: From BCS to rDCS

In 1995, the Biopharmaceutics Classification System (BCS) was introduced which highlights the critical influence of solubility and permeability on the oral drug absorption (Amidon et al., 1995). The BCS classifies drugs into four categories based on their solubility and intestinal permeability (Figure 1-1). A compound is categorized as highly soluble if its highest dose strength can dissolve in 250 ml or less of aqueous media across a pH range of 1.0 to 7.5. Drugs are classified as highly permeable when human data show that at least 85% of the administered dose is absorbed after oral administration. Conversely, drugs requiring more than 250 ml to dissolve or exhibiting less than 85% bioavailability after oral administration are classified as poorly soluble or poorly permeable, respectively. If human in vivo data is not available to assess bioavailability, alternative methods can be used to evaluate drug

permeability. Validated and standardized in vitro methods using Caco-2 cells for example were proven to be useful to assess the permeability of a compound (Mehta et al., 2017).

The BCS has served as a strategic tool for industrial formulation during early drug development, although it represents a relatively conservative classification in the context of current drug product development. (Han et al., 2022). Therefore, it has proven valuable for regulatory agencies that implemented the BCS to support biowaivers for in vivo bioequivalence testing, while for the oral drug product development of novel compounds exhibiting highly unfavourable biopharmaceutical properties, further advances were made through progressive modifications of the BCS during the last decades (Mehta et al., 2023).

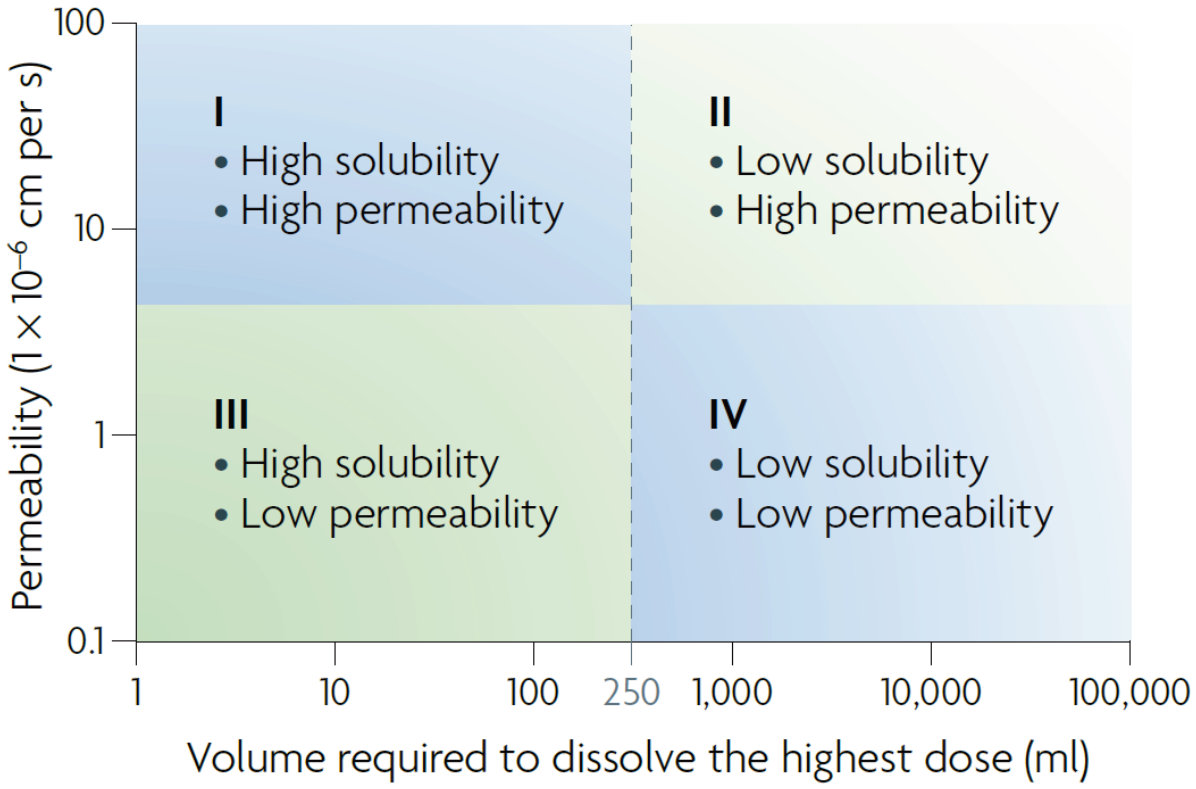


Figure 1-1: The Biopharmaceutics Classification System as proposed from (Amidon et al., 1995), adapted from (Rautio et al., 2008). Drugs are classified according to the lowest volume to dissolve the highest dose over the pH range from 1 – 7.5 (x-axis). Hence, for drugs with pH-dependent solubility, classification is based on the lowest solubility observed across the pH range (worst-case scenario). The permeability can be assessed by either in vitro assays as depicted on the y-axis or by in vivo bioavailability determination.

Ten years after the introduction of the BCS, Wu and Benet identified a notable correlation between the rate of intestinal permeability and the extent of drug metabolism, leading to the development of the Biopharmaceutics Drug Disposition Classification System (BDDCS) (Wu and Benet, 2005). This classification system divides drug substances into four categories based on their solubility and extent of metabolism. A drug is classified as undergoing extensive metabolism if at least 70% of the administered oral dose is metabolized in humans. Wu and Benet observed that for drugs with high permeability, metabolism was the primary elimination pathway, whereas drugs with low permeability were predominantly eliminated unchanged via renal or biliary excretion. The BDDCS offers a framework for predicting drug disposition rather than drug absorption, understanding potential drug-drug interactions, and analysing the interplay between transporters and enzymes (Benet et al., 2008).

The next significant advancement of the BCS was made by Butler and Dressman in 2010, introducing the Developability Classification System (DCS). Focussing the early-stage development of novel small molecules, the DCS classifies drugs based on their dose/solubility ratio, dissolution rate, and permeability (Butler and Dressman, 2010a). The DCS offers an approach to evaluate risks in early development stages within the framework of quality by design. Solubility measurements are performed in biorelevant media, mimicking actual conditions in the gastrointestinal fluids, while the permeability measurements are also standardized. By incorporating the concept of a solubility-limited absorbable dose, poorly soluble drugs are further divided into two subcategories. The oral absorption of DCS class IIa drugs is expected to be limited by the dissolution rate, while class IIb drugs display solubility-limited drug absorption. This subdivision provides more targeted insights for selecting appropriate formulation strategies. For improving oral drug absorption, particle size reduction is typically employed in the case of class IIa drugs (dissolution rate limited absorption) while class IIb drugs (solubility limited absorption) typically require enabling formulation techniques such as solid dispersions or lipid-based formulations.

An extension of the DCS, the refined Developability Classification System (rDCS), was published in 2018 by implementing recent scientific progress into the predictive model (Rosenberger et al., 2018). Standardized investigations of the rDCS include solubility and permeability measurements, similarly to BCS and DCS. Depending on the outcome of the standardized investigations, customized investigations can be triggered. These customized investigations are dissolution or precipitation tests, preferably in small-scale, which are useful to anticipate the behaviour of the drug under physiological conditions. For example, a supersaturation/precipitation experiment is recommended for weak bases classified as rDCS class IIb and IV. Also, for all dissolution rate limited compounds as well as rDCS class I and III compounds below 100 µg/ml aqueous solubility, a (small-scale) dissolution experiment is triggered to support decision making in early-stage formulation development.

The rDCS framework was recently advanced to improve its practical application and guiding formulation design (Beran et al., 2024a). Firstly, for dissolution rate-limited compounds (rDCS class IIa), a set of novel equations were provided to calculate a target particle radius below which dissolution limitations are expected to be overcome (Beran et al., 2023). Depending on the available data, the target particle size can be calculated using either the drug intrinsic dissolution rate (IDR) or solubility as input (Figure 1-2). The framework also provides different equations depending on whether in vivo dissolution is expected to occur under sink or non-sink conditions.

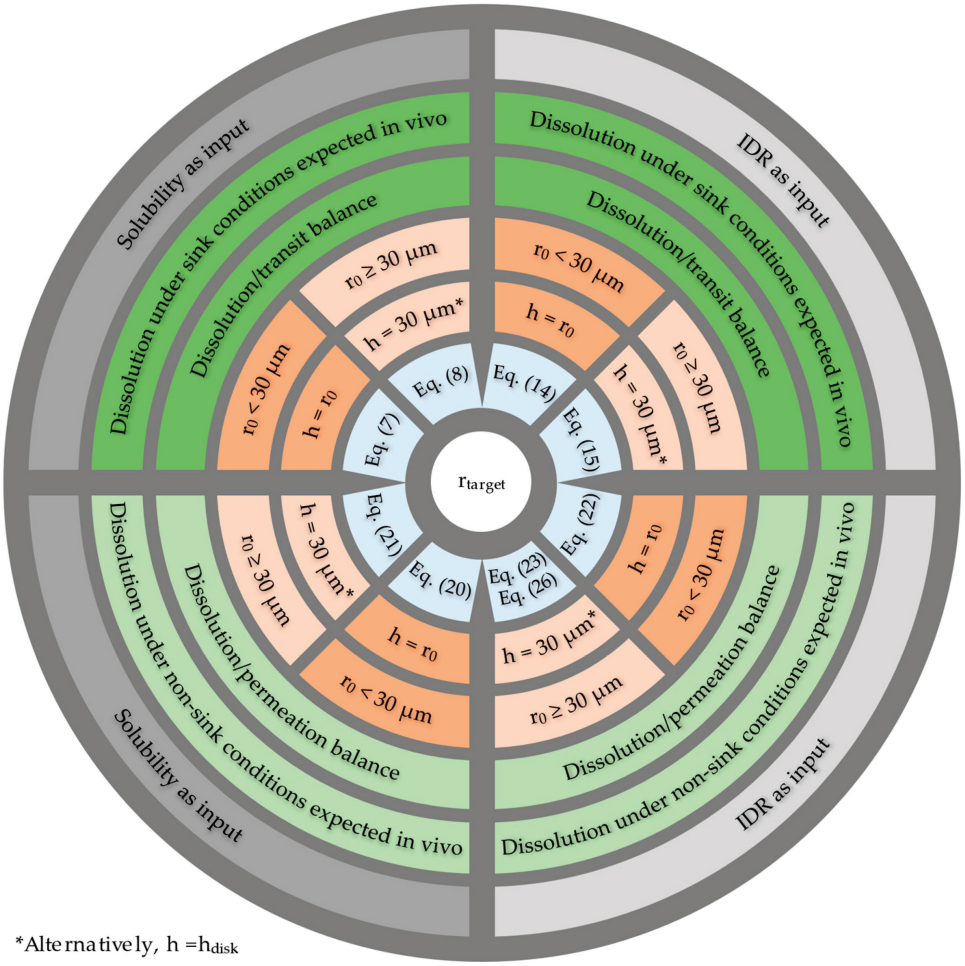


Figure 1-2: The "decision wheel" for the calculation of the target particle radius to overcome dissolution rate limited absorption, extracted from (Beran et al., 2023). The decision process begins with either solubility or intrinsic dissolution rate (IDR) as input (outer ring), followed by an assessment of whether sink or non-sink conditions are expected in vivo.

Secondly, the application of the rDCS was advanced for solubility-limited compounds by considering supersaturation and precipitation effects of enabling formulations (Beran et al., 2024b). Based on two-stage dissolution experiments in the gastric and intestinal phases, four different scenarios, "ambitious"; "optimistic"; "pessimistic" and "worst case", can be projected into the rDCS (Figure 1-3).

For weak bases, the four scenarios can be determined for both the unformulated drug as

"baseline scenarios" and the enabling formulation as "enabling scenarios". They are calculated using the measured gastric solubility ("ambitious"), intestinal solubility ("worst case"), maximum intestinal supersaturation ("optimistic"), and average intestinal drug concentration ("pessimistic") during dissolution testing, resulting in different dose/solubility (D/S) ratios on the x-axis of the rDCS classification scheme.

In the case of weakly acidic drugs, baseline scenarios are calculated using the gastric solubility as the "worst case" and intestinal solubility as the "best case" for the free acid, while enabling scenarios are based on intestinal supersaturation ("optimistic") and the average concentration ("pessimistic") of the salt form.

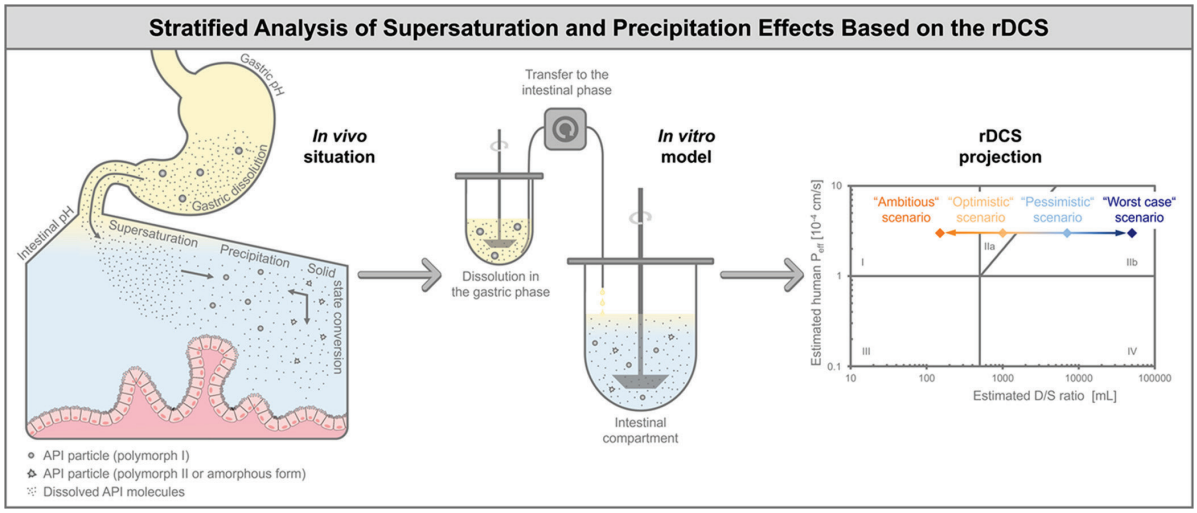


Figure 1-3: Schematic representation of the analysis of supersaturation and precipitation effects based on the rDCS, extracted from (Beran et al., 2024b). The in vivo situation involves drug dissolution in the stomach, supersaturation upon intestinal transfer, and potential precipitation. These processes are simulated using a two-stage in vitro dissolution model. Experimentally derived measured gastric solubility, intestinal solubility, maximum intestinal supersaturation, and average intestinal drug concentration allow the projection of different scenarios into the rDCS diagram to support formulation strategy decisions.

1.2 Formulation strategies to overcome dissolution rate and solubility limited drug absorption

The BCS and its extended frameworks have highlighted poorly water-soluble drugs as a focal point of interest due to the significant challenges they pose in formulation development (Cook et al., 2008). To address poor dissolution and solubility, numerous formulation strategies have been explored that have the potential for enhancing the oral absorption of small molecule drugs by improving dissolution in the gastrointestinal fluid. Improved dissolution can be achieved, for instance, by converting a crystalline drug into its amorphous form within a polymer-stabilized amorphous solid dispersion, or by reducing the drug particle size (Knopp et al., 2018; Liu et al., 2021). In addition, several advanced formulation strategies have been developed to improve the solubility and oral bioavailability of poorly water-soluble drugs (Reppas et al., 2023). One widely applied approach involves the use of lipid-based drug delivery systems, where the drug is solubilized in oils, surfactants, or self-emulsifying formulations (Holm et al., 2023; Kuentz, 2012). These systems enhance drug absorption by promoting solubilization in the gastrointestinal tract and, in some cases, facilitating lymphatic transport, thereby partially bypassing hepatic first-pass metabolism (Suys et al., 2018).

Salt formation is another commonly used strategy, in which the drug is converted into a more soluble ionic form by reacting with a suitable counterion (Saal and Becker, 2013; Zöller et al., 2024). This approach is particularly effective for ionizable compounds and can significantly improve dissolution rate and, consequently, bioavailability (Bae et al., 2015; Drozd et al., 2022; Zhang et al., 2024). However, it is limited to compounds with appropriate functional groups and may pose stability challenges, such as salt disproportionation (Stegemann et al., 2023).

A further promising technique for the pharmaceutical industry is co-crystallization, where the drug is crystallized with a pharmaceutically acceptable co-former to form a multi-component crystal (Guidetti et al., 2023; Taylor et al., 2021). This approach can enhance drug solubility, and even mechanical properties, while obtaining the drug in a crystalline solid state (Guidetti

et al., 2025). Since not every drug-co-former combination results in a co-crystal, owing to the lack of favorable intermolecular interactions and crystal packing compatibility, screening suitable drug-excipient combinations to identify potential co-crystals has been of great interest over the past decade (Malamatari et al., 2017; Sarjeant et al., 2024; Wu et al., 2021).

The production of a drug polymorph exhibiting better dissolution properties compared to the thermodynamically stable form is another potential way to enhance the bioavailability of a drug after oral administration (Censi and Di Martino, 2015; Parlier et al., 2025; Wang et al., 2023). While effective, these modifications require thorough characterization to ensure stability, reproducibility, and consistent performance throughout the product's shelf life (Hilfiker and Raumer, 2018).

1.3 Application of milling to improve oral drug absorption

Milling of solids is a fundamental operation in pharmaceutical manufacturing (Seibert et al., 2019). Terms such as crushing, comminution, grinding, and pulverization are often used interchangeably with milling (Loh et al., 2015). During the milling process, particle surfaces are subjected to mechanical stress, which causes them to deform and accumulate internal strain. When the applied stress exceeds a critical threshold, cracks begin to form within the particle structure. These cracks can propagate and ultimately lead to the fracture and breakage of particles (Meier et al., 2009).

A range of commercially available milling equipment exists suitable for laboratory, pilot and production scale (table 1-1). While ball milling benefits from a simple setup and the ability to perform both dry and wet processes, it suffers from poor scalability (Giraud et al., 2021). Nevertheless, it remains the preferred milling method in research laboratories (Priestley et al., 2023). The selection of suitable milling equipment in pharmaceutical manufacturing depends largely on the physical properties of the raw materials and the desired specifications

of the final product (Seibert et al., 2019). Key factors for evaluating the appropriate stress conditions include fragmentation behaviour, elasticity, hardness of the solids, and the solid-state form of the product. For the production of fine powders, jet milling has proven to be highly effective in industrial contexts (Kushimoto et al., 2023). It operates without balls, which minimizes heat generation. However, it is an energy-intensive process and less suitable for sticky or moisture-sensitive materials. A jet mill can only be used for dry milling. A dry drug milling process typically leads to drugs in the lower micrometre range, whereas wet milling has the potential to produce nanoparticles under well-defined conditions (Malamatari et al., 2018).



Figure 1-4: Laboratory-scale ball mill (MM 400, Retsch, Haan, Germany). The stainless-steel milling jars are mounted onto the milling unit and secured using blue locking wheels. On the right, the interior of the milling jars is shown, along with the milling balls. The white balls are made of zirconium oxide, while the others are composed of stainless steel.

Table 1-1: Overview and comparison of commonly used milling technologies in pharmaceutical development and production. The table summarizes typical scale applicability, suitability for dry and wet milling, key advantages and disadvantages, and typical application areas for each mill type.

Mill Type	Scale	Dry Milling	Wet Milling	Advantages	Disadvantages	Typical Applications
Jet Mill	Lab, Pilot, Production	✓	✗	Fine particles (<10 µm), low heat production	Energy intensive, poorly suitable for sticky materials	Inhalables, fine APIs
Hammer Mill	Lab, Pilot, Production	✓	✗	Robust design, high throughput, widely used	Heat generation, noisy during operation, limited particle size control	Granule resizing, excipients
Ball Mill	Lab, limited Pilot and Production	✓	✓	Simple setup, suitable for brittle materials	Long process duration and cleaning process, not scale-friendly	Research, preformulation
Pin Mill	Lab, Pilot, Production	✓	✗	Uniform particle size, moderate energy demand	Less suitable for sticky or moist materials	Powder milling, intermediates
Cone Mill (Conical)	Lab, Pilot, Production	✓	✓	Gentle size reduction, easy cleaning	Less effective for large size reduction	De-agglomeration, post-drying
Colloid Mill	Lab, Pilot, Production	✗	✓	High shear, ideal for emulsions/suspensions	Not for dry solids, needs cleaning	Creams, gels, emulsions
Roller Mill	Production	✓	✗	Low dust production, energy-efficient	Limited effectiveness for hard or brittle substances	Granulation, powder compaction

A common purpose of milling is particle size reduction (comminution) to achieve a specific particle size distribution, for example, to enhance the dissolution properties of a drug. However, in addition to particle size reduction, milling has the potential to play a pivotal role for the production of drugs with enhanced bioavailability by modifying the physical properties of solid compounds (Bhalani et al., 2022). It can be employed to induce amorphization or to produce drug polymorphs with enhanced solubility (Parlier et al., 2025). Moreover, the incorporation of excipients during milling enables the mechanochemical synthesis of co-crystals or the formation of (partially) amorphous solid dispersions (Dedroog et al., 2019; Friščić and Jones, 2009; Guidetti et al., 2023; Patterson et al., 2007; Wu et al., 2021).

One of the major advantages of mechanochemistry, which is fundamentally based on milling techniques, is its minimal or even complete avoidance of solvent waste (Do and Friščić, 2017). This not only aligns with green chemistry principles but also anticipates potential future regulations that may restrict or ban the use of certain hazardous solvents (Dutta et al., 2022). Mechanochemical processes are therefore typically not only less harmful to the environment and human health but also offer a more sustainable and regulatory-compliant alternative to conventional solvent-based methods. The required mechanical energy of milling processes is derived from electrical energy, which, due to the growing use of renewable sources, is increasingly generated in a sustainable manner and is consistent with the goals of the United Nations Sustainable Development Goals (Zholdassov et al., 2024).

However, from an energetic perspective, dry milling is a highly inefficient yet strategically powerful unit operation, as only a small fraction of the supplied mechanical energy contributes directly to particle breakage and the generation of new surface area, while the majority is dissipated as heat, noise, vibration, and irreversible deformation (Martelli and Di Nunzio, 2025). Energy is transferred through mechanical stresses such as impact, compression, shear, and attrition, arising from direct contacts between milling media, particles, and the mill walls in the absence of a liquid phase. Despite the intense stressing conditions, experimental and theoretical studies consistently show that typically less than 5% of the input energy is

effectively utilized for comminution in dry milling processes (Atashin et al., 2015). The remaining energy is largely dissipated through elastic and plastic deformation of particles and milling media. Additional losses occur through frictional heating at contact interfaces, which is particularly pronounced in dry milling due to the lack of convective heat removal. Inelastic media–media and media–wall collisions further reduce the fraction of useful energy and contribute to temperature rise (Heidari et al., 2025).

While mechanochemistry has gained renewed relevance through the implementation of milling-based techniques as alternatives to solvent-based methods, particularly in industrial manufacturing and especially within the pharmaceutical industry, the effects of milling drug substances remain a highly complex phenomenon (Bodach et al., 2024). Consequently, further research and deeper mechanistic insights into mechanochemistry in pharmaceutical formulation are urgently needed.

1.3.1 Mechanisms of milling induced disorder

The transformation of a crystalline solid into an amorphous form can occur through two primary mechanisms (Figure 1-4). The first, known as fluid-mediated transformation or amorphization on the thermodynamic pathway, involves the intermediate conversion of the crystalline solid into a non-crystalline state (e.g., solution or melt), which subsequently solidifies into an amorphous form via techniques such as melt-quenching, spray-drying, or freeze-drying (Kim et al., 2021).

The second mechanism involves the direct transformation of a crystalline solid into an amorphous or disordered state through mechanical treatment, a process referred to as mechanical activation or solid-state amorphization via the kinetic pathway (Willart and Descamps, 2008). The typically used technique to induce solid-state amorphization via the kinetic pathway is milling.

Although various theories have been proposed to explain the transformation of crystalline solids into amorphous forms during milling, the precise physical mechanisms underlying milling-induced disorder remain poorly understood. The first proposed theory to explain amorphization via the kinetic pathway involves the generation of defects within the crystal lattice, leading to the formation of amorphous regions once a critical defect density is reached (Descamps and Willart, 2016). Defects may take various forms, such as vacancies or dislocations in the crystal lattice or may result from the fragmentation of crystallites (Caron et al., 2011b). These defects can significantly increase the lattice energy of the solid with processing time until a disordered amorphous solid is obtained which lacks characteristic peaks of crystals in X-ray diffractograms (Figure 1-5) (Dujardin et al., 2013).

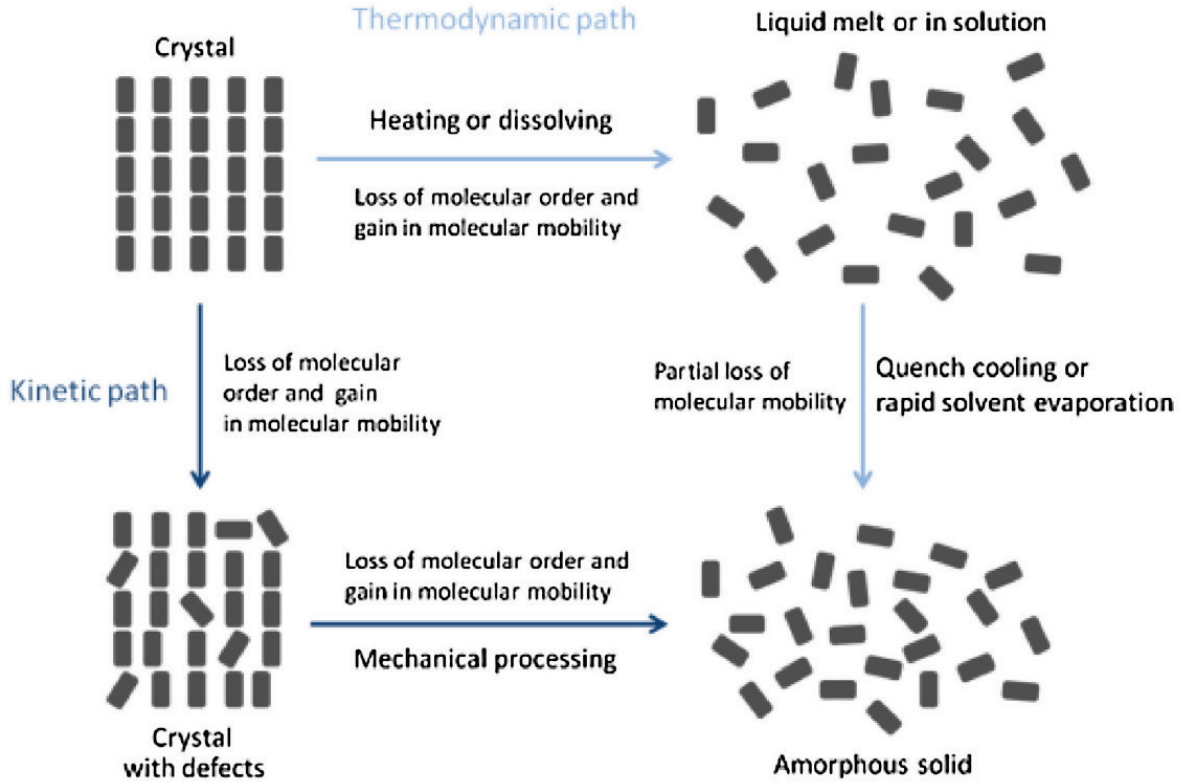


Figure 1-5: Schematic representation of transformation routes from a crystal to an amorphous solid, extracted from (Blaabjerg et al., 2017a). A crystal can lose its crystalline order via mechanical processing (milling) on the kinetic pathway or on the thermodynamic pathway by quench cooling the melt or rapid solvent evaporation.

The second mechanism involves the formation of an amorphous domain through localized melting, caused by frictional heat generated as particles slide against one another, followed by a rapid solidification process known as vitrification (Descamps and Willart, 2016).

Despite theories proposed to explain mechanical activation, the processes of comminution and amorphization in a milling operation remain inherently complex, relying on intricate interactions between material properties and operational parameters. Furthermore, the relationship between material properties at the molecular level and drug amorphization by milling is poorly understood. To achieve the desired combination of particle size reduction and amorphization often necessitates comprehensive optimization of both process- and material-related variables. The nature and extent of disorder introduced into a material depends on both its intrinsic properties and the specific mechanical process applied. To analyse the characteristics of disorder in a solid, it is essential to understand the mechanisms responsible for inducing it.

1.3.2 Co-milling of poorly water-soluble drugs

Milling of poorly water-soluble drugs together with excipients can further enhance both the in vitro dissolution and in vivo bioavailability of drugs (Isaac et al., 2016; Li et al., 2019, 2017a; Slámová et al., 2021; Xiong et al., 2019). The process of milling a drug with an excipient is referred to as "co-milling". Pharmaceutical co-milling has been investigated using a variety of excipients, including hydrophilic polymers, amino acids, crystalline co-formers, sugar alcohols, cyclodextrins, and inorganic materials (Chambers et al., 2021; Kamil and Bayoumi, 2023; Maggi et al., 2013a; Slámová et al., 2021; Varghese and Ghoroi, 2017; Xiong et al., 2019). The underlying mechanisms responsible for the dissolution enhancement span from excipient-mediated support of drug particle size reduction to the stabilization of milling-induced crystal lattice disorder by excipients on the molecular-level (Lim et al., 2016; Liu et al., 2021; Löbmann et al., 2013; Patera et al., 2022; Xiong et al., 2019). The interactions that

occur during co-milling are inherently complex, highly diverse and influenced by both the milling conditions as well as the chosen drug–excipient combination.

1.3.3 Co-milling with hydrophilic polymers

Drug milling with hydrophilic polymers is an often employed process to enhance apparent solubility or the dissolution rate of poorly water-soluble drugs (Loh et al., 2015). Commonly used Polymers are cellulose ethers such as Hydroxypropyl Methylcellulose (HPMC) or Polyvinylpyrrolidone (PVP). Most of the co-milled formulations reveal residual drug crystallinity (Bolourchian et al., 2019; Hussain et al., 2018; Isaac et al., 2016; Lim et al., 2013; Varghese and Ghoroi, 2017). A marketed technology containing residual drug crystallinity, i.e. a partially amorphous drug prepared by milling in combination with a hydrophilic polymer, is SoluMatrix® (Desjardins et al., 2015). However, a commonly recognized drawback of co-milled drug products is that residual crystallinity can serve as a nucleus for recrystallization processes, potentially compromising the product's shelf life (Bhujbal et al., 2021). However, different studies could show that it was possible to prepare amorphous solid dispersions via ball milling using hydrophilic polymers (Caron et al., 2013, 2011; Dedroog et al., 2019; Lim et al., 2013; Patterson et al., 2007). The nature of mechanically activated amorphous solid dispersions produced by ball milling typically differs from those prepared via the thermodynamic pathway. These differences arise not only from the disordered state of the drug but also because milling can induce mechanical degradation of the polymer. Such process-induced changes can further alter the properties of the resulting formulation and potentially impact its performance (Pas et al., 2020; Peterson et al., 2020). Milling at lower temperatures in a cryogenic process typically promotes the drug amorphization for the preparation of amorphous solid dispersions with hydrophilic polymers (Pas et al., 2020).

1.3.4 Mechanically activated “co-amorphous” drug formulations

During the last decade, “co-amorphous” formulations have attracted significant attention in pharmaceutical development, which consist of drug and small molecule-excipient and forming a homogeneous single-phase amorphous system (Kasten et al., 2018; Lim et al., 2016; Löbmann et al., 2013). The majority of investigated excipients in these formulations were amino acids as small molecule alternatives to produce amorphous solid dispersions (Liu et al., 2021). While hydrophilic polymers usually have a drug loading capacity of 20-30%, amino acids usually stabilize in a lower weight ratio than the amorphous drug, usually in a drug to amino acid molar ratio of 1:1 (Shi et al., 2022). Co-amorphous formulations were prepared in different studies either on the kinetic or the thermodynamic pathway. However, the most investigated preparation method was the kinetic pathway by milling (Liu et al., 2021). While long-term stability tests are still missing, mechanically activated, co-amorphous drug material could show increased drug bioavailability (Kasten et al., 2018) (Figure 1-6). In this study, naproxen, a poorly water-soluble compound, was used as a model drug and processed either through liquid assisted grinding or conventional dry ball milling, both in the presence of the amino acid arginine. The liquid assisted grinding process resulted in the formation of a crystalline salt with a melting point of 230 °C and showed no statistically significant differences in AUC or c_{max} compared to the unprocessed crystalline form when administered to Wistar rats. In contrast, dry ball milling produced a co-amorphous salt characterized by a single glass transition temperature (T_g), which significantly enhanced the oral naproxen absorption in rats.

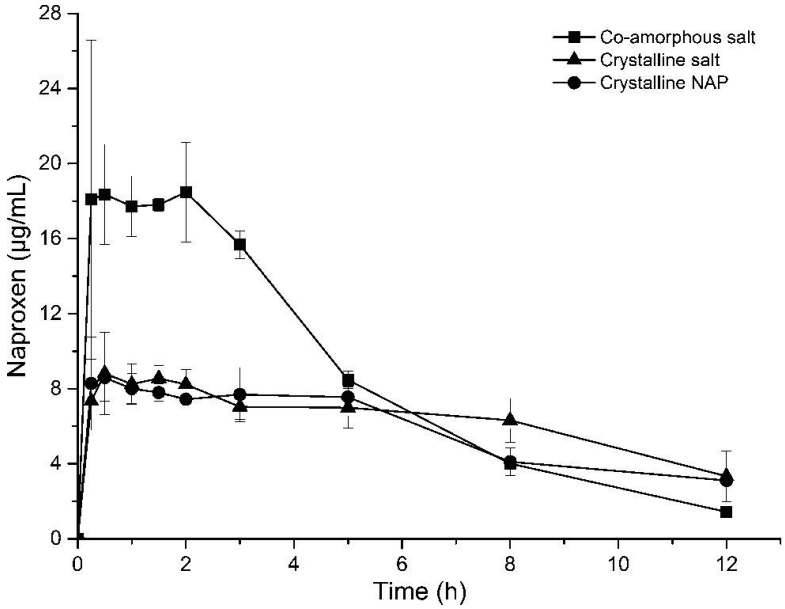


Figure 1-6: Plasma concentration–time profiles of naproxen in Wistar rats following oral administration of co-amorphous salt, crystalline salt, and crystalline naproxen formulations. The co-amorphous salt, prepared by dry ball milling with arginine, showed significantly higher c_{max} and faster absorption compared to the crystalline forms. Crystalline salt produced via liquid assisted grinding exhibited similar pharmacokinetic behaviour to unprocessed crystalline naproxen.

1.3.5 Inclusion complexation by Co-milling

The preparation of complexes containing poorly water-soluble drugs and cyclodextrins is a widely investigated and promising formulation technique to improve oral bioavailability (Brewster and Loftsson, 2007). Due to its lipophilic interior, the complex can interact with lipophilic drugs to form stable complexes, while its hydrophilic exterior typically increases the apparent solubility of the drug in aqueous environments (Bartkowiak et al., 2021). Milling is one solvent free approach for the preparation of these complexes in the solid state and produces minimal chemical waste (Jug and Mura, 2018).

While the naturally existing α-, β- and γ-cyclodextrin already showed partial and in some cases full amorphization after co-milling, modulated cyclodextrins such as randomly methylated β-cyclodextrin (RAMEB) typically showed even higher inclusion efficiency of drugs applying comparable mechanical energy during the co-milling process (Mura et al., 2001).

The product amorphization in the solid state is thereby generally accepted as an indicator of an inclusion complex formation (Jug and Mura, 2018).

1.3.6 Co-milling with pharmaceutical silicates

While silica in solid oral dosage forms are typically used to improve the processability of powders before pressing the tablet, several studies used these excipients as co-milling excipient (Bahl et al., 2008; Bahl and Bogner, 2006; Gupta et al., 2003; Vadher et al., 2009). These studies could show amorphous drugs prepared by co-milling with silicates such as mesoporous silica, Neusilin US2 or Aerosil 200. The excipient related silanol groups are hypothetically contributing to the stabilization of the amorphous drug by hydrogen bonding (Moutamenni et al., 2023). However, more studies are needed to further investigate mechanisms or mechanically activated drug material prepared with pharmaceutical silicates. No study to date could present in vivo bioavailability improvements of poorly water-soluble drugs co-milled formulations with pharmaceutical silica.

1.3.7 Co-milling with Surfactants

Co-milling of poorly water-soluble drugs with surfactants was shown to be an effective approach to accelerate in vitro dissolution. Poloxamer F-127 showed in one study a higher dissolution enhancement compared to amorphous silica and mannitol as co-milling agents in the same drug to excipient ratio (Maggi et al., 2013a). Another study also evaluated poloxamer F-127 as well as sucrose stearate as co-milling carriers, showing not only improved drug dissolution rate and solubility, but also chemical stability and biocompatibility of the co-milled product (Gaggero et al., 2020). Furthermore, one study ball milled a model drug with Soluplus® to investigate its suitability as a co-former of a mechanically activated amorphous solid dispersion (Caron et al., 2013). Interestingly, in contrast to the traditionally used polymer PVP, Soluplus® as a carrier did not lead to a single T_g of both components. A single T_g is typically an indicator of an amorphous solid dispersion of carrier and drug. The

two different T_gs suggest that co-milling with Soluplus® resulted in a rather heterogeneous system, whereas using PVP as the carrier led to a homogeneous dispersion. However, stability studies showed that Soluplus®-based formulations absorbed less moisture compared to those prepared with the traditionally used hydrophilic polymer PVP. Therefore, Soluplus® appears to offer advantages in terms of stability.

Despite the promising in vitro results, there is no in vivo data available for co-milled drugs with surfactants alone. However, ternary complexes consisting of sodium lauryl sulfate (SLS) as a surfactant and PVP as a carrier were ball-milled with various poorly water-soluble drugs, resulting in enhanced bioavailability in rats (Nkansah et al., 2013). Interestingly, these ternary complexes with surfactant led to a nanosized drug after dry milling in the solid state without the use of a solvent. Another study dry milled the poorly water-soluble drug probucol with the hydrophilic polymer Kollidon® VA64 (Vinylpyrrolidone/vinyl acetate (60/40)) and the non-ionic surfactant Cremophor® RH40 (Li et al., 2017). The in vivo bioavailability of the milled drug was significantly improved compared to the marketed formulation (Figure 1-7).

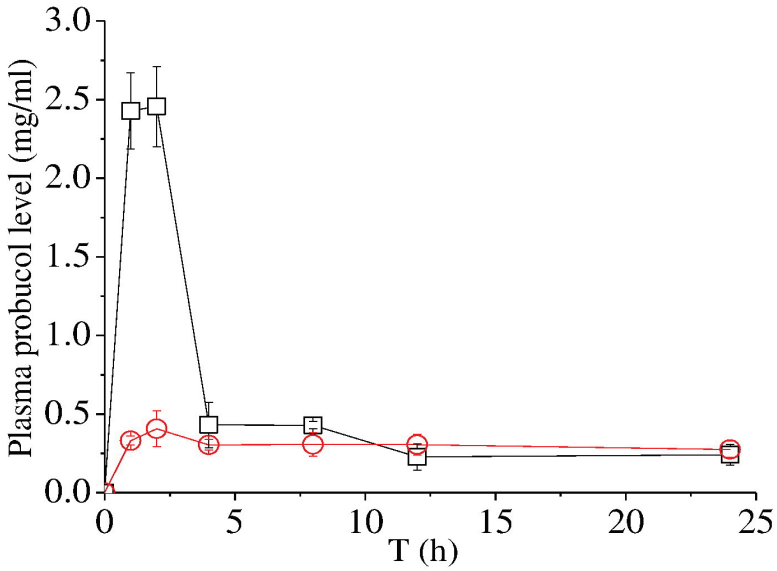


Figure 1-7: Example of a mechanically activated formulation that successfully enhanced the in vivo bioavailability of a poorly water-soluble drug. Depicted are plasma concentrations of orally administered probucol in rats (n = 6), extracted from (Li et al., 2017). The black squares represent the dry milled ternary complex of probucol with the hydrophilic polymer Kollidon® VA64 and the non-ionic surfactant Cremophor® RH40, while the red cycles show the plasma concentration of the marketed formulation.

1.3.8 Co-milling with sugar alcohols

Sugar alcohols such as mannitol are widely used excipients in oral solid dosage forms (Ohrem et al., 2014). Hence, investigations of the suitability of these excipients as co-milling agents were performed (Ibraheem and Wagner, 2021; Maggi et al., 2013b; Mártha et al., 2014). In all of the studies, co-milled mixtures of drug and mannitol contained residual crystallinity. In one study, the in vitro dissolution enhancement of mannitol was lower compared to polymeric excipients (Maggi et al., 2013b). Similar findings were observed in another study that investigated the solubility and dissolution of ibuprofen after high-pressure compaction combined with a co-milling step. This study used the polymeric excipient HPC and the polyols mannitol, sorbitol, and isomalt (Ibraheem and Wagner, 2021). In this study, substantial partial amorphization was observed only for formulation using the polymeric excipient, not for the

polyols. Consequently, the polymer-based mixture of ibuprofen exhibited higher solubility and dissolution enhancement compared to the binary mixtures with the polyols. While these studies suggest that sugar alcohols may not be the most effective excipients for stabilizing milling-induced disorder on solid drug particles, one in vivo study demonstrated a significant improvement in the bioavailability of a mannitol-based co-milled mixture with a poorly water-soluble drug. (Kubo and Mizobe, 1997).

1.3.9 Co-milling with proteins

A newly investigated protein for the stabilization of drugs in an amorphous solid dispersion is beta lactoglobulin (Zhuo et al., 2024). The drug loading of amorphous solid dispersions prepared by milling or spray drying drugs in beta lactoglobulin can exceed 50% (w/w) (Kabedev et al., 2022). In vitro dissolution results indicate a high potential of beta lactoglobulin as carrier compared to traditionally used excipients. However, in vivo data is still missing, because regulatory agencies need to accept beta lactoglobulin as a pharmaceutical excipient.

1.3.10 Co-milling to produce Co-crystals

Milling can be used to produce co-crystals either in a dry process using simply both crystalline compounds or in a liquid assisted process adding a liquid to catalyse the co-crystallization process during milling (Karimi-Jafari et al., 2018). While salt formation involves proton transfer and ionic bond creation between an acid and a base, co-crystal formation requires neutral molecules associating through non-ionic interactions (Deng et al., 2023). The mechanisms of co-crystal formation during dry milling goes typically via an amorphous intermediate state produced during milling, which recrystallises as a cocrystal. If one or both reactants exhibit significant vapor pressures in the solid state, the co-crystal formation can also go via molecular diffusion (Friščić and Jones, 2009). Co-crystal co-formers are often small molecule acids, such as fumaric acid or oxalic acid, but they can also be various types of non-ionic substances, including sugar alcohols, basic heterocycles, or amides (Wu et al., 2021).

1.4 Integration of Artificial Intelligence methods in computational pharmaceutics

Over the past decade, computational pharmaceutics has integrated artificial intelligence (AI) techniques, offering the potential to transform the current formulation development paradigm (Reppas et al., 2023). Computational methodologies have become indispensable across different areas of pharmaceutical research and development, spanning from atomic-level phenomena to whole-body simulations. As illustrated in figure 1-7, a diverse array of in silico tools supports and accelerates various stages of formulation development (Wang et al., 2021). At the nanoscale, quantum mechanical calculations enable detailed electronic-level insights, which are crucial for understanding molecular interactions, stability, and drug solubility (Alsenz and Kuentz, 2019; Hossain et al., 2019). Progressing to the microscopic and mesoscopic scales, molecular dynamics simulations provide a dynamic perspective on structural flexibility, solvation behaviour, and phase transitions (De Vivo et al., 2016). Mathematical modelling and process simulations then bridge the gap to macroscale phenomena, enabling quantitative analysis and optimization of manufacturing and formulation processes. At the human-body level, physiologically based pharmacokinetic modelling (PBPK) offers a systems-level understanding of drug absorption, distribution, metabolism, and excretion (ADME), aiding in dose prediction and clinical translation (Kostewicz et al., 2014). Computational methods are now integral across all domains of pharmaceutics, including a wide range of techniques such as quantum mechanics, molecular dynamics simulations, mathematical modelling, process simulations, AI/machine learning (ML) algorithms and PBPK modelling, as depicted in Figure 1-8 (Wang et al., 2021).

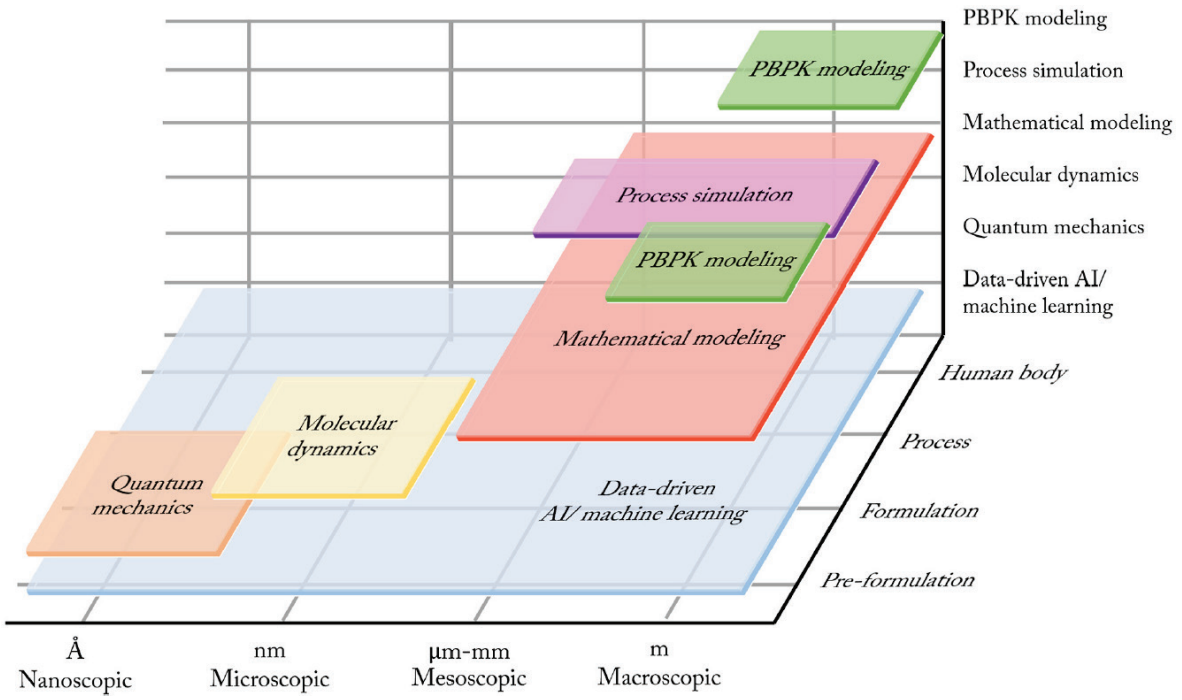


Figure 1-8: Schematic overview of computational pharmaceutics, extracted from (Wang et al., 2021). The x-axis represents spatial scale from nanoscopic (Å) to macroscopic (m) levels while the y-axis reflects stages of pharmaceutical development, from pre-formulation to modelling of performance in humans. The z-axis shows the types of computational approaches used, including quantum mechanics, molecular dynamics, mathematical and process modelling, PBPK modelling, and data-driven AI or machine learning, each mapped to the scales and processes where they are most applicable,

Importantly, data-driven approaches are integrated across nearly all levels of this computational framework. These techniques support the identification of complex patterns, the development of predictive models, and informed decision-making based on both experimental and simulated data (Dong et al., 2023). Their application enhances the accuracy, robustness, and efficiency of mechanistic as well as empirical modelling efforts. The combined deployment of computational methods, ranging from quantum mechanical simulations to physiologically based pharmacokinetic modeling, signifies a fundamental shift toward model-informed drug development. This transformation promotes a more predictive,

mechanistically grounded, and data-rich understanding of pharmaceutical systems (Sliwoski et al., 2014).

1.4.1 Machine Learning algorithms

Machine learning, a specialized domain within artificial intelligence (AI), focuses on developing algorithms that can learn from data and make decisions or predictions without being explicitly programmed for every task. Unlike traditional rule-based systems, where predefined instructions dictate behaviour, machine learning models are capable of autonomously identifying patterns and structures in data. The primary aim is to generalize effectively from observed data to previously unseen scenarios, allowing systems to perform complex tasks with minimal human intervention (Greener et al., 2022). Machine learning can be broadly categorized into four main types: supervised learning, unsupervised learning, semi-supervised learning, and reinforcement learning (figure 1-9) (Taye, 2023). Each of these categories encompasses distinct objectives, methodologies, and algorithmic approaches.

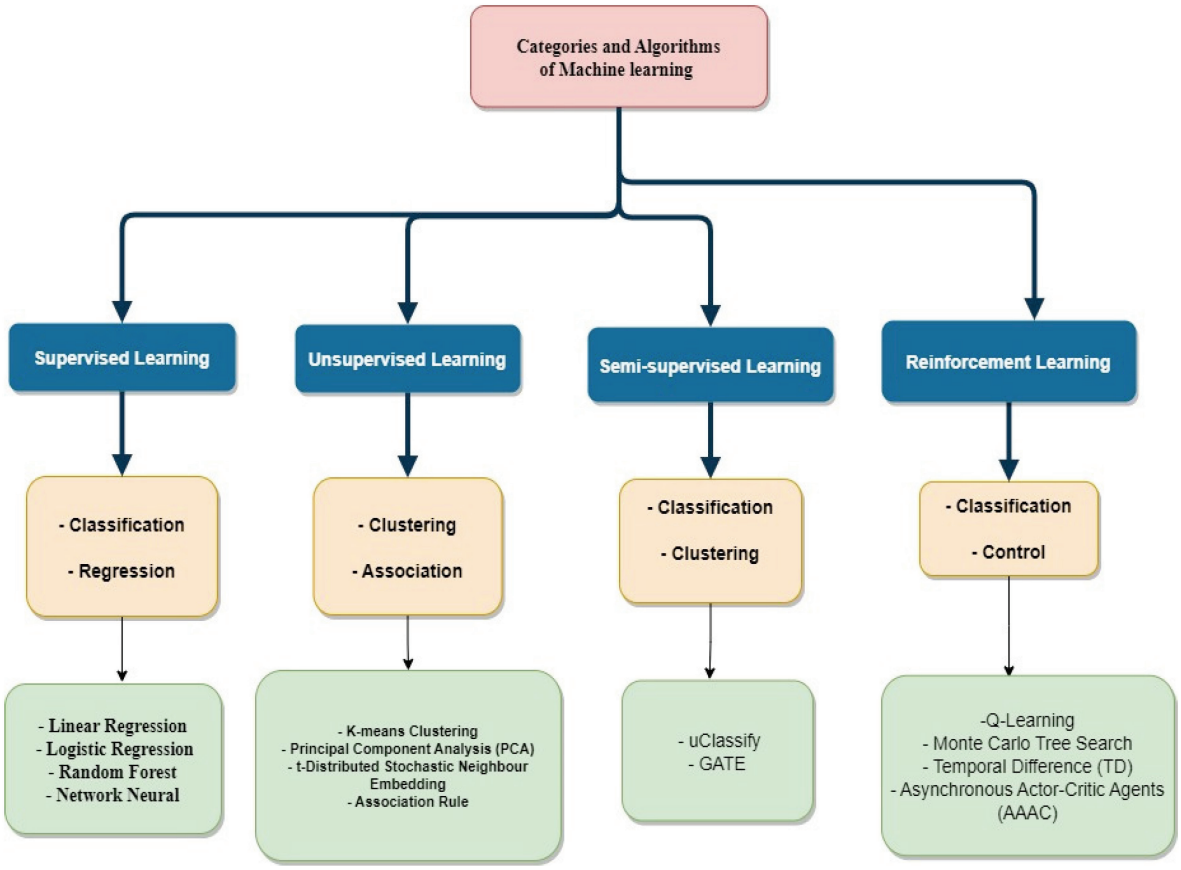


Figure 1-9: Overview of the main categories and representative algorithms of machine learning, extracted from (Taye, 2023). The diagram distinguishes four major learning paradigms: Supervised learning, unsupervised learning, semi-supervised learning, and reinforcement learning. Each category is associated with specific tasks such as classification, regression or clustering and employs characteristic algorithms tailored to its objectives.

Supervised learning involves training a model on a labelled dataset, where each input is associated with a corresponding output. The model learns to map inputs to outputs, making it particularly effective for tasks such as classification and regression. Commonly used supervised learning algorithms include linear regression, logistic regression, random forest, and neural networks (Bzdok et al., 2018). These methods rely on the minimization of a loss function to optimize predictive accuracy and are widely applied in pharmaceutical research (Alhalaweh et al., 2014; Bennett-Lenane et al., 2021a, 2021b; Hossain et al., 2019).

In contrast, unsupervised learning deals with datasets that lack explicit labels. The primary goal here is to uncover hidden patterns or intrinsic structures within the data. Tasks such as clustering and association rule mining are central to this category. Common algorithms include K-means clustering, Principal Component Analysis (PCA), t-distributed stochastic neighbour embedding, and various association rule learning methods (Trezza et al., 2024). These techniques are especially useful for exploratory data analysis by dimensionality reduction.

Semi-supervised learning represents a hybrid approach, leveraging a small set of labelled data alongside a large volume of unlabelled data (Obaido et al., 2024). This method is particularly advantageous in scenarios where labelling is costly or time-consuming. As indicated in figure 1-9, algorithms enabling both classification and clustering with limited supervision. These models aim to extrapolate the structure present in the unlabelled data to improve predictive performance.

Finally, reinforcement learning focuses on training agents to make sequences of decisions by interacting with an environment. The agent learns a policy that maximizes cumulative rewards through trial and error. This paradigm is well-suited for dynamic, real-time applications such as robotics and autonomous systems (Moos et al., 2022).

In summary, the taxonomy presented in Figure 1-9 highlights the diversity and depth of machine learning methodologies. Each category addresses specific types of learning problems and is supported by a suite of algorithms tailored to its objectives. Understanding these categories is essential for selecting appropriate techniques in real-world applications and for advancing research in intelligent systems.

1.4.2 Applications of Machine Learning in drug formulation development

The initial applications of machine learning in drug formulation development date back to the 1990s when artificial neural networks were employed to predict the properties of immediate-release oral tablets. These early studies involved the preparation and evaluation of various tablet formulations, with the resulting data used to train artificial neural networks for the prediction of tablet properties (i.e., tensile strength, friability, capping, disintegration time, and dissolution at various time points) after tablet compression (Bourquin et al., 1998, 1997; Kesavan and Peck, 1996; Turkoglu et al., 1999). These pioneering studies showcased the potential of machine learning to predict drug formulation performance.

Recent advancements in applying machine learning techniques have enabled the prediction of a wide range of parameters for advanced oral delivery systems, such as release rates, stability or to guide excipient selection. For example, different works could establish models to predict drug release rates from sustained-release tablets using matrices that consists of Eudragit RS PO or polyethylene oxide (Barmpalexis et al., 2010; Ibri et al., 2002; Petrović et al., 2009). Another study used 8 different machine learning techniques for the assessment of long-term physical stabilities of amorphous solid dispersions (Han et al., 2019). Among the 8 applied algorithms, a random forest model could achieve the best score (82.5%) to predict the stability of these amorphous formulations based on molecular descriptors.

Machine learning was also used to predict the complex formation of cyclodextrins and guest molecules as well as drugs in phospholipid systems (Gao et al., 2020; Zhao et al., 2019). Another widely investigated field in pharmaceutical formulation and machine learning is the prediction of co-crystal formability of a drug and a crystalline co-former. Different Co-crystal screenings were designed based on machine learning algorithms, such as Partial least squares discriminant analysis (PLS-DA), random forest models or different artificial neural networks to predict the formability of a co-crystal based on physicochemical properties of drug and excipient (Alharby and Huwaimel, 2025; Essen and Luedeker, 2023; Liang et al., 2024; Mswahili et al., 2021; Song et al., 2025). In addition to the field of co-crystals, co-amorphous

formulations have also gained attention in recent decades. For co-amorphous systems, the co-formability has also been predicted based on molecular descriptors using PLS-DA. The technique correctly predicted 95% of mebendazole - amino acid combinations after ball milling (Meng-Lund et al., 2018).

Despite the well-established use of lipid-based formulations for decades, machine learning could reveal new insights into effects on the molecular level. Recently, artificial neural networks and partial least squares regression have been employed to predict improvements in biorelevant solubility based on key physicochemical properties of drug substances (Alskär and Bergström, 2015; Bennett-Lenane et al., 2021b). It was further demonstrated that the impact of lipid-based formulations on the Developability Classification System (DCS) could be accurately predicted. (Bennett-Lenane et al., 2021a).

The parameters predicted by these models, such as improvements in drug solubility, release rates, stability, and compatibility with excipients, reflect key challenges in the development of advanced oral delivery systems. These studies highlight the potential of machine learning to address these issues and to support the design and optimization of such formulations.

1.5 Aims of the thesis

This work aimed to investigate co-milling as a strategy for enhancing the drug dissolution rate from multiple perspectives. While most existing co-milling studies have focused on a limited number of drug compounds, the objective of this project was to conduct broader screenings to improve the reproducibility, generalizability, and predictability of dissolution enhancement. To this end, the usefulness of machine learning techniques was investigated to gain deeper insights into the co-milling process, with the goal of training models capable of forecasting formulation performance. Such models could be leveraged during preclinical development to assess the potential of co-milling as a formulation strategy for individual novel drug candidates aimed at improving drug dissolution.

Following the identification of such trends, another aim of the project was to mechanistically investigate particularly noteworthy phenomena observed among specific drug candidates in the wider screening. Co-milling can induce crystal lattice disorder on the surface or within the core of drug particles. Understanding the induction and stability of lattice disorder was a key objective, especially in relation to relevant molecular descriptors that may relate to drug supersaturation. In addition to focusing on drug properties, this project aimed to shift perspective by examining the role of excipients. One of the aims was to explore novel or under-researched excipient classes with high potential for co-milling applications. These excipients should be evaluated both for their practical applicability and for their biopharmaceutical relevance, using the most recent developments within the Developability Classification System (DCS) as a predictive framework for oral drug absorption.

An essential objective of drug milling is the reduction of particle size. However, the incorporation of excipients can influence this process by affecting both the fragmentation and agglomeration behaviour of drug particles. Accordingly, one aim of this project was to investigate the impact of polymer-assisted milling on particle size reduction, with particular emphasis on its potential to reduce drug particle aggregation.

Chapter 2: Predictive computational models for assessing the impact of co-milling on drug dissolution

Nicolas Pätzmann[1,2], Patrick J. O'Dwyer[1], Josef Beránek[2], Martin Kuentz[3], Brendan T. Griffin[1]

[1] *School of Pharmacy, University College Cork, Cork, Ireland*

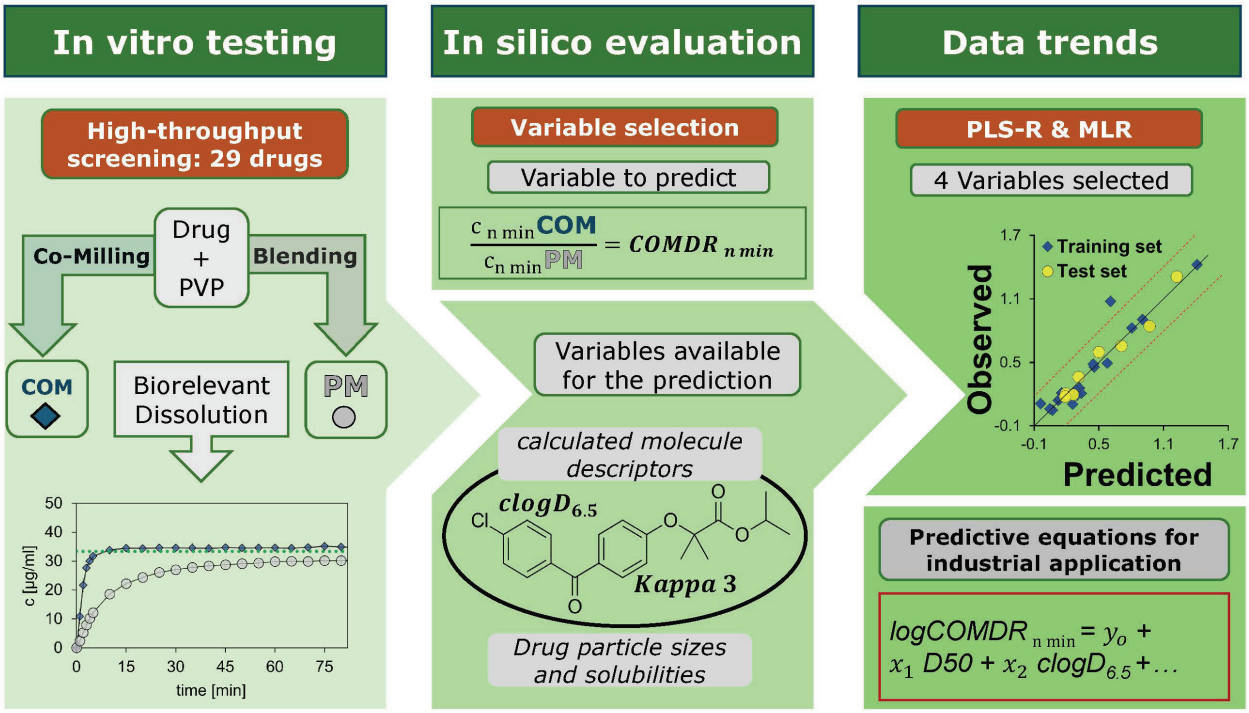
[2] *Department Preformulation and Biopharmacy, Zentiva, k.s., Prague, Czech Republic*

[3] *Institute of Pharma Technology, University of Applied Sciences and Arts Northwestern Switzerland, Muttenz, Switzerland*

Published in: European Journal of Pharmaceutical Sciences (2024), Volume 198

DOI: 10.1016/j.ejps.2024.106780

2.1 Graphical abstract



2.2 Abstract

Co-milling is an effective technique for improving dissolution rate limited absorption characteristics of poorly water-soluble drugs. However, there is a scarcity of models available to forecast the magnitude of dissolution rate improvement caused by co-milling. Therefore, this study endeavoured to quantitatively predict the increase in dissolution by co-milling based on drug properties. Using a biorelevant dissolution setup, a series of 29 structurally diverse and crystalline drugs were screened in co-milled and physically blended mixtures with Polyvinylpyrrolidone K25. Co-Milling Dissolution Ratios after 15 min ($COMDR_{15\ min}$) and 60 min ($COMDR_{60\ min}$) drug release were predicted by variable selection in the framework of a partial least squares (PLS) regression. The model forecasts the $COMDR_{15\ min}$ (R^2 = 0.82 and Q^2 = 0.77) and $COMDR_{60\ min}$ (R^2 = 0.87 and Q^2 = 0.84) with small differences in root mean square errors of training and test sets by selecting four drug properties. Based on three of these selected variables, applicable multiple linear regression equations were developed with a high predictive power of R^2 = 0.83 ($COMDR_{15\ min}$) and R^2 = 0.84 ($COMDR_{60\ min}$). The most influential predictor variable was the median particle size of the pure drug, followed by the calculated drug $logD_{6.5}$ value, the calculated molecular descriptor Kappa 3 and the apparent solubility of pure drug after 24 h dissolution. The study demonstrates the feasibility of forecasting the dissolution rate improvements of poorly water-soluble drugs through co-milling. These models can be applied as computational tools to guide formulation in early-stage development.

2.3 Introduction

Formulating drugs with dissolution rate limited absorption in oral solid dosage forms remains a challenge for pharmaceutical development (Grady et al., 2018). The Developability Classification System (DCS) enables the identification of potential candidates with dissolution rate limited absorption in the early-stage drug development (Butler and Dressman, 2010b). For drug candidates with dissolution rate limited absorption (DCS class IIa drugs) the DCS proposes a target particle size to be achieved, below which the risk of dissolution rate limiting the extent of absorption is considered low. Recently, further advancements have been proposed for calculating the appropriate degree of particle size reduction needed to mitigate dissolution limitations for DCS Class IIa drug candidates (Beran et al., 2023). These approaches are already good starting points for identifying and addressing dissolution rate limitations of emerging drug candidates in the early phase of drug development. In practice, reducing drug particles by milling to a calculated size may not be sufficient in every case to overcome dissolution rate absorption. For these scenarios, the inclusion of excipients as a milling aid may be required to further bioenhance the drug in order to achieve desired drug absorption.

Numerous studies have confirmed that the dissolution rate of drugs can be successfully improved by various formulation strategies such as micronisation, spray drying, solid dispersions, inclusion complexes and co-milling (Ibraheem and Wagner, 2021; Saharan et al., 2010). Co-milling has been identified as an industrially scalable, solvent-free and green process in which a drug powder is milled with an excipient to improve its dissolution rate (Maggi et al., 2013b; Varghese and Ghoroi, 2017). The process not only promotes mixing and reduces particle size but can also induce drug amorphization. Additionally, specific drug-excipient interactions and other mechanisms may come into play (Slámová et al., 2021). Therefore, it is assumed that a combination of different factors is responsible for the improvement of the dissolution rate (Brokešová et al., 2022; Vogt et al., 2008a).

Polyvinylpyrrolidone (PVP) has been demonstrated in various studies to be a promising excipient for co-milled formulations (Patterson et al., 2007; Chingunpitak et al., 2008; Patterson et al., 2007; Yang et al., 2012). The polymer exhibits the potential to stabilize the produced amorphous state of co-milled drugs leading to an enhanced dissolution rate of the drug (Asgreen et al., 2020; Meiland et al., 2022). Prior investigations with PVP as an excipient in co-milled formulations confirmed successful dissolution rate enhancement of a few drug candidates (Bolourchian et al., 2019; Mura et al., 2002). However, data-driven, computational approaches based on a high-throughput screening to predict drug dissolution after co-milling are lacking.

To guide industrial scientists in the development of orally administered formulations, data driven prediction models were established in recent years (Bannigan et al., 2021). Considerable progress has been made in computational models for solubility prediction, covering a wide range of models, such as quantitative structure property relationships (QSPR) (Kuentz and Bergström, 2021). By utilising obtained predictive models, industrial scientists can move beyond the traditional trial-and-error approach and adopt more rational procedures that anticipate outcomes. For example, QSPR models for lipid-based formulations to assess the solubility gain helped to streamline the industrial development of drugs with solubility limited absorption by unlocking early indicators of success (Alskär and Bergström, 2015; Bennett-Lenane et al., 2021b; Bergström et al., 2016). However, for the development of oral solid dosage forms containing drugs with dissolution rate limited absorption, such QSPR models for a technique to improve dissolution rate have not yet been developed.

The objective of this study was therefore to explore the establishment of a computational model that could be applied for early-stage industrial development to predict dissolution rate enhancement achieved by co-milling based on drug properties. The experimental aims were to screen 29 drugs in binary co-milled mixtures (COM) and blended physical mixtures (PM) with PVP. Obtained dissolution profiles combined with measured and calculated drug properties were used for computational modelling.

2.4 Materials and Methods

2.4.1 Materials

Sertraline, ceritinib, etoricoxib, rivaroxaban, enzalutamide, candesartan cilexetil and PVP K25 were provided by Zentiva, k.s. (Prague, Czech Republic), apremilast, ezetimibe, tadalafil and dasatinib by MSN Pharmaceuticals Inc. (New Jersey, USA), apixaban and aripiprazole by Sanofi S.A. (Paris, France), nilotinib by Teva Pharmaceutical Industries Limited (Petach Tikwa, Israel), celecoxib by Cadila Pharmaceuticals (Ahmedabad, Gujarat, India), deferasirox by Neuland Laboratories Ltd. (Telangana, India), olaparib by Taizhou Crene Biotechnology Co. Ltd. (Taizhou Zhejiang, China) and sorafenib by Qilu Antibiotics Pharmaceutical Co., Ltd. (Jinan, China). Further model drugs cinnarizine, glibenclamide, griseofulvin, dipyridamole, fenofibrate, albendazole, mefenamic acid, gemfibrozil, carbamazepine, indomethacin, thiabendazole and nimesulide were purchased from Sigma-Aldrich (Prague, Czech Republic). Reagents for the medium sodium chloride, sodium hydroxide, di-sodium hydrogen phosphate were provided by Sigma-Aldrich (Prague, Czech Republic) and Simulated Intestinal Fluids powder was sourced from Biorelevant.com Ltd. (London, United Kingdom).

2.4.2 Compound selection and characteristics

29 poorly water-soluble model drugs with diverse molecular structures and physicochemical properties were selected (Table 2-1). The dataset contains substances with a wide range of molecular weight (201.3 – 610.7 g/mol, lipophilicity ($clogD_{6.5}$ 1.2 – 5.2), hydrogen bond acceptors (1-12), hydrogen bond donors (0-4) and rotatable bonds (0-12). Acidic, basic, neutral and ampholyte compounds were included to enhance the structural diversity of the dataset. All model drugs have UV-light absorbing chromophores to enable quantitative determination during dissolution test using in-situ UV probe.

Table 2-1: Selection of physicochemical and molecular properties of investigated compounds. clogD$_{6.5}$ and Polar surface area were calculated using ADMET Predictor software (Version 9.5, Simulation Plus, California, USA). Following abbreviations were used: clogD$_{6.5}$ = calculated decadic logarithm of the distribution coefficient (Octanol/water) at pH 6.5, PSA = Polar surface area; HBA = Number of hydrogen bond acceptors; HBD = Number of hydrogen bond donors; RBC = Rotatable bond count.

Drug Compound	Molecular Weight [g/mol]	Calculated logD$_{6.5}$	Acidic/ Basic/ Neutral/ Ampholyte	Calculated PSA [Å^2]	HBA	HBD	RBC
Albendazole	265.34	2.81	Ampholyte	67.01	4	2	6
Apixaban	459.51	2.16	Neutral	110.76	8	1	3
Apremilast	460.51	1.81	Neutral	119.08	9	1	9
Aripiprazole	448.39	4.08	Basic	44.81	5	1	7
Candesartan Cilexetil	610.67	2.89	Ampholyte	143.34	10	1	10
Carbamazepine	236.28	2.40	Basic	46.33	3	1	1
Celecoxib	381.38	3.81	Acidic	77.98	4	1	2
Ceritinib	558.15	2.60	Ampholyte	105.24	8	3	9
Cinnarizine	368.53	4.08	Basic	6.48	2	0	5
Dasatinib	488.01	2.30	Basic	106.51	9	3	7
Deferasirox	373.37	1.16	Acidic	108.47	6	3	0
Dipyridamole	504.64	2.96	Basic	145.44	12	4	12
Enzalutamide	464.44	3.57	Neutral	76.44	6	1	4
Etoricoxib	358.85	3.35	Basic	59.92	4	0	1

Drug Compound	Molecular Weight [g/mol]	Calculated $logD_{6.5}$	Acidic/ Basic/ Neutral/ Ampholyte	Calculated PSA [$Å^2$]	HBA	HBD	RBC
Ezetimibe	409.44	4.18	Neutral	60.77	4	2	6
Fenofibrate	360.84	5.20	Neutral	52.60	4	0	5
Gemfibrozil	250.34	2.41	Acidic	46.53	3	1	6
Glibenclamide	494.01	3.84	Acidic	113.6	8	3	10
Griseofulvin	352.77	2.51	Neutral	71.06	6	0	3
Indomethacin	357.79	1.45	Acidic	68.53	4	1	3
Mefenamic acid	241.29	2.36	Acidic	49.33	3	2	2
Nilotinib	529.53	4.97	Basic	97.62	7	2	5
Nimesulide	308.31	2.45	Acidic	101.22	6	1	4
Olaparib	434.47	2.26	Neutral	86.37	6	1	5
Rivaroxaban	435.89	1.97	Neutral	88.18	8	1	5
Sertraline	306.24	2.56	Basic	12.03	1	1	2
Sorafenib	464.83	5.00	Basic	92.35	7	3	8
Tadalafil	389.41	1.60	Neutral	74.87	6	1	1
Thiabendazole	201.25	2.31	Basic	41.57	2	1	0

2.4.3 Preparation of COM, PM and milled drugs

COM and milled drugs were prepared using a vibrational ball mill (MM 200, Retsch, Haan, Germany). A drug to excipient ratio of 1:2 (w/w) was chosen for the preparation of COM. 250 mg (± 0.1 mg) of a model drug, 500 mg (± 0.2 mg) of PVP K25 and three 9 mm stainless steel balls were placed in a 25 mL stainless steel milling jar. The milling process took 15 min at a frequency of 15 Hz. To prepare the milled drug samples (i.e., milled drug without PVP K25 present), the same preparation process was carried out without the addition of an excipient.

PM of a model drug and PVP K25 in a ratio of 1:2 (w/w) were mixed in a 3D shaker mixer (Turbula type T2F, WAB AG, Switzerland). A 250 mL glass container was filled with 250 mg (± 0.1 mg) of model drug and 500 mg (± 0.2 mg) of PVP K25. The mixing conditions were set to 10 min and 50 rpm.

2.4.4 Dissolution medium preparation

Fasted State Simulated Intestinal Fluid (FaSSIF) has been produced in accordance with the standard operating procedures provided by biorelevant.com Ltd. The pH was adjusted to 6.50 (± 0.05) and the medium was used within 24 h.

2.4.5 Dissolution tests and apparent solubility measurements

Dissolution was tested in a USP2 vessel with a stirring speed of 50 rpm in 250 mL FaSSIF at 37°C. Using fibre-optic UV probes connected to the Rainbow Dynamic Dissolution Monitor Instrument (Pion Inc., Billerica, MA, USA), the duration of the dissolution experiments were 80 min. Standard curves were established using the second derivative of the UV absorbance. The highest wavelength and a range of 10 nm were chosen to generate seven-point calibration curves with an R^2 of > 0.99 for each compound. Depending on the UV absorbance of the drug, a UV probe with a path length of 2, 5 or 10 mm was used. The freshly prepared samples (120 ± 30 min after preparation) were added to the medium in triplicate.

The dose added to dissolution tests corresponded to three times the apparent solubility after 24 h of dissolution which was measured in the same instrument at a stirring speed of 100 rpm in 250 mL FaSSIF V1, 37°C (n = 3) with the pure drug. An excess amount of the drug compound was added to the medium and the average concentration after 24 h calculated to obtain the apparent solubility.

2.4.6 Particle size distribution

The particle size distribution was measured for 29 poorly water-soluble drugs by laser diffraction analysis (Mastersizer 2000 with Hydro 2000S, Malvern Instruments Co. Ltd., Solihull, UK). Drug powders (200 mg) were added to 50 mL of water and 0.05 mL of Tween 80. To prepare a dispersion, the samples were stirred and mixed for 10 min (± 30 s) and then immediately placed in the Hydro S instrument until a stable obscuration between 10 and 20 % was achieved. The refractive index for the dispersion medium water was set to 1.33 and for the particles the values were selected according to refractive indices of the respective compounds from published data. The stirring speed was set to 2100 rpm and the measurement took 30 seconds. All measurements were carried out in triplicate and average values calculated. Since the highest measured apparent FaSSIF solubility of the drugs in the study was 667 µg/mL (supplementary material, Table S1) and the prepared dispersions contained a concentration of 4000 µg/mL in water, it can be assumed that highly saturated dispersions were prepared.

2.4.7 X-Ray powder diffraction (XRPD)

X-ray powder diffraction was analysed to evaluate changes in the solid state after milling of powders and mixtures. Powder X-ray diffractograms were collected using a Bruker-AXS D8 Advance powder diffractometer (Karlsruhe, Germany). Measurements were conducted in reflection geometry using a flat sample holder. A CuKα radiation (λ = 1.5418 Å) was operated at 40 kV, 40 mA and ambient temperature. The theta-theta geometry ranges from 2 to 40º with

a scan rate of 0.02º/s. The generated diffractograms were treated with standard background subtraction and smoothing procedures and the crystallinity of PM and COM was determined by automatized refinement procedures. XRPD patterns were aligned with published data of the investigated compounds to confirm their identity.

2.4.8 Calculation of Co-Milling Dissolution Ratios

The measured released drug concentration [µg/mL] after timepoint $\mathrm{n}\ [\mathrm{min}]$ of dissolution of COM $(\mathrm{c}(\mathrm{drug}_{\mathrm{n\ min,COM}}))$ and PM $(\mathrm{c}(\mathrm{drug}_{\mathrm{n\ min,PM}}))$ were used to calculate the Co-Milling Dissolution ratio (COMDR) for 29 drugs at different timepoints via equation 2-1:

$$\mathrm{Co-Milling\ Dissolution\ Ratio}\ (\mathrm{COMDR}_{15\ \mathrm{min}}) = \frac{\bar{\mathrm{x}}\ \mathrm{COM}_{\mathrm{n\ min}}}{\bar{\mathrm{x}}\ \mathrm{PM}_{\mathrm{n\ min}}} \qquad (2-1)$$

Where $\bar{\mathrm{x}}\ \mathrm{COM}_{\mathrm{n\ min}}$ and $\bar{\mathrm{x}}\ \mathrm{PM}_{\mathrm{n\ min}}$ describe the mean concentration of released drug after n min dissolution of a COM and of a PM.

The standard error of COMDR was calculated from equation 2-2 (Fagerberg et al., 2012):

$$SE_{COMDR} = COMDR * \sqrt{\frac{SE_{\bar{x}COM}{}^2}{\bar{x}COM^2} + \frac{SE_{\bar{x}PM}{}^2}{\bar{x}PM^2}} \qquad (2-2)$$

$\mathrm{SE}_{\bar{\mathbf{x}}\mathrm{COM}}$ and $\mathrm{SE}_{\bar{\mathbf{x}}\mathrm{PM}}$ are the standard errors of the mean concentration of released drug in the respective mixtures.

2.4.9 Statistics and model development

To investigate the influence of molecular, physicochemical and measured drug properties on the improvement of dissolution after co-milling with PVP K25, multivariate data analysis was performed using Simca (Version 15.0, Sartorius, Germany). ADMET Predictor software (Version 9.5, Simulation Plus, USA) was used to generate molecular descriptors. SMILES

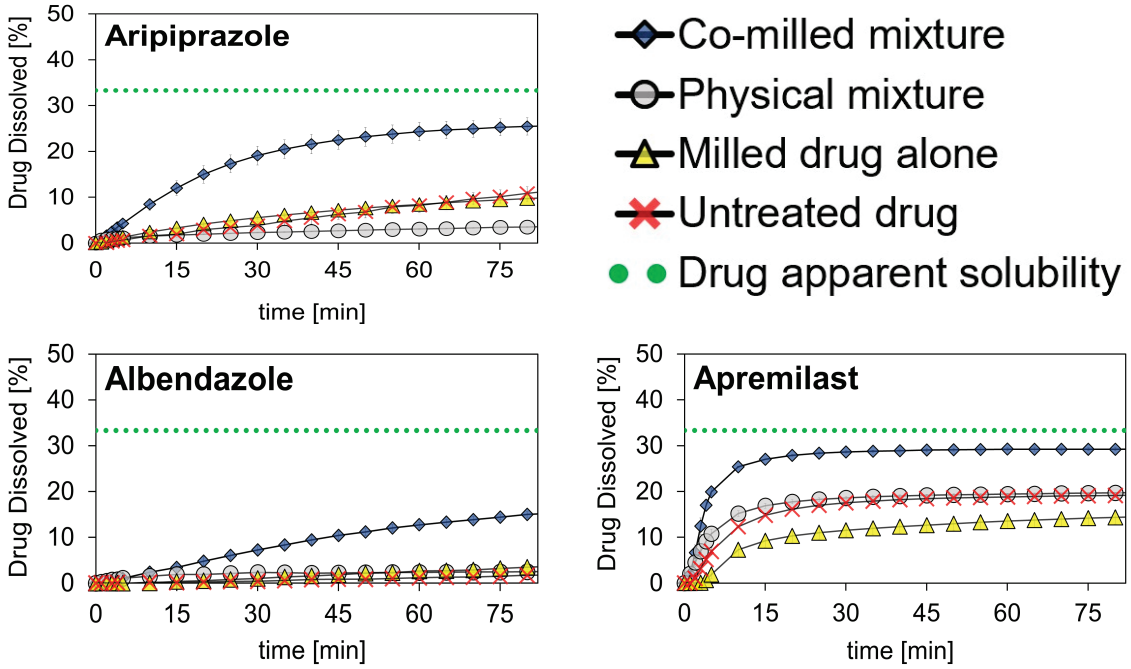
strings of all model drugs were obtained from PubChem as inputs for the ADMET Predictor and compounds were randomly assigned to training and test sets. A principal component analysis (PCA) and a Hotelling T2 ellipse (95% confidence interval) of all descriptors were performed to identify potential outliers that would have been assigned to the test set to avoid such compounds affecting the training set. Partial least squares projection to latent structures (PLS) models were developed to identify important variables and for quantitative predictions. Descriptors from ADMET Predictor, results of particle size distribution measurements (D50) and the measured apparent solubility in FaSSIF after 24 h dissolution values were added to the dataset and used as inputs for PLS modelling. The logarithm of the COMDR after 15 and 60 min of dissolution were used as response. In a first step, the descriptors were de-identified and standardised by mean centring and scaled to unit variance. Descriptors with the same value for all model drugs were removed. Subsequently, 244 standardised descriptors were submitted for variable selection. Based on the variable importance in projection (VIP) diagram, all variables except the 100 most important for the response were excluded. In a next step, variables whose exclusion resulted in an increase or no change in R^2 and Q^2 were permanently removed from the model. Q^2 was validated using 7 leave-one-out cross-validation groups. To ensure accuracy, PLS regressions were validated using root mean square error of cross validation ($RMSE_{CV}$) and permutation tests (100 iterations). Final models were validated with the test sets. A limit of four variables resulting in a maximum Q^2 value were selected to avoid overfitting.

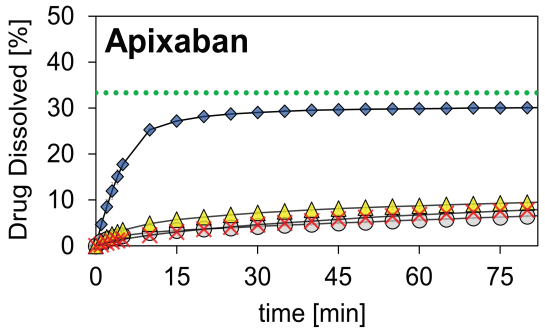
Multiple linear regression (MLR) equations to quantitatively predict Co-Milling Dissolution Ratios were generated using SPSS Statistics (Version 26, IBM Corporation, US). MLR equations were established based on selected variables from PLS models. The combination of three of the four variables selected in PLS models that yielded the highest R^2 values was used to generate MLR equations, considering multicollinearity. The same training and test sets were employed as for the PLS models.

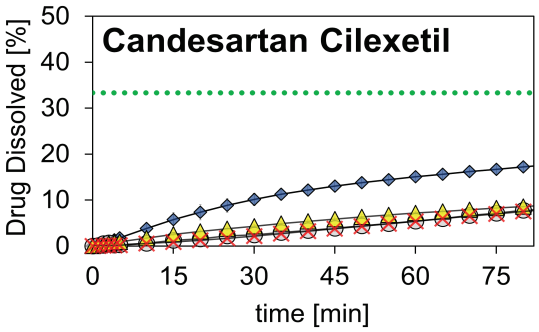
2.5 Results and discussion

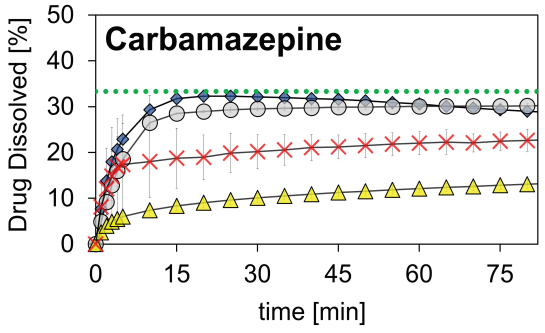
2.5.1 Dissolution profiles

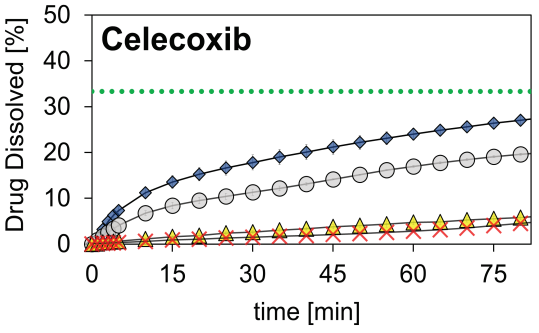
Figure 2-1 illustrates the dissolution profiles of 29 structurally diverse drug substances under different processing conditions, i.e. as unmilled powder, milled powder, PM and COM. For the evaluation of dissolution profiles, one timepoint in the early phase (15 min) of the dissolution process and one timepoint in a later stage (60 min) of COM and PM were selected. The 15 minute and 60 min dissolution timepoints are of industrial relevance to achieve specifications in bioequivalence studies to prove similarity of dissolution profiles and biowaiver approvals of immediate release formulations (Ono et al., 2023).

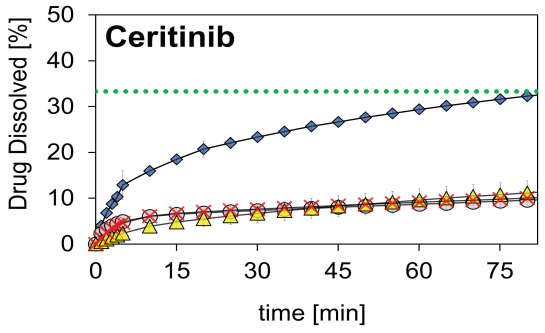


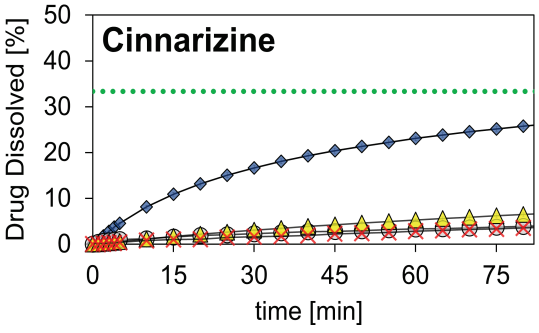

Apixaban
Drug Dissolved [%]
time [min]

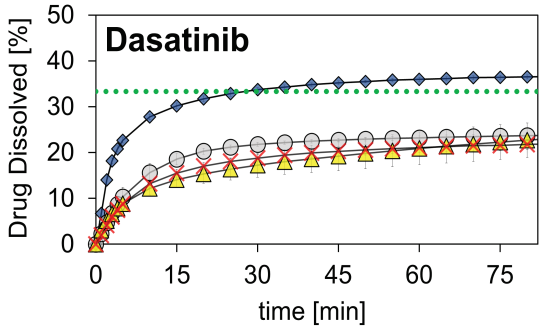

Candesartan Cilexetil
Drug Dissolved [%]
time [min]

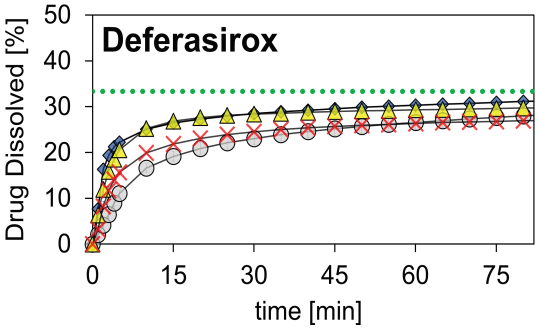

Carbamazepine
Drug Dissolved [%]
time [min]

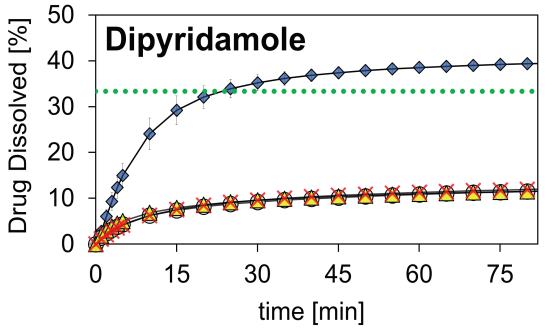

Celecoxib
Drug Dissolved [%]
time [min]

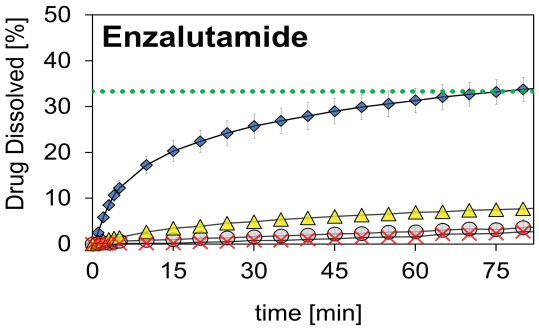

Ceritinib
Drug Dissolved [%]
time [min]

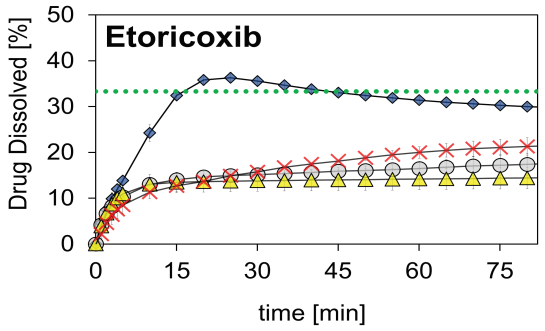

Cinnarizine
Drug Dissolved [%]
time [min]

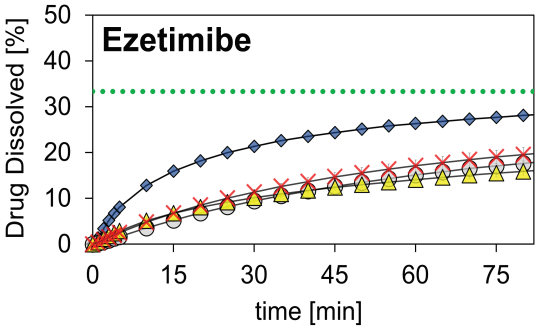

Dasatinib
Drug Dissolved [%]
time [min]

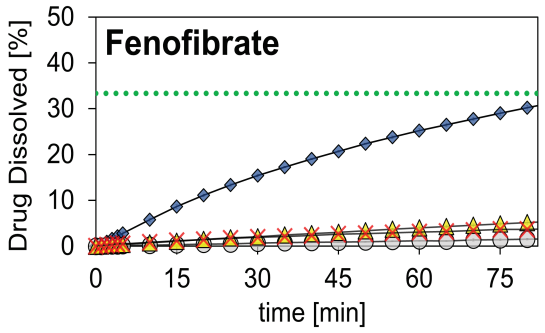

Deferasirox
Drug Dissolved [%]
time [min]

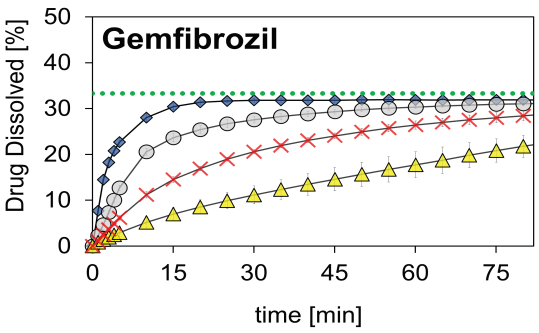

Dipyridamole
Drug Dissolved [%]
time [min]

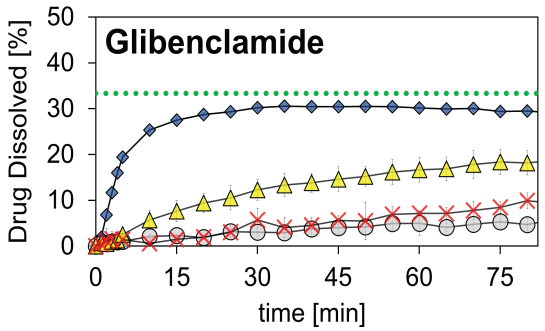

Enzalutamide
Drug Dissolved [%]
time [min]

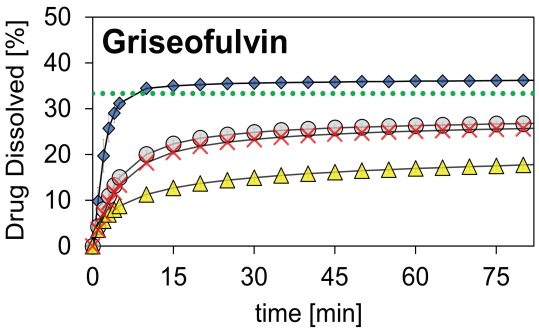

Etoricoxib
Drug Dissolved [%]
time [min]

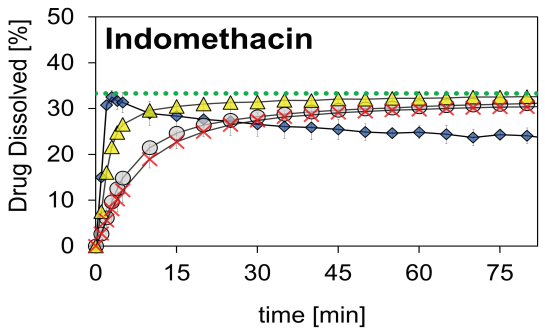

Ezetimibe
Drug Dissolved [%]
time [min]

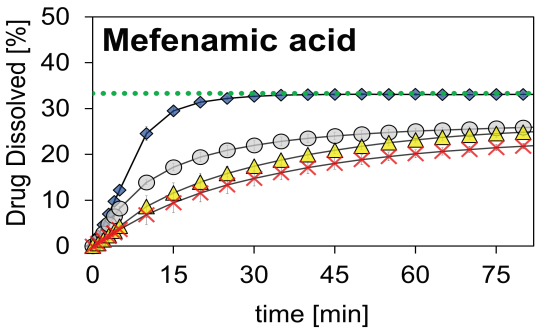

Fenofibrate
Drug Dissolved [%]
time [min]

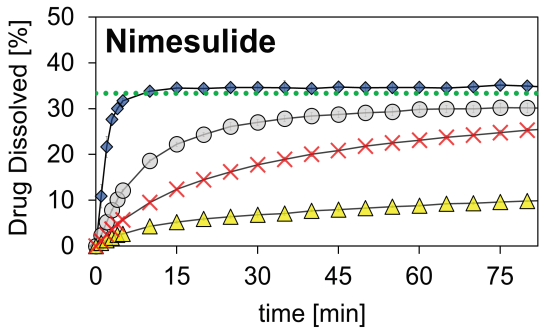

Gemfibrozil
Drug Dissolved [%]
time [min]

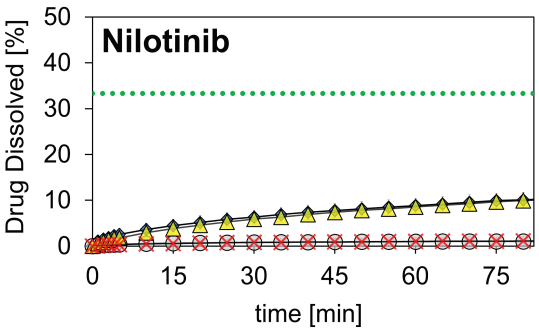

Glibenclamide
Drug Dissolved [%]
time [min]


Griseofulvin
Drug Dissolved [%]
time [min]


Indomethacin
Drug Dissolved [%]
time [min]


Mefenamic acid
Drug Dissolved [%]
time [min]


Nimesulide
Drug Dissolved [%]
time [min]


Nilotinib
Drug Dissolved [%]
time [min]

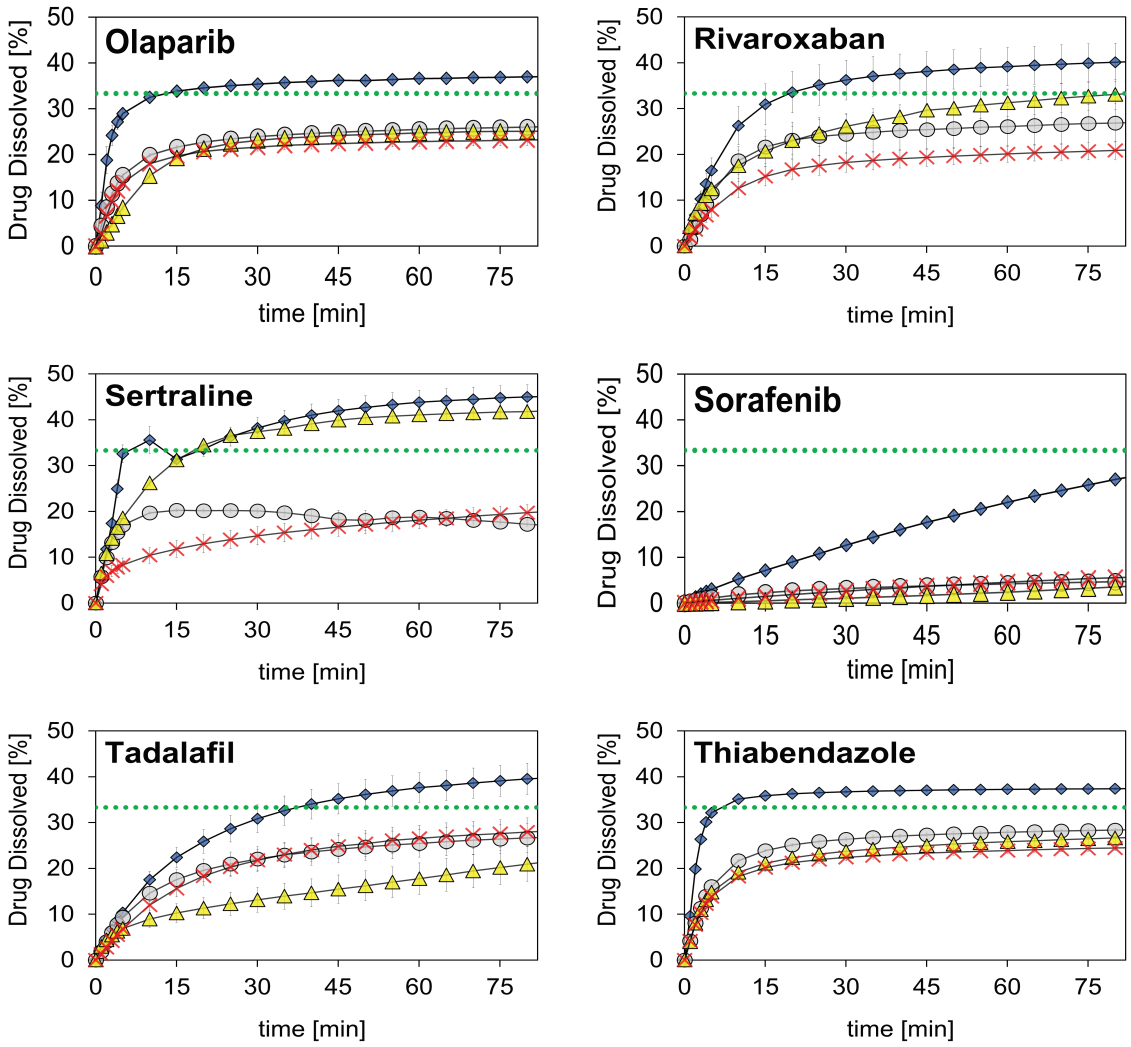


Figure 2-1: Dissolution profiles of drug powders, milled drug powders, binary physical and co-milled mixtures with PVP K25 as carrier for 29 compounds are shown (n = 3). Depicted as blue squares are measurement points of co-milled mixtures, those of physical mixtures are grey filled circles, the initial drug powders are shown as red crosses and the dissolution profiles of milled drug powders are labelled as yellow triangles. The apparent solubility after 24 h dissolution of each drug is plotted as a green dotted line. An excess of three times the apparent solubility of each drug was added to the dissolution experiments. Some error bars are small and only barely visible.

Considering the 15 minutes timepoint, the $COMDR_{15\ min}$ ranges from 1.11 (carbamazepine) to 26.48 (fenofibrate) (Figure 2-2 and supplementary materials, Table S3). In 26 of 29 cases, a two-sided t-test showed a significantly higher dissolved drug concentration from COM compared to PM (*$p < 0.05$). Non-significant differences were observed for tadalafil ($p = 0.055$), rivaroxaban ($p = 0.051$) and indomethacin ($p = 0.064$). These compounds have in common

that the measured pre-milled median drug particle sizes were among the smallest in the data set (tadalafil = 15.89 ± 3.89 µm; rivaroxaban = 9.5 ± 1.54 µm; carbamazepine = 15.87 ± 2.74 µm). Further, the calculated $logD_{6.5}$-values of these compounds were low which suggests that these compounds are among the least lipophilic within the data set (tadalafil 1.60; rivaroxaban 1.97; carbamazepine 2.40). It may reflect that these compounds benefit less from the potential wetting enhancement and subsequent dissolution enhancement through their embedding in the polymer matrix than more lipophilic compounds.

After 60 min of dissolution, fenofibrate was the drug substance with the highest COMDR with a value of 21.48 and indomethacin the lowest with 0.82 (Figure 2-2 and supplementary materials, Table S4). Fenofibrate has the largest particle size (255.3 ± 3.4 µm) and the calculated lipophilicity, expressed by clogD6.5 (5.2), of the investigated drugs. In the entire screening, indomethacin is the only substance with a lower dissolved concentration in COM than in PM after 60 minutes (p = 0.005). No significant differences could be measured for carbamazepine (p = 0.46). Within the 27 remaining compounds, a higher concentration of the drug was released from COM than from PM after 60 minutes of dissolution (*p < 0.05).

The dissolution profiles of co-milled and milled drugs allow comparison of the influence of the addition of an excipient to the ball milling process. For 24 out of 29 compounds, the dissolved fraction of the drug was significantly higher from co-milled blends. Dissolution of milled and co-milled sertraline (p = 0.83), nilotinib (p = 0.47), indomethacin (p = 0.24) and deferasirox (p = 0.068) did not result in statistically significant differences after 15 min drug release. After 60 min, again sertraline (p = 0.19) and nilotinib (p = 0.77) did not dissolve to a significantly different degree as well as rivaroxaban (p = 0.057). Deferasirox and rivaroxaban revealed very small initial particle sizes (5.2 ± 0.2 and 9.5 ± 1.6 µm) and also low calculated logD6.5 values (deferasirox 1.16 and rivaroxaban 1.97) which may be reasons that the addition of the excipient in a co-milling process did not significantly influence the dissolution enhancement compared to milling the drug without excipient.

The shape of the dissolution profile of co-milled Indomethacin was atypical and did not match standard zero or first order release kinetics. A rapid initial increase in apparent drug

concentration was observed during the first two minutes of dissolution. After that initial “spring effect”, the measured apparent concentration of indomethacin in FaSSIF decreased slowly, potentially due to partial precipitation in the metastable zone of a dissolution profile with “spring and parachute” characteristics. The spring effect may have been caused by structural disorder and amorphization on drug particle surfaces created during the co-milling process. Recent studies presented the tendency of Indomethacin to transit into the amorphous state by milling with excipients (Iemtsev et al., 2022; Lim et al., 2016).

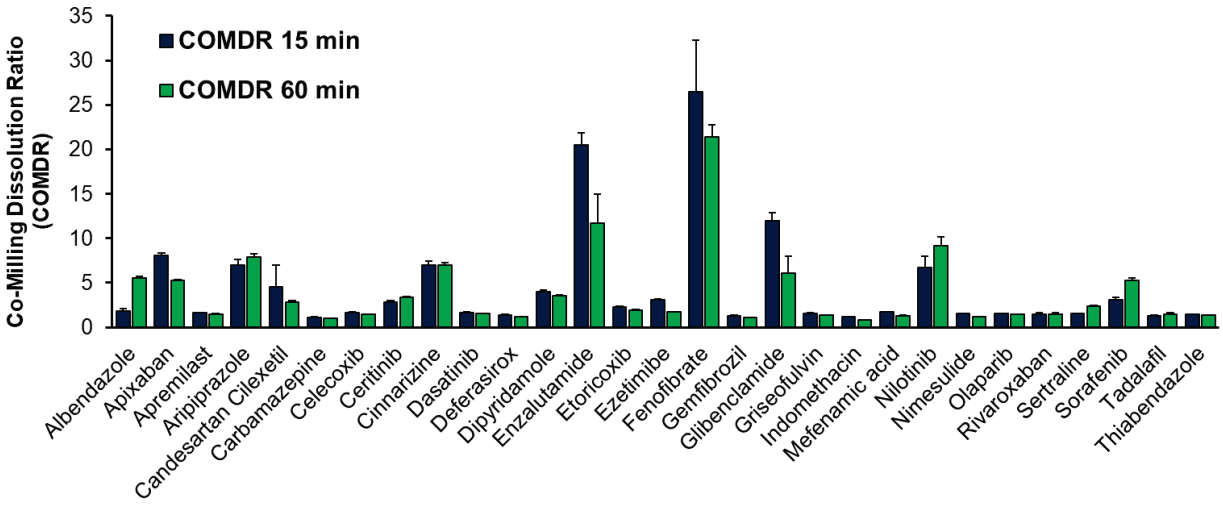


Figure 2-2: Co-Milling Dissolution Ratios (COMDR) of all 29 drugs used in the study with standard errors after 15 minutes (green) and 60 minutes (blue) of dissolution (n = 3). The COMDR is the ratio of mean released drug concentration in co-milled and physical mixtures with PVP K25 in a drug to excipient ratio of 1 to 2 (w/w) at above mentioned timepoints.

2.5.2 Influence of co-milling on solid state properties of drug substances

XRPD measurements were used to investigate whether the milling processes caused polymorphic changes in investigated drugs and to evaluate the loss in crystallinity during co-milling. XRPD patterns are presented in the supplementary material, Figures S1 – S58. Sharp Bragg peaks in the diffractograms of all model drugs confirmed a high initial degree of crystallinity before milling. In addition, sharp peaks were still visible in all diffractograms of

COM after 15 minutes of drug ball milling with PVP. In 21 of 29 diffractograms of COM, peak intensity was reduced compared to PM, indicating a partial loss of crystallinity due to milling-induced disorder of the solid drug substance particles.

All polymorphs of investigated compounds are listed in supplementary materials, table S6. The diffractograms of binary mixtures did not result in changes of the basic patterns which suggests that no major polymorphic changes were produced during co-milling of binary mixtures. An exception is an initial polymorphic transformation of ceritinib (polymorphic form 2b) that can be assumed since new peaks are visible in the X-Ray diffractogram of the co-milled mixture. Interestingly, milling of drugs without the addition of the excipient resulted in a polymorphic change of enzalutamide from form R1 to R2. A beginning polymorphic transition of tadalafil was observed which was originally in form a.

2.5.3 Prediction of Co-Milling Dissolution Ratios

A PCA based on molecular properties was conducted to initially explore the structural diversity of the screened model drugs. The plot confirmed that investigated compounds are covering a wide chemical space as drug substances are well distributed on the PCA-X graph (Figure 2-3). Drugs from the training and test set are also widely distributed over the chemical space. Subsequently, PLS models were developed to explore the feasibility of predicting the $COMDR_{15\ min}$ and $COMDR_{60\ min}$. In the framework of PLS modelling, it was examined which properties of drug substances have an influence on the rate of dissolution after applying the co-milling technique with PVP K25. The variable importance in projection plots of $COMDR_{15\ min}$ and $COMDR_{60\ min}$ are added to the supplementary material, Figure S59 and S60. The logarithm of COMDR at the respective time points were used to build linear models. In addition to the calculated molecular properties, measured median particle sizes of drug powders with a broad span of 3.6 µm to 255 µm and apparent solubilities of pure drug substances after 24 h of dissolution were included as variables in the PLS models (Supplementary material, Tables S1 and S2).

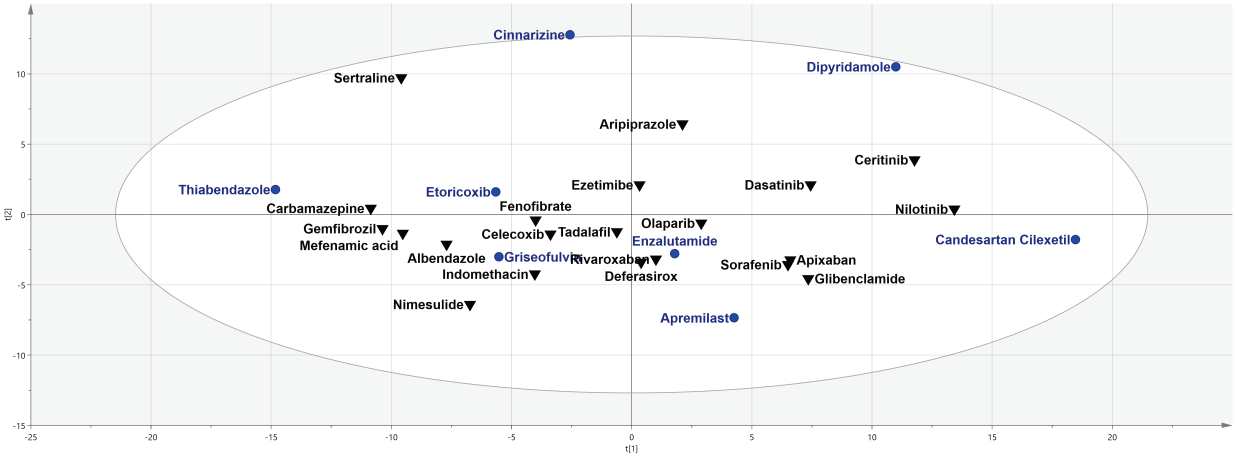


Figure 2-3: Principal component analysis of the chemical space based on the calculated molecular properties of investigated compounds. For the development of predictive models, the compounds were randomly assigned to a training set (black) and a test set (blue). Drugs of training and test are well distributed over the chemical space.

The highest Q^2 value of the training set with $COMDR_{15\ min}$ was obtained with the inclusion of the median particle size (D50) of initial pre-milled drug particle size, the measured apparent solubility of the drug and the calculated molecular descriptors $clogD_{6.5}$ and Kappa 3 (Table 2-2). An R^2 value of 0.82 and a Q^2 value of 0.77 and only small differences in root mean square error ($RMSE_{Tr}$ = 0.12, $RMSE_{Te}$ 0.17) and root mean square error of cross validations ($RMSE_{CV, Tr}$ = 0.15, $RMSE_{CV, Te}$ = 0.18) of training and test set allows the prediction to be considered as valid. As illustrated in Figure 2-4, each value of the test is within the prediction interval of the training set. There is one outlier in the training set (glibenclamide), all other drugs are within the prediction interval of the trained model. The observed $logCOMDR_{15min}$ (1.08) is considerably higher than the predicted $logCOMDR_{15min}$ (0.76). This under-prediction could be a result of the low apparent solubility value of glibenclamide (4.0 ± 0.5 µg/mL), which may not be captured by this model. Since the validation with the test set showed that all substances

are in the prediction interval and therefore the outlier appears to not strongly influence the predictive accuracy of the model, the outlier remained in the model.

Table 2-2: Results from PLS model development for the logarithm of the ratio of released drug in co-milled and physical mixtures (LogCOMDR) after 15 and 60 min of dissolution, The following abbreviations are used: Root mean square error (RMSE), Training set (Tr), Test set (Te), Cross Validation (CV), measured median drug particle size (D50), calculated decadic logarithm of the distribution coefficient (Octanol/water) at pH 6.5 ($clogD_{6.5}$), degree of branching at the center of a molecule (Kappa 3), Relative topological diameter of the hydrogen-suppressed molecular graph (T_RDmtr)

	R^2	Q^2	$RMSE_{Tr}$	$RMSE_{Te}$	$RMSE_{CV, Tr}$	$RMSE_{CV,Te}$	Selected variables
$LogCOMDR_{15\ min}$	0.82	0.77	0.12 (n = 21)	0.17 (n = 8)	0.15 (n = 21)	0.18 (n = 8)	D50, $clogD_{6.5}$, Kappa 3, apparent solubility,
$LogCOMDR_{60\ min}$	0.87	0.84	0.13 (n = 21)	0.11 (n = 8)	0.13 (n = 21)	0.12 (n = 8)	D50, $clogD_{6.5}$, T_RDmtr, apparent solubility

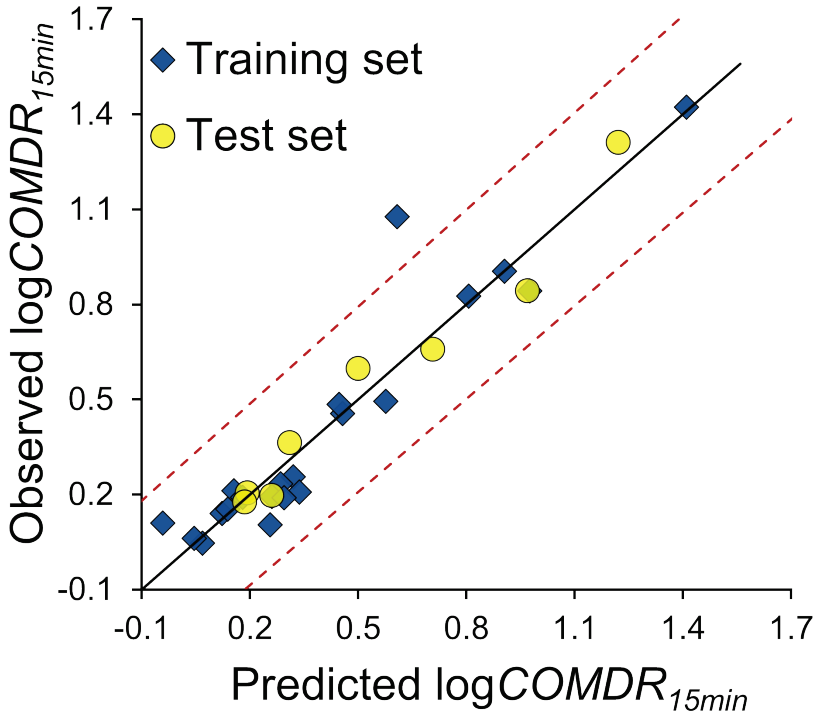


Figure 2-4: PLS model results of the logarithm of Co-milling Dissolution Ratios after 15 min of dissolution (logCOMDR$_{15min}$). Drugs in the training set are depicted as blue squares and candidates of the test set as yellow circles.

Another PLS model was developed for the ratio of the 60 min time points to detect possible effects and influences of variables on the further progression of the dissolution process. The variable selection considered again the median particle size D50, the apparent solubility of the pure drug and the calculated descriptor clogD$_{6.5}$. This time, the molecular descriptor T_RDmtr ended up in the model instead of Kappa 3 (Table 2-2). The model achieved a high predictivity (R^2 = 0.87, Q^2 = 0.84). The root mean square error ($RMSE_{Tr}$ = 0.13, $RMSE_{Te}$ = 0.11) and the root mean square error of cross validation ($RMSE_{CV, Tr}$ = 0.13, $RMSE_{CV, Te}$ = 0.12) of training and test set differ only slightly, confirming a good prediction. All timepoints are in the prediction interval, which is shown graphically in Figure 2-5.

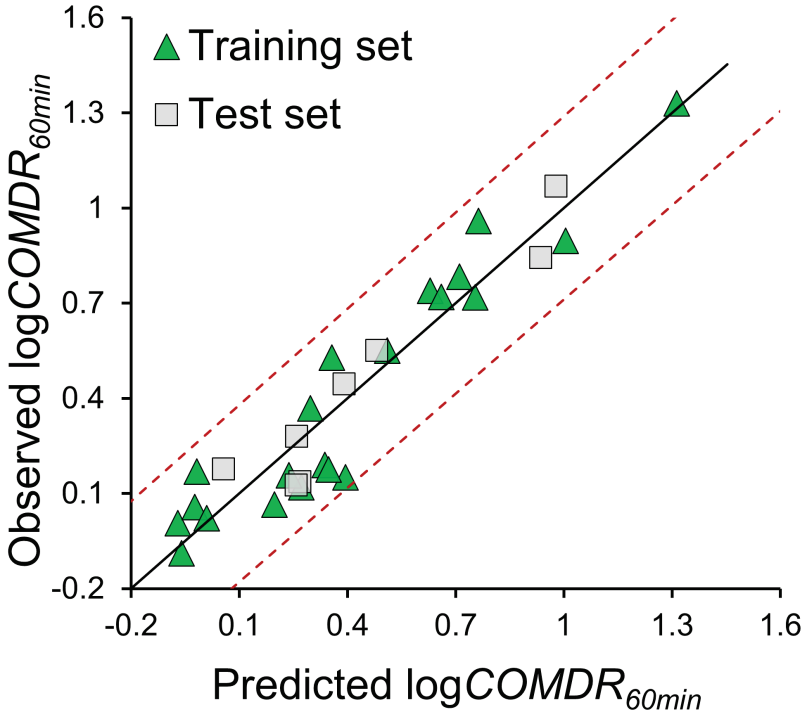


Figure 2-5: PLS model results of the logarithm of Co-Milling Dissolution Ratios after 60 min of dissolution (log$COMDR_{60min}$). Drugs from the training set are shown as green triangles and candidates from the test set are shown as grey squares.

The inclusion of a particle size parameter in the models is explainable as reducing the particle size leads to an increase in the particle surface area, which according to the Nernst-Brunner equation results in an improvement of dissolution rate (Brunner, 1904; Nernst, 1904). Co-milling is designed to reduce particle size, and the positive correlation between initial drug particle size and the enhancement of dissolution rate through co-milling suggests that larger drug particles before co-milling may have a higher potential for size reduction, leading to an increased dissolution rate. However, very small drug particles may have the tendency to aggregate during the milling process.

In contrast to molecular descriptors and substance specific properties, particle sizes vary from batch to batch. Milling of drugs commonly leads to a particle size reduction up to a grinding limit where particle agglomeration and particle size breakage are in equilibrium (Knieke et al., 2009). The grinding limit is the result of a balance between material properties and the energy

applied to the drug particles during the milling process (Luciani, 2018). Other batches with different particle sizes would also lead to a reduction in particle size near to the grinding limit and therefore also to a dissolution enhancement which appears to also depend on the initial particle size of the drug batch. The present model was trained for particle sizes from 3.62 ± 0.03 µm to 255.26 ± 3.35 µm, which is the range for which the model is applicable.

The second parameter present in each model is the lipophilicity/distribution coefficient $clogD_{6.5}$ as calculated by the ADMET predictor, which is a parameter for the lipophilicity of a molecule (Kah and Brown, 2008). The higher the $clogD_{6.5}$ of a molecule, and thus its lipophilicity, the lower may be the wettability of particle surfaces. A poor wettability may result in decreased dissolution rates and several studies confirmed that drug powders embedded in a polymer matrix of a co-milled mixture exhibit increased wettability (Gu et al., 2012; Maggi et al., 2013b; Varghese and Ghoroi, 2017). Drugs with more lipophilic surfaces may benefit more from the embedding in polymer matrices by co-milling in terms of wettability, and therefore the dissolution rate can also be improved to a higher degree.

The 15 min model includes the calculated molecular descriptor Kappa 3 which indicates the shape of organic molecules neglecting hydrogen by describing atomic radii and the number of topological paths (Kier, 1985). Bigger and more complex molecules tend to have less rigid structures, which facilitates the formation and persistence of amorphous fractions in molecules (Alhalaweh et al., 2014; Baird et al., 2010; Mahlin and Bergström, 2013). In line with this, higher Kappa 3 values may indicate an increased tendency to induce mechanically surface disorder and partial amorphization during co-milling. Derived by automated refinement procedures of X-Ray diffractograms, Figure 2-6 confirms a correlation of computed Kappa 3 values and the residual drug crystallinity in co-milled formulations. Drug compounds with median particle sizes above 100 µm (apixaban, aripiprazole, enzalutamide and fenofibrate) were excluded since the particle size may influence the reliability of the assessment. The relationship (R^2 = 0.61) between the residual crystallinity of drugs in co-milled formulations and the Kappa 3 value of

drug substances indicates that with increasing complexity of the molecules, the loss of crystallinity due to co-milling increases and consequently the dissolution as extracted from the modelling procedure (equation 2-3).

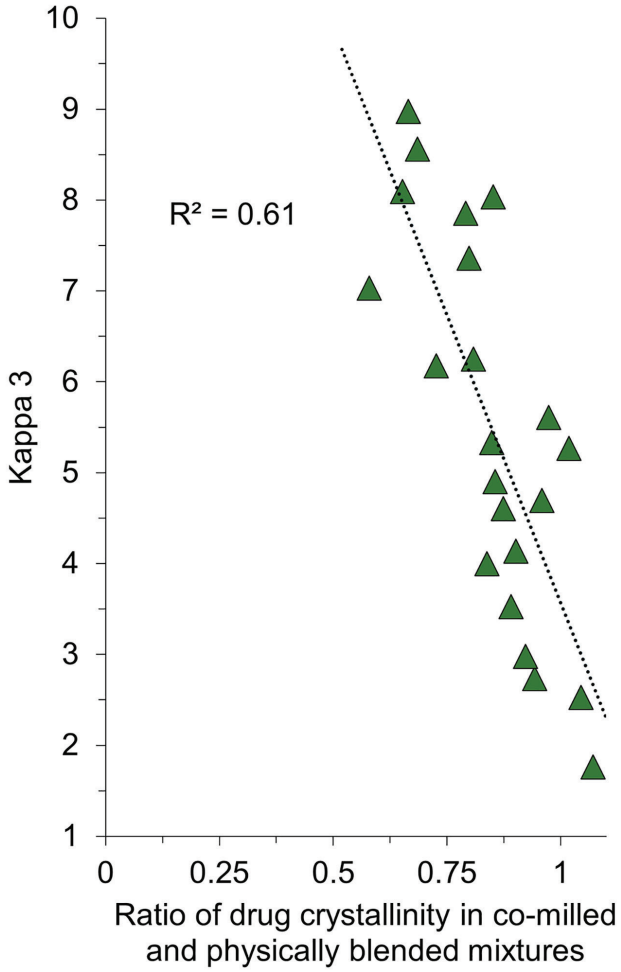


Figure 2-6: Correlation between the calculated molecular descriptor Kappa 3 and the residual crystallinity of the drug in co-milled formulations. Kappa 3 was extracted by variable selection as part of partial least squares regression modelling. The residual crystallinity of the drug in the co-milled formulations was derived from the ratio of the calculated crystallinity of physical mixtures and co-milled formulations in an automated refinement procedure of the X-ray diffractograms.

Another selected molecular descriptor refers to the topology (T_RDmtr, 60 min COMDR) of the molecule (Bloomingdale and Mager, 2019). The calculated molecular descriptors T_RDmtr and $logD_{6.5}$ provide first indications which properties of a molecule could be associated with a successful dissolution rate enhancement by co-milling.

The results of PLS models were used to generate applicable MLR equations that predict the Co-Milling Dissolution Ratios after 15 and 60 min of dissolution by applying co-milling with PVP K25 under the experimental conditions based on only three of the selected variables that yielded in the highest R^2 value (equation 2-3 and 2-4). Results of MLR equations are summarized in Table 2-3. A test of multicollinearity is a requirement for the validity of MLR equations. Multicollinearity exists if the variable inflation factor is greater than 5 or less than 0.2. Furthermore, a conditions index of 10-30 indicates multicollinearity, above 30 a strong multicollinearity (Kim, 2019). The variable inflation factors are 1.1 and 1.6, and the condition indices 7.8 and 8.1, indicating that there is no considerable multicollinearity in the generated MLR equations (Supplementary material, Table S5). These identified equations would be readily applied in early-stage drug development to guide formulators on the potential improvements in dissolution via co-milling.

$$logCOMDR_{15\ min} = -0.319 + 0.00377 * D50 + 0.098 * clogD_{6.5} + 0.05 * Kappa\ 3 \quad (2\text{-}1)$$

$$logCOMDR_{60\ min} = -0.141 + 0.00325 * D50 + 0.142 * clogD_{6.5} - 0.00051 * c_s \quad (2\text{-}2)$$

Table 2-3: Summarized results of multiple linear regression equations. The following abbreviations are used: Root mean square error (RMSE); Training set (Tr); Te = Test set, measured median drug particle size (D50), calculated decadic logarithm of the distribution coefficient (Octanol/water) at pH 6.5 ($clogD_{6.5}$), degree of branching at the center of a molecule (Kappa 3), c_s = Measured apparent solubility of drug in FaSSIF at 37°C after 24 h dissolution of pure drug substance.

	R^2	$RMSE_{Tr}$	$RMSE_{Te}$	F-value	p-value	Variables
$logCOMDR_{15\ min}$	0.83	0.128 (n = 21)	0.190 (n = 8)	46.52	$2.2 * 10^{-10}$	D50, $clogD_{6.5}$, Kappa3
$logCOMDR_{60\ min}$	0.84	0.117 (n = 21)	0.144 (n = 8)	51.65	$7.4 * 10^{-11}$	D50, $clogD_{6.5}$, c_s

The generated MLR equations have R^2 values of 0.83 and 0.84, indicating a high predictivity (Table 2-3). Importantly, the difference between RMSE values were small which suggests that valid prediction models were given in line with the obtained *p*-values. In both formulas, the median particle size of the original drug powder and the $clogD_{6.5}$ values were included in the equations. For the 15 min timepoint, the calculated molecule descriptor Kappa 3 was included as a third descriptor, whereas at the 60 min timepoint, the measured apparent solubility was included. The different equations for early and later-stage time points were data-driven findings, but it can be also justified from a mechanistic viewpoint. The presence of Kappa 3 in the dissolution formula at 15 minutes, and its absence at 60 minutes, may refer to produced high-energy sites on the surface of drug particles. Such high energy sites would be expected as surface-induced disorder that can progress from the surface to a more pronounced partial amorphization (Niederquell and Kuentz, 2014). Nevertheless, these effects are anticipated to be less significant in the later stages of dissolution. Therefore, it makes sense to employ separate models for the early and later stages.

To estimate the influence of every variable on the Co-Milling Dissolution Ratios, beta standardized coefficients of MLR equations were calculated. At the time of 15 min, all variables contributed positively to the increase in the amount released in co-milled materials, i.e., the higher the median particle size D50, $clogD_{6.5}$, and Kappa 3 values of the drug substance the greater the expected increase in the proportion of dissolved drug after co-milling (Table 2-4). The size of the median particle had the biggest influence on the $COMDR_{15\ min}$ (0.284), followed by $clogD_{6.5}$ (0.105) and Kappa 3 (0.095). After 60 min of dissolution the median particle size had again the highest influence on the COMDR (0.214) followed again by $clogD_{6.5}$ (0.154). The apparent solubility contributed with -0.077 negatively to the $COMDR_{60\ min}$ which means that the higher the apparent solubility was, the lower tends to be the expected $COMDR_{60\ min}$.

Table 2-4: Beta Standardized coefficients of variables selected for multiple linear regression equations. The following abbreviations are used: Median drug particle size (D50), calculated decadic logarithm of the distribution coefficient (Octanol/water) at pH 6.5 ($clogD_{6.5}$), degree of branching at the center of a molecule (Kappa 3), c_s = measured apparent solubility of drug in FaSSIF at 37°C after 24 h dissolution of pure drug substance.

	D50	$clogD_{6.5}$	Kappa 3	c_s
$logCOMDR_{15\ min}$	0.284	0.105	0.095	-
$logCOMDR_{60\ min}$	0.214	0.154	-	-0.077

The purpose of this study was to develop a co-milling model that is specifically designed for dissolution rate limitations in industry. Thus, a comparatively short milling time of 15 minutes was selected for this study. By applying longer co-milling times the production of structural disorder and amorphous regions is expected to increase which could be of interest to improve the solubility of the compounds (Asgreen et al., 2020). A limitation of this study is that the whole model was performed only with PVP. As a consequence, outcomes of the study may not be

generalisable to other excipients. In addition, within the pharmaceutical field the screening contains a comparatively large number of 29 drug compounds. However, it represents a small number for partial least squares regression modelling. An extended dataset would therefore be desirable to enable a broader applicability of co-milling in pharmaceutical drug development.

The use of an in-line UV probe enabled significantly faster data acquisition compared with conventional manual sampling at predefined time points followed by external concentration determination, for example using a traditional HPLC–UV system. Nevertheless, this approach constitutes an alternative method for the quantification of dissolved drug concentration; therefore, validation of the in-line UV probe measurements is essential. As a consequence, the in-line UV probe dissolution setup in this industry-standard laboratory is routinely validated against HPLC–UV measurements.

2.6 Conclusion

This study successfully predicted the impact of co-milling with PVP on the dissolution of drug compounds. The key factors were identified as the median particle size of drug powders, the calculated molecular descriptors $clogD_{6.5}$ and Kappa 3, and the apparent solubility of drugs. Multiple linear regression equations were derived based on computationally selected variables, making them suitable for industrial applications. Future studies could further validate established in silico predictions of this work to enable rational decision-making in the development of co-milled formulations.

Chapter 3: Co-milling of glass forming ability class III drugs: Comparing the impact of low and high glass transition temperatures

Author names and affiliations:

Nicolas Pätzmann[1,2], Josef Beránek[2], Brendan T. Griffin[1], Martin Kuentz[3], Patrick J. O'Dwyer[1]

[1] *School of Pharmacy, University College Cork, Cork, Ireland*

[2] *Department Preformulation and Biopharmacy, Zentiva, k.s., Prague, Czechia*

[3] *Institute of Pharma Technology, University of Applied Sciences and Arts Northwestern Switzerland, Muttenz, Switzerland*

Corresponding Author:

Patrick J. O'Dwyer

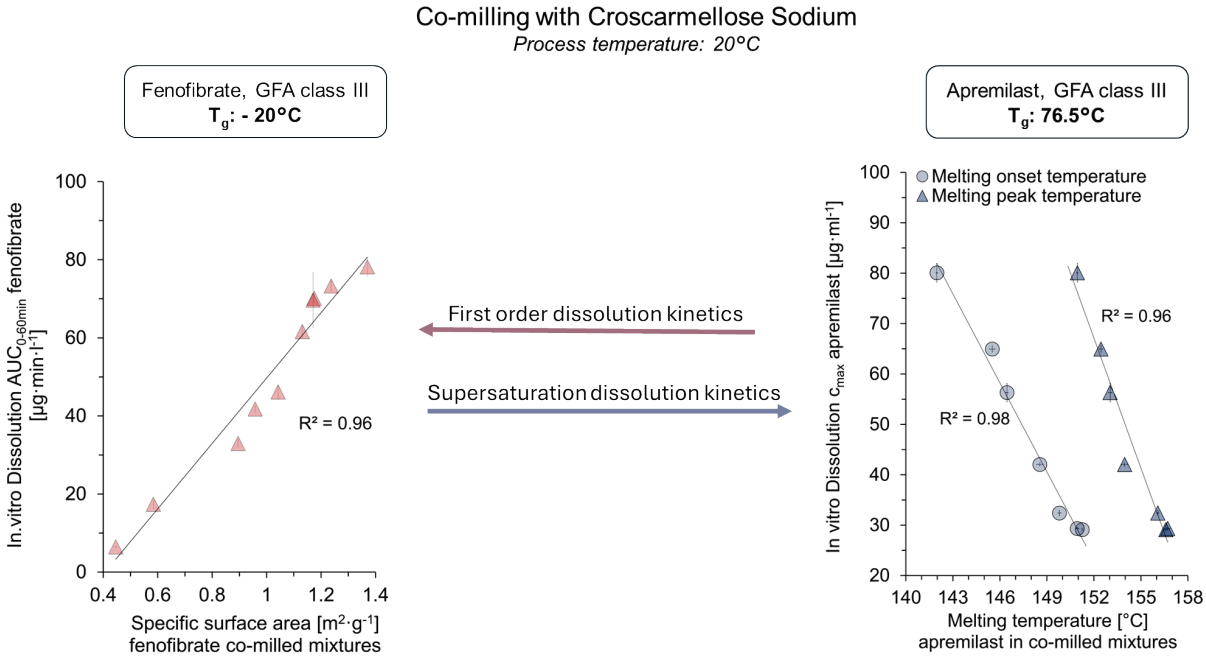
Keywords:

Co-milling, Ball milling, Glass transition temperature, Drug supersaturation, Melting point depression

Published in: European Journal of Pharmaceutical Sciences (2025), Volume 209

DOI: https://doi.org/10.1016/j.ejps.2025.107081

3.1 Graphical abstract



3.2 Abstract

With an increasing focus on sustainable technologies in the pharmaceutical industry, milling provides a solvent-free approach to improve drug dissolution. Milling of drugs with an excipient offers additional opportunities to achieve supersaturation kinetics. Therefore, this work aims to present insights of co-milling fenofibrate and apremilast, two good glass formers with low and high glass transition temperatures (T_gs) respectively. Drugs were co-milled with croscarmellose sodium for various process durations followed by thermal analysis, investigation of crystallinity, surface area and dissolution. The dissolution enhancement of the low-T_g glass former fenofibrate highly correlated with the process induced increase in surface area of co-milled systems (R^2 = 0.96). In contrast, the high-T_g glass former apremilast, lost its crystalline order gradually after ≥ 10 min of co-milling, and favourable supersaturation kinetics during biorelevant dissolution testing were observed. Interestingly, the melting point of co-milled apremilast decreased and linearly correlated with the highest measured drug concentration (c_{max}) during in vitro dissolution (onset temperature R^2 = 0.98; peak temperature R^2 = 0.96). The melting point depression remained stable after 90 days for apremilast, whereas fenofibrate co-milled for 20 minutes or more showed an increase in melting point upon storage. This study demonstrated that co-milling with croscarmellose sodium is ideally suited to good glass formers with a high T_g. The melting point depression is thereby proposed as an easily accessible critical quality attribute to estimate likely dissolution performance of drugs in dry co-milled formulations.

3.3 Introduction

Milling is a well-established particle size reduction technology for tackling dissolution rate-limited absorption (Brokešová et al., 2022). While milling reduces particle size to a certain extent, it can also induce disorder in the crystal lattices of processed substances (Oliveira et al., 2018; Zimper et al., 2010b). Highly disordered, amorphous drug material prepared by milling can be desirable, because it typically results in a higher apparent solubility compared to ordered crystalline forms (Descamps and Willart, 2016; Murdande et al., 2010; Štukelj et al., 2019). However, the high-energy state of the crystal lattice disorder and amorphous material can lead to stability issues (Priemel et al., 2016). Hence, stabilizing lattice disorder remains a key challenge for the pharmaceutical industry to fully exploit the potential biopharmaceutical benefits of milling (Slámová et al., 2021).

Co-milling with excipients has been demonstrated as an effective strategy to further enhance drug dissolution (Asgreen et al., 2020; Slámová et al., 2021; Vogt et al., 2008a). The mechanisms by which excipients contribute to the drug dissolution enhancement are diverse, including the inhibition of particle agglomeration, an increase in wettability, molecular interactions and the stabilization of such produced lattice disorder on drug particles due to the milling process (Balani et al., 2010; Chipakwe et al., 2020; Löbmann et al., 2013; Patterson et al., 2007). Several studies have shown a positive effect of co-milling on the oral bioavailability of poorly water-soluble drugs (Jagadish et al., 2010; Kasten et al., 2018; Vogt et al., 2008b). Despite those advances on a lab scale in pharmaceutical research, co-milling is not yet widely used for manufacturing enabling formulations due to the risk of residual drug crystallinity (Bhujbal et al., 2021).

Amorphous drug material can be obtained in different ways (Blaabjerg et al., 2017b). Milling can produce highly disordered amorphous material in the solid state by gradually disrupting the crystal lattice until a lack of long-range order is achieved, which is amorphisation on the “kinetic pathway”. However, an alternative strategy to obtain amorphous drug material is quench cooling a melt or by solvent evaporation via the “thermodynamic pathway”. Previous

studies investigated drugs for their ability to form a glass using the thermodynamic pathway by classifying them according to their ability to form and remain stable as an amorphous solid after quench cooling (Alhalaweh et al., 2014; Baird et al., 2010; Blaabjerg et al., 2016; Wyttenbach et al., 2016). A subsequent elaboration of both the thermodynamic and the kinetic pathway revealed a correlation between glass forming ability classes (thermodynamic pathway) of drugs and their ease to amorphise via milling (kinetic pathway) (Blaabjerg et al., 2017b). However, the addition of an excipient to a drug milling process may further impact the extent of produced crystal lattice disorder on the kinetic pathway. Therefore, studying the mechanisms of co-milling induced lattice disruption could deliver useful insights to support the design of stable co-milled formulations.

Fenofibrate, a poorly water-soluble drug, has been extensively studied using various formulation strategies to improve its oral bioavailability (Ejskjær et al., 2024; Griffin et al., 2014; Lentz et al., 2021; Suys et al., 2018). The glass transition temperature (T_g) of fenofibrate is around −20 °C, which is far below the temperature of a common milling process (Tipduangta et al., 2015). Previous research hypothesised that a drug T_g far below the process temperature negatively impacts the extent of milling-induced crystal lattice disorder (Descamps et al., 2007; Descamps and Willart, 2016). Another poorly water-soluble drug is apremilast, which has also been tested in various formulation approaches to improve its oral absorption (Abushal et al., 2022; Yang et al., 2021; Zhang et al., 2022). In contrast to fenofibrate, the T_g of apremilast is considerably higher than common milling temperatures (Tipduangta et al., 2015; Zhang et al., 2021). Co-milling these drugs with excipients may further influence the formation of crystal lattice disorder. The widely used tablet disintegrant croscarmellose sodium has also been shown to be effective as a co-milling co-former, making it a potentially attractive option for oral solid dosage forms (Kamil and Bayoumi, 2023).

Therefore, the objective of the current study was to explore the impact of co-milling on the crystal lattice disruption of two stable glass formers with T_gs located above and below the milling temperature. The influence of co-milling on the solid state and impact on *in vitro*

dissolution testing were investigated. Finally, an approach to evaluate the degree of drug crystal lattice disorder in co-milled formulations is presented.

3.4 Materials and Methods

3.4.1 Materials

Apremilast and croscarmellose sodium were kindly provided by the Zentiva Group k.s. (Prague, Czech Republic). Fenofibrate as well as dissolution medium reagents sodium chloride, sodium hydroxide and di-sodium hydrogen phosphate were purchased from Sigma-Aldrich (Prague, Czechia). The Simulated Intestinal Fluids powder to prepare the dissolution medium was sourced from Biorelevant.com Ltd. (London, United Kingdom).

3.4.2 Sample preparation by ball milling and blending

Ball milling was performed in a vibrational ball mill (MM 200, Haan, Retsch GmbH, Germany). To prepare co-milled mixtures, 250 mg (± 0.1 mg) of fenofibrate or apremilast and 500 mg (± 0.2 mg) croscarmellose sodium were placed in a 25 mL stainless steel milling jar with three stainless steel balls (9 mm diameter). The co-milling times were 1, 2, 5, 10, 20, 30 and 60 min, while fenofibrate was additionally co-milled for total durations of 0.25, 0.5, and 1.5 min. Co-milled mixtures of both drugs were stored in closed conditions protected from light at 20°C and a relative humidity of 40%. To produce milled drugs, apremilast and fenofibrate were prepared without excipient under the same ball milling conditions and a milling time of 15 min. Physical mixtures were mixed in a 250 mL glass container with an orbital mixer (Turbula type T2F, Willy A Bachofen AG, Muttenz, Switzerland). The glass container was filled with 250 mg (± 0.1 mg) of drug and 500 mg (± 0.2 mg) of croscarmellose and mixed at 50 rpm for 10 min. The unmilled drug samples were used as received.

3.4.3 Dissolution medium preparation

Fasted State Simulated Intestinal Fluid (FaSSIF) was prepared in line with standard operating procedures supplied by Biorelevant.com Ltd (London, UK). The pH was set to 6.50 (± 0.1) and the medium was utilised within 24 hours.

3.4.4 Biorelevant dissolution Testing

Dissolution testing was performed in 250 mL FaSSIF using a USP2 apparatus with a stirring speed of 50 rpm. Fibre-optic UV probes with a path length of 10 mm were employed to measure dissolved drug concentration. The UV probes were linked to the Rainbow Dynamic Dissolution Monitor (Pion Inc., Forest Row, UK) and the second derivative of the UV absorbance of fenofibrate and apremilast used to establish calibration curves with an R^2 of > 0.99. The calibration curves were generated with concentrated stock solutions and consisted of ten different measurement points. The dose added to the dissolution experiments was approximately three times the amount soluble in 250 mL of FaSSIF at 37°C, ensuring comparable non-sink dissolution conditions for both drugs. To determine the solubility, an excess of drug was added to FaSSIF at 37°C and stirred with 100 rpm. The concentration of the dissolution curve plateau was used as solubility. These measured solubility values in FaSSIF, 12.2 $\mu g \cdot ml^{-1}$ for fenofibrate and 31.5 $\mu g \cdot ml^{-1}$ for apremilast, were taken as reference for dissolution experiments. To initiate dissolution, formulations equivalent to 23.63 mg of apremilast and 9.15 mg of fenofibrate were added to the vessel, corresponding to 71 mg (± 0.1) apremilast and 27.5 mg (± 0.1) fenofibrate co-milled 33.3% (w/w) mixtures. The dissolution experiments were carried out in quadruplicate.

3.4.5 Particle size distribution determination

Particle size distribution was measured of unmilled and milled drug substances with laser diffraction analysis by using the Mastersizer 2000 (Malvern Instruments Co. Ltd., Solihull, UK). Fenofibrate or apremilast was added to 50 mL water and 0.05 mL of Tween 80. After 10 min (± 30 s) of mixing and stirring, the samples were immediately placed in the Hydro S instrument. A measurement began when a stable obscuration between 10 and 20 % was achieved. The refractive index was set to 1.33 for the dispersion medium (water), 1.612 for apremilast, and 1.55 for fenofibrate. One measurement took 30 sec with a stirring speed of 2100 rpm, which was repeated as triplicates to determine mean values.

3.4.6 Specific surface area measurements

The specific surface area of binary mixtures was determined from the adsorption isotherm using the Brunauer-Emmett-Teller method. The measurements were performed with the NOVA 2000e Surface and Pore Size Analyzer (Anton Paar QuantaTec Inc**.**, Boynton Beach, USA). Samples were degassed for 2 hours at 40 °C in a vacuum. Specific surface area measurements were made by nitrogen adsorption at 77 K in the relative pressure range p/p0 = 0.05-0.30.

3.4.7 X-ray powder diffraction (XRPD)

Powder X-ray diffractograms were recorded using a Bruker-AXS D8 Advance powder diffractometer (Bruker, Karlsruhe, Germany). At ambient temperature, a CuKα radiation (λ = 1.5418 Å) operated at 40 kV and 40 mA . The applied scan rate was 0.02º/s at a theta-theta geometry from 4 to 40º. Finally, the generated diffractograms were modified by standard smoothing procedures and background subtraction.

3.4.8 Differential scanning calorimetry (DSC)

Differential scanning calorimetry was based on a Discovery DSC (Waters TA instruments, New Castle, USA). The measurements were performed under modulated conditions. Samples were weighed in triplicates between 3 and 8 mg in a standard aluminium pan with an accuracy of 0.001 mg. Under nitrogen atmosphere (50 ml min^{-1}), prepared samples were transferred into the instrument and scanned. The instrument was heated from 0°C to 200°C with a heating rate of 5°C min^{-1}. Additionally, the glass forming ability classes of pure drug compounds were evaluated by quench cooling the melt with a cooling rate of 20°C min^{-1} according to Baird et al., 2010. The recrystallization behaviour was assessed by a heating rate of 10°C min^{-1}. The T_gs of apremilast and fenofibrate were extracted by using the midpoint of the thermal event from the quench cooled melt.

3.5 Results

3.5.1 Impact of milling and co-milling on the drug crystallinity assessed by X-Ray powder diffraction

The influence of the milling and co-milling process on the crystallinity of fenofibrate and apremilast was evaluated using X-ray powder diffraction. The general diffraction patterns of both drugs milled for 15 min in the absence of an excipient remained mainly unchanged (Figure 3-1). Most of the Bragg peaks after milling fenofibrate reveal a lower intensity, which could be a sign of a lower crystal order of the milled drug. However, also higher Bragg peak intensities after milling of fenofibrate were observed e.g. the two peaks between 16° and 17° and the peaks at 19° as well as 26°. These higher peak intensities after milling fenofibrate indicate changes of the crystalline arrangement. This effect was not observed for the high T_g drug apremilast, which showed a general lower Bragg peak intensity after neat drug milling.

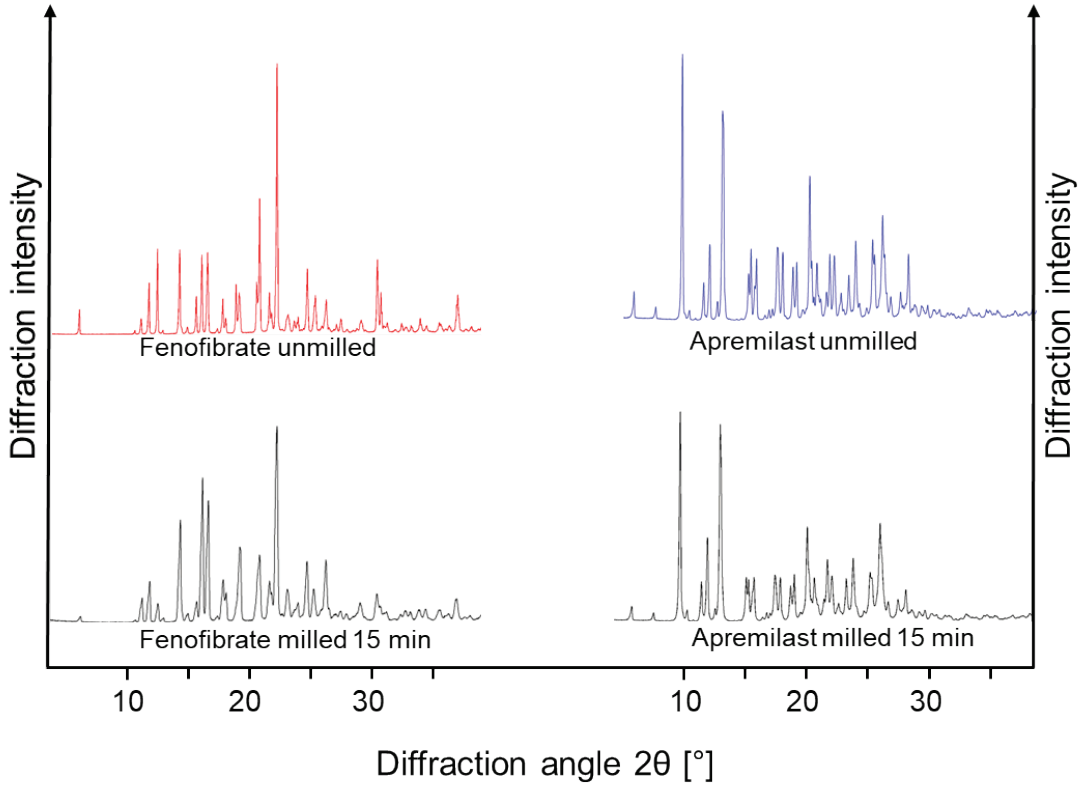


Figure 3-1: X-ray powder diffractograms of fenofibrate (left, red) and apremilast (right, blue) as unmilled drug powder and both drugs after 15 min ball milling (black).

Co-milling fenofibrate mixtures had the same basic diffraction pattern, even after 60 min of (Figure 3-2). None of the clearly visible peaks of the physically mixed mixture disappeared in diffractograms of co-milled mixtures, indicating a high degree of drug crystallinity. However, a peak broadening is also visible for co-milled fenofibrate compared to the physically blended mixture. In contrast, lower intensities of drug diffraction peaks were observed in apremilast mixtures with increased co-milling times. A reduced diffraction intensity was observed from 10 min of co-milling onwards, indicating a higher degree of drug crystal lattice disorder in co-milled mixtures. After 30 and 60 min of co-milling, almost all sharp Bragg peaks were missing in co-milled mixtures of the high-T_g glass former apremilast.

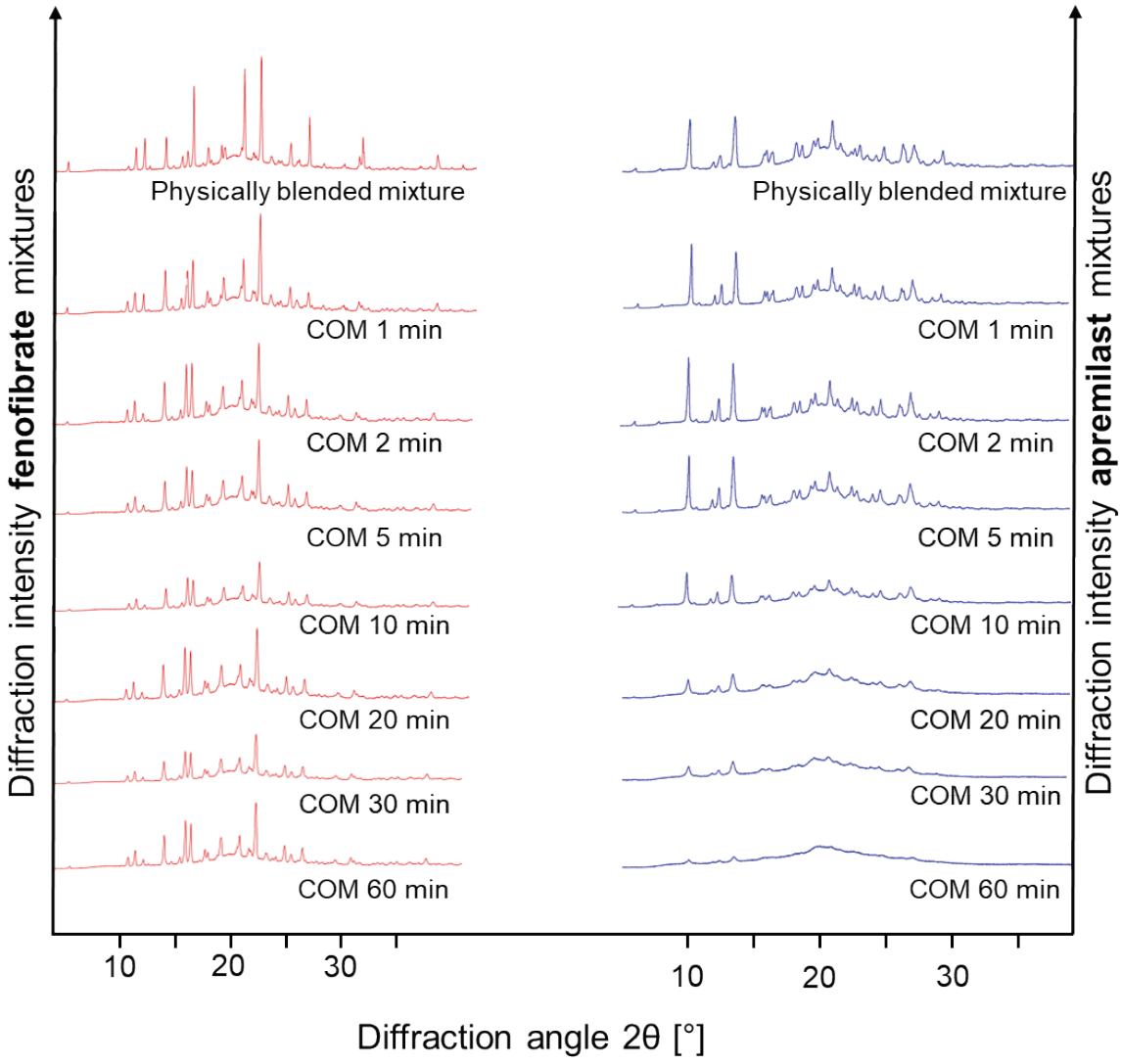


Figure 3-2: X-ray powder diffractograms of fenofibrate (red) and apremilast (blue) in physically blended mixtures and co-milled mixtures (COM) at different milling times.

3.5.2 Glass forming ability class determination of fenofibrate and apremilast

The glass forming ability classification determinations of fenofibrate and apremilast are depicted in Figure 3-3. During cooling of the melt, no exothermic peaks indicating recrystallization were observed for both drugs. In addition, the absence of a second crystallisation peak during reheating indicates that both compounds did not recrystallize during the entire experiment and therefore belong to glass forming ability class III. Fenofibrate had a measured T_g of −20 °C (midpoint of the thermal event) at a cooling rate of 20 °C min^{-1} whereas the determined T_g of apremilast was 76.5 °C.

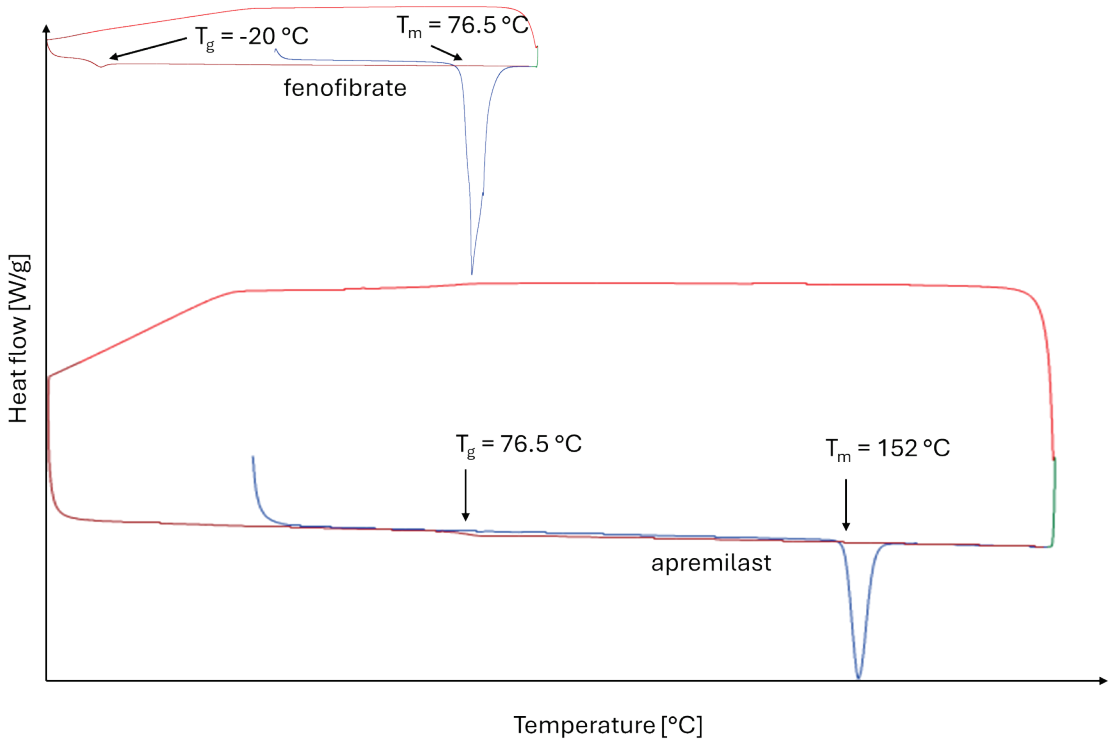


Figure 3-3: Glass forming ability class determinations of apremilast and fenofibrate. The glass transition temperatures (T_g) were extracted by using the midpoint of the thermal event from the quenched cooled melt and the onset of the melting peak was used to determine the melting point (T_m).

3.5.3 In vitro Dissolution profiles of apremilast and fenofibrate in different formulations

Dissolution of fenofibrate as unmilled and milled drug (without excipient) displayed no significant differences in drug release after 15 and 60 min Figure 3-4), as determined by a two-sided *t*-test ($p > 0.05$), despite of a particle size reduction on the D10, D50 and D90 levels (table S7). The addition of croscarmellose sodium to the unmilled powder, which was physically blended for 10 min, also had no significant effect on the measured drug concentration after 15- and 60- min dissolution ($p > 0.05$). However, co-milling for 0.25 min already revealed a significant dissolution enhancement compared to the physical mixture, unmilled and milled drug, considering these two dissolution timepoints ($p < 0.05$). Prolonging the co-milling process resulted in a further significant increase in dissolution, observed up to 10 min of co-milling ($p < 0.05$). Co-milling for 10 min or longer resulted in no further significant dissolution

The dissolved drug concentration of milled apremilast was significantly lower than of the unmilled drug at the 15- and 60-min dissolution timepoints ($p < 0.05$). Faster drug release was observed for the physical mixture as well as for 1- and 2- min co-milled mixtures, which showed significantly higher drug concentrations at the 15- and 60- min timepoints compared to unmilled apremilast ($p < 0.05$). Highest dissolution enhancement was measured for mixtures co-milled for 5 min and longer. After 10 min of co-milling, the dissolution profile exhibited drug supersaturation (c_{max} = 42.05 ± 0.31 µg·ml^{-1}). The maximum apparently supersaturated drug concentration grew further with the applied co-milling time up to 80.07 ± 1.95 µg·ml^{-1} for the 60 min co-milled samples, and did not fall below the equilibrium solubility (black dotted line) throughout the duration of the dissolution experiment.

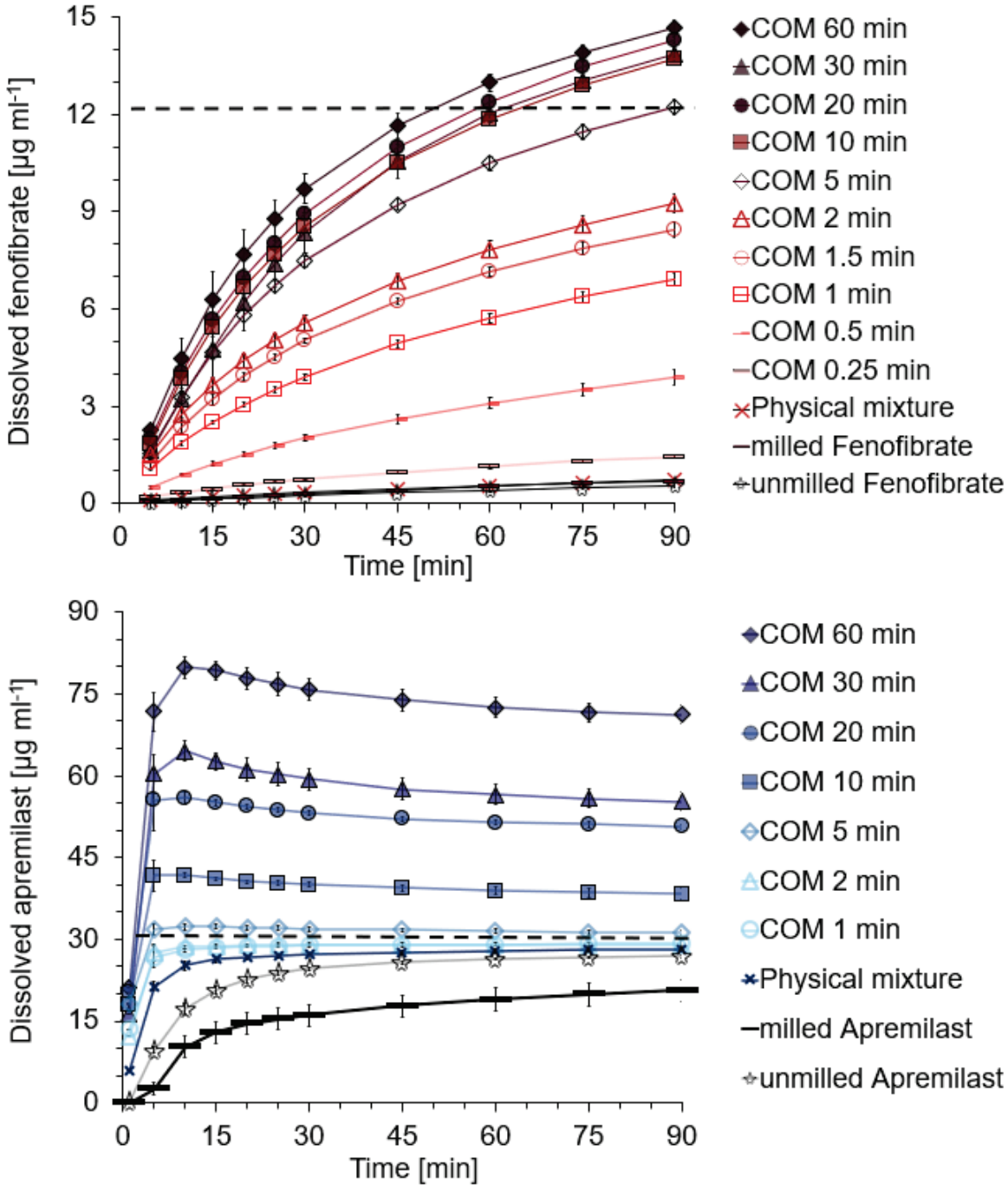


Figure 3-4: Dissolution profiles of fenofibrate and apremilast as unmilled drugs, milled drugs, physically blended and co-milled mixtures (COM) at different milling times with croscarmellose sodium in a drug to excipient ratio of 1:2 (w/w) (n = 4). The black dotted line expresses the equilibrium solubility of the respective drugs in the used medium FaSSIF V1 at 37°C.

3.5.4 Relationship between surface area of co-milled mixtures and drug dissolution

Drug dissolution of the low-T_g glass former fenofibrate, represented by the area under the dissolution curve (AUC) in the first 60 min, was in good agreement with the specific surface areas of the co-milled mixtures (Figure 3-5, $R^2 = 0.96$). In contrast, the $AUC_{0–60\ min}$ of the high-T_g glass former apremilast did not correlate well with the surface area of the co-milled mixtures (Figure 3-5, $R^2 = 0.07$). The relationship between co-milling time and the specific surface area is attached to the supplementary materials in Figure S61.

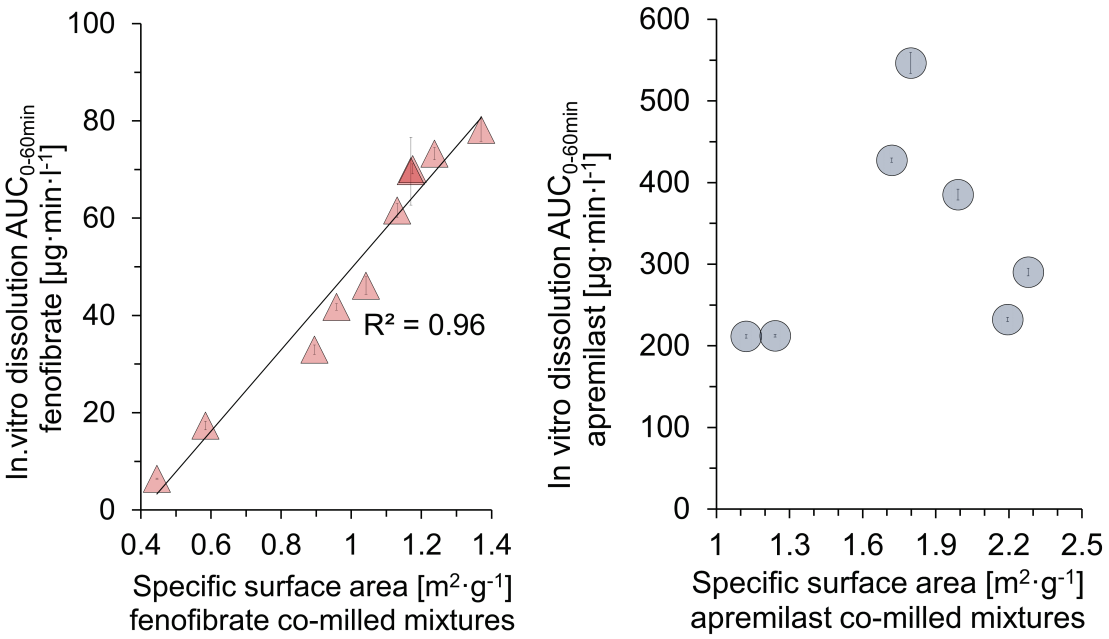


Figure 3-5: Relationship of the area under the curve (AUC) of the first 60 min in vitro dissolution of fenofibrate (left) and apremilast (right) (n = 4) in co-milled mixtures versus the specific surface area of these co-milled systems.

3.5.5 Melting point depression of co-milled drugs and its correlation with the in vitro dissolution c_{max} of the high-T_g glass former apremilast

The melting point of both co-milled drugs, extracted from the onset of the melting peak from DSC thermograms, decreased to different extents (Figure 3-6). While the drug melting point of the low-T_g glass former fenofibrate depressed with the processing time by around 1.5 °C after 60 min co-milling, it decreased by >10 °C for the high-T_g glass former apremilast.

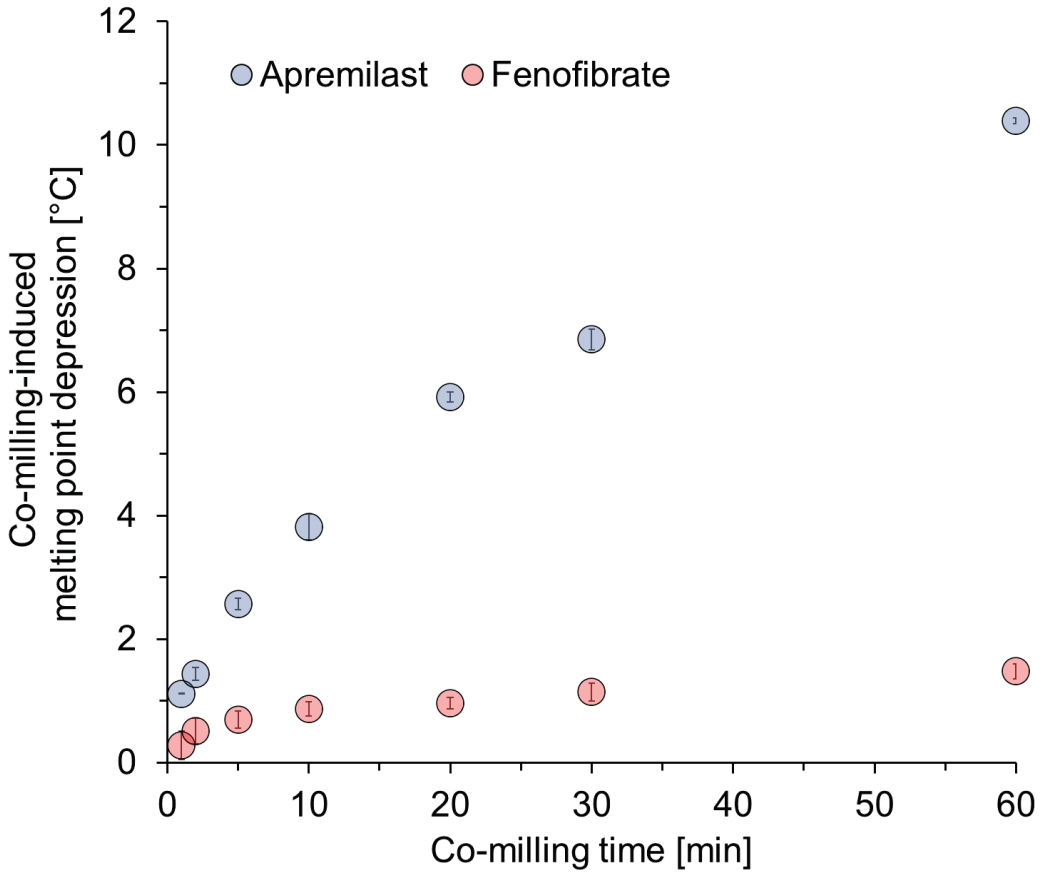


Figure 3-6: Melting point depression, extracted from the onset of the drug melting peak, of co-milled apremilast (high-T_g glass former) and fenofibrate (low-T_g glass former) (n = 3) after various co-milling process duration.

The dissolution profiles of Figure 3-4 showed that co-milled fenofibrate dissolved according to first order kinetics whereas ≥ 10 min co-milled apremilast release profiles rather followed "spring and parachute" characteristics i.e. the drug substance supersaturated in the dissolution medium. Subsequently, the highest measured apremilast concentration during *in vitro* dissolution (c_{max}), a parameter reflecting drug supersaturation, was chosen to relate with parameters of co-milled mixtures of apremilast. Notably, the melting point depression of co-milled apremilast correlated with the co-milling induced increase of the *in vitro* dissolution c_{max} (Figure 3-7). A linear relationship was observed for the onset (R^2 = 0.98) as well as for the tip of the melting peak (R^2 = 0.96).

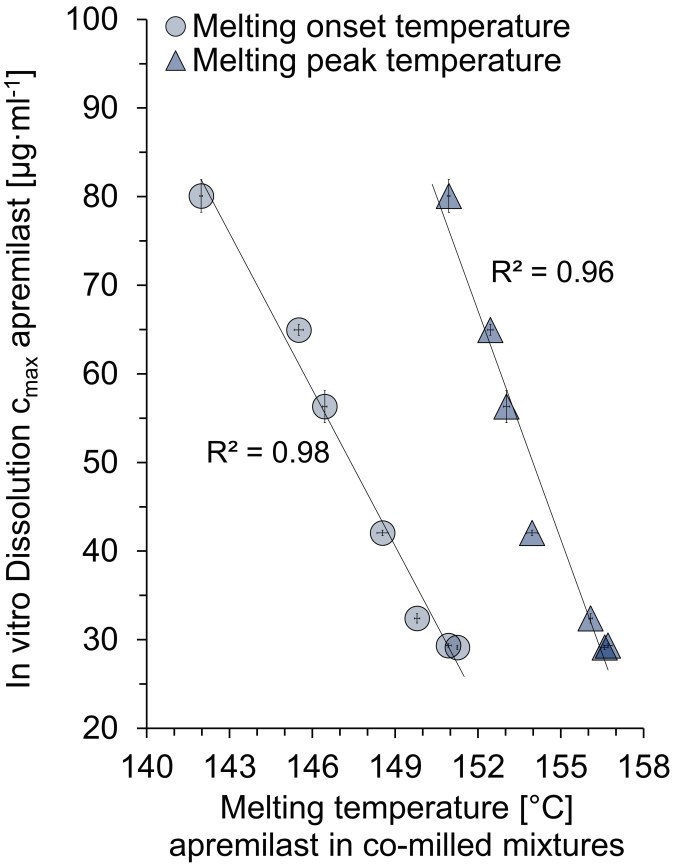


Figure 3-7: The melting point depression of the high-T_g glass former apremilast as a function of the highest measured apremilast concentration (c_{max}) during the in vitro dissolution process. Apremilast was co-milled with croscarmellose sodium at different milling times from 1 to 60 min (n = 3).

3.5.6 Stability study of co-milled drugs based on the melting point depression approach

To evaluate the change in crystallinity of the co-milled drugs, stored samples were measured directly after preparation and 90 days of storage using DSC. The change in onset temperature of the melting peak of a DSC measurement was used for the evaluation (Figure 3-8), the corresponding thermograms are added to the supplementary materials (Figures S62 - S101). No notable changes in the melting onset of co-milled fenofibrate which had been co-milled for 10 min or less were observed during storage. However, the onset of the melting peak in samples co-milled for 20 min or longer was notably higher after storage. Despite the higher co-milling induced melting point depression of apremilast, the melting point did not change noticeably for all co-milled mixtures of this high-T_g glass former during storage. The stability conditions (90 days under closed storage at 20 °C and 40% relative humidity) were selected to be mild, as the crosslinked polymer in the co-milled formulations is highly hydrophilic. Moisture uptake can act as a plasticizing agent, increasing molecular mobility and thereby promoting recrystallization of these disordered formulations.

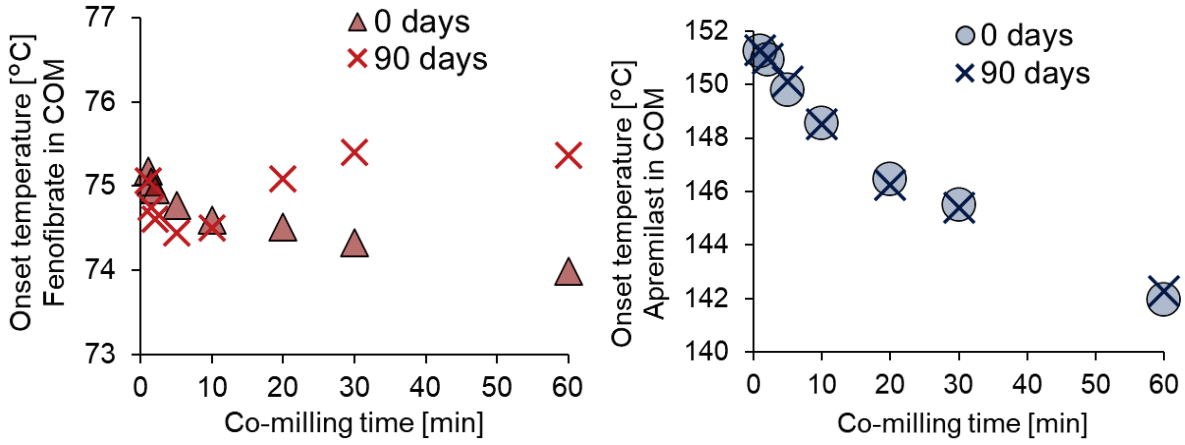


Figure 3-8: Stability study of co-milled drugs using the melting point depression approach. Depicted are onset temperatures of co-milled drugs directly after preparation and after 90 days of storage under closed conditions, 20°C and 40% relative humidity.

3.6 Discussion

The aim of this study was to gain insights into co-milling of two drugs belonging to glass forming ability class III by exploring extremes in drug T_gs, which are located far below and above the milling temperature. Co-milling of the high-T_g drug apremilast led to drug supersaturation in the dissolution medium for milling times of 10 min and longer (Figure 3-4), as highest measured dissolved apremilast concentration exceeded the equilibrium (crystalline) solubility of the compound in FaSSIF. In contrast, milling without an excipient did not achieve drug supersaturation and resulted in the slowest dissolution rate among all preparations (Figure 3-4) which may be explained by particle aggregation (Table S1). Similar cases have also been observed in studies where compounds were milled without excipient (Pätzmann et al., 2024; Zimper et al., 2010a). The melting point of apremilast decreased with increased co-milling time, dropping by more than 10 °C after 60 min of co-milling (Figure 3-6). Interestingly, the melting point depression highly correlated with the dissolution c_{max} of apremilast during *in vitro* dissolution (R^2 = 0.98, melting peak onset temperature; R^2 = 0.96, melting peak temperature, (Figure 3-7). On storage, the pronounced melting point depression of this high-T_g glass former remained stable (Figure 3-8). A possible explanation for the melting point depression may be the increased chemical potential of the disordered drug material, which is higher compared to the non-milled crystals, while the chemical potential of the liquid state remains the same (Ahmed et al., 2020). As a result, the energy required to melt the ball milled crystal, with a higher degree of disorder is lower and the drug material melts earlier (Alsayed et al., 2005; Chikhalia et al., 2006; Lipson and Polturak, 2024). The reduced diffraction peak intensity X-ray diffractograms of co-milled apremilast suggest the introduction of pronounced crystal lattice defects due to a processing time of ≥ 10 min (Figure 3-2). Since disordered drug material appear to melt earlier, the melting point depression may be a critical quality attribute of a co-milled product to monitor the degree of crystal lattice disorder and drug supersaturation. It could therefore have applications as an easily accessible parameter in industrial settings in compliance with ICH Q8. Although DSC measurements were performed in modulated mode

in this study, the correlation is also applicable in standard, non-modulated mode for determining the melting point depression of the drug in binary, co-milled mixtures.

The melting point depression of the low-T_g glass former fenofibrate reduced by < 2 °C after 60 min co-milling. This reduction is considerably less than for apremilast whose T_g is above milling temperature (Figure 3-6). However, despite the lower melting point depression of co-milled fenofibrate, it did not remain stable as the melting point of samples co-milled for 20 min or more increased during storage (Figure 3-8). It could be a sign of effects on the particle surfaces and may indicate reparation processes of structural disorder generated during co-milling. The dissolution rate enhancement of the low-T_g glass former fenofibrate highly correlated with the specific surface area of co-milled mixtures (R^2 = 0.96, Figure 3-5). Sharp Bragg peaks in all diffractograms of fenofibrate containing mixtures reveal that this low-T_g glass former remained in a highly ordered crystalline state, despite 60 min of high energy dry ball milling in a stainless-steel ball mill (Figure 3-2). This strengthens the hypothesis that the driving force for the dissolution enhancement of this low-T_g glass former was mainly the increase in surface area and not due to the co-milling induced drug crystal lattice disorder. Other studies showed that it was not possible to amorphise low-T_g drugs via milling (Blaabjerg et al., 2017a; Descamps et al., 2007). The addition of croscarmellose sodium to the milling process appeared to not overcome this phenomenon for fenofibrate by stabilizing the crystal lattice disorder.

The dissolution enhancement of co-milled fenofibrate appears specific to the co-milling process. When fenofibrate was milled alone for 15 min, dissolution did not improve compared to the physically blended or unmilled drug, despite a reduction in particle size and an expected increase in surface area (Table S1). However, adding croscarmellose sodium during co-milling significantly improved dissolution, with effects observed after just 15 s of co-milling (Figure 3-4). The superdisintegrant may have enhanced the wettability of lipophilic fenofibrate (Bennett-Lenane et al., 2021a). As a result, the wettability issues of this lipophilic compound appeared to be overcome by the addition of the excipient to the milling process. Another study confirmed

that co-milling with a polymer can increase the wettability of a drug (Varghese and Ghoroi, 2017).

A limitation of this work is that it screened only one high-T_g glass former. More studies with high-T_g glass formers and different excipients are required to strengthen the hypothesis that dry co-milling is a suitable technique for the development of stable supersaturable formulations. The correlation between drug melting point depression with dissolution parameters also needs further investigation using other drug-excipient combinations. This correlation is only applicable for co-milled formulations which contain residual crystallinity, because fully amorphous systems do not have a melting point.

Future studies could investigate interactions between drug substances and excipients due to co-milling. Since the milled material remains in the solid state throughout the process, interactions at the molecular level might be less pronounced compared to formulations produced by spray drying or hot melt extrusion. Nonetheless, even weak interactions such as van der Waals forces or hydrogen bonds created by co-milling may have a significant impact on dissolution, especially when using a swellable excipient like croscarmellose sodium. These interactions could lead to favourable particle arrangements of co-milled material, particularly benefiting highly lipophilic and brittle drugs. Future research could investigate drug-excipient interactions generated by co-milling using e.g. FT-IR or solid state NMR, as well as the influence of drug deformation behaviour on the degree of co-milling-induced lattice disorder.

Overall, this work demonstrated that co-milling of high-T_g glass formers such as apremilast appears to be a promising approach to produce stable formulations with supersaturation kinetics. The drug melting point depression correlated with the dissolution enhancement of this high-T_g glass former and may be a critical quality attribute for the design of partially crystalline formulations prepared by co-milling. Further, this study delivered additional data where a low-T_g drug lost to a much lower extent crystallinity due to the milling process compared to the high-T_g candidate, even though both compounds belong to glass forming ability class III. The addition of croscarmellose sodium to the milling process seemed not to have a positive effect

on the stabilization of crystal lattice disorder of this lipophilic low-T_g compound but the dissolution was significantly improved.

3.7 Conclusion

This study showed that applying the same co-milling conditions on two stable glass formers with T_gs below and above milling temperature can lead to significantly different degrees of produced crystal lattice disorder. The low-T_g glass former fenofibrate remained mainly in an ordered crystalline state after one hour of co-milling and the dissolution rate enhancement correlated with the surface increase of the co-milled system. A higher degree of structural disorder was measured for the high-T_g glass former apremilast and supersaturation kinetics during in vitro dissolution were observed. The milling induced entropy increase in crystal lattices led to a melting point depression, which highly correlated with the *in vitro* dissolution enhancement of co-milled apremilast. Thus, a co-milling related melting point depression may be a useful critical quality attribute for the production of co-milled formulations to assess the degree of process induced structural disorder and to anticipate drug supersaturation.

Chapter 4: Exploring co-milling of poorly water-soluble drugs with swellable polymers to enhance the dissolution rate

Nicolas Pätzmann[1,2], Josef Beránek[2], Brendan T. Griffin[1], Martin Kuentz[3], Patrick J. O'Dwyer[1*]

[1] *School of Pharmacy, University College Cork, Cork, Ireland*

[2] *Zentiva, k.s., U Kabelovny 130, Prague 10, 102 00, Czech Republic*

[3] *University of Applied Sciences and Arts Northwestern Switzerland, Institute of Pharma Technology, Hofackerstrasse, 30, CH-4132 Muttenz, Switzerland*

*Corresponding Author:

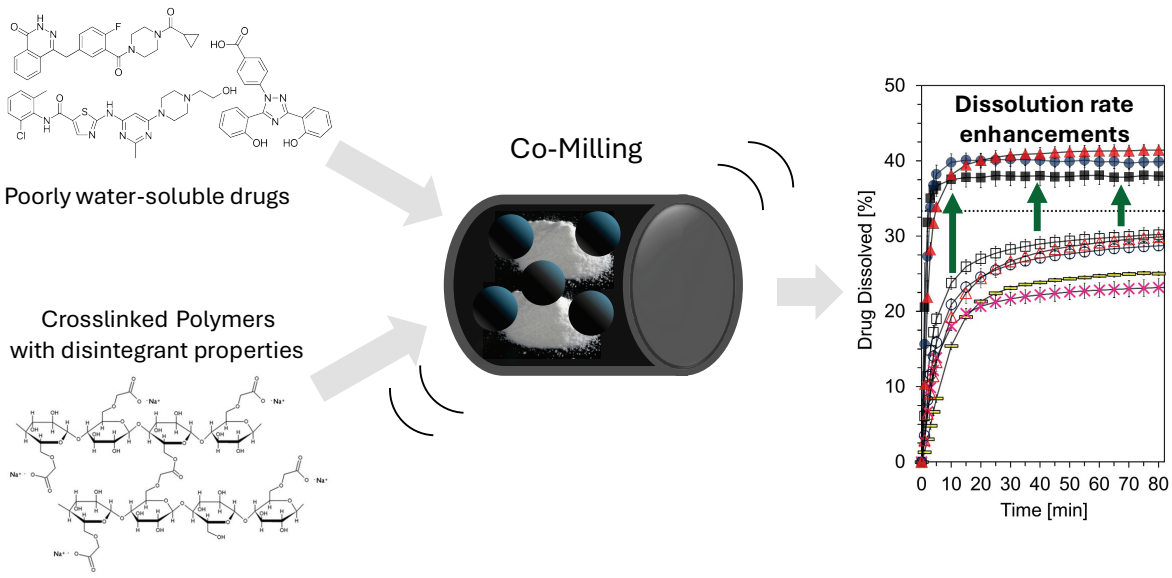
Dr. Patrick J. O'Dwyer;

E-mail address: patrick.odwyer@ucc.ie

Keywords: Co-milling, co-grinding, ball milling, dissolution rate limited absorption, tablet disintegrants, refined Developability Classification System

Published in: AAPS PharmSciTech (2026), Volume 27, DOI: 10.1208/s12249-025-03270-w

4.1 Graphical Abstract



4.2 Abstract

Co-milling with excipients offers an effective solvent-free strategy to enhance the dissolution of drugs in the pharmaceutical industry. Nonetheless, the range of excipients available for co-milling, as well as the selection criteria, remains relatively unexplored. Therefore, this study aims to evaluate the effect of co-milling with crosslinked swellable polymers on the dissolution of poorly water-soluble drugs. A structurally diverse set of crystalline compounds (n = 13) were co-milled with the three commonly used tablet disintegrants: Croscarmellose sodium, sodium starch glycolate and crospovidone. *In vitro* dissolution profiles were assessed to evaluate the excipient performance and identify crucial drug descriptors relating to co-milling induced dissolution enhancement. All 39 co-milled formulations showed an increased drug intrinsic dissolution rate (IDR), with drug properties such as molecular size and polar surface area showing a positive correlation with the extent of IDR enhancement following co-milling. Moreover, co-milling consistently yielded greater initial dissolution ($AUC_{0\text{-}5min}$) across all excipients compared to milling the drug without an excipient. On average, milling with croscarmellose sodium produced the greatest improvement in the early stages of dissolution for neutral and basic compounds, while sodium starch glycolate was more effective in enhancing the dissolution of co-milled acidic drugs. Furthermore, an assessment within the refined Developability Classification System (rDCS) revealed that co-milling was effective to overcome dissolution rate limitations for all rDCS class IIa drugs. This study establishes a practical framework for the broader application of co-milling with tablet disintegrants and demonstrates its relevance within the latest rDCS paradigm for overcoming dissolution rate-limited absorption.

4.3 Introduction

The formulation of drugs with dissolution rate-limited absorption remains a considerable challenge for the pharmaceutical industry (Vinarov et al., 2021). A useful tool to predict the risk of limited oral absorption by a low drug dissolution rate for a novel compound in the development pipeline is provided by the Developability Classification System (DCS) (Butler and Dressman, 2010a). The DCS, which was refined in 2021 (rDCS), supports formulation decision-making by assessing risk levels and categorizing compounds to guide appropriate formulation strategies (Rosenberger et al., 2018). For compounds with dissolution rate limited absorption, milling-based particle size reduction remains a practical and widely used alternative to more complex bio-enabling strategies such as amorphous dispersions or lipid-based drug delivery systems. Within the framework of the rDCS, recent work by Dressman and colleagues has introduced an advanced approach to calculate target particle size needed to overcome dissolution rate limited absorption (Beran et al., 2023). The estimation of the target particle size is based on the compound's intrinsic dissolution rate (IDR) or solubility, along with the expected in vivo dissolution behaviour under either sink or non-sink conditions.

An alternative bio-enabling approach to enhance the dissolution rate is co-milling of drugs with excipients (Maggi et al., 2013b; Slámová et al., 2021). Previous studies showed a successful dissolution rate enhancement *in vitro* as well as an increase of in vivo bioavailability after applying this industrially scalable process (Isaac et al., 2016; Vogt et al., 2008b). Proposed mechanisms for the enhancement of dissolution are particle size reduction, crystal lattice disorder and excipient related effects (Löbmann et al., 2013; Varghese and Ghoroi, 2017; Zimper et al., 2010a). Co-milling with different excipients has been applied for a variety of formulation approaches, such as co-crystals with organic acids, co-amorphous systems with amino acids, or amorphous solid dispersions with hydrophilic polymers (Caron et al., 2013; Holzapfel et al., 2023; Shaikh et al., 2021). Given the range of existing approaches, further investigation into the formulation performance of additional excipients, and their effects on processed drugs, is warranted to fully realise the potential of pharmaceutical co-milling.

Croscarmellose sodium, sodium starch glycolate, and crospovidone are widely used tablet disintegrants which are typically included in orally administered tablet formulations (Quodbach and Kleinebudde, 2015). These excipients have undergone crosslinking, which enables them to swell upon exposure to gastrointestinal fluids supporting the disintegration of tablets. (Azad et al., 2015). This superior ability to promote tablet disintegration has led to their classification as “superdisintegrants” (Quodbach et al., 2014). One study showed enhanced oral bioavailability of raloxifene when co-milled with crospovidone both *in vitro* and in vivo in rats (Jagadish et al., 2010). Realizing the potential of superdisintegrant-based co-milling calls for further investigations involving a wider range of poorly water-soluble drugs, along with deeper insights into the mechanisms responsible for enhanced dissolution.

Therefore, this study aimed to investigate the efficacy of three superdisintegrants as co-milling aids, and applying the technique across a diverse set of thirteen poorly water-soluble drugs. *In vitro* dissolution data was used to assess the dissolution enhancement from both an excipient and drug properties perspective. Furthermore, the utility of co-milling with superdisintegrants to overcome dissolution rate-limited characteristics was evaluated within the framework of the rDCS, and therein support the wider application of this technique as a bioenabling strategy for dissolution rate-limited drug candidates.

4.3 Materials and Methods

4.3.1 Materials

Gefitinib, indapamide, meloxicam, rivaroxaban, croscarmellose sodium (Ac-Di-Sol), sodium starch glycolate type A and crospovidone (Polyplasdone XL) were provided by Zentiva k.s. (Prague, Czechia). Dipyridamole, griseofulvin, mefenamic acid, nimesulide, the dissolution medium reagents sodium hydroxide, sodium chloride and di-sodium hydrogen phosphate were purchased from Sigma-Aldrich (Prague, Czechia). Deferasirox was obtained from Neuland Laboratories Ltd. (Telangana, India), olaparib from Taizhou Crene Biotechnology Co. Ltd. (Taizhou Zhejiang, China), and apremilast, tadalafil and dasatinib from MSN Pharmaceuticals Inc. (New Jersey, USA). Simulated Intestinal Fluids powder was purchased from Biorelevant.com Ltd. (London, United Kingdom).

4.3.2 Preparation of milled drugs, physical blends and co-milled mixtures

Milling was performed 15 min at a frequency of 15 Hz in a vibrational ball mill (MM 200, Retsch, Haan, Germany). The 25 mL stainless steel milling jar was filled with three 9 mm diameter stainless steel balls and 250 mg (± 0.1 mg) of drug to prepare milled drugs. To prepare co-milled mixtures, either 500 mg (± 0.2 mg) of croscarmellose sodium or sodium starch glycolate, or 250 mg (± 0.1 mg) of crospovidone, was added to the drug. Preliminary dissolution studies using candesartan cilexetil indicated that the optimal excipient-to-drug ratio was 2:1 for croscarmellose sodium and sodium starch glycolate, while a 1:1 ratio was optimal for crospovidone. Physical mixtures were prepared by blending the drug and excipients in the same ratios as the co-milled samples. Mixing was carried out in a 250 mL glass container using an orbital mixer (Turbula type T2F, WAB AG, Muttenz, Switzerland) at 50 rpm for 10 minutes. Drug powders were used as received.

4.3.3 Biorelevant Dissolution testing and intrinsic dissolution rate determination

Fibre-optic UV probes of a Rainbow Dynamic Dissolution Monitor Instrument (Pion Inc., East Sussex, United Kingdom) were used for dissolution testing. All drugs were tested for 80 minutes in their unmilled, milled, physically blended, and co-milled forms. Testing was conducted in a USP2 vessel containing 250 mL of Fasted State Simulated Intestinal Fluid (FaSSIF), pre-heated to 37°C, with stirring at 50 rpm. The biorelevant medium was prepared according to standard operating procedures from Biorelevant.com Ltd. (London, United Kingdom). A range of 10 nm from the second derivative of the UV absorbance from every drug was used to generate at least seven-point calibration curves with an R^2 > 0.99, covering the entire concentration range of all dissolution experiments. Based on the UV absorption and solubility of the drug, a path length of 2, 5 or 10 mm on UV probes was used to quantify the dissolved drug. The same path length was used for all samples of a given drug. Solubility was determined for each drug to guide the amount of drug dose used in the dissolution experiments. This was done by adding an excess of drug in triplicate to pre-heated FaSSIF (37°C) and stirred with 100 rpm until a concentration plateau was reached. The average of the plateau concentration was taken as thermodynamic solubility. Formulations equivalent to three times the drug amount soluble in 250 mL of biorelevant medium were added to initiate the dissolution experiments A triplicate of freshly prepared samples was added to the medium. Tsinman and colleagues established a method which allows determination of the IDR from powder dissolution testing, particularly suitable for poorly water-soluble drugs (Tsinman et al., 2009). This method is integrated in AuPRO™ (version 6.1.0.354) of the Pion Rainbow and was used to calculate IDRs of powder dissolution approaches.

Dissolved drug concentrations at different time points of the same drug in two formulations were analysed using an independent samples t-test (two-tailed) with consideration of the respective p-values at a significance level of $\alpha = 0.05$ (Excel 2024, Microsoft, USA). The area under the first 5 minutes dissolution curve ($AUC_{0\text{-}5min}$) was calculated using the same software

by including the average concentration values after 30s, 60s, 90s, 120s, 150s, 180s, 210s, 240s, 270s and 300s of the dissolution experiments. The $AUC_{0\text{-}5min}$ was normalized by z-standardisation to the mean for each drug in co-milled mixtures, as milled drugs without excipient and unmilled drugs used as received.

Table 4-1: Overview of the experimental conditions used for dissolution testing.

Parameter	**Condition**
Apparatus Type	USP 2, Paddle
Rotation Speed	50 rpm
Medium	FaSSIF
Volume	250 mL
Bath Temperature	37°C
Detection	In-line UV probe
Quantification	10 nm range of the second derivative of the drug's UV spectrum
Duration of Experiment	80 minutes
Measurement Frequency	Every 30 seconds

4.3.4 X-Ray powder diffraction

X-ray diffraction analysis was performed on drug powders before their use to evaluate the crystallinity and determine the polymorph. Diffractograms were generated using a Bruker-AXS D8 Advance powder diffractometer (Karlsruhe, Germany). By an applied scan rate of 0.02º/s, the theta-theta geometry ranged from 4 to 40º.

4.3.5 Particle size determination

The particle size distribution of drug powders was determined by laser diffraction analysis (Mastersizer 2000 with Hydro 2000S, Malvern Instruments Co. Ltd., Solihull, UK). Solid drug particles (200 ± 0.5 mg) were mixed with 50 mL of water, 0.05 mL Tween 80 and stirred for 10

min to prepare a dispersion. After that, the dispersion was added to the Hydro S element of the instrument until a steady obscuration between 10 and 20% was achieved. Refractive indices of drug substances were set according to published data and 1.33 for the dispersion medium water. Measurements were performed at 30 s intervals with 2100 rpm. Every measurement was conducted in triplicate and averages calculated. It can be assumed that highly saturated dispersions were prepared because the highest FaSSIF solubility of investigated drugs was 149.3 µg/mL and the dispersions for particle size distribution measurements contained 4000 µg/mL of drug substance in water.

4.3.6 Specific surface area measurements

The specific surface area of co-milled mixtures was measured using the Brunauer-Emmett-Teller method from the adsorption isotherm. The experiments were conducted with the NOVA 2000e Surface and Pore Size Analyzer (Quantachrome, Odelzhausen, Germany). Co-milled mixtures were degassed in vacuum for 120 min at 313 K. Measurements were performed in a relative pressure range of p/p0 = 0.05-0.30 by nitrogen adsorption at 77 K.

Since particle size determination by water-based laser diffraction analysis would lead to swelling of the tablet disintegrants and, consequently, unreliable particle size data, specific surface area measurements were used to derive the particle size of the drugs in the co-milled mixtures. Based on the assumption of spherical particle shapes, a particle size can be calculated from equation 4-1:

$$d = \frac{6}{(w/w_{drug} * \rho_{drug}) + (w/w_{excipient} * \rho_{excipient})\, SSA} \quad (4\text{-}1)$$

d = Particle diameter [µm]

SSA = Specific surface area of co − milled system [m^2/g]

w/w = Mass fraction of drug or excipient in the co − milled mixture

ρ_{drug} = Drug density [g/cm^3]

$$\rho_{excipient} = \text{Excipient density } [g/cm^3]$$

Milling tends to produce particles with a spherical nature (Blanco et al., 2025), however, the nature of a milled material still deviates from an ideally spherical morphology. Hence, the shape coefficient of ideally spherical particles of equation 4-1, which is 6, needed modifications in order to approach a more realistic drug particle size in co-milled formulations. A shape factor between 11.1 (smooth surface) and 12 (rough surface) for particles with low sphericity was determined (Maroof et al., 2020). Consequently, the drug particle sizes in co-milled formulations were estimated with equation 4-2:

$$d = \frac{12}{(w/w_{drug} * \rho_{drug}) + (w/w_{excipient} * \rho_{excipient})\, SSA} \quad (4\text{-}2)$$

The density of used excipients was obtained from the handbook of pharmaceutical excipients and drug densities were predicted by ACD labs (Advanced Chemistry Development Inc., Toronto, Canada) based on SMILES strings of respective drug molecules.

4.3.7 Thermal analysis via differential scanning calorimetry

Differential scanning calorimetry was performed with a Discovery DSC (Waters TA instruments, New Castle, USA). The drugs were weighed into aluminium pans in quantities between 3 and 8 mg. Under nitrogen atmosphere (50 ml min^{-1}), samples were heated with a rate of 5 °C min^{-1} until they exceeded the melting point (T_m) of the substances. The onset of the melting peak was extracted. Furthermore, the glass forming ability classes of all compounds were measured. Hence, the melt was quench cooled with a cooling rate of 20 °C min^{-1}. After that, the recrystallization behaviour was assessed by a heating rate of 10 °C min^{-1}. The glass transition temperature (T_g) of drugs were determined as the midpoint of the thermal event from the quench cooled melt.

4.3.8 Descriptor variables calculation and statistical analysis

The molecule descriptors molecular weight (MW), Polar surface area (PSA) and $LogD_{6.5}$ of investigated drug substances were calculated using ADMET Predictor software (Version 9.5, Simulation Plus, USA) by using Simplified Molecular Input Line Entry System (SMILES) strings of these molecules as input data. Subsequently, a Principal Component Analysis (PCA) was conducted in SPSS Statistics (Version 26, IBM Corporation, USA) using measured melting points and solubility values, along with the calculated MW and $LogD_{6.5}$. Drugs Pearson correlations with IDR ratios (equation 4-3) based on measured and calculated drug descriptors were obtained using the same software.

$$\text{Intrinsic Dissolution Rate Ratio(IDRR)} = \frac{\text{IDR}_{\text{co-milled drug}}}{\text{IDR}_{\text{crystalline drug}}} \quad (4\text{-}3)$$

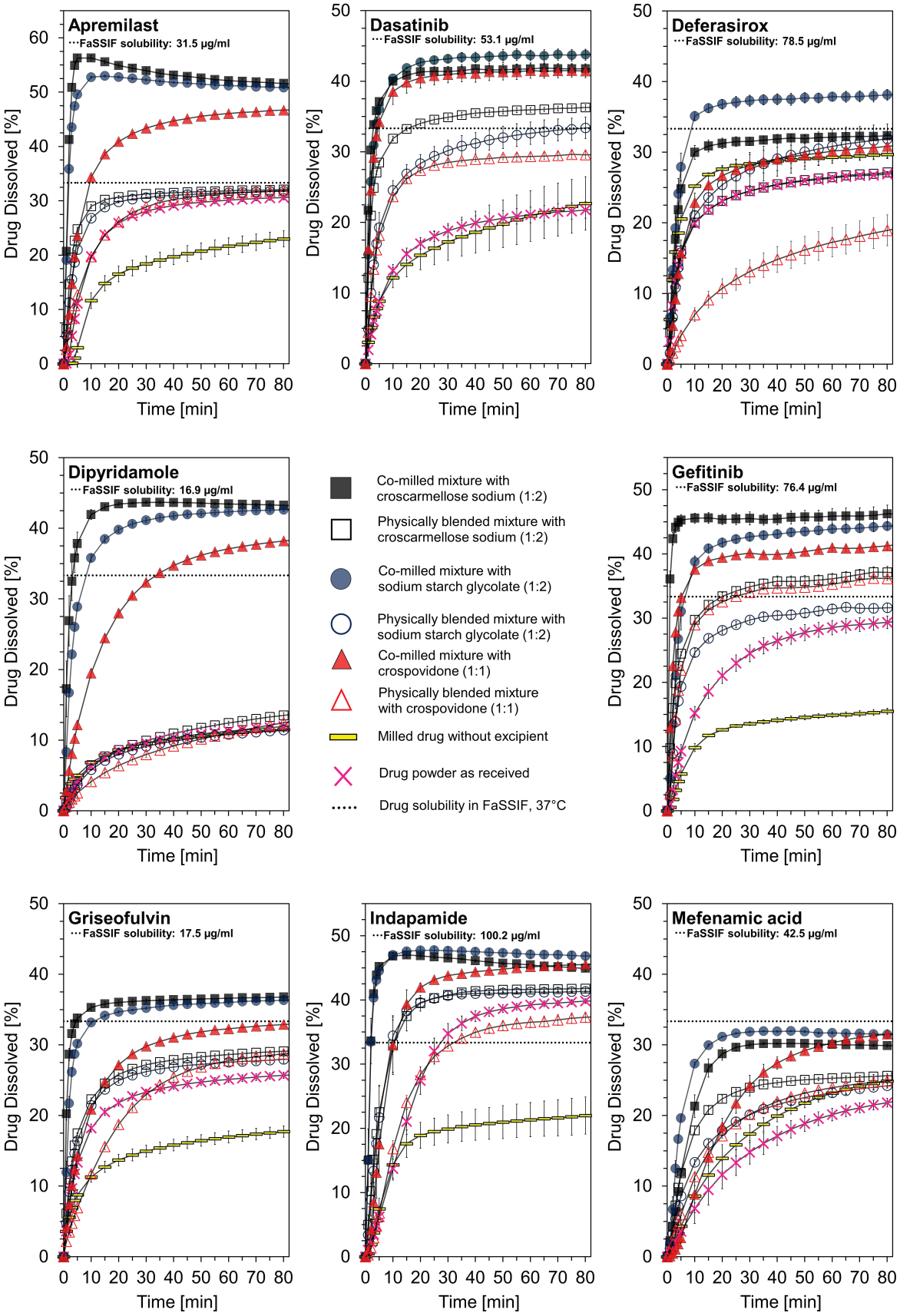
4.3.9 Analysis based on the refined Developability Classification System

Measured solubility data, usual marketed doses and predicted P_{eff} values from ADMET Predictor software (Version 9.5, Simulation Plus, USA) were used as inputs to classify compounds in the refined Developability Classification System (rDCS). In addition, dissolution conditions and measured IDR values of drugs after co-milling were used as inputs in the excel sheet enclosed to the paper of Dressman and colleagues (Beran et al., 2023). By assuming non sink conditions in vivo, target particle radii were calculated using the IDR based dissolution permeation balance. If the calculated r_{target} was < 30 µm, the assumption $h_{particle} = r_0$ was used and if the calculated r_{target} was ≥ 30 µm, the assumption $h_{particle}$ = 30 µm was applied. Obtained particle radii were compared to measured drug particle sizes in co-milled formulations for the evaluation of absorption risks of orally administered co-milled drug material.

4.4 Results and discussion

4.4.1 Influence of co-milling on the dissolution of poorly water-soluble drugs

The *in vitro* dissolution profiles of 13 poorly water-soluble drugs in different formulations are presented in Figure 4-1. Co-milling resulted in increased dissolution for all drug-excipient combinations, with significantly higher dissolved drug concentrations observed after 15 and 60 minutes of dissolution ($p < 0.05$), compared to unmilled drug powder. Compared to the physically blended mixtures of drug and excipient, co-milling with croscarmellose sodium or sodium starch glycolate also resulted in a significantly higher dissolved drug concentration after 15 and 60 min dissolution among all 13 drugs. In the case of co-milled mixtures with crospovidone, 12 out of 13 drugs showed higher apparent concentrations at both dissolution time points compared to the equivalent physically blended drug-excipient mixtures. However, for mefenamic acid, the dissolved drug concentration was not significantly higher relative to physical mixtures at the 15 min time point. Mefenamic acid is the only glass-forming ability (GFA) class I drug within the group of model drugs evaluated and also has the smallest molecular weight within the set (241.29 g/mol) (Table 4-1) (Alhalaweh et al., 2014; Slámová et al., 2021). This observation, albeit for one of the excipients, may indicate that the extent of milling-induced disorder or formation of glassy regions on drug particle surfaces, which typically enhances dissolution rate, may be less pronounced in the case of the GFA class I drug mefenamic acid compared to the other GFA class II and III drugs investigated in this study.


Apremilast
···FaSSIF solubility: 31.5 µg/ml
Dasatinib
···FaSSIF solubility: 53.1 µg/ml
Deferasirox
···FaSSIF solubility: 78.5 µg/ml
Dipyridamole
···FaSSIF solubility: 16.9 µg/ml
Gefitinib
···FaSSIF solubility: 76.4 µg/ml
Griseofulvin
···FaSSIF solubility: 17.5 µg/ml
Indapamide
···FaSSIF solubility: 100.2 µg/ml
Mefenamic acid
···FaSSIF solubility: 42.5 µg/ml
Drug Dissolved [%]
Time [min]
Co-milled mixture with croscarmellose sodium (1:2)
Physically blended mixture with croscarmellose sodium (1:2)
Co-milled mixture with sodium starch glycolate (1:2)
Physically blended mixture with sodium starch glycolate (1:2)
Co-milled mixture with crospovidone (1:1)
Physically blended mixture with crospovidone (1:1)
Milled drug without excipient
Drug powder as received
Drug solubility in FaSSIF, 37°C

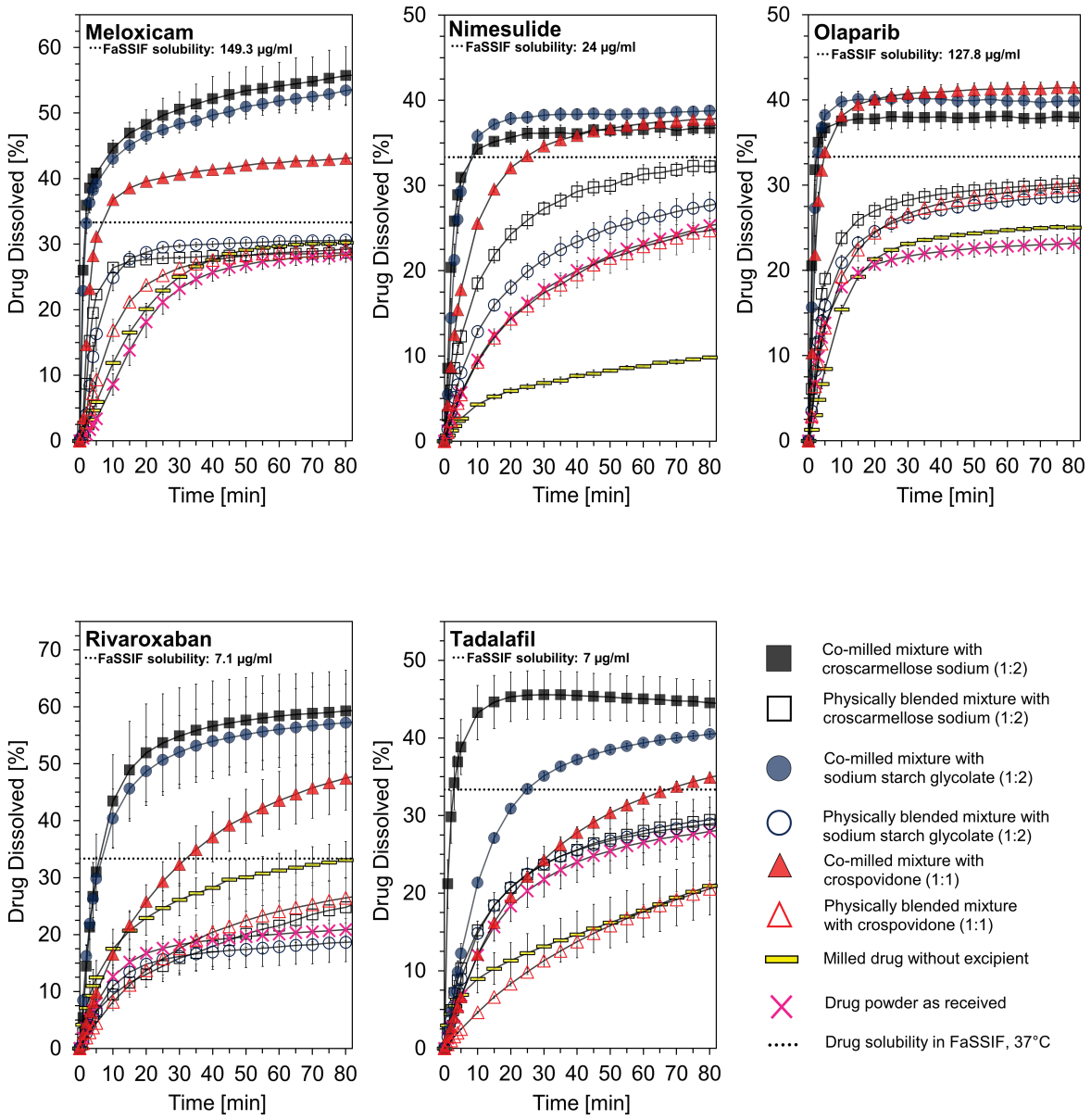


Figure 4-1: In vitro Dissolution profiles of thirteen poorly water-soluble drugs in different formulations (n = 3). Drugs were dissolved in Fasted State Simulated Intestinal Fluid (FaSSIF) as binary co-milled and physically blended mixtures with croscarmellose Sodium (black squares) and sodium starch glycolate (blue circles) in a drug to excipient ratio of 1:2 (w/w), as well as with crospovidone (red triangles, drug to excipient ratio 1:1 (w/w)). All drugs were also tested as milled powder without excipient (yellow quadrangles) and as drug powder used as received (pink crosses). The black dotted line represents the thermodynamic solubility of the respective compounds in FaSSIF. A drug amount three times the previously measured thermodynamic solubility of each drug was added to initiate dissolution.

Comparing milling alone to co-milling with excipient, the addition of croscarmellose sodium or sodium starch glycolate to the drug milling process led in all cases to a dissolution enhancement at the 15 min and 60 min dissolution timepoint ($p < 0.05$). Crospovidone was also effective as a co-former, with 11 out of 13 drugs showing significantly higher amounts dissolved at the 15 and 60 min dissolution timepoint, relative to milling without excipient addition ($p < 0.05$). Non-significant concentration differences were firstly observed in the case of deferasirox at the 15 min as well as the 60 min dissolution time point. Deferasirox is an acid so predominantly exists in its charged state in the dissolution medium at pH 6.5 (Remko, 2009; Steinbrueck et al., 2021). The high polarity of this acidic compound may have potentially reduced the impact of hydrophilic co-formers on dissolution enhancement in aqueous medium. In the case of rivaroxaban, no significant differences were observed between milling alone and co-milling blends at the 15 min timepoint but were evident at the 60 min time point.

Table 4-2: List of screened compounds in the study. The 13 compounds were selected based on their physicochemical properties, with poor water solubility as the primary criterion, and additional requirements including a diverse range of molecular weights (MW) (241.3 – 504.6 g/mol) and lipophilicity (cLogD6.5 1.16 – 3.63). The onset of the melting point (T_m) as well as the midpoint of the glass transition temperatures (T_g) were measured via differential scanning calorimetry and used to calculate the ratio of both (T_g/T_m). The glass-forming ability (GFA) classes were determined according to (Baird et al., 2010). For every drug, the particle size before its use was measured and the polymorph determinations were performed after evaluation of X-Ray diffraction patterns which were aligned with published data. Further abbreviations were used: Calculated log$D_{6.5}$ (c$LogD_{6.5}$); Molecular weight (MW).

Compound name	**Polymorph**	**D90 particle size [µm]**	**T_m [°C]**	**T_g [°C]**	**T_g/T_m**	**GFA class**	**c$LogD_{6.5}$**	**MW [g/mol]**
Apremilast	Form B	32.1	157.7	75.6	0.81	3	1.81	460.5
Dasatinib	Form C	10.2	281.8	127.2	0.72	3	2.30	488.0
Deferasirox	Form A	16.8	263.6	104.1	0.71	3	1.16	373.4
Dipyridamole	Form II	205.9	163.3	40.5	0.72	2	2.96	504.6
Gefitinib	Form I	191.4	191.1	67.1	0.74	2	3.63	446.9
Griseofulvin	Form I	43.5	214.8	91.3	0.75	2	2.51	352.8
Indapamide	Form I	15.7	159.1	105.1	0.88	3	2.13	365.8
Mefenamic acid	Form I	173.5	228.1	-	-	1	2.36	241.3
Meloxicam	Form I	12.9	250.0	98.0	0.71	3	1.18	351.4
Nimesulide	Form I	84.9	145.8	21.1	0.71	2	2.45	308.3
Olaparib	Form A	488.5	205.8	96.6	0.78	3	2.26	435.1
Rivaroxaban	Form A	290.1	231.2	83.5	0.71	3	1.97	435.9
Tadalafil	Form A	152.9	298.9	139.0	0.72	3	1.60	389.4

In 33 out of 39 cases, drugs in co-milled formulations exceeded the previously measured thermodynamic crystalline solubility of the pure drug compound. Milling-induced disorder may be a major driving force behind the observed spring effect, potentially supported by swelling and wicking effects from the crosslinked polymers to enhance the wettability of the drug particle surfaces. It also cannot be ruled out that milling reduced some particles to the nanoscale, which would further promote supersaturation. Additionally, it cannot be excluded that the

thermodynamic solubility of some drugs was slightly underestimated, as true equilibrium may require a prolonged time to establish. The excipient matrix may have inhibited the aggregation of these finely crushed drug particles, as none of the milled drugs without excipient exhibited supersaturation during the dissolution experiments. However, the complexity and heterogeneity of the underlying mechanisms make it challenging to pinpoint a definitive explanation for excipient effects during co-milling and dissolution, and current interpretations remain largely speculative. Future mechanistic studies could therefore aim to quantify the degree of milling induced disorder using a combination of X-ray powder diffraction, differential scanning calorimetry, and Raman spectroscopy following co-milling, or investigate the presence of drug nanoparticles using imaging techniques such as scanning electron microscopy.

While the majority of co-milled blends successfully promoted supersaturation, it is also noteworthy that this was not followed by rapid precipitation of supersaturated drug within the timeframe of the dissolution studies conducted. This behaviour is best exemplified by apremilast co-milled with sodium starch glycolate and croscarmellose, where a pronounced ‘parachute’ effect is observed. While the parachute effect is more frequently observed with hydrophilic polymers like PVP and HPMC, which can stabilize drugs in a supersaturated state, its occurrence in crosslinked excipients, known for their poor solubility, is less commonly documented. However, since the dissolution studies were conducted in FaSSIF, this micelle-rich environment may have facilitated enhanced interactions between the drug and the crosslinked polymer, leading to the stabilization of the supersaturated state. Nevertheless, further mechanistic studies are needed to better understand the factors and interactions contributing to maintained supersaturation effect in co-milled formulations with superdisintegrants.

Griseofulvin co-milled with crospovidone was one of 6 formulations (out of 39) that did not exceed the measured thermodynamic solubility during dissolution experiments. While griseofulvin was reported in some studies as non-glass former (Alhalaweh et al., 2014; Baird

et al., 2010), other studies reported a glass forming ability for griseofulvin (Blaabjerg et al., 2018; Mahlin and Bergström, 2013). In the present study, the DSC cycles of griseofulvin showed properties of a non-stable glass former (GFA II) (table 4-2). The apparently poor glass forming ability of griseofulvin may be a reason for the lack of supersaturation after crospovidone co-milling. Co-milled griseofulvin with the other two excipients exceeded the thermodynamic solubility to a minor extent. Moreover, the previously discussed non-glass former mefenamic acid did not exceed the thermodynamic solubility in all co-milled formulations throughout the entire *in vitro* dissolution experiments. In the case of deferasirox, only sodium starch glycolate containing co-milled mixtures exceeded the thermodynamic solubility of the compound. The underlying mechanisms remain unclear, particularly with regard to why supersaturation is observed exclusively in the co-milled formulation of deferasirox with sodium starch glycolate, while no such effect is seen with the other excipients tested.

This study demonstrated that milling the drug alone negatively impacted dissolution for 5 of 13 drugs, relative to unmilled drug, considering the 15 min and 60 min dissolution timepoint. While it might have been expected that the disorder generated by milling would increase the dissolution rate, a potential explanation for the observed results for apremilast, gefitinib, griseofulvin, indapamide and nimesulide could be the particle agglomeration into compacts during the milling process, which may have decreased the surface area available for dissolution. In these cases, the milling compacts seemed to reduce the dissolution rate more than the disorder in the crystal lattice increased it. A similar phenomenon was observed in other studies (Pätzmann et al., 2024; Zimper et al., 2010a).

4.4.2 Influence of superdisintegrant selection on the initial drug release from co-milled formulations

Co-milling with superdisintegrants may have a pronounced effect on the initial part of the drug dissolution process because the swelling effect is expected to be most prominent at this stage. Moreover, any milling induced crystal lattice disorder on crushed drug particle surfaces may similarly have a bigger impact on the beginning of the dissolution process and may differ with the excipient selection. To capture this, the area under the first 5 min *in vitro* dissolution curve by including concentration measurements every 30 s were normalised to compare the effect of different preparations on every drug (Figure 4-2).

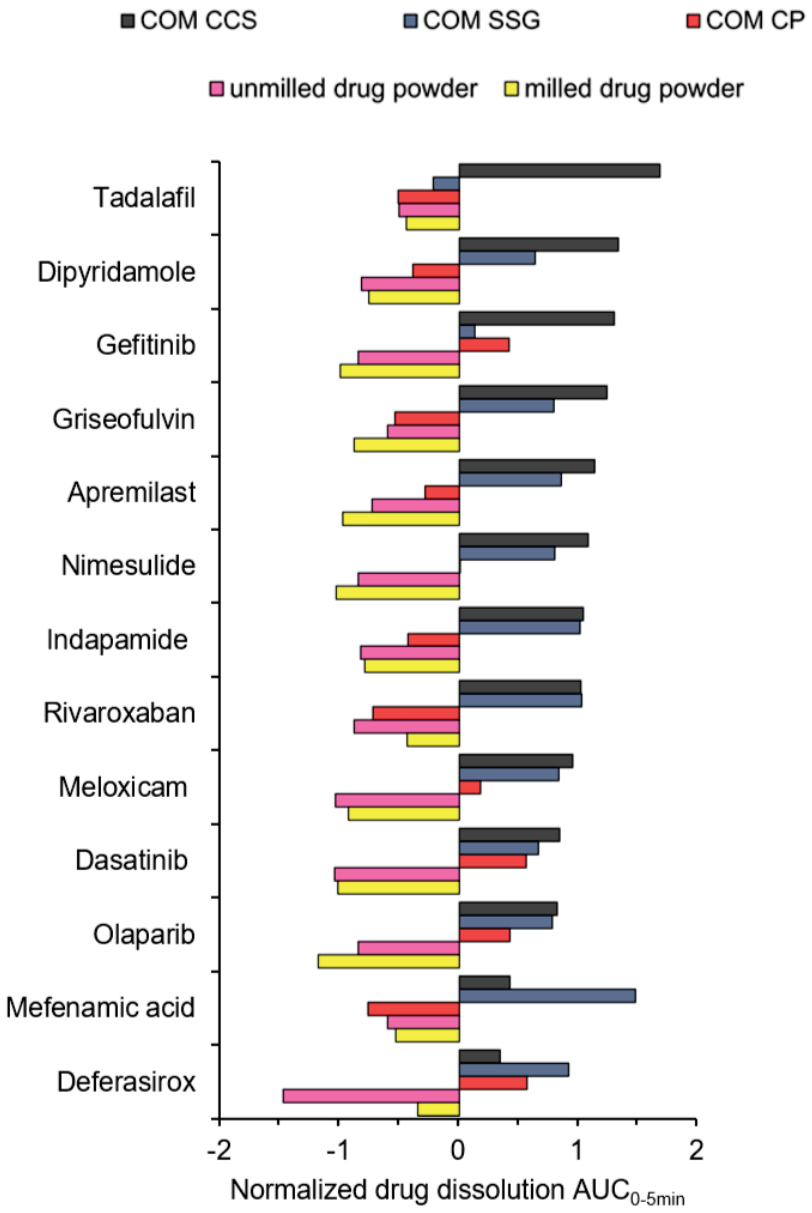


Figure 4-2: A z-Standardisation was applied for the normalisation of initial dissolution performances to compare different preparations of every drug (n = 3). The drug dissolution $AUC_{0\text{-}5min}$ was normalized to the mean for every investigated drug, based on measured dissolved drug concentrations every 30 s in the first 5 min. A normalized value above zero for a formulation indicates that the drug dissolved to a greater extent compared to the average of the five different preparations of this compound. Hence, values below zero indicate a lower extent of dissolution relative to the average. The following abbreviations were used: Co-milling with croscarmellose sodium (COM CCS); co-milling with sodium starch glycolate (COM SSG); co-milling with crospovidone (COM CP).

Figure 4-2 shows that all co-milled formulations of croscarmellose sodium (black) and sodium starch glycolate (blue) have a positive normalized value, which indicates a higher dissolution $AUC_{0\text{-}5min}$ compared to the average of the five preparations of each drug. Unmilled (pink) and milled drug alone (yellow) have for every drug negative value and consequently a lower measured $AUC_{0\text{-}5min}$ compared to the average of the five preparations. Normalized values of co-milling with crospovidone (red) led for 5 drugs to positive and in 8 cases to negative values. The sums of these normalized values are presented in table 4-3 and made it possible to create an overall ranking of the efficiency of used excipients in co-milled formulations as follows: Croscarmellose sodium (13.94) followed by sodium starch glycolate (10.24) and crospovidone (-1.57). The proposed mechanism of action for crospovidone differs significantly from that of sodium starch glycolate and croscarmellose sodium. While the latter two primarily facilitate tablet disintegration through swelling upon water uptake, crospovidone acts mainly via shape recovery (elastic expansion) (Quodbach and Kleinebudde, 2015). This mechanistic difference is reflected in its water uptake behavior: crospovidone exhibits less than half the water absorption compared to sodium starch glycolate and croscarmellose sodium, which may be attributed to its distinct disintegration mechanism (Quodbach and Kleinebudde, 2014). This difference in mechanism and lower water uptake potential may contribute to the generally lower dissolution enhancement of co-milled drugs with crospovidone in the early stages of dissolution.

Interestingly, for the two acidic compounds investigated in this study (deferasirox and mefenamic acid), sodium starch glycolate proved to be the most effective co-milling co-former in terms of improving dissolution, as shown in Figure 4-2. The mechanistic explanation may lie in the different chemical nature of these two crosslinked polymers. While sodium starch glycolate is produced by crosslinking starch, croscarmellose sodium undergoes carboxymethylation prior to crosslinking the cellulose backbone, resulting in a higher degree of substitution and thus a greater anionic charge density (Berardi et al., 2022). These structural differences may influence drug release behavior after co-milling. Acidic compounds, being

negatively charged at pH 6.5, may experience electrostatic repulsion from the highly anionic croscarmellose sodium, potentially leading to improved release when formulated with the less charged sodium starch glycolate. In contrast, basic drugs, which are positively charged under the same conditions, may form favorable ionic interactions with croscarmellose sodium, supporting enhanced dispersion and dissolution. Neutral compounds, lacking charge-based interactions, may therefore primarily benefit from the pronounced swelling capacity and porous matrix formation of croscarmellose sodium, which may facilitate faster water penetration and diffusion-driven release. Milling the drug without excipient led to a summed standardized $AUC_{0\text{-}5\ min}$ value of -11.68 which was on a similar level to the unmilled drug (-10.93).

Table 4-3: Sum of normalized drug dissolution from different preparations. The area under the first 5 min in vitro dissolution ($AUC_{0\text{-}5min}$) was z-standardised and the sum for all 13 drugs are depicted in the table.

Preparation	**Sum of normalized $AUC_{0\text{-}5min}$ drug dissolution**
Co-milling with croscarmellose sodium	13.94
Co-milling with sodium starch glycolate	10.24
Co-milling with crospovidone	-1.57
Drug milling without excipient	-11.68
Unmilled drug	-10.93

4.4.3 Statistical analysis to identify relationships between drug properties and Co-milling-induced Intrinsic Dissolution Rate enhancement

Measured IDR values of investigated drugs in different formulations are presented in table 4-4. The co-milling step led in all 39 drug-excipient combinations to a higher measured powder IDR compared to the unmillled, crystalline drug.

Table 4-4: Powder Intrinsic Dissolution Rates (pIDR) [mg/min/cm^2] of all screened compounds in Fasted State Simulated Intestinal Fluid of drug powder, milled drug and co-milled drugs with Croscarmellose Sodium (CCS, drug to excipient ratio 1:2), Sodium Starch Glycolate (SSG, drug to excipient ratio 1:2), and Crospovidone (CP, drug to excipient ratio 1:1) (n = 3).

Drug Compound	**pIDR drug [mg/min/cm^2]**	**pIDR milled drug [mg/min/cm^2]**	**pIDR COM CCS [mg/min/cm^2]**	**pIDR COM SSG [mg/min/cm^2]**	**pIDR COM CP [mg/min/cm^2]**
Apremilast	1.81 ± 0.01	1.53 ± 0.32	3.04 ± 0.03	2.98 ± 0.02	2.67 ± 0.04
Dasatinib	2.27 ± 0.26	2.45 ± 0.27	4.26 ± 0.06	4.22 ± 0.04	4.39 ± 0.19
Deferasirox	3.99 ± 0.32	4.86 ± 0.45	5.33 ± 0.09	6.19 ± 0.08	4.96 ± 0.14
Dipyridamole	0.44 ± 0.00	0.43 ± 0.02	1.44 ± 0.01	1.39 ± 0.02	1.28 ± 0.00
Gefitinib	5.48 ± 0.21	3.88 ± 0.05	7.13 ± 0.07	6.86 ± 0.03	6.22 ± 0.01
Griseofulvin	0.81 ± 0.01	0.63 ± 0.04	1.34 ± 0.01	1.24 ± 0.00	1.14 ± 0.00
Indapamide	8.46 ± 0.43	4.33 ± 0.82	9.10 ± 0.02	9.61 ± 0.02	9.27 ± 0.02
Mefenamic acid	2.47 ± 0.21	2.69 ± 0.29	3.04 ± 0.10	3.21 ± 0.01	3.28 ± 0.06
Meloxicam	8.63 ± 0.22	8.64 ± 0.17	11.23 ± 0.43	11.17 ± 0.12	10.43 ± 0.14
Nimesulide	1.54 ± 0.04	0.84 ± 0.00	2.01 ± 0.03	2.01 ± 0.04	1.98 ± 0.01
Olaparib	8.29 ± 0.13	8.56 ± 0.01	9.38 ± 0.06	9.78 ± 0.12	9.95 ± 0.03
Rivaroxaban	0.41 ± 0.01	0.55 ± 0.05	0.83 ± 0.22	0.77 ± 0.31	0.70 ± 0.17
Tadalafil	0.28 ± 0.02	0.31 ± 0.05	0.55 ± 0.11	0.60 ± 0.01	0.57 ± 0.12

The structural diversity of drug compounds in this study was investigated in figure 4-3, prior to the subsequent statistical analysis relating to the co-milling-induced gain in IDR. A wide distribution of compounds on the PCA-X graph on the first and second principal component suggests a high structural diversity of drugs, regarding molecule size, lipophilicity, and the measured solubility as well as melting points of screened drugs. This is a desired prerequisite to increase the reliability of a subsequent statistical analysis. Moreover, a PCA-X graph allows the classification of drugs, which was performed in figure 4-3 by marking high and low co-milling induced IDR ratios. Interestingly, the classification led to a separation of drugs with a high IDRR (orange circles) from candidates with a low IDRR (black). Consequently, a more detailed analysis was performed in figure 4-4 by investigating Pearson correlations of single drug substance properties and the IDRR among different co-milled formulations.

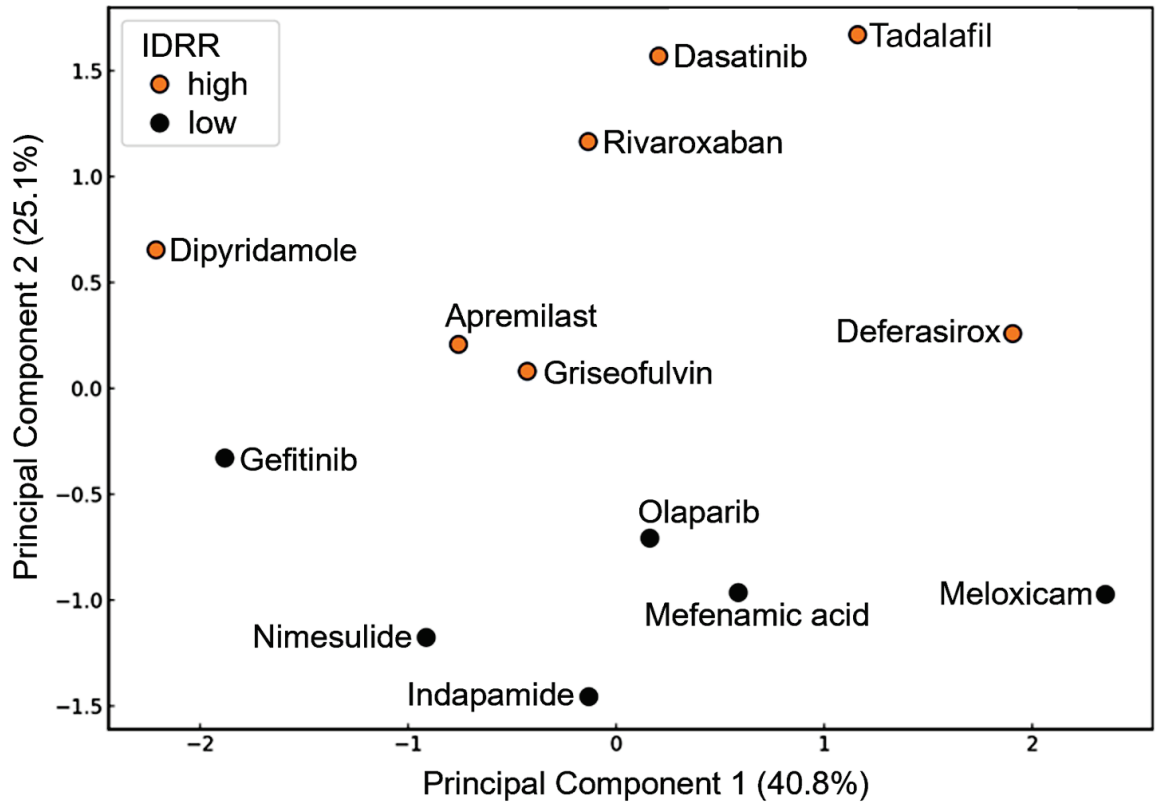


Figure 4-3: Scores plot of a Principal Component Analysis (PCA) based on drug substance properties. Input variables of the PCA-X refer to the lipophilicity and size of drug molecules as well as their solubilities and melting points to investigate the structural diversity of screened compounds. Compounds whose average intrinsic dissolution rate ratio (IDRR) after co-milling is below the median value among

the dataset are marked black, whereas drugs whose IDRR ≥ the median value are depicted as orange circles.

Molecular weight of the drug, as well as the Polar Surface Area (PSA) were found to be positively correlated with the IDRR of co-milled samples. The IDR gain typically results from crystal lattice disorder i.e. amorphous/glassy-like regions induced by milling. Studies empirically determined an approximate threshold value of a molecular weight of 300 g/mol above which compounds tend to be glass-formers (Alhalaweh et al., 2014; Wyttenbach et al., 2016). However, this data was determined on the "thermodynamic pathway" by quench cooling a melt of a drug and evaluating the recrystallization behaviour. Milling induces disorder mechanically by gradually inducing defects in the crystal lattice on the "kinetic pathway" (Blaabjerg et al., 2017b). The data also indicates that on the kinetic pathway, the size and complexity of molecules play a crucial role in determining the extent of generated disorder on drug particle surfaces.

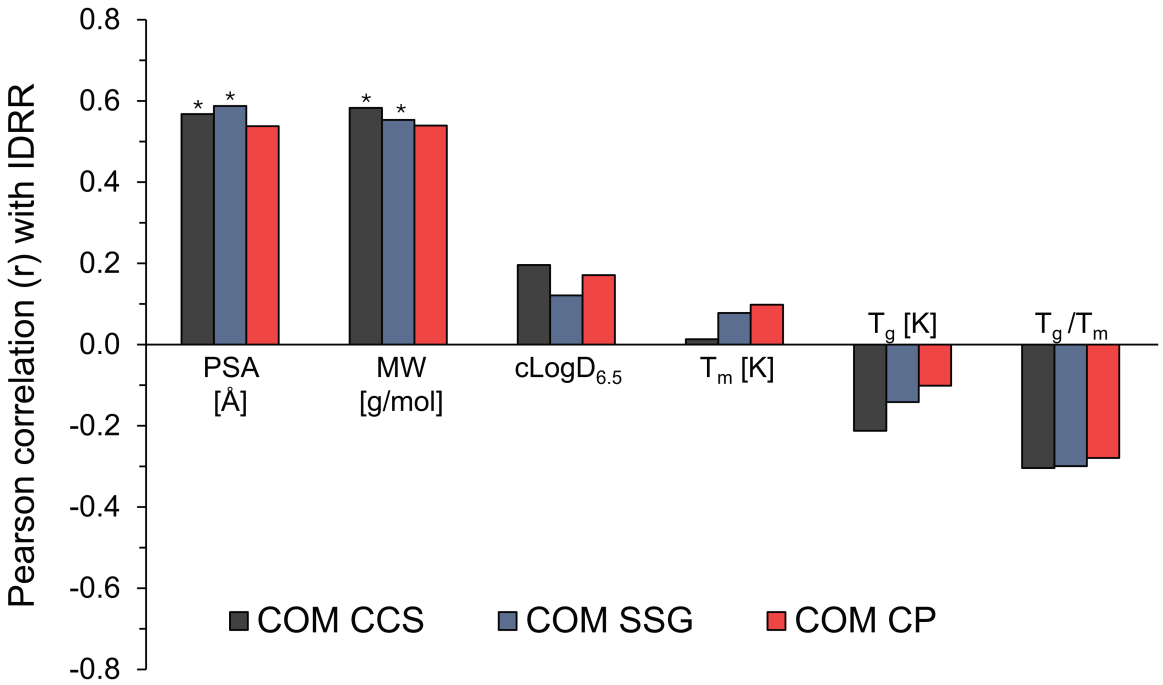


Figure 4-4: Pearson correlations of different single drug properties with the Intrinsic dissolution rate ratio (IDRR), which describes the ratio of the IDR of a co-milled drug divided by the IDR of unmilled drug powder. Following abbreviations were used: Polar Surface Area (PSA); Molecular Weight (MW);

Calculated logarithm of the distribution coefficient (Octanol/water) at pH 6.5 (cLogD6.5); Melting point (T_m); Glass transition temperature (T_g); Co-milling with croscarmellose sodium (COM CCS); Co-milling with sodium starch glycolate (COM SSG); Co-milling with crospovidone (COM CP).

The T_m and the T_g did not correlate strongly with the drug IDR gain after co-milling, independently of the used co-former (figure 4-4). It has also been reported that the T_m and the T_g did not correlate with classes of glass forming ability (Baird et al., 2010). However, previous studies could show that the location of the T_g in relation to the milling temperature plays a crucial role in determining the extent to which disorder on drug particles is retained or restored (Descamps et al., 2007; Pätzmann et al., 2025). Since none of the investigated drugs have a T_g significantly below the milling temperature, this relationship might not be reflected in this analysis (table 4-2).

The T_g/T_m ratio contributed for all co-formers weakly negative to the IDR gain without showing statistical relevance ($p > 0.05$). This is rather unexpected since a higher T_g/T_m would have an expected higher glass forming ability, but this original observation was not in the context of co-milling, nor does it account for the complexity of excipient effects (Baird et al., 2010; Turnbull, 1969).

4.4.4 Using the refined Developability Classification System to assess the impact of co-milling on dissolution rate limited absorption

The thirteen investigated drugs were classified in the refined Developability Classification System based (figure 4-5). Of these, 8 compounds were categorised as rDCS class IIa which indicates a dissolution rate-limited absorption after oral administration. For these rDCS class IIa compounds, a target particle radius was determined by applying the recently proposed equations in the framework of the rDCS (Beran et al., 2023) (table 4-5). Applying this approach, complete drug absorption after oral administration is expected for dissolution rate-limited compounds when the drug particle size is below the calculated target particle radius.

Conversely, if the particle size of an rDCS class IIa candidate exceeds the calculated target radius, the risk of incomplete oral absorption is expected to persist.

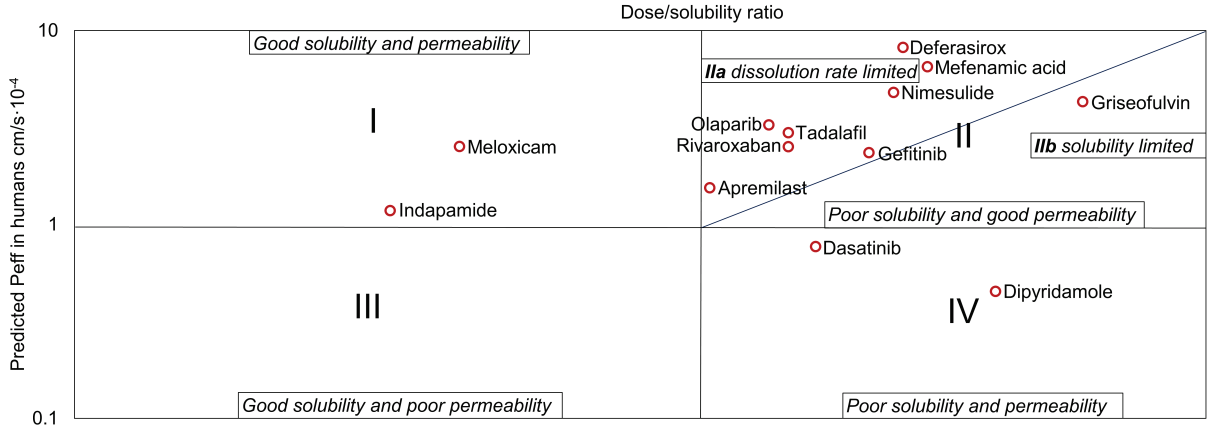


Figure 4-5: The drugs examined in this study were categorised according to the refined Developability Classification System. Usual doses of these compounds in marketed orally administered drug formulations were used to classify the compounds.

Table 4-5: Overview of the 8 dissolution rate limited drugs (rDCS class IIa) investigated in this study. Calculated target particle radii to overcome dissolution limitations are presented next to actual measured drug particle sizes of these drugs in co-milled mixtures (COM). In addition, a dose diversity risk assessment was performed to determine the rDCS risk level classes of dissolution rate-limited drugs.

Compound	**rDCS risk level classification**	**Calculated target particle radius (r_{target}) [µm]**	**Measured drug particle size in COM [µm]**		
			COM CCS	**COM SSG**	**COM CP**
Apremilast	R2	23.9 - 25.5	5.0	5.1	6.9
Deferasirox	R1	47.8 - 59.7	5.6	5.1	5.6
Gefitinib	R1	148.3 – 170.0	4.1	4.4	4.6
Mefenamic acid	R1	47.3 – 51.0	6.5	6.0	8.1
Nimesulide	R2	29.8 – 30.0	5.8	6.3	6.4
Olaparib	R1	58.1 - 61.6	5.1	4.6	5.7
Rivaroxaban	R3	14.3 - 15.6	4.3	5.4	7.8
Tadalafil	R3	11.7 - 12.2	5.0	4.5	6.2

The measured drug particle sizes in the co-milled mixtures are in all cases smaller than the corresponding calculated target particle radii (table 4-5). For all risk level class 1 candidates, target particle radii exceeded measured sizes by significant margins, ranging from 8.5-fold ($r_{target,deferasiroxCOMCP}$ = 47.8 µm vs. $measured_{deferasiroxCOMCP}$ = 5.6 µm) to over 40-fold differences ($r_{target,gefitinibCOMCCS}$ = 170.0 µm vs. $measured_{gefitinibCOMCCS}$ = 4.1 µm). Smaller IDR based target particle radii were calculated for co-milled risk level 2 candidates apremilast and nimesulide. The differences between measured and calculated particle sizes are consequently lower but still range from 3.5-fold ($r_{target,apremilastCOMCP}$ = 23.9 µm vs. $measured_{apremilastCOMCP}$ = 6.9 µm) to more than 5-fold ($r_{target,nimesulideCOMCCS}$ = 30.0 µm vs. measured $_{nimesulideCOMCCS}$ = 5.8 µm). However, since the rDCS-based calculations yield particle radii while the measured values represent diameters, the actual differences are likely to be greater. Consequently, the dissolution limitations of these co-milled risk level 2 drugs are expected to be low.

Despite the significantly increased IDR resulting from co-milling of the risk level 3 candidates rivaroxaban and tadalafil (Table 4-4), the calculated target particle radii remain comparatively small, ranging from 11.7 to 15.6 µm. These small target particle sizes highlight the need for a carefully controlled milling process that prevents particle aggregation and yields in a highly fine powder. The use of milling aids, such as the excipients employed in this study, can help to inhibit particle aggregation (Przwara and Kwade, 2020). Consequently, the particle sizes achieved after co-milling were between 4.3 and 7.8 µm, which is still clearly below the calculated target radii and indicate complete absorption after oral administration.

While co-milling led to reduced particle sizes, the outcomes should be interpreted considering potential limitations, particularly for the risk level class 3 candidates rivaroxaban and tadalafil. Unexpected deviations from manufacturing specifications, such as particle agglomeration during milling or measurement uncertainties in IDR as well as particle size determination in this study could potentially lead to dissolution rate limitations for these two compounds. As a result, a residual risk of dissolution rate-limited oral absorption remains for co-milled rivaroxaban and tadalafil. Therefore, other formulation strategies such as nanosized drugs

prepared in a wet milling process, amorphous solid dispersions or lipid based formulations may need to be considered to further reduce the risk of incomplete oral absorption in these risk level 3 drug candidates.

The quantity of superdisintegrant plays a crucial role in determining whether a developed tablet exhibits fast or slow drug release. At an optimal concentration, superdisintegrants promote rapid water uptake and efficient tablet disintegration, resulting in fast drug dissolution and immediate release. When used in insufficient amounts, tablet disintegration can be delayed, leading to slower drug release. Conversely, excessive concentrations may cause gel formation or reduced tablet porosity, thereby hindering drug diffusion and slowing dissolution (Bolhuis et al., 1997). However, ball-milled materials may influence gel formation due to the presence of finely crushed particles; therefore, further investigation into the gel-forming behavior of co-milled drug materials containing different superdisintegrants is warranted to fully harness the potential of co-milling strategies.

Future work could also investigate the solid-state properties of selected drug–excipient combinations both before and after co-milling. This would enable a more mechanistic understanding of drug–excipient compatibility and provide insights into co-milling-induced lattice disorder and polymorph formation. Furthermore, co-milling stability studies could offer deeper insight into which compounds retain their solid-state characteristics and dissolution advantages over time.

4.5 Conclusion

The study showed that co-milling with superdisintegrants is a highly effective method to enhance *in vitro* dissolution rates for poorly water-soluble drugs. Among the disintegrants tested, croscarmellose sodium proved most effective for basic and neutral drugs, while sodium starch glycolate showed superior performance for acidic compounds. A positive correlation was observed between the improvement in intrinsic dissolution rate (IDR) and the drug's molecular weight and polar surface area. Finally, the rDCS based analysis revealed that co-milling with superdisintegrants appeared to be effective for reducing the risk of incomplete drug absorption after oral administration for dissolution rate-limited (rDCS Class IIa) drugs, particularly in the case of drugs considered to be risk level R1 and R2. The findings also suggest that this approach holds promise for addressing dissolution challenges in rDCS risk level 3 drugs. However, due to the very small target particle sizes required for these candidates, additional formulation strategies may be necessary. Overall, the results highlight co-milling with disintegrants as a practical and effective method within the rDCS framework to mitigate the risk of dissolution-limited oral drug absorption.

University College Cork, Ireland
Coláiste na hOllscoile Corcaigh

CORA
Cork Open Research Archive
Cartlann Taighde Oscailte Chorcaí

Pätzmann, N. 2025. Exploring co-milling as a strategy to improve the dissolution of poorly water-soluble drugs. PhD Thesis, University College Cork.

Please note that Chapter 5 (pp. 110-125) is unavailable due to a request by the author.

CORA Cork Open Research Archive http://cora.ucc.ie

Chapter 6: Thesis discussion

6.1 Overview and Summary

Insufficient dissolution in gastrointestinal fluids remains a major limitation to the oral absorption and therapeutic performance of numerous drug candidates in the development pipeline. (Vinarov et al., 2021). The DCS serves as a framework for the early identification of drug candidates with limitations in oral drug absorption during preclinical development (Butler and Dressman, 2010b). Building on this foundation, recent advancements have introduced more refined strategies identifying these drug candidates with dissolution rate limitations and to guide suitable formulation approaches that possibly enable effective drug absorption (Beran et al., 2023; Rosenberger et al., 2018; Beran et al., 2024a, 2024b).

While drug milling remains the standard technique for reducing particle size in the pharmaceutical industry, co-milling of drugs with excipients has been shown to further improve dissolution characteristics under in vitro conditions (Caron et al., 2013; Isaac et al., 2016b; Varghese and Ghoroi, 2017). Consequently, selected co-milled formulations identified through in vitro testing were evaluated in vivo, where improvements in the bioavailability of poorly water-soluble drug candidates could be observed (Kasten et al., 2018). The mechanisms proposed to explain these in vivo benefits are diverse. On one hand, the stabilization of disorder/amorphization induced during milling by the presence of the excipient has been reported (Shi et al., 2022). Additionally, enhanced particle size reduction when milling in the presence of excipients, and improved wetting of poorly soluble drugs co-milled with hydrophilic carriers, are also considered important contributing factors for improved bioavailability (Kubo and Mizobe,1997).

Co-milling represents a practically simple technique that can be readily integrated into industrial processes. Its ability to operate without solvents and to run entirely on prospectively sustainable generated electrical energy, makes it particularly appealing in the context of a more environmentally responsible pharmaceutical industry. However, despite its practical advantages, the mechanochemical transformations that occur during milling are highly

complex, especially in the presence of excipients. This complexity leads to limited predictability of the process outcomes and continues to hinder its broader implementation in pharmaceutical development.

Based on these considerations, this thesis firstly aimed to establish a data-driven approach to support the understanding and predictivity of co-milling for poorly water-soluble drugs. A dataset of 29 structurally diverse drug compounds was assembled and explored for predictive relationships. The objective was to relate drug properties with improved dissolution when co-milled with the widely used hydrophilic polymer PVP. This strategy aims to reduce reliance on trial and error during preclinical development by enabling prediction of co-milling success for novel compounds. The second objective was to support rational excipient selection by evaluating the performance of different polymers across a range of drug compounds and assess their biopharmaceutical relevance. Third, the aim was to investigate co-milling–related phenomena in more detail using selected drug candidates, with a particular focus on the generation of lattice disorder, the induction of drug supersaturation, and the stability of such disordered formulations. Finally, the objective was to assess the influence of drug particle size reduction in the presence of a polymer during the milling process, in order to provide guidance for industrial scientists developing co-milling processes.

The experimental work addressing these goals was described in the previous chapters. The following section presents a combined discussion of the main results and places them in the context of current scientific knowledge.

6.2 Identification of suitable drug candidates for co-milling

With the increasing focus on advancing artificial intelligence tools in formulation development, one of the objectives of this thesis was to explore the potential of machine learning techniques to provide predictive insights into co-milling as a strategy for enhancing drug dissolution rates. To this end, Chapter 2 presents the largest dataset of co-milled drugs reported in the literature to date, in terms of the number of drug substances investigated. The dissolution profiles of 29

different poorly water-soluble drugs were evaluated before and after co-milling with PVP. The ratios of measured drug concentrations at 15 and 60 min dissolution pre- and post-co-milling were used to identify the most influential drug descriptors contributing to co-milling induced dissolution enhancement via MLR and PLS regression. This analysis was based on 244 calculated molecular descriptors and measured physicochemical properties of the screened drug substances.

Among all variables, the median drug particle size (measured before milling) emerged as the most influential factor for co-milling-induced dissolution enhancement. This data-driven approach is consistent with theoretical understanding, given that co-milling inherently reduces particle size, thereby increasing surface area, a relationship described by the Noyes–Whitney and Nernst–Brunner equations, which link dissolution rate to surface area. (Brunner, 1904; Nernst, 1904). Drugs with larger initial particle sizes are more likely to experience significant surface area increases upon co-milling, resulting in greater enhancement of the dissolution rate.

Since the particle size is not an intrinsic molecular property, additional focus was placed on where this data-driven approach can uncover relationships between molecular descriptors and dissolution enhancement. Notably, the calculated logD at pH 6.5, a surrogate for the drug lipophilicity, was consistently among the top predictors in the models developed. A plausible mechanistic explanation is that co-milling may enhance drug wettability, particularly for lipophilic drug surfaces. Poor wettability is known to inhibit the dissolution process, and previous studies have demonstrated that embedding drug particles in a polymer matrix (via co-milling) can improve wettability (Gu et al., 2012; Maggi et al., 2013; Varghese & Ghoroi, 2017). Thus, lipophilic drugs with high logD6.5 values appear to benefit more from co-milling due to improved wettability and enhanced dissolution.

Another important molecular descriptor identified in Chapter 2 was Kappa 3, which was particularly influential at the 15 min dissolution time point. Kappa 3 is a topological descriptor that reflects molecular shape and complexity, incorporating atomic radii, topological path counts and molecular weight (Kier, 1985). Higher Kappa 3 values are indicative of more

complex molecular structures. Interestingly, Kappa 3 not only contributed to the predictive dissolution model but also correlated with co-milling-induced crystallinity loss as measured by XRPD (R^2 = 0.61). This suggests that structurally complex molecules may undergo greater degrees of amorphization and crystal lattice disorder during co-milling, thereby enhancing dissolution.

In Chapter 4, molecular descriptors related to drug molecular size were also found to significantly influence the outcomes of co-milling with superdisintegrants. This analysis focused on the enhancement of intrinsic dissolution rate (IDR), a surface-area-independent parameter that allows greater focus for the investigation of molecular effects. A positive Pearson correlation coefficient was found between molecular weight ($r = 0.61$, $p < 0.05$) as well as the polar surface area ($r = 0.62$, $p < 0.05$) with the co-milling-induced IDR gain, both indicating that larger molecules may benefit more from co-milling with superdisintegrants. The chapter also examined the role of the drug's T_g in IDR enhancement. No consistent correlation was found between T_g [K] and milling induced IDR gain across the three swellable excipients studied. This observation does not appear to align directly with previous findings (Blaabjerg et al., 2017; Descamps et al., 2007), which suggest that milling below a drug substance's T_g typically does not yield fully amorphous material, whereas milling above T_g can. Amorphous drug material typically has an increased dissolution rate. However, in the current study all drugs had T_g values above the ambient milling temperature. As a result, the relationship of the drug T_g and the milling induced intrinsic dissolution may not be captured in this analysis. In fact, in 10 out of 13 cases, co-milling with high-T_g compounds resulted in dissolved concentrations exceeding the thermodynamic solubility of the non-milled crystalline form, likely due to induced structural disorder. Exceptions included mefenamic acid, griseofulvin, and deferasirox, for which supersaturation was not achieved in any of the co-milled formulations. These three drugs share relatively low molecular weights (241.29 g/mol (mefenamic acid), 352.76 g/mol (griseofulvin), and 373.37 g/mol (deferasirox), suggesting that smaller molecules may be less responsive to co-milling in terms of achieving supersaturation.

6.3 Excipient selection in pharmaceutical co-milling

The selection of appropriate excipients is critical for the successful development of oral solid dosage forms containing co-milled drug materials. The data presented in this thesis support rational excipient selection, particularly for the use of hydrophilic polymeric excipients. Data from Chapter 2 and 4 show more than 65 drug–excipient combinations screened under consistent milling and dissolution conditions. Data using the same drugs from both chapters were used for the following section, enabling direct comparison of the dissolution behaviour of used excipients as co-milling co-former.

The initial phase of drug dissolution is crucial to ensure complete dissolution in gastrointestinal fluids. Hence, to assess the excipient performance, firstly the initial dissolution rate of drugs in dissolution experiments was used for the excipient comparison (table 6-1). Concentrations in solution were measured every 30 seconds and the slope of the linear regression for the first 7 measurement points i.e. first 3 min of dissolution was used as initial dissolution rate. In contrast to Chapter 4 of this thesis, where the $AUC_{0\text{-}5min}$ was used to evaluate the initial dissolution performance of superdisintegrants, we employ the slope of the linear regression in this section for comparison. The slope directly reflects a dissolution rate and is therefore more intuitive, as it allows a clear interpretation of how much more of the dose is released per minute as a result of co-milling. All linear regressions to extract a dissolution rate have R^2 values above 0.9.

Table 6-1: Initial dissolution rate, using the linear initial dissolution slope of the first 3 minutes from the dissolution profile of drugs in various preparations. Drugs powders in either unmilled or milled form (without excipients) were compared with co-milled mixtures. Excipients used in co-milled mixtures include Croscarmellose Sodium (CCS), Polyvinylpyrrolidone K25 (PVP), Sodium Starch Glycolate (SSG), and Crosslinked Povidone (CP).

Drug substance	**Initial dissolution rate [µg/mL/min]**					
	Drug Powders		Co-milled mixtues			
	Unmilled	Milled	CCS	PVP	SSG	CP
Apremilast	1.5	0.03	**15.7**	6.0	13.4	4.5
Dasatinib	3.3	3.5	**17.3**	10.3	16.7	15.2
Deferasirox	9.9	12.8	14.1	**16.6**	15.1	7.5
Dipyridamole	0.5	0.6	**5.5**	1.6	4.0	1.4
Griseofulvin	1.7	1.2	**5.3**	4.7	4.8	1.8
Mefenamic acid	0.9	1.0	2.7	3.0	**5.5**	0.4
Nimesulide	0.9	0.4	6.7	**7.0**	5.4	3.1
Olaparib	13.3	6.3	**45.9**	33.1	44.1	38.4
Rivaroxaban	0.4	0.6	**1.6**	0.7	1.5	0.5
Tadalafil	0.3	0.4	**2.2**	0.5	0.5	0.3

Co-milling improved the initial dissolution rate in most of the cases compared to the unmilled and milled drug powder without excipient. Notably, CCS exhibited the highest initial dissolution rate for 7 out of 10 co-milled drugs, suggesting that the swelling capacity of superdisintegrants may be preserved post co-milling (table 6-1). This, in addition to induced disorder on drug

particles and particle size reduction, appears to positively influence dissolution performance. Interestingly, for the two acidic model compounds, CCS did not yield the best results. For mefenamic acid, sodium starch glycolate (SSG) led to a higher initial dissolution rate, and for deferasirox, polyvinylpyrrolidone (PVP) performed best. However, SSG also outperformed CCS for deferasirox, indicating potential interactions between acidic functional groups and the crosslinked matrices of SSG and CCS. These findings warrant further investigation to clarify the mechanistic basis of these effects.

Crospovidone (CP) also enhanced initial dissolution in most cases compared to milling alone. However, CP showed the slowest overall initial dissolution enhancement among the tested excipients and, in some instances (mefenamic acid, rivaroxaban, tadalafil), even resulted in lower initial dissolution rates than pure drug powders.

Another important parameter of tested excipients is the comparison of the highest drug concentration (c_{max}) observed in the dissolution profiles following co-milling with the selected hydrophilic polymers, since it may indicate the polymers property to stabilize disorder on the drug particles. In all cases, co-milled mixtures reached higher c_{max} values than any of the respective controls, including the drug alone and the drug milled alone (table 6-2). This indicates that co-milling has a distinct effect beyond simple particle size reduction. It may contribute to the stabilization of amorphous domains within the excipient matrix or promote the dispersion of nanofragments formed during milling. Both mechanisms could enhance the apparent solubility and subsequently increase the maximum achievable drug concentration during dissolution testing.

When the results are analysed by excipient it was evident that CCS and SSG achieved the highest c_{max} values in 6 out of 10 drugs while the Povidone based polymers PVP and CP achieved the highest c_{max} for two drugs. Similar to the results for initial dissolution, CCS was not the most effective excipient for the acidic drugs deferasirox and mefenamic acid. However, the difference for deferasirox with SSG as co-former to the CCS performance was bigger compared to the benefits of PVP for mefenamic acid compared to CCS (table 6-2).

Table 6-2: The peak concentration (c_{max}) of drugs during biorelevant dissolution testing using various preparation methods. Drugs were tested either as pure powders, in their unmilled form or after undergoing a milling process (milled), without excipients. Additionally, binary mixtures of the drug with excipients were prepared in fixed drug-to-excipient ratios, either as physical blends or co-milled formulations. The excipients used in the binary mixtures included Croscarmellose Sodium (CCS), Polyvinylpyrrolidone K25 (PVP), Sodium Starch Glycolate (SSG), and Crosslinked Povidone (CP).

Drug Substance	**Highest drug concentration (c_{max}) during dissolution testing [µg/mL]**					
	Drug Powders		Co-milled mixtues			
	Unmilled	Milled	CCS	PVP	SSG	CP
Apremilast	26.9	20.6	**49.6**	41.0	46.4	41.0
Dasatinib	35.2	37.5	67.3	58.7	**70.1**	66.8
Deferasirox	63.9	70.1	76.7	74.0	**90.2**	73.5
Dipyridamole	6.3	6.1	**22.7**	20.6	22.2	20.0
Griseofulvin	13.5	9.4	**19.1**	**18.9**	**19.0**	17.2
Mefenamic acid	28.7	32.4	38.7	**42.5**	41.0	40.7
Nimesulide	18.9	7.5	**26.7**	25.3	**28.0**	**27.5**
Olaparib	89.6	97.1	146.3	142.8	**154.4**	**159.4**
Rivaroxaban	4.5	7.1	**12.5**	8.5	**12.1**	10.3
Tadalafil	6.0	4.7	**9.6**	8.4	8.6	7.5

Linear excipients as co-milling excipients are typically water soluble and dissolve readily, thereby potentially promoting drug dissolution and stabilizing supersaturated solutions, an effect that is well established for PVP (Bolourchian et al., 2019b; Caron et al., 2013). In contrast, for insoluble crosslinked excipients, one would expect that the excipient does not

dissolve and therefore would not contribute to the stabilization of drug supersaturation. Interestingly, drug supersaturation has also been observed in the presence of crosslinked polymers, and in some cases the supersaturated state remains stable in solution.

At higher concentrations of crosslinked polymers, gel formation can occur. This phenomenon has not yet been observed in studied co-milled systems, suggesting that a more detailed investigation of the structure of the milled crosslinked co-milled products is required. Such structural insights may reveal additional mechanisms contributing to supersaturation stabilization. Overall, these findings indicate that crosslinked excipients may have greater potential than initially assumed. This is further supported by the results presented in Chapter 3 of this thesis, where apremilast exhibited long term supersaturation with pronounced spring and parachute behavior when formulated with crosslinked excipients.

6.4 The relationship between the drug's glass transition temperature (T_g) and the co-milling temperature

While the majority of the screened drugs investigated in Chapters 2 and 4 had T_gs above the applied milling temperature, chapter 3 focused on two model compounds chosen specifically for their contrasting T_g values, one significantly below and one significantly above the milling temperature. Unlike previous studies focusing on the relationship between glass transition temperature (T_g) and milling-induced disorder, this study incorporated croscarmellose sodium to the milling process to evaluate its effect on the stabilization of disordered states of the drug and the influence on dissolution characteristics.

Fenofibrate, a low-T_g compound (~ –20 °C), was investigated under these conditions. Given that milling was performed at ambient temperature i.e. above T_g but below T_m (78°C), the system allowed for considerable molecular mobility and, consequently, increased potential for recrystallization. In contrast, apremilast, with a T_g of ~75 °C, was milled below its T_g, where

molecular mobility is expected to be substantially lower, thus limiting the ability of the system to restore crystallographic order. This lower molecular mobility favours the accumulation of lattice disorder and promotes the formation of amorphous material.

One aim of the study was to examine whether co-milling of the low-T_g drug fenofibrate could stabilize lattice disorder and induce supersaturation. Varying milling times were applied to assess the impact of mechanical energy input on the dissolution behaviour. Fenofibrate maintained sharp diffraction peaks in its XRPD pattern even after 60 minutes of co-milling, signifying a high degree of residual crystallinity. One recent study hypothesized that the GFA class impacts the drug dissolution enhancement after co-milling (Slámová et al., 2021). Our data of chapter 3 show that the GFA class alone is not sufficient to predict the co-milling induced dissolution enhancement, because fenofibrate is a GFA class III compound and did not substantially lose crystallinity nor supersaturate in dissolution medium. However, the location of the T_g appears to play a significant role for the expected lattice disorder and thus the expected dissolution enhancement. Also, the presence of croscarmellose sodium did not appear to significantly hinder the reordering of the crystal lattice disorder or stabilize amorphous regions formed during the co-milling process on fenofibrate particles. Interestingly, milling the drug without excipient led to certain diffraction peak intensities increased while others decreased, suggesting the occurrence of polymorphic transitions-phenomena that have also been reported in other studies involving drugs milled below their T_g (Willart et al., 2006, 2005; Zhang et al., 2002). This effect was not visible in X-Ray diffractograms of co-milled fenofibrate, so the addition of the excipient to the ball milling process of the low-T_g-compound appeared to prevent this effect.

In contrast, XRPD analysis of co-milled apremilast demonstrated a progressive reduction in Bragg peak intensity with increasing milling time. After 60 minutes of co-milling, nearly all diffraction peaks had disappeared, indicating the formation of a predominantly amorphous material with minimal residual crystallinity. Correspondingly, in vitro dissolution testing in FaSSIF revealed that supersaturation was achieved for co-milling durations of 10 minutes or longer. The extent of supersaturation increased with longer milling times, likely due to the

accumulation of lattice defects and the formation of greater quantities of amorphous apremilast.

The mechanistic hypothesis for milling-induced amorphization via the kinetic pathway suggests that prolonged mechanical stress gradually introduces lattice defects, eventually resulting in a complete loss of long-range order and the formation of a phase with amorphous character (Mishra et al., 2018). However, experimental data of Blaabjerg and coworkers demonstrated that when a drug's T_g is below the milling temperature, amorphization is not achieved, likely due to dynamic recrystallization or the restoration of crystallographic order during processing (Blaabjerg et al., 2017a). Above T_g, but still below the melting temperature, the amorphous state is supposed to be thermodynamically metastable and behaves like a supercooled liquid, characterized by higher molecular mobility (Roudaut et al., 2004). This increased mobility above T_g facilitates the reorganization of molecules back into a crystalline structure, thereby reducing the effectiveness of the amorphization process.

These findings suggest that, for GFA class III compounds, co-milling is more effective in inducing amorphization when the drug's T_g lies above the milling temperature. Under such conditions, the low molecular mobility limits the ability of the system to restore crystalline order, as observed with apremilast. Conversely, compounds with low T_g values, such as fenofibrate, appear to restore milling-induced disorder, despite of the addition of a polymeric excipient to the drug milling process.

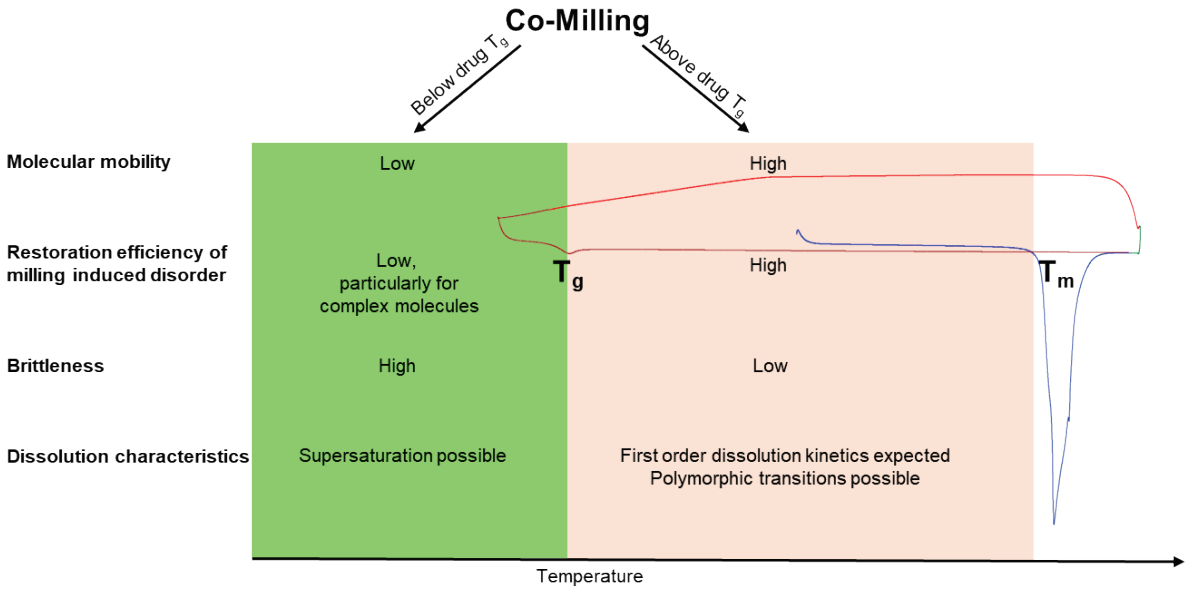


Figure 6-4: Schematic representation of the relationship of the drug glass transition temperature (T_g) to the co-milling temperature. Co-milling below T_g, a low molecular mobility and high brittleness favour the retention of milling-induced disorder is expected, especially in structurally complex molecules, enabling supersaturation in dissolution. Co-milling above drug T_g, an increased molecular mobility is promotes the restoration of crystallinity with first-order dissolution kinetics expected. The diagram highlights the critical role of T_g in determining whether co-milling results in stabilized disorder or structural reorganization, and thus its impact on dissolution enhancement. The thermogram is an example of a drug after and quench cooling cycle and serves as a visual orientation for the locations of the T_g and T_m.

6.5 The role of melting point depression for supersaturating co-milled drug formulations

In Chapter 3, the high-T_g drug apremilast exhibited supersaturation in FaSSIF in formulations co-milled for 10 minutes or longer, characterized by the typical "spring-and-parachute" dissolution profile. The degree of supersaturation increased proportionally with milling duration and was accompanied by a melting point depression exceeding 10 °C. Notably, a strong linear relationship was observed between the maximum dissolved concentration (c_{max}) of apremilast and the extent of its melting point depression, with R^2 values of 0.98 for the onset temperature

and 0.96 for the peak of the endothermic event, as measured by differential scanning calorimetry (DSC).

Several factors must be considered to interpret the correlation of drug supersaturation with melting point depression and evaluate its relevance for pharmaceutical quality control. It is well-established that simple physical mixing of a crystalline drug with an amorphous polymer can lead to a reduction in the drug's melting point (Marsac et al., 2009). This phenomenon is commonly used to assess drug-polymer miscibility by quantifying the degree of melting point depression (Pezzoli et al., 2018). In the present study, all co-milled formulations contained the same excipient in the same drug: excipient ratio which would result in the same melting point depression. However, the observed melting point depression increased with longer milling durations and this additional depression correlated strongly with increasing dissolution c_{max}.

While melting point depression can also occur with the production of nanoscale materials, this mechanism is unlikely in the present context. Dry co-milling typically yields particle sizes in the lower micrometer range due to a dynamic balance between particle size reduction and agglomeration. In fact, Chapter 5 established a grinding limit for drugs in co-milled formulations with PVP applying the same milling setup, showing a median particle size in average of 16.9 µm. Moreover, the specific surface area of apremilast-containing co-milled formulations did not increase after 10 minutes of co-milling, despite continued melting point depression and increased supersaturation. These findings suggest that particle size reduction is not the driver of the observed effects.

Instead, the generation of lattice defects during prolonged co-milling likely plays a central role for this correlation. The accumulation of such defects can introduce substantial lattice disorder and facilitate either partial or full amorphisation of the drug. In such cases, residual crystalline regions exhibit a melting point that decreases as structural disorder increases. Mechanochemical activation raises the chemical potential (µ) of the crystal, thereby reducing the energy barrier for melting (Ahmed et al., 2020). Consequently, the observed melting point depression with longer milling times likely reflects the progressive destabilization of the crystalline lattice due to defect accumulation. This mechanistic pathway helps explain both the

enhanced dissolution performance and its strong correlation with melting point depression. Interestingly, milling apremilast without an excipient did not result in supersaturation. Therefore, the melting point depression effect illustrated in Figure 6-2 was only relevant for co-milled formulations that included an excipient.

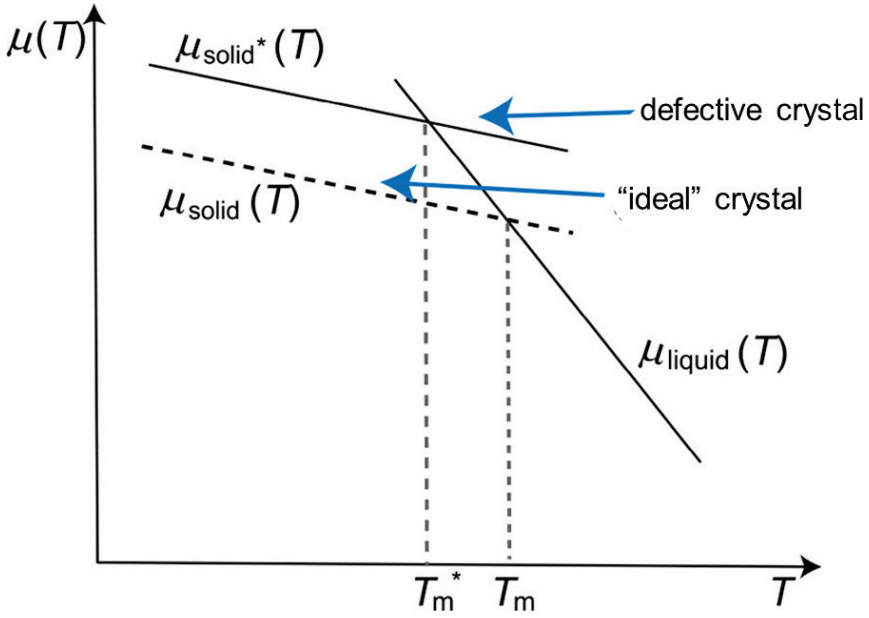


Figure 6-5: Thermodynamic illustration of the effect of crystal defects on the melting behaviour of solids, extracted and edited from (Ahmed et al., 2020). The graph shows the temperature dependence of the chemical potential (μ) for an "ideal" crystal (μ_{solid}) and a defective crystal (μ_{solid^*}), compared to the liquid phase (μ_{liquid}). Due to higher free energy, defective crystals exhibit a lower melting temperature (T_m^*) than the ideal crystalline form (T_m). The introduction of defects increases the chemical potential of the solid, promoting melting and phase transitions at reduced temperatures.

The co-milling-induced melting point depression of the high-T_g compound apremilast remained stable during storage, suggesting effective stabilization of lattice disorder. In contrast, the melting point of the low-T_g compound fenofibrate increased over time, indicating recrystallization processes occurring on drug particle surfaces. These observations highlight

firstly the importance of T_g in predicting the physical stability of co-milled formulations and underline the relevance of drug melting point depression monitoring as a surrogate marker for solid-state changes over time in co-milled formulations.

The melting point of a dry co-milled sample appears to serve as an indicator of the degree of lattice disorder within the material. Given that mechanically activated formulations may be susceptible to instability during storage, differential scanning calorimetry (DSC), which requires only microgram-scale sample quantities, is proposed as a practical analytical approach for assessing the structural state of co-milled materials that retain residual crystallinity. This method offers a rapid and efficient method for assessing the extent of co-milling-induced disorder and can be particularly beneficial for as a stability indicating quality control method during storage. For such applications, DSC measurements should be standardized, using consistent conditions across batches. Threshold values for the melting point can be established, beyond which deviations would indicate potential instabilities. Any observed increase in melting point over time may signal recrystallization or structural reorganization, which could compromise the supersaturation potential and, consequently, impact drug product performance in patients. This approach can serve as an alternative approach to quantitative XRPD or Raman spectroscopy for a future study assessing the stability of highly disordered co-milled formulations.

6.6 Mechanisms of particle aggregation inhibition and size reduction of Co-milling with Polyvinylpyrrolidone

Milling is the most commonly employed method for particle size reduction of drugs in the pharmaceutical industry (Loh et al., 2015). Dry milling techniques, such as those using zirconium oxide beads or stainless-steel balls, typically produce micron-sized particles, while wet milling can be employed to obtain nanoscale drug particles (Al-Kassas et al., 2017; Negrini et al., 2017; Peltonen and Hirvonen, 2010; Sigfridsson et al., 2019). A key objective in milling processes is to establish conditions that yield reproducible and consistent particle size distributions. For crystalline small-molecule drugs, dry milling often reaches a dynamic equilibrium between particle fragmentation and re-agglomeration. At this point, the applied mechanical energy defines a "grinding limit," beyond which further size reduction becomes inefficient, and a stable particle size distribution is achieved (Matveeva et al., 2025).

Chapter 5 investigated the influence of the PVP addition on milling-induced drug particle size reduction. Milling the drug without any excipient led to particle agglomeration in several cases, making the conventional approach prone to producing suboptimal drug products with inconsistent particle size distributions. In contrast, the addition of PVP during co-milling resulted in a significantly greater degree of particle size reduction for most drugs. Remarkably, the extent and range of particle size reduction were predictable based solely on the initial particle size of the drug, regardless of the co-milled drug compound. PVP likely reduced surface adhesion forces between crushed drug particles, effectively acting as a "grinding aid" in pharmaceutical milling (Cayirli, 2022). This effect contributed to the stabilization of smaller drug particles and a consistent lowering of the grinding limit.

6.7 Scale-up of Co-milling

The scale-up of milling processes is challenging and requires mechanistic understanding to ensure reliable transfer from laboratory to industrial scale. In dry co-milling techniques, as investigated in this study, drugs with a high T_g were found to progressively lose their crystalline order with increasing milling time, while particle sizes were simultaneously reduced into the lower micrometer range. At the early stages of dry co-milling, particle size reduction is typically the dominant mechanism, as the applied mechanical stresses primarily lead to fragmentation of the crystalline material (Capece et al., 2015). With continued milling, however, structural changes within the crystal lattice become increasingly pronounced, resulting in elevated lattice disorder or partial amorphization of the drug substance (Guerain et al., 2025). This mechanistic evolution clearly differs from wet milling approaches, such as those employed for the production of nanosuspensions, or liquid-assisted grinding used for co-crystal formation, where the presence of a liquid phase facilitates molecular mobility and promotes recrystallization processes that can counteract mechanically induced lattice disorder (Malamatari et al., 2018). In contrast, dry co-milling lacks such solvent-mediated relaxation mechanisms, allowing crystal lattice defects to accumulate over time.

Consequently, when addressing the upscaling of dry co-milling processes, particle size and crystal lattice disorder should be regarded as the critical target parameters, as both are key determinants of dissolution behavior and ultimately drug bioavailability. Despite this, the majority of co-milling studies reported in the literature are conducted using laboratory-scale ball milling systems, even though dry ball milling is particularly difficult to scale up. This limitation arises from the heat production in bigger scales, batch-wise nature of the process, limited control over the spatial and temporal distribution of energy input, and the inherently non-uniform application of mechanical stresses within the milling chamber. These factors lead that dry ball milling unsuitable for continuous, large-scale pharmaceutical manufacturing. As a result, alternative milling technologies such as jet milling or pin milling must be considered for industrial scale-up. Successful translation from laboratory to pilot and production scales requires a rational strategy that links milling energy input over time to the resulting particle size

reduction and degree of crystal lattice disorder in the co-milled drug product. However, this approach remains complex, as the mechanical stresses responsible for particle breakage and lattice disorder, including impact, shear, and frictional forces, differ fundamentally in magnitude and distribution depending on the milling technology employed, thereby further complicating direct scale-up of dry co-milling processes. However, comparing the yield particle size distribution and the crystal lattice disorder of the different milling processes in laboratory and pilot-/porduction scale by calculating the input energies could be a first way to upscale co-milling with hydrophilic polymers.

An interesting approach may be pin milling followed by a ball milling process. The pin mill enables rapid pre-comminution via impact-dominated stress, producing a narrow intermediate particle size distribution and effective deagglomeration. This preconditioning minimizes overloading and inefficient breakage regimes in the subsequent ball milling step. The ball mill then operates predominantly in an attrition- and abrasion-controlled mode, allowing precise control of fine and ultrafine particle generation. Consequently, the two-step milling strategy enhances energy efficiency and may be a promising strategy for the industrial scale production of highly disordered co-milled formulations.

7 Conclusions

Co-milling demonstrated high efficacy in enhancing the dissolution rate in over 90% of 65 tested drug–excipient combinations, employing hydrophilic polymers such as PVP and crosslinked tablet disintegrants including CCS, SSG and CP. For formulations co-milled with PVP, dissolution enhancement could be predicted based on specific drug characteristics. Statistical analysis revealed that, under the applied high-intensity co-milling conditions, particle size was the most significant factor influencing dissolution enhancement, followed by drug lipophilicity, and finally the molecular shape and size of the compound. Furthermore, the loss of crystallinity in co-milled formulations was found to correlate with Kappa 3, suggesting a relationship between molecular complexity and the tendency toward disorder.

In addition, co-milling with croscarmellose sodium was found to be able to induce supersaturation, with the extent of supersaturation correlating with a process-induced melting point depression that remained stable on storage. Owing to its ease of measurement, melting point depression emerges as an important and readily accessible parameter for assessing the physical stability of supersaturating co-milled formulations with residual crystallinity.

Co-milling promoted particle size reduction by inhibiting drug particle agglomeration during processing. Finally, an investigation within the latest framework of the rDCS calculating a target particle size confirmed that co-milling with tablet disintegrants represents an effective approach to overcome dissolution rate-limited absorption following oral administration.

8 Future perspectives

An important direction for future research could be the investigation of a broader range of excipients to develop an additional co-milling dissolution rate prediction model. It may provide a clearer distinction between excipient-related and drug-specific effects within the model established in chapter 2. In this context, it would be particularly valuable to explore drug–excipient interactions in greater detail using advanced analytical techniques. Gaining insights into which combinations form interactions or bonds during co-milling in the solid state, what types of interactions occur, and how these affect milling-induced disorder could further contribute meaningfully to formulation design.

Since drugs with a high T_g have shown the potential to exhibit supersaturation following co-milling, future research could focus on predicting the extent of supersaturation that can be achieved under varying conditions. A further logical next step would be to examine the relationship between melting point depression and supersaturation across different drug–excipient combinations.

Another promising line of investigation involves the molecular modeling of drug crystal structures to better understand the mechanisms underlying the induction and potential repair of mechanically induced lattice disorder. Such studies could help clarify the molecular processes responsible for the formation, stability, and possible reversibility of structural disorder, thereby supporting a more mechanistic understanding of how disorder arises during milling. Finally, the development of comprehensive datasets on the physical stability of co-milled formulations would lay the groundwork for predictive models to assist formulation scientists and industrial developers. Different techniques such as the melting point depression method and in vitro dissolution as proposed in chapter 3 could be used for the stability evaluation. Such models could help to support the design of more robust formulations early in development. Moreover, further research into the scalability of co-milling would be essential for its broader implementation as an enabling technology, contributing to more sustainable pharmaceutical manufacturing with reduced solvent use and lower process waste.

9 References

Abushal, A.S., Aleanizy, F.S., Alqahtani, F.Y., Shakeel, F., Iqbal, M., Haq, N., Alsarra, I.A., 2022. Self-Nanoemulsifying Drug Delivery System (SNEDDS) of Apremilast: In Vitro Evaluation and Pharmacokinetics Studies. Molecules 27, 3085. https://doi.org/10.3390/molecules27103085

Ahmed, E., Karothu, D.P., Pejov, L., Commins, P., Hu, Q., Naumov, P., 2020. From Mechanical Effects to Mechanochemistry: Softening and Depression of the Melting Point of Deformed Plastic Crystals. J Am Chem Soc 142, 11219–11231. https://doi.org/10.1021/jacs.0c03990

Alhalaweh, A., Alzghoul, A., Kaialy, W., Mahlin, D., Bergström, C.A.S., 2014. Computational Predictions of Glass-Forming Ability and Crystallization Tendency of Drug Molecules. Mol Pharm 11, 3123–3132. https://doi.org/10.1021/mp500303a

Alharby, T.N., Huwaimel, B., 2025. Machine learning analysis of pharmaceutical cocrystals solubility parameters in enhancing the drug properties for advanced pharmaceutical manufacturing. Sci Rep 15, 29970. https://doi.org/10.1038/s41598-025-12886-8

Al-Kassas, R., Bansal, M., Shaw, J., 2017. Nanosizing techniques for improving bioavailability of drugs. Journal of Controlled Release 260, 202–212. https://doi.org/10.1016/j.jconrel.2017.06.003

Alsayed, A.M., Islam, M.F., Zhang, J., Collings, P.J., Yodh, A.G., 2005. Premelting at Defects Within Bulk Colloidal Crystals. Science (1979) 309, 1207–1210. https://doi.org/10.1126/science.1112399

Alsenz, J., Kuentz, M., 2019. From Quantum Chemistry to Prediction of Drug Solubility in Glycerides. Mol Pharm 16, 4661–4669. https://doi.org/10.1021/acs.molpharmaceut.9b00801

Alskär, L.C., Bergström, C.A.S., 2015. Models for Predicting Drug Absorption From Oral Lipid-Based Formulations. Curr Mol Biol Rep 1, 141–147. https://doi.org/10.1007/s40610-015-0023-1

Amidon, G.L., Lennernäs, H., Shah, V.P., Crison, J.R., 1995. A theoretical basis for a biopharmaceutic drug classification: the correlation of in vitro drug product dissolution and in vivo bioavailability . Pharm Res 12, 413–420. https://doi.org/10.1023/A:1016212804288

Asgreen, C., Knopp, M.M., Skytte, J., Löbmann, K., 2020. Influence of the Polymer Glass Transition Temperature and Molecular Weight on Drug Amorphization Kinetics Using Ball Milling. Pharmaceutics 12, 483. https://doi.org/10.3390/pharmaceutics12060483

Atashin, S., Wen, J.Z., Varin, R.A., 2015. Investigation of milling energy input on structural variations of processed olivine powders for CO2 sequestration. J Alloys Compd 618, 555–561. https://doi.org/10.1016/J.JALLCOM.2014.08.142

Azad, M., Afolabi, A., Bhakay, A., Leonardi, J., Davé, R., Bilgili, E., 2015. Enhanced physical stabilization of fenofibrate nanosuspensions via wet co-milling with a superdisintegrant and an adsorbing polymer. European Journal of Pharmaceutics and Biopharmaceutics 94, 372–385. https://doi.org/10.1016/J.EJPB.2015.05.028

Bae, S.K., Park, J.B., Seo, J.H., Choi, W.-K., Park, S., Sung, Y.J., Oh, E., 2015. Improved oral absorption of cilostazol via sulfonate salt formation with mesylate and besylate. Drug Des Devel Ther 3961. https://doi.org/10.2147/DDDT.S87687

Bahl, D., Bogner, R.H., 2006. Amorphization of Indomethacin by Co-Grinding with Neusilin US2: Amorphization Kinetics, Physical Stability and Mechanism. Pharm Res 23, 2317–2325. https://doi.org/10.1007/s11095-006-9062-x

Bahl, D., Hudak, J., Bogner, R.H., 2008. Comparison of the Ability of Various Pharmaceutical Silicates to Amorphize and Enhance Dissolution of Indomethacin Upon Co-grinding. Pharm Dev Technol 13, 255–269. https://doi.org/10.1080/10837450802012869

Baird, J.A., Van Eerdenbrugh, B., Taylor, L.S., 2010. A Classification System to Assess the Crystallization Tendency of Organic Molecules from Undercooled Melts. J Pharm Sci 99, 3787–3806. https://doi.org/10.1002/jps.22197

Balani, P.N., Ng, W.K., Tan, R.B.H., Chan, S.Y., 2010. Influence of excipients in comilling on mitigating milling-induced amorphization or structural disorder of crystalline pharmaceutical actives. J Pharm Sci 99, 2462–2474. https://doi.org/10.1002/jps.21998

Bannigan, P., Aldeghi, M., Bao, Z., Häse, F., Aspuru-Guzik, A., Allen, C., 2021. Machine learning directed drug formulation development. Adv Drug Deliv Rev 175, 113806. https://doi.org/10.1016/j.addr.2021.05.016

Barmpalexis, P., Kanaze, F.I., Kachrimanis, K., Georgarakis, E., 2010. Artificial neural networks in the optimization of a nimodipine controlled release tablet formulation. European Journal of Pharmaceutics and Biopharmaceutics 74, 316–323. https://doi.org/10.1016/J.EJPB.2009.09.011

Bartkowiak, A., Matyszewska, D., Krzak, A., Zaborowska, M., Broniatowski, M., Bilewicz, R., 2021. Incorporation of simvastatin into lipid membranes: Why deliver a statin in form of inclusion complex with hydrophilic cyclodextrin. Colloids Surf B Biointerfaces 204, 111784. https://doi.org/10.1016/J.COLSURFB.2021.111784

Bejaoui, M., Djemi, R., Kouass, S., Galai, H., 2024. Physical Stability of Ibuprofen Upon Co-Milling with Caffeine and Polyvinylpyrrolidone at Room Temperature. Pharm Chem J 58, 320–326. https://doi.org/10.1007/s11094-024-03148-4

Benet, L.Z., Amidon, G.L., Barends, D.M., Lennernäs, H., Polli, J.E., Shah, V.P., Stavchansky, S.A., Yu, L.X., 2008. The Use of BDDCS in Classifying the Permeability of Marketed Drugs. Pharm Res 25, 483–488. https://doi.org/10.1007/s11095-007-9523-x

Bennett-Lenane, H., Koehl, N.J., O'Dwyer, P.J., Box, K.J., O'Shea, J.P., Griffin, B.T., 2021a. Applying Computational Predictions of Biorelevant Solubility Ratio Upon Self-Emulsifying Lipid-Based Formulations Dispersion to Predict Dose Number. J Pharm Sci 110, 164–175. https://doi.org/10.1016/j.xphs.2020.10.055

Bennett-Lenane, H., O'Shea, J.P., Murray, J.D., Ilie, A.-R., Holm, R., Kuentz, M., Griffin, B.T., 2021b. Artificial Neural Networks to Predict the Apparent Degree of Supersaturation in Supersaturated Lipid-Based Formulations: A Pilot Study. Pharmaceutics 13, 1398. https://doi.org/10.3390/pharmaceutics13091398

Beran, K., Hermans, E., Holm, R., Sepassi, K., Dressman, J., 2024a. Using the refined Developability Classification System (rDCS) to guide the design of oral formulations. J Pharm Sci 113, 3497–3517. https://doi.org/10.1016/j.xphs.2024.09.022

Beran, K., Hermans, E., Holm, R., Sepassi, K., Dressman, J., 2024b. A Stratified Analysis of Supersaturation and Precipitation Effects Based on the Refined Developability Classification System (rDCS). J Pharm Sci 113, 2940–2946. https://doi.org/10.1016/j.xphs.2024.06.014

Beran, K., Hermans, E., Holm, R., Sepassi, K., Dressman, J., 2023. Projection of Target Drug Particle Size in Oral Formulations Using the Refined Developability Classification System (rDCS). Pharmaceutics 15. https://doi.org/10.3390/pharmaceutics15071909

Berardi, A., Janssen, P.H.M., Dickhoff, B.H.J., 2022. Technical insight into potential functional-related characteristics (FRCs) of sodium starch glycolate, croscarmellose sodium and crospovidone. J Drug Deliv Sci Technol 70, 103261. https://doi.org/10.1016/J.JDDST.2022.103261

Bergström, C.A.S., Charman, W.N., Porter, C.J.H., 2016. Computational prediction of formulation strategies for beyond-rule-of-5 compounds. Adv Drug Deliv Rev 101, 6–21. https://doi.org/10.1016/j.addr.2016.02.005

Bhalani, D. V., Nutan, B., Kumar, A., Singh Chandel, A.K., 2022. Bioavailability Enhancement Techniques for Poorly Aqueous Soluble Drugs and Therapeutics. Biomedicines 10, 2055. https://doi.org/10.3390/biomedicines10092055

Bhujbal, S. V., Mitra, B., Jain, U., Gong, Y., Agrawal, A., Karki, S., Taylor, L.S., Kumar, S., (Tony) Zhou, Q., 2021. Pharmaceutical amorphous solid dispersion: A review of manufacturing strategies. Acta Pharm Sin B 11, 2505–2536. https://doi.org/10.1016/j.apsb.2021.05.014

Blaabjerg, L.I., Lindenberg, E., Löbmann, K., Grohganz, H., Rades, T., 2018. Is there a correlation between the glass forming ability of a drug and its supersaturation propensity? Int J Pharm 538, 243–249. https://doi.org/10.1016/j.ijpharm.2018.01.013

Blaabjerg, L.I., Lindenberg, E., Löbmann, K., Grohganz, H., Rades, T., 2016. Glass Forming Ability of Amorphous Drugs Investigated by Continuous Cooling and Isothermal Transformation. Mol Pharm 13, 3318–3325. https://doi.org/10.1021/acs.molpharmaceut.6b00650

Blaabjerg, L.I., Lindenberg, E., Rades, T., Grohganz, H., Löbmann, K., 2017a. Influence of preparation pathway on the glass forming ability. Int J Pharm 521, 232–238. https://doi.org/10.1016/j.ijpharm.2017.02.042

Blanco, D., Pätzmann, N., García-Triñanes, P., 2025. Microdynamic Flowability for Early API Characterisation: A Case Study on Palbociclib. Pharmaceutical Science Advances 100069. https://doi.org/10.1016/J.PSCIA.2025.100069

Bloomingdale, P., Mager, D.E., 2019. Machine Learning Models for the Prediction of Chemotherapy-Induced Peripheral Neuropathy. Pharm Res 36, 35. https://doi.org/10.1007/s11095-018-2562-7

Bodach, A., Portet, A., Winkelmann, F., Herrmann, B., Gallou, F., Ponnusamy, E., Virieux, D., Colacino, E., Felderhoff, M., 2024. Scalability of Pharmaceutical Co-Crystal Formation by Mechanochemistry in Batch. ChemSusChem 17. https://doi.org/10.1002/cssc.202301220

Bolhuis, G.K., Zuurman, K., Te Wierik, G.H.P., 1997. Improvement of dissolution of poorly soluble drugs by solid deposition on a super disintegrant. II. The choice of super disintegrants and effect of granulation. European Journal of Pharmaceutical Sciences 5, 63–69. https://doi.org/10.1016/S0928-0987(96)00256-4

Bolourchian, N., Talamkhani, Z., Nokhodchi, A., 2019a. Preparation and physicochemical characterization of binary and ternary ground mixtures of carvedilol with PVP and SLS aimed to improve the drug dissolution. Pharm Dev Technol 24, 1115–1124. https://doi.org/10.1080/10837450.2019.1641516

Bourquin, J., Schmidli, H., Van Hoogevest, P., Leuenberger, H., 1998. Comparison of artificial neural networks (ANN) with classical modelling techniques using different experimental designs and data from a galenical study on a solid dosage form. European Journal of Pharmaceutical Sciences 6, 287–300. https://doi.org/10.1016/S0928-0987(97)10025-2

Bourquin, J., Schmidli, H., van Hoogevest, P., Leuenberger, H., 1997. Application of Artificial Neural Networks (ANN) in the Development of Solid Dosage Forms. Pharm Dev Technol 2, 111–121. https://doi.org/10.3109/10837459709022616

Brewster, M.E., Loftsson, T., 2007. Cyclodextrins as pharmaceutical solubilizers. Adv Drug Deliv Rev 59, 645–666. https://doi.org/10.1016/J.ADDR.2007.05.012

Brokešová, J., Slámová, M., Zámostný, P., Kuentz, M., Koktan, J., Krejčík, L., Vraníková, B., Svačinová, P., Šklubalová, Z., 2022. Mechanistic study of dissolution enhancement by interactive mixtures of chitosan with meloxicam as model. European Journal of Pharmaceutical Sciences 169, 106087. https://doi.org/10.1016/j.ejps.2021.106087

Brunner, E., 1904. Reaktionsgeschwindigkeit in heterogenen Systemen. Zeitschrift für Physikalische Chemie 47U, 56–102. https://doi.org/10.1515/zpch-1904-4705

Butler, J.M., Dressman, J.B., 2010. The Developability Classification System: Application of Biopharmaceutics Concepts to Formulation Development. J Pharm Sci 99, 4940–4954. https://doi.org/10.1002/jps.22217

Bzdok, D., Krzywinski, M., Altman, N., 2018. Machine learning: supervised methods. Nat Methods 15, 5–6. https://doi.org/10.1038/nmeth.4551

Capece, M., Davé, R.N., Bilgili, E., 2015. On the origin of non-linear breakage kinetics in dry milling. Powder Technol 272, 189–203. https://doi.org/10.1016/J.POWTEC.2014.11.040

Caron, V., Hu, Y., Tajber, L., Erxleben, A., Corrigan, O.I., McArdle, P., Healy, A.M., 2013. Amorphous Solid Dispersions of Sulfonamide/Soluplus® and Sulfonamide/PVP Prepared by Ball Milling. AAPS PharmSciTech 14, 464–474. https://doi.org/10.1208/s12249-013-9931-7

Caron, V., Tajber, L., Corrigan, O.I., Healy, A.M., 2011a. A Comparison of Spray Drying and Milling in the Production of Amorphous Dispersions of Sulfathiazole/Polyvinylpyrrolidone and Sulfadimidine/Polyvinylpyrrolidone. Mol Pharm 8, 532–542. https://doi.org/10.1021/mp1003674

Caron, V., Willart, J.F., Lefort, R., Derollez, P., Dande, F., Descamps, M., 2011b. Solid state amorphization kinetic of alpha lactose upon mechanical milling. Carbohydr Res 346, 2622–2628. https://doi.org/10.1016/J.CARRES.2011.09.004

Cayirli, S., 2022. Analysis of grinding aid performance effects on dry fine milling of calcite. Advanced Powder Technology 33, 103446. https://doi.org/10.1016/J.APT.2022.103446

Censi, R., Di Martino, P., 2015. Polymorph Impact on the Bioavailability and Stability of Poorly Soluble Drugs. Molecules 20, 18759–18776. https://doi.org/10.3390/molecules201018759

Chamarthy, S.P., Pinal, R., 2008. The nature of crystal disorder in milled pharmaceutical materials. Colloids Surf A Physicochem Eng Asp 331, 68–75. https://doi.org/10.1016/J.COLSURFA.2008.06.040

Chambers, L.I., Grohganz, H., Palmelund, H., Löbmann, K., Rades, T., Musa, O.M., Steed, J.W., 2021. Predictive identification of co-formers in co-amorphous systems. European

Journal of Pharmaceutical Sciences 157, 105636. https://doi.org/10.1016/j.ejps.2020.105636

Chikhalia, V., Forbes, R.T., Storey, R.A., Ticehurst, M., 2006. The effect of crystal morphology and mill type on milling induced crystal disorder. European Journal of Pharmaceutical Sciences 27, 19–26. https://doi.org/10.1016/j.ejps.2005.08.013

Chingunpitak, J., Puttipipatkhachorn, S., Chavalitshewinkoon-Petmitr, P., Tozuka, Y., Moribe, K., Yamamoto, K., 2008. Formation, Physical Stability and In Vitro Antimalarial Activity of Dihydroartemisinin Nanosuspensions Obtained by Co-grinding Method. Drug Dev Ind Pharm 34, 314–322. https://doi.org/10.1080/03639040701662388

Chipakwe, V., Semsari, P., Karlkvist, T., Rosenkranz, J., Chelgani, S.C., 2020. A critical review on the mechanisms of chemical additives used in grinding and their effects on the downstream processes. Journal of Materials Research and Technology 9, 8148–8162. https://doi.org/10.1016/j.jmrt.2020.05.080

Cook, J., Addicks, W., Wu, Y.H., 2008. Application of the Biopharmaceutical Classification System in Clinical Drug Development—An Industrial View. AAPS J 10, 306–310. https://doi.org/10.1208/s12248-008-9036-5

De Vivo, M., Masetti, M., Bottegoni, G., Cavalli, A., 2016. Role of Molecular Dynamics and Related Methods in Drug Discovery. J Med Chem 59, 4035–4061. https://doi.org/10.1021/acs.jmedchem.5b01684

Dedroog, S., Huygens, C., Van den Mooter, G., 2019. Chemically identical but physically different: A comparison of spray drying, hot melt extrusion and cryo-milling for the formulation of high drug loaded amorphous solid dispersions of naproxen. European Journal of Pharmaceutics and Biopharmaceutics 135, 1–12. https://doi.org/10.1016/J.EJPB.2018.12.002

Deng, Y., Liu, S., Jiang, Y., Martins, I.C.B., Rades, T., 2023. Recent Advances in Co-Former Screening and Formation Prediction of Multicomponent Solid Forms of Low Molecular Weight Drugs. Pharmaceutics 15, 2174. https://doi.org/10.3390/pharmaceutics15092174

Descamps, M., Willart, J.F., 2016. Perspectives on the amorphisation/milling relationship in pharmaceutical materials. Adv Drug Deliv Rev 100, 51–66. https://doi.org/10.1016/j.addr.2016.01.011

Descamps, M., Willart, J.F., Dudognon, E., Caron, V., 2007. Transformation of Pharmaceutical Compounds upon Milling and Comilling: The Role of Tg. J Pharm Sci 96, 1398–1407. https://doi.org/10.1002/jps.20939

Desjardins, P.J., Olugemo, K., Solorio, D., Young, C.L., 2015. Pharmacokinetic Properties and Tolerability of Low-dose SoluMatrix Diclofenac. Clin Ther 37, 448–461. https://doi.org/10.1016/J.CLINTHERA.2014.10.018

Ditzinger, F., Price, D.J., Ilie, A.-R., Köhl, N.J., Jankovic, S., Tsakiridou, G., Aleandri, S., Kalantzi, L., Holm, R., Nair, A., Saal, C., Griffin, B., Kuentz, M., 2019. Lipophilicity and hydrophobicity considerations in bio-enabling oral formulations approaches – a PEARRL review. Journal of Pharmacy and Pharmacology 71, 464–482. https://doi.org/10.1111/jphp.12984

Do, J.-L., Friščić, T., 2017. Mechanochemistry: A Force of Synthesis. ACS Cent Sci 3, 13–19. https://doi.org/10.1021/acscentsci.6b00277

Dong, Y., Yang, T., Xing, Y., Du, J., Meng, Q., 2023. Data-Driven Modeling Methods and Techniques for Pharmaceutical Processes. Processes 11, 2096. https://doi.org/10.3390/pr11072096

Dressman, J.B., Fleisher, D., Amidon, G.L., 1984. Physicochemical Model for Dose-Dependent DrugAbsorption. J Pharm Sci 73, 1274–1279. https://doi.org/10.1002/JPS.2600730922

Drozd, K. V., Manin, A.N., Boycov, D.E., Perlovich, G.L., 2022. Simultaneous Improvement of Dissolution Behavior and Oral Bioavailability of Antifungal Miconazole via Cocrystal and Salt Formation. Pharmaceutics 14, 1107. https://doi.org/10.3390/pharmaceutics14051107

Dujardin, N., Willart, J.F., Dudognon, E., Danède, F., Descamps, M., 2013. Mechanism of Solid State Amorphization of Glucose upon Milling. J Phys Chem B 117, 1437–1443. https://doi.org/10.1021/jp3069267

Dutta, P., McGranaghan, A., Keller, I., Patil, Y., Mulholland, N., Murudi, V., Prescher, H., Smith, A., Carson, N., Martin, C., Cox, P., Stierli, D., Boussemghoune, M., Barreteau, F., Cassayre, J., Godineau, E., 2022. A case study in green chemistry: the reduction of hazardous solvents in an industrial R&D environment. Green Chemistry 24, 3943–3956. https://doi.org/10.1039/D2GC00698G

Ejskjær, L., O'Dwyer, P.J., Ryan, C.D., Holm, R., Kuentz, M., Box, K.J., Griffin, B.T., 2024. Developing an in vitro lipolysis model for real-time analysis of drug concentrations during digestion of lipid-based formulations. European Journal of Pharmaceutical Sciences 194, 106681. https://doi.org/10.1016/j.ejps.2023.106681

Essen, C. von, Luedeker, D., 2023. In silico co-crystal design: Assessment of the latest advances. Drug Discov Today 28, 103763. https://doi.org/10.1016/J.DRUDIS.2023.103763

Fagerberg, J.H., Al-Tikriti, Y., Ragnarsson, G., Bergström, C.A.S., 2012. Ethanol Effects on Apparent Solubility of Poorly Soluble Drugs in Simulated Intestinal Fluid. Mol Pharm 9, 1942–1952. https://doi.org/10.1021/mp2006467

Friščić, T., Jones, W., 2009. Recent Advances in Understanding the Mechanism of Cocrystal Formation via Grinding. Cryst Growth Des 9, 1621–1637. https://doi.org/10.1021/cg800764n

Gaggero, A., Jurišić Dukovski, B., Radić, I., Šagud, I., Škorić, I., Cinčić, D., Jug, M., 2020. Co-grinding with surfactants as a new approach to enhance in vitro dissolution of praziquantel. J Pharm Biomed Anal 189, 113494. https://doi.org/10.1016/j.jpba.2020.113494

Gao, Haoshi, Ye, Z., Dong, J., Gao, Hanlu, Yu, H., Li, H., Ouyang, D., 2020. Predicting drug/phospholipid complexation by the lightGBM method. Chem Phys Lett 747, 137354. https://doi.org/10.1016/J.CPLETT.2020.137354

Giraud, M., Gatumel, C., Vaudez, S., Nos, J., Gervais, T., Bernard-Granger, G., Berthiaux, H., 2021. Investigating grinding mechanisms and scaling criteria in a ball mill by dimensional analysis. Advanced Powder Technology 32, 2988–3001. https://doi.org/10.1016/J.APT.2021.06.016

Grady, H., Elder, D., Webster, G.K., Mao, Y., Lin, Y., Flanagan, T., Mann, J., Blanchard, A., Cohen, M.J., Lin, J., Kesisoglou, F., Hermans, A., Abend, A., Zhang, L., Curran, D., 2018. Industry's View on Using Quality Control, Biorelevant, and Clinically Relevant Dissolution Tests for Pharmaceutical Development, Registration, and Commercialization. J Pharm Sci 107, 34–41. https://doi.org/10.1016/j.xphs.2017.10.019

Greener, J.G., Kandathil, S.M., Moffat, L., Jones, D.T., 2022. A guide to machine learning for biologists. Nat Rev Mol Cell Biol 23, 40–55. https://doi.org/10.1038/s41580-021-00407-0

Griffin, B.T., Kuentz, M., Vertzoni, M., Kostewicz, E.S., Fei, Y., Faisal, W., Stillhart, C., O'Driscoll, C.M., Reppas, C., Dressman, J.B., 2014. Comparison of in vitro tests at various levels of complexity for the prediction of in vivo performance of lipid-based formulations: Case studies with fenofibrate. European Journal of Pharmaceutics and Biopharmaceutics 86, 427–437. https://doi.org/10.1016/j.ejpb.2013.10.016

Gu, F.G., Wang, Y., Meng, G.D.L., Han, H.B., Wu, C.Z., 2012. Investigation of a fenofibrate-hydroxypropyl-beta-cyclodextrin system prepared by a co-grinding method. Pharmazie 67, 143–6.

Guerain, M., Dupont, A., Danède, F., Barkhatova, D., Willart, J.-F., 2025. New Kinetic Investigations to Better Understand the Mechanism of Polymorphic Transformations of Pharmaceutical Materials Induced by Milling. Pharmaceutics 17, 1404. https://doi.org/10.3390/pharmaceutics17111404

Guidetti, M., Hilfiker, R., De Paul, S.M., Bauer-Brandl, A., Blatter, F., Kuentz, M., 2025. Discovery of Cilnidipine Cocrystals with Enhanced Dissolution by the Use of Computational Tools and Semiautomatic High-Throughput Screening. Cryst Growth Des. https://doi.org/10.1021/acs.cgd.5c00184

Guidetti, M., Hilfiker, R., Kuentz, M., Bauer-Brandl, A., Blatter, F., 2023. Exploring the Cocrystal Landscape of Posaconazole by Combining High-Throughput Screening Experimentation with Computational Chemistry. Cryst Growth Des 23, 842–852. https://doi.org/10.1021/acs.cgd.2c01072

Gupta, M.K., Vanwert, A., Bogner, R.H., 2003. Formation of Physically Stable Amorphous Drugs by Milling with Neusilin. J Pharm Sci 92, 536–551. https://doi.org/10.1002/jps.10308

Han, M., Xu, J., Lin, Y., 2022. Approaches of formulation bridging in support of orally administered drug product development. Int J Pharm 629, 122380. https://doi.org/10.1016/J.IJPHARM.2022.122380

Han, R., Xiong, H., Ye, Z., Yang, Y., Huang, T., Jing, Q., Lu, J., Pan, H., Ren, F., Ouyang, D., 2019. Predicting physical stability of solid dispersions by machine learning techniques. Journal of Controlled Release 311–312, 16–25. https://doi.org/10.1016/J.JCONREL.2019.08.030

Heidari, H., Vargas, A., Macris, A., Muller, F., Pikhard, O., Guner, G., Clancy, D.J., Bilgili, E., 2025. Control of temperature rise during wet stirred media milling. Advanced Powder Technology 36, 104981. https://doi.org/10.1016/J.APT.2025.104981

Hilfiker, R., Raumer, M. von (Eds.), 2018. Polymorphism in the Pharmaceutical Industry. Wiley. https://doi.org/10.1002/9783527697847

Holm, R., Kuentz, M., Ilie-Spiridon, A.-R., Griffin, B.T., 2023. Lipid based formulations as supersaturating oral delivery systems: From current to future industrial applications. European Journal of Pharmaceutical Sciences 189, 106556. https://doi.org/10.1016/j.ejps.2023.106556

Holzapfel, K., Rades, T., Leopold, C.S., 2023. Co-amorphous systems consisting of indomethacin and the chiral co-former tryptophan: Solid-state properties and molecular mobilities. Int J Pharm 636, 122840. https://doi.org/10.1016/j.ijpharm.2023.122840

Hossain, S., Kabedev, A., Parrow, A., Bergström, C.A.S., Larsson, P., 2019. Molecular simulation as a computational pharmaceutics tool to predict drug solubility, solubilization processes and partitioning. European Journal of Pharmaceutics and Biopharmaceutics 137, 46–55. https://doi.org/10.1016/J.EJPB.2019.02.007

Hussain, A., Smith, G., Khan, K.A., Bukhari, N.I., Pedge, N.I., Ermolina, I., 2018. Solubility and dissolution rate enhancement of ibuprofen by co-milling with polymeric excipients. European Journal of Pharmaceutical Sciences 123, 395–403. https://doi.org/10.1016/J.EJPS.2018.08.001

Ibraheem, B., Wagner, K.G., 2021. Influence of high pressure compaction on solubility and intrinsic dissolution of ibuprofen binary mixtures employing standard excipients. Int J Pharm X 3, 100075. https://doi.org/10.1016/j.ijpx.2021.100075

Ibri, S., Jovanovi, M., Djuri, Z., Parojči, J., Solomun, L., 2002. The application of generalized regression neural network in the modeling and optimization of aspirin extended release tablets with Eudragit® RS PO as matrix substance. Journal of Controlled Release 82, 213–222. https://doi.org/10.1016/S0168-3659(02)00044-5

Iemtsev, A., Zemánková, A., Hassouna, F., Mathers, A., Klajmon, M., Slámová, M., Malinová, L., Fulem, M., 2022. Ball milling and hot-melt extrusion of indomethacin–l-arginine–vinylpyrrolidone-vinyl acetate copolymer: Solid-state properties and dissolution performance. Int J Pharm 613, 121424. https://doi.org/10.1016/j.ijpharm.2021.121424

Isaac, J., Ganguly, S., Ghosh, A., 2016. Co-milling of telmisartan with poly(vinyl alcohol) – An alkalinizer free green approach to ensure its bioavailability. European Journal of Pharmaceutics and Biopharmaceutics 101, 43–52. https://doi.org/10.1016/j.ejpb.2016.01.016

Iyer, J., Brunsteiner, M., Modhave, D., Paudel, A., 2023. Role of Crystal Disorder and Mechanoactivation in Solid-State Stability of Pharmaceuticals. J Pharm Sci 112, 1539–1565. https://doi.org/10.1016/J.XPHS.2023.02.019

Jagadish, B., Yelchuri, R., K, B., Tangi, H., Maroju, S., Rao, V.U., 2010. Enhanced Dissolution and Bioavailability of Raloxifene Hydrochloride by Co-grinding with Different Superdisintegrants. Chem Pharm Bull (Tokyo) 58, 293–300. https://doi.org/10.1248/cpb.58.293

Jug, M., Mura, P.A., 2018. Grinding as Solvent-Free Green Chemistry Approach for Cyclodextrin Inclusion Complex Preparation in the Solid State. Pharmaceutics 10, 189. https://doi.org/10.3390/pharmaceutics10040189

Kabedev, A., Zhuo, X., Leng, D., Foderà, V., Zhao, M., Bergström, C.A.S., Löbmann, K., 2022. Stabilizing Mechanisms of β-Lactoglobulin in Amorphous Solid Dispersions of Indomethacin. Cite This: Mol. Pharmaceutics 19, 3933. https://doi.org/10.1021/acs.molpharmaceut.2c00397

Kah, M., Brown, C.D., 2008. LogD: Lipophilicity for ionisable compounds. Chemosphere 72, 1401–1408. https://doi.org/10.1016/j.chemosphere.2008.04.074

Kamil, M.M., Bayoumi, A.A., 2023. Co-Milling: A Successful Approach to Enhance Solubility of a Poorly Soluble Antihypertensive Drug. Indonesian Journal of Pharmacy. https://doi.org/10.22146/ijp.7072

Karimi-Jafari, M., Padrela, L., Walker, G.M., Croker, D.M., 2018. Creating Cocrystals: A Review of Pharmaceutical Cocrystal Preparation Routes and Applications. Cryst Growth Des 18, 6370–6387. https://doi.org/10.1021/acs.cgd.8b00933

Kasten, G., Lobo, L., Dengale, S., Grohganz, H., Rades, T., Löbmann, K., 2018. In vitro and in vivo comparison between crystalline and co-amorphous salts of naproxen-arginine.

European Journal of Pharmaceutics and Biopharmaceutics 132, 192–199. https://doi.org/10.1016/J.EJPB.2018.09.024

Kesavan, J.G., Peck, G.E., 1996. Pharmaceutical Granulation and Tablet Formulation Using Neural Networks. Pharm Dev Technol 1, 391–404. https://doi.org/10.3109/10837459609031434

Kier, L.B., 1985. A Shape Index from Molecular Graphs. Quantitative Structure-Activity Relationships 4, 109–116. https://doi.org/10.1002/qsar.19850040303

Kim, D., Kim, Y., Tin, Y.-Y., Soe, M.-T.-P., Ko, B., Park, S., Lee, J., 2021. Recent Technologies for Amorphization of Poorly Water-Soluble Drugs. Pharmaceutics 13, 1318. https://doi.org/10.3390/pharmaceutics13081318

Kim, J.H., 2019. Multicollinearity and misleading statistical results. Korean J Anesthesiol 72, 558–569. https://doi.org/10.4097/kja.19087

Knieke, C., Sommer, M., Peukert, W., 2009. Identifying the apparent and true grinding limit. Powder Technol 195, 25–30. https://doi.org/10.1016/j.powtec.2009.05.007

Knopp, M.M., Wendelboe, J., Holm, R., Rades, T., 2018. Effect of amorphous phase separation and crystallization on the in vitro and in vivo performance of an amorphous solid dispersion. European Journal of Pharmaceutics and Biopharmaceutics 130, 290–295. https://doi.org/10.1016/j.ejpb.2018.07.005

Kostewicz, E.S., Aarons, L., Bergstrand, M., Bolger, M.B., Galetin, A., Hatley, O., Jamei, M., Lloyd, R., Pepin, X., Rostami-Hodjegan, A., Sjögren, E., Tannergren, C., Turner, D.B., Wagner, C., Weitschies, W., Dressman, J., 2014. PBPK models for the prediction of in vivo performance of oral dosage forms. European Journal of Pharmaceutical Sciences 57, 300–321. https://doi.org/10.1016/j.ejps.2013.09.008

Krupa, A., Descamps, M., Willart, J.-F., Strach, B., Wyska, E., Jachowicz, R., Danède, F., 2016. High-Energy Ball Milling as Green Process To Vitrify Tadalafil and Improve Bioavailability. Mol Pharm 13, 3891–3902. https://doi.org/10.1021/acs.molpharmaceut.6b00688

KUBO, H., MIZOBE, M., 1997. Improvement of Dissolution Rate and Oral Bioavailability of a Sparingly Water-Soluble Drug, (.+-.)-5-((2-(2 Naphthalenylmethyl)-5-benzoxazolyl)-methyl)-2,4-thiazolidinedione, in Co-ground Mixture with D-Mannitol. Biol Pharm Bull 20, 460–463. https://doi.org/10.1248/bpb.20.460

Kuentz, M., 2012. Lipid-based formulations for oral delivery of lipophilic drugs. Drug Discov Today Technol 9, e97–e104. https://doi.org/10.1016/j.ddtec.2012.03.002

Kuentz, M., Bergström, C.A.S., 2021. Synergistic Computational Modeling Approaches as Team Players in the Game of Solubility Predictions. J Pharm Sci 110, 22–34. https://doi.org/10.1016/j.xphs.2020.10.068

Kushimoto, K., Suzuki, K., Ishihara, S., Soda, R., Ozaki, K., Kano, J., 2023. Analysis of the particle collision behavior in spiral jet milling. Advanced Powder Technology 34, 103993. https://doi.org/10.1016/J.APT.2023.103993

Lentz, K.A., Plum, J., Steffansen, B., Arvidsson, P.-O., Omkvist, D.H., Pedersen, A.J., Sennbro, C.J., Pedersen, G.P., Jacobsen, J., 2021. Predicting in vivo performance of fenofibrate amorphous solid dispersions using in vitro non-sink dissolution and dissolution permeation setup. Int J Pharm 610, 121174. https://doi.org/10.1016/j.ijpharm.2021.121174

Levy, G., Hollister, L.E., 1965. Dissolution Rate Limited Absorption in Man. J Pharm Sci 54, 1121–1125. https://doi.org/10.1002/jps.2600540805

Li, F., Li, L., Wang, Shaoning, Yang, Y., Li, J., Liu, D., Zhang, S., Wang, Siling, Xu, H., 2019. Improved dissolution and oral absorption by co-grinding active drug probucol and ternary stabilizers mixtures with planetary beads-milling method. Asian J Pharm Sci 14, 649–657. https://doi.org/10.1016/J.AJPS.2018.12.001

Li, J., Yang, Y., Zhao, M., Xu, H., Ma, J., Wang, S., 2017a. Improved oral bioavailability of probucol by dry media-milling. Materials Science and Engineering: C 78, 780–786. https://doi.org/10.1016/J.MSEC.2017.04.141

Li, J., Yang, Y., Zhao, M., Xu, H., Ma, J., Wang, S., 2017b. Improved oral bioavailability of probucol by dry media-milling. Materials Science and Engineering: C 78, 780–786. https://doi.org/10.1016/j.msec.2017.04.141

Liang, X., Liu, S., Li, Z., Deng, Y., Jiang, Y., Yang, H., 2024. Efficient cocrystal coformer screening based on a Machine learning Strategy: A case study for the preparation of imatinib cocrystal with enhanced physicochemical properties. European Journal of Pharmaceutics and Biopharmaceutics 196, 114201. https://doi.org/10.1016/j.ejpb.2024.114201

Lim, A.W., Löbmann, K., Grohganz, H., Rades, T., Chieng, N., 2016. Investigation of physical properties and stability of indomethacin–cimetidine and naproxen–cimetidine co-amorphous systems prepared by quench cooling, coprecipitation and ball milling. Journal of Pharmacy and Pharmacology 68, 36–45. https://doi.org/10.1111/jphp.12494

Lim, R.T.Y., Ng, W.K., Tan, R.B.H., 2013. Dissolution enhancement of indomethacin via amorphization using co-milling and supercritical co-precipitation processing. Powder Technol 240, 79–87. https://doi.org/10.1016/J.POWTEC.2012.07.004

Lipson, S.G., Polturak, E., 2024. Experimental investigation of the premelting process in Sn. Phys Rev B 109, 024109. https://doi.org/10.1103/PhysRevB.109.024109

Liu, J., Grohganz, H., Löbmann, K., Rades, T., Hempel, N.-J., 2021. Co-Amorphous Drug Formulations in Numbers: Recent Advances in Co-Amorphous Drug Formulations with Focus on Co-Formability, Molar Ratio, Preparation Methods, Physical Stability, In Vitro

and In Vivo Performance, and New Formulation Strategies. Pharmaceutics 13, 389. https://doi.org/10.3390/pharmaceutics13030389

Löbmann, K., Laitinen, R., Strachan, C., Rades, T., Grohganz, H., 2013. Amino acids as co-amorphous stabilizers for poorly water-soluble drugs – Part 2: Molecular interactions. European Journal of Pharmaceutics and Biopharmaceutics 85, 882–888. https://doi.org/10.1016/j.ejpb.2013.03.026

Loh, Z.H., Samanta, A.K., Sia Heng, P.W., 2015. Overview of milling techniques for improving the solubility of poorly water-soluble drugs. Asian J Pharm Sci 10, 255–274. https://doi.org/10.1016/J.AJPS.2014.12.006

Luciani, C. V., 2018. Impact of Process Parameters on the Grinding Limit in High-Shear Wet Milling. Org Process Res Dev 22, 1328–1333. https://doi.org/10.1021/acs.oprd.8b00251

Maggi, L., Bruni, G., Maietta, M., Canobbio, A., Cardini, A., Conte, U., 2013a. II. Technological approaches to improve the dissolution behavior of nateglinide, a lipophilic insoluble drug: Co-milling. Int J Pharm 454, 568–572. https://doi.org/10.1016/j.ijpharm.2013.06.085

Maggi, L., Bruni, G., Maietta, M., Canobbio, A., Cardini, A., Conte, U., 2013b. I. Technological approaches to improve the dissolution behavior of nateglinide, a lipophilic insoluble drug: Nanoparticles and co-mixing. Int J Pharm 454, 562–567. https://doi.org/10.1016/j.ijpharm.2013.06.084

Mahlin, D., Bergström, C.A.S., 2013. Early drug development predictions of glass-forming ability and physical stability of drugs. European Journal of Pharmaceutical Sciences 49, 323–332. https://doi.org/10.1016/j.ejps.2013.03.016

Malamatari, M., Ross, S.A., Douroumis, D., Velaga, S.P., 2017. Experimental cocrystal screening and solution based scale-up cocrystallization methods. Adv Drug Deliv Rev 117, 162–177. https://doi.org/10.1016/j.addr.2017.08.006

Malamatari, M., Taylor, K.M.G., Malamataris, S., Douroumis, D., Kachrimanis, K., 2018. Pharmaceutical nanocrystals: production by wet milling and applications. Drug Discov Today 23, 534–547. https://doi.org/10.1016/j.drudis.2018.01.016

Maroof, M.A., Mahboubi, A., Noorzad, A., 2020. A new method to determine specific surface area and shape coefficient of a cohesionless granular medium. Advanced Powder Technology 31, 3038–3049. https://doi.org/10.1016/J.APT.2020.05.028

Marsac, P.J., Li, T., Taylor, L.S., 2009. Estimation of Drug–Polymer Miscibility and Solubility in Amorphous Solid Dispersions Using Experimentally Determined Interaction Parameters. Pharm Res 26, 139–151. https://doi.org/10.1007/s11095-008-9721-1

Martelli, S., Di Nunzio, P.E., 2025. Powder ball milling: An energy balance approach to particle size reduction. J Mater Res 40, 292–308. https://doi.org/10.1557/s43578-024-01502-6

Mártha, C., Jójárt-Laczkovich, O., Ulrich, J., Szabó-Révész, P., 2014. Investigation of the crystallinity of sugar alcohols co-ground with polymeric excipients. J Therm Anal Calorim 115, 2479–2486. https://doi.org/10.1007/s10973-013-3590-5

Matveeva, A.G., Skripkina, T.S., Nekrasov, V.M., Nikiforova, U.E., Bukhtoyarov, V.A., Bychkov, A., Lomovskiy, I., 2025. Particle aggregation and the grinding limit in high energy ball mill. Powder Technol 449, 120370. https://doi.org/10.1016/j.powtec.2024.120370

Mehta, M., Polli, J.E., Seo, P., Bhoopathy, S., Berginc, K., Kristan, K., Cook, J., Dressman, J.B., Mandula, H., Munshi, U., Shanker, R., Volpe, D.A., Gordon, J., Veerasingham, S., Welink, J., Almeida, S., Gonzalez, P., Painter, D., Tsang, Y.C., Vaidyanathan, J., Velagapudi, R., 2023. Drug Permeability - Best Practices for Biopharmaceutics Classification System (BCS)-Based Biowaivers: A workshop Summary Report. J Pharm Sci 112, 1749–1762. https://doi.org/10.1016/j.xphs.2023.04.016

Mehta, M.U., Uppoor, R.S., Conner, D.P., Seo, P., Vaidyanathan, J., Volpe, D.A., Stier, E., Chilukuri, D., Dorantes, A., Ghosh, T., Mandula, H., Raines, K., Dhanormchitphong, P., Woodcock, J., Yu, L.X., 2017. Impact of the US FDA “Biopharmaceutics Classification System” (BCS) Guidance on Global Drug Development. Mol Pharm 14, 4334–4338. https://doi.org/10.1021/acs.molpharmaceut.7b00687

Meier, M., John, E., Wieckhusen, D., Wirth, W., Peukert, W., 2009. Influence of mechanical properties on impact fracture: Prediction of the milling behaviour of pharmaceutical powders by nanoindentation. Powder Technol 188, 301–313. https://doi.org/10.1016/J.POWTEC.2008.05.009

Meiland, P., Larsen, B.S., Knopp, M.M., Tho, I., Rades, T., 2022. A new method to determine drug-polymer solubility through enthalpy of melting and mixing. Int J Pharm 629, 122391. https://doi.org/10.1016/j.ijpharm.2022.122391

Meng-Lund, H., Kasten, G., Jensen, K.T., Poso, A., Pantsar, T., Rades, T., Rantanen, J., Grohganz, H., 2018. The use of molecular descriptors in the development of co-amorphous formulations. European Journal of Pharmaceutical Sciences 119, 31–38. https://doi.org/10.1016/J.EJPS.2018.04.014

Mishra, J., Löbmann, K., Grohganz, H., Rades, T., 2018. Influence of preparation technique on co-amorphization of carvedilol with acidic amino acids. Int J Pharm 552, 407–413. https://doi.org/10.1016/J.IJPHARM.2018.09.070

Moos, J., Hansel, K., Abdulsamad, H., Stark, S., Clever, D., Peters, J., 2022. Robust Reinforcement Learning: A Review of Foundations and Recent Advances. Mach Learn Knowl Extr 4, 276–315. https://doi.org/10.3390/make4010013

Moutamenni, B., Tabary, N., Mussi, A., Dhainaut, J., Ciotonea, C., Fadel, A., Paccou, L., Dacquin, J.-P., Guinet, Y., Hédoux, A., 2023. Milling-Assisted Loading of Drugs into

Mesoporous Silica Carriers: A Green and Simple Method for Obtaining Tunable Customized Drug Delivery. Pharmaceutics 15, 390. https://doi.org/10.3390/pharmaceutics15020390

Mswahili, M.E., Lee, M.-J., Martin, G.L., Kim, J., Kim, P., Choi, G.J., Jeong, Y.-S., 2021. Cocrystal Prediction Using Machine Learning Models and Descriptors. Applied Sciences 11, 1323. https://doi.org/10.3390/app11031323

Mura, P., Cirri, M., Faucci, M.T., Ginès-Dorado, J.M., Bettinetti, G.P., 2002. Investigation of the effects of grinding and co-grinding on physicochemical properties of glisentide. J Pharm Biomed Anal 30, 227–237. https://doi.org/10.1016/S0731-7085(02)00252-2

Mura, P., Faucci, M.T., Parrini, P.L., 2001. Effects of Grinding with Microcrystalline Cellulose and Cyclodextrins on the Ketoprofen Physicochemical Properties. Drug Dev Ind Pharm 27, 119–128. https://doi.org/10.1081/DDC-100000478

Murdande, S.B., Pikal, M.J., Shanker, R.M., Bogner, R.H., 2010. Solubility advantage of amorphous pharmaceuticals: I. A thermodynamic analysis. J Pharm Sci 99, 1254–1264. https://doi.org/10.1002/jps.21903

Negrini, R., Aleandri, S., Kuentz, M., 2017. Study of Rheology and Polymer Adsorption Onto Drug Nanoparticles in Pharmaceutical Suspensions Produced by Nanomilling. J Pharm Sci 106, 3395–3401. https://doi.org/10.1016/J.XPHS.2017.07.006

Nernst, W., 1904. Theorie der Reaktionsgeschwindigkeit in heterogenen Systemen. Zeitschrift für Physikalische Chemie 47U, 52–55. https://doi.org/10.1515/zpch-1904-4704

Niederquell, A., Kuentz, M., 2014. Biorelevant dissolution of poorly soluble weak acids studied by UV imaging reveals ranges of fractal-like kinetics. Int J Pharm 463, 38–49. https://doi.org/10.1016/j.ijpharm.2013.12.049

Nkansah, P., Antipas, A., Lu, Y., Varma, M., Rotter, C., Rago, B., El-Kattan, A., Taylor, G., Rubio, M., Litchfield, J., 2013. Development and evaluation of novel solid nanodispersion system for oral delivery of poorly water-soluble drugs. Journal of Controlled Release 169, 150–161. https://doi.org/10.1016/j.jconrel.2013.03.032

Obaido, G., Mienye, I.D., Egbelowo, O.F., Emmanuel, I.D., Ogunleye, A., Ogbuokiri, B., Mienye, P., Aruleba, K., 2024. Supervised machine learning in drug discovery and development: Algorithms, applications, challenges, and prospects. Machine Learning with Applications 17, 100576. https://doi.org/10.1016/J.MLWA.2024.100576

Ohrem, H.L., Schornick, E., Kalivoda, A., Ognibene, R., 2014. Why is mannitol becoming more and more popular as a pharmaceutical excipient in solid dosage forms? Pharm Dev Technol 19, 257–262. https://doi.org/10.3109/10837450.2013.775154

Oliveira, P.F.M., Willart, J.-F., Siepmann, J., Siepmann, F., Descamps, M., 2018. Using Milling To Explore Physical States: The Amorphous and Polymorphic Forms of

Dexamethasone. Cryst Growth Des 18, 1748–1757. https://doi.org/10.1021/acs.cgd.7b01664

Ono, A., Kurihara, R., Terada, K., Sugano, K., 2023. Bioequivalence Dissolution Test Criteria for Formulation Development of High Solubility-Low Permeability Drugs. Chem Pharm Bull (Tokyo) 71, c22-00685. https://doi.org/10.1248/cpb.c22-00685

Parlier, É.M.S., Al Amir, K., Métro, T.-X., Granjon, P., Laurencin, D., Leroy, C., 2025a. Listening to the Formation of Polymorphs in a Ball Mill. Anal Chem 97, 2922–2931. https://doi.org/10.1021/acs.analchem.4c05608

Pas, T., Bergonzi, A., Michiels, E., Rousseau, F., Schymkowitz, J., Koekoekx, R., Clasen, C., Vergauwen, B., Van den Mooter, G., 2020a. Preparation of Amorphous Solid Dispersions by Cryomilling: Chemical and Physical Concerns Related to Active Pharmaceutical Ingredients and Carriers. Mol Pharm 17, 1001–1013. https://doi.org/10.1021/acs.molpharmaceut.9b01265

Pas, T., Smeets, B., Ramon, H., Van Schepdael, A., Mansour, M., Koekoekx, R., Clasen, C., Vergauwen, B., Van den Mooter, G., 2020b. Mechanodegradation of Polymers: A Limiting Factor of Mechanochemical Activation in the Production of Amorphous Solid Dispersions by Cryomilling. Mol Pharm 17, 2987–2999. https://doi.org/10.1021/acs.molpharmaceut.0c00376

Patera, J., Němečková, P., Zámostný, P., 2022. Dissolution Kinetics of Meloxicam Formulations Co-Milled with Sodium Lauryl Sulfate. Pharmaceutics 14, 2173. https://doi.org/10.3390/pharmaceutics14102173

Patterson, J.E., James, M.B., Forster, A.H., Lancaster, R.W., Butler, J.M., Rades, T., 2007. Preparation of glass solutions of three poorly water soluble drugs by spray drying, melt extrusion and ball milling. Int J Pharm 336, 22–34. https://doi.org/10.1016/j.ijpharm.2006.11.030

Pätzmann, N., Beránek, J., Griffin, B.T., Kuentz, M., O'Dwyer, P.J., 2025. Co-milling of glass forming ability class III drugs: Comparing the impact of low and high glass transition temperatures. European Journal of Pharmaceutical Sciences 209, 107081. https://doi.org/10.1016/J.EJPS.2025.107081

Pätzmann, N., O'Dwyer, P.J., Beránek, J., Kuentz, M., Griffin, B.T., 2024. Predictive computational models for assessing the impact of co-milling on drug dissolution. European Journal of Pharmaceutical Sciences 198, 106780. https://doi.org/10.1016/j.ejps.2024.106780

Peltonen, L., Hirvonen, J., 2010. Pharmaceutical nanocrystals by nanomilling: critical process parameters, particle fracturing and stabilization methods. Journal of Pharmacy and Pharmacology 62, 1569–1579. https://doi.org/10.1111/j.2042-7158.2010.01022.x

Peterson, G.I., Ko, W., Hwang, Y.-J., Choi, T.-L., 2020. Mechanochemical Degradation of Amorphous Polymers with Ball-Mill Grinding: Influence of the Glass Transition Temperature. Macromolecules 53, 7795–7802. https://doi.org/10.1021/acs.macromol.0c01510

Petrović, J., Ibrić, S., Betz, G., Parojčić, J., Durić, Z., 2009. Application of dynamic neural networks in the modeling of drug release from polyethylene oxide matrix tablets. European Journal of Pharmaceutical Sciences 38, 172–180. https://doi.org/10.1016/J.EJPS.2009.07.007

Pezzoli, R., Lyons, J.G., Gately, N., Higginbotham, C.L., 2018. Investigation of miscibility estimation methods between indomethacin and poly(vinylpyrrolidone-co-vinyl acetate). Int J Pharm 549, 50–57. https://doi.org/10.1016/J.IJPHARM.2018.07.039

Priemel, P.A., Grohganz, H., Rades, T., 2016. Unintended and in situ amorphisation of pharmaceuticals. Adv Drug Deliv Rev 100, 126–132. https://doi.org/10.1016/J.ADDR.2015.12.014

Priestley, I., Battilocchio, C., Iosub, A. V., Barreteau, F., Bluck, G.W., Ling, K.B., Ingram, K., Ciaccia, M., Leitch, J.A., Browne, D.L., 2023. Safety Considerations and Proposed Workflow for Laboratory-Scale Chemical Synthesis by Ball Milling. Org Process Res Dev 27, 269–275. https://doi.org/10.1021/acs.oprd.2c00226

Prziwara, P., Kwade, A., 2020. Grinding aids for dry fine grinding processes – Part I: Mechanism of action and lab-scale grinding. Powder Technol 375, 146–160. https://doi.org/10.1016/j.powtec.2020.07.038

Quodbach, J., Kleinebudde, P., 2015. A critical review on tablet disintegration. Pharm Dev Technol 1–12. https://doi.org/10.3109/10837450.2015.1045618

Quodbach, J., Kleinebudde, P., 2014. Systematic classification of tablet disintegrants by water uptake and force development kinetics. Journal of Pharmacy and Pharmacology 66, 1429–1438. https://doi.org/10.1111/jphp.12276

Quodbach, J., Moussavi, A., Tammer, R., Frahm, J., Kleinebudde, P., 2014. Tablet Disintegration Studied by High-Resolution Real-Time Magnetic Resonance Imaging. J Pharm Sci 103, 249–255. https://doi.org/10.1002/jps.23789

Rautio, J., Kumpulainen, H., Heimbach, T., Oliyai, R., Oh, D., Järvinen, T., Savolainen, J., 2008. Prodrugs: design and clinical applications. Nat Rev Drug Discov 7, 255–270. https://doi.org/10.1038/nrd2468

Remko, M., 2009. Molecular structure, lipophilicity, solubility, absorption, and polar surface area of novel anticoagulant agents. Journal of Molecular Structure: THEOCHEM 916, 76–85. https://doi.org/10.1016/j.theochem.2009.09.011

Reppas, C., Kuentz, M., Bauer-Brandl, A., Carlert, S., Dallmann, A., Dietrich, S., Dressman, J., Ejskjaer, L., Frechen, S., Guidetti, M., Holm, R., Holzem, F.L., Karlsson, E.,

Kostewicz, E., Panbachi, S., Paulus, F., Senniksen, M.B., Stillhart, C., Turner, D.B., Vertzoni, M., Vrenken, P., Zöller, L., Griffin, B.T., O'Dwyer, P.J., 2023. Leveraging the use of in vitro and computational methods to support the development of enabling oral drug products: An InPharma commentary. European Journal of Pharmaceutical Sciences 188, 106505. https://doi.org/10.1016/J.EJPS.2023.106505

Ribeiro, A., Montes, F., Sousa, J., Pais, A., 2025. Comminution technologies in the pharmaceutical industry: a comprehensive review with recent advances. Reviews in Chemical Engineering 41, 69–100. https://doi.org/10.1515/revce-2024-0059

Rosenberger, J., Butler, J., Dressman, J., 2018. A Refined Developability Classification System. J Pharm Sci 107, 2020–2032. https://doi.org/10.1016/j.xphs.2018.03.030

Roudaut, G., Simatos, D., Champion, D., Contreras-Lopez, E., Le Meste, M., 2004. Molecular mobility around the glass transition temperature: a mini review. Innovative Food Science & Emerging Technologies 5, 127–134. https://doi.org/10.1016/J.IFSET.2003.12.003

Saal, C., Becker, A., 2013. Pharmaceutical salts: A summary on doses of salt formers from the Orange Book. European Journal of Pharmaceutical Sciences 49, 614–623. https://doi.org/10.1016/J.EJPS.2013.05.026

Saharan, V., Kukkar, V., Kataria, M., Gera, M., Choudhury, P., 2010. Dissolution enhancement of drugs. part i: technologies and effect of carriers. International Journal of Health Research 2. https://doi.org/10.4314/ijhr.v2i2.55401

Sarjeant, A., Abourahma, H., Thomas, S., Cook, C., Yin, Z., 2024. On the Road to Cocrystal Prediction: A Screening Study for the Validation of In Silico Methods. Cryst Growth Des 24, 5486–5493. https://doi.org/10.1021/acs.cgd.4c00220

Seibert, K.D., Collins, P.C., Luciani, C. V., Fisher, E.S., 2019. MILLING OPERATIONS IN THE PHARMACEUTICAL INDUSTRY, in: Chemical Engineering in the Pharmaceutical Industry. Wiley, pp. 861–879. https://doi.org/10.1002/9781119600800.ch38

Shaikh, R., Shirazian, S., Guerin, S., Sheehan, E., Thompson, D., Walker, G.M., Croker, D.M., 2021. Understanding solid-state processing of pharmaceutical cocrystals via milling: Role of tablet excipients. Int J Pharm 601, 120514. https://doi.org/10.1016/j.ijpharm.2021.120514

Shi, Q., Wang, Y., Moinuddin, S.M., Feng, X., Ahsan, F., 2022. Co-amorphous Drug Delivery Systems: a Review of Physical Stability, In Vitro and In Vivo Performance. AAPS PharmSciTech 23, 259. https://doi.org/10.1208/s12249-022-02421-7

Sigfridsson, K., Rydberg, H., Strimfors, M., 2019. Nano- and microcrystals of griseofulvin subcutaneously administered to rats resulted in improved bioavailability and sustained release. Drug Dev Ind Pharm 45, 1477–1486. https://doi.org/10.1080/03639045.2019.1628769

Slámová, M., Prausová, K., Epikaridisová, J., Brokešová, J., Kuentz, M., Patera, J., Zámostný, P., 2021. Effect of co-milling on dissolution rate of poorly soluble drugs. Int J Pharm 597, 120312. https://doi.org/10.1016/j.ijpharm.2021.120312

Sliwoski, G., Kothiwale, S., Meiler, J., Lowe, E.W., Barker, E.L., 2014. Computational Methods in Drug Discovery. Pharmacol Rev 66, 334–395. https://doi.org/10.1124/pr.112.007336

Song, Y., Ding, Y., Su, J., Li, J., Ji, Y., 2025. Unlocking the Potential of Machine Learning in Co-crystal Prediction by a Novel Approach Integrating Molecular Thermodynamics. Angewandte Chemie International Edition 64. https://doi.org/10.1002/anie.202502410

Stegemann, S., Moreton, C., Svanbäck, S., Box, K., Motte, G., Paudel, A., 2023. Trends in oral small-molecule drug discovery and product development based on product launches before and after the Rule of Five. Drug Discov Today 28, 103344. https://doi.org/10.1016/J.DRUDIS.2022.103344

Steinbrueck, A., Sedgwick, A.C., Hwang, S.-M., Sen, S., Zhao, M.Y., Huang, D.-Y., Knoll, D.M., Wang, Y.-Y., Sessler, J.L., 2021. A Deferasirox Derivative That Acts as a Multifaceted Platform for the Detection and Quantification of Fe3+. Chemosensors 9, 68. https://doi.org/10.3390/chemosensors9040068

Štukelj, J., Svanbäck, S., Agopov, M., Löbmann, K., Strachan, C.J., Rades, T., Yliruusi, J., 2019. Direct Measurement of Amorphous Solubility. Anal Chem 91, 7411–7417. https://doi.org/10.1021/acs.analchem.9b01378

Sugano, K., Terada, K., 2015. Rate- and Extent-Limiting Factors of Oral Drug Absorption: Theory and Applications. J Pharm Sci 104, 2777–2788. https://doi.org/10.1002/jps.24391

Suys, E.J.A., Chalmers, D.K., Pouton, C.W., Porter, C.J.H., 2018. Polymeric Precipitation Inhibitors Promote Fenofibrate Supersaturation and Enhance Drug Absorption from a Type IV Lipid-Based Formulation. Mol Pharm 15, 2355–2371. https://doi.org/10.1021/acs.molpharmaceut.8b00206

Taye, M.M., 2023. Understanding of Machine Learning with Deep Learning: Architectures, Workflow, Applications and Future Directions. Computers 12, 91. https://doi.org/10.3390/computers12050091

Taylor, L.S., Braun, D.E., Steed, J.W., 2021. Crystals and Crystallization in Drug Delivery Design. Cryst Growth Des 21, 1375–1377. https://doi.org/10.1021/acs.cgd.0c01592

Tipduangta, P., Takieddin, K., Fábián, L., Belton, P., Qi, S., 2015. A New Low Melting-Point Polymorph of Fenofibrate Prepared via Talc Induced Heterogeneous Nucleation. Cryst Growth Des 15, 5011–5020. https://doi.org/10.1021/acs.cgd.5b00956

Trezza, A., Visibelli, A., Roncaglia, B., Spiga, O., Santucci, A., 2024. Unsupervised Learning in Precision Medicine: Unlocking Personalized Healthcare through AI. Applied Sciences 14, 9305. https://doi.org/10.3390/app14209305

Tsinman, K., Avdeef, A., Tsinman, O., Voloboy, D., 2009. Powder Dissolution Method for Estimating Rotating Disk Intrinsic Dissolution Rates of Low Solubility Drugs. Pharm Res 26, 2093–2100. https://doi.org/10.1007/s11095-009-9921-3

Türeli, N.G., Türeli, A.E., 2020. Upscaling and GMP production of pharmaceutical drug delivery systems. Drug Delivery Trends: Volume 3: Expectations and Realities of Multifunctional Drug Delivery Systems 3, 215–229. https://doi.org/10.1016/B978-0-12-817870-6.00011-0

Turkoglu, M., Aydin, I., Murray, M., Sakr, A., 1999. Modeling of a roller-compaction process using neural networks and genetic algorithms. European Journal of Pharmaceutics and Biopharmaceutics 48, 239–245. https://doi.org/10.1016/S0939-6411(99)00054-5

Turnbull, D., 1969. Under what conditions can a glass be formed? Contemp Phys 10, 473–488. https://doi.org/10.1080/00107516908204405

Vadher, A.H., Parikh, J.R., Parikh, R.H., Solanki, A.B., 2009. Preparation and Characterization of Co-Grinded Mixtures of Aceclofenac and Neusilin US2 for Dissolution Enhancement of Aceclofenac. AAPS PharmSciTech 10, 606–614. https://doi.org/10.1208/s12249-009-9221-6

Varghese, S., Ghoroi, C., 2017. Improving the wetting and dissolution of ibuprofen using solventless co-milling. Int J Pharm 533, 145–155. https://doi.org/10.1016/j.ijpharm.2017.09.062

Vinarov, Z., Abrahamsson, B., Artursson, P., Batchelor, H., Berben, P., Bernkop-Schnürch, A., Butler, J., Ceulemans, J., Davies, N., Dupont, D., Flaten, G.E., Fotaki, N., Griffin, B.T., Jannin, V., Keemink, J., Kesisoglou, F., Koziolek, M., Kuentz, M., Mackie, A., Meléndez-Martínez, A.J., McAllister, M., Müllertz, A., O'Driscoll, C.M., Parrott, N., Paszkowska, J., Pavek, P., Porter, C.J.H., Reppas, C., Stillhart, C., Sugano, K., Toader, E., Valentová, K., Vertzoni, M., De Wildt, S.N., Wilson, C.G., Augustijns, P., 2021. Current challenges and future perspectives in oral absorption research: An opinion of the UNGAP network. Adv Drug Deliv Rev 171, 289–331. https://doi.org/10.1016/j.addr.2021.02.001

Vogt, M., Kunath, K., Dressman, J.B., 2008a. Dissolution improvement of four poorly water soluble drugs by cogrinding with commonly used excipients. European Journal of Pharmaceutics and Biopharmaceutics 68, 330–337. https://doi.org/10.1016/j.ejpb.2007.05.009

Vogt, M., Vertzoni, M., Kunath, K., Reppas, C., Dressman, J.B., 2008b. Cogrinding enhances the oral bioavailability of EMD 57033, a poorly water soluble drug, in dogs. European

Journal of Pharmaceutics and Biopharmaceutics 68, 338–345. https://doi.org/10.1016/j.ejpb.2007.06.011

Wang, M., Gong, J., Rades, T., Martins, I.C.B., 2023. Amorphization of different furosemide polymorphic forms during ball milling: Tracking solid-to-solid phase transformations. Int J Pharm 648, 123573. https://doi.org/10.1016/j.ijpharm.2023.123573

Wang, W., Ye, Z., Gao, H., Ouyang, D., 2021. Computational pharmaceutics - A new paradigm of drug delivery. Journal of Controlled Release 338, 119–136. https://doi.org/10.1016/J.JCONREL.2021.08.030

Willart, J.F., Descamps, M., 2008. Solid State Amorphization of Pharmaceuticals. Mol Pharm 5, 905–920. https://doi.org/10.1021/mp800092t

Willart, J.F., Descamps, N., Caron, V., Capet, F., Danède, F., Descamps, M., 2006. Formation of lactose-mannitol molecular alloys by solid state vitrification. Solid State Commun 138, 194–199. https://doi.org/10.1016/J.SSC.2006.02.034

Willart, J.F., Lefebvre, J., Danède, F., Comini, S., Looten, P., Descamps, M., 2005. Polymorphic transformation of the Γ-form of d-sorbitol upon milling: structural and nanostructural analyses. Solid State Commun 135, 519–524. https://doi.org/10.1016/J.SSC.2005.04.048

Wu, C.-Y., Benet, L.Z., 2005. Predicting Drug Disposition via Application of BCS: Transport/Absorption/ Elimination Interplay and Development of a Biopharmaceutics Drug Disposition Classification System. Pharm Res 22, 11–23. https://doi.org/10.1007/s11095-004-9004-4

Wu, D., Zhang, B., Yao, Q., Hou, B., Zhou, L., Xie, C., Gong, J., Hao, H., Chen, W., 2021a. Evaluation on Cocrystal Screening Methods and Synthesis of Multicomponent Crystals: A Case Study. Cryst Growth Des 21, 4531–4546. https://doi.org/10.1021/acs.cgd.1c00415

Wyttenbach, N., Kirchmeyer, W., Alsenz, J., Kuentz, M., 2016. Theoretical Considerations of the Prigogine–Defay Ratio with Regard to the Glass-Forming Ability of Drugs from Undercooled Melts. Mol Pharm 13, 241–250. https://doi.org/10.1021/acs.molpharmaceut.5b00688

Xiong, X., Zhang, M., Hou, Q., Tang, P., Suo, Z., Zhu, Y., Li, H., 2019. Solid dispersions of telaprevir with improved solubility prepared by co-milling: formulation, physicochemical characterization, and cytotoxicity evaluation. Materials Science and Engineering: C 105, 110012. https://doi.org/10.1016/j.msec.2019.110012

Yang, C., Xu, X., Wang, J., An, Z., 2012. Use of the Co-grinding Method to Enhance the Dissolution Behavior of a Poorly Water-Soluble Drug: Generation of Solvent-Free Drug–Polymer Solid Dispersions. Chem Pharm Bull (Tokyo) 60, 837–845. https://doi.org/10.1248/cpb.c12-00034

Yang, L., Wu, P., Xu, J., Xie, D., Wang, Z., Wang, Q., Chen, Y., Li, C.H., Zhang, J., Chen, H., Quan, G., 2021. Development of Apremilast Solid Dispersion Using TPGS and PVPVA with Enhanced Solubility and Bioavailability. AAPS PharmSciTech 22, 142. https://doi.org/10.1208/s12249-021-02005-x

Zhang, G.G.Z., Gu, C., Zell, M.T., Burkhardt, R.T., Munson, E.J., Grant, D.J.W., 2002. Crystallization and Transitions of Sulfamerazine Polymorphs. J Pharm Sci 91, 1089–1100. https://doi.org/10.1002/jps.10100

Zhang, Q., Durig, T., Blass, B., Fassihi, R., 2022. Development of an amorphous based sustained release system for apremilast a selective phosphodiesterase 4 (PDE4) inhibitor. Int J Pharm 615, 121516. https://doi.org/10.1016/j.ijpharm.2022.121516

Zhang, Q., Li, A., Yan, Y., Wu, Y., Zhang, X., 2021. Systematic thermodynamic analysis of apremilast polymorphs via solubility measurement with modeling: Mechanism evaluation through molecular simulation. European Journal of Pharmaceutical Sciences 165, 105958. https://doi.org/10.1016/j.ejps.2021.105958

Zhang, X.-R., Wu, B.-L., Han, J.-J., Li, J.-Q., 2024. Simultaneous Improvement in Dissolution Behavior and Oral Bioavailability of Naproxen via Salt Formation. Crystals (Basel) 14, 1104. https://doi.org/10.3390/cryst14121104

Zhao, Q., Ye, Z., Su, Y., Ouyang, D., 2019. Predicting complexation performance between cyclodextrins and guest molecules by integrated machine learning and molecular modeling techniques. Acta Pharm Sin B 9, 1241–1252. https://doi.org/10.1016/J.APSB.2019.04.004

Zholdassov, Y.S., Kwok, R.W., Shlain, M.A., Patel, M., Marianski, M., Braunschweig, A.B., 2024. Kinetics of primary mechanochemical covalent-bond-forming reactions. RSC Mechanochemistry 1, 11–32. https://doi.org/10.1039/D3MR00018D

Zhuo, X., Jasiukenaite, I., Löbmann, K., 2024. β-Lactoglobulin-based amorphous solid dispersions: A graphical review on the state-of-the-art. European Journal of Pharmaceutics and Biopharmaceutics 202, 114396. https://doi.org/10.1016/J.EJPB.2024.114396

Zimper, U., Aaltonen, J., Krauel-Goellner, K., Gordon, K.C., Strachan, C.J., Rades, T., 2010a. The Influence of Milling on the Dissolution Performance of Simvastatin. Pharmaceutics 2, 419–431. https://doi.org/10.3390/pharmaceutics2040419

Zimper, U., Aaltonen, J., McGoverin, C.M., Gordon, K.C., Krauel-Goellner, K., Rades, T., 2010b. Quantification of Process Induced Disorder in Milled Samples Using Different Analytical Techniques. Pharmaceutics 2, 30–49. https://doi.org/10.3390/pharmaceutics2010030

Zöller, L., Avdeef, A., Karlsson, E., Borde, A., Carlert, S., Saal, C., Dressman, J., 2024. A comparison of USP 2 and µDISS ProfilerTM apparatus for studying dissolution

phenomena of ibuprofen and its salts. European Journal of Pharmaceutical Sciences 193, 106684. https://doi.org/10.1016/j.ejps.2023.106684

10 Supplementary materials

10.1 Appendix Chapter 2

10.1.1 Thermodynamic Solubility values of investigated compounds in FaSSIF

Table S1: Thermodynamic solubility values of investigated compounds in Fasted State Simulated Intestinal Fluid (FaSSIF) at 37°C after 24 h of dissolution and a stirring speed of 100 rpm with standard deviations

Drug Compound	**Apparent solubility [µg/ml] ± SD**
Albendazole	3.3 ± 0.8
Apixaban	53.2 ± 1.2
Apremilast	46.7 ± 1.4
Aripiprazole	27.8 ± 0.9
Candesartan Cilexetil	19.9 ± 1.2
Carbamazepine	383.6 ± 3.0
Celecoxib	42.7 ± 0.8
Ceritinib	35.9 ± 1.8
Cinnarizine	14.7 ± 0.6
Dasatinib	53.1 ± 2.1
Deferasirox	78.5 ± 3.2
Dipyridamole	16.9 ± 0.6
Enzalutamide	5.4 ± 0.1
Etoricoxib	137.9 ± 2.9
Ezetimibe	14.9 ± 1.2
Fenofibrate	4.6 ± 0.6
Gemfibrozil	667 ± 8.9
Glibenclamide	4.0 ± 0.5
Griseofulvin	17.5 ± 2.2
Indomethacin	426 ± 22.0
Mefenamic acid	42.5 ± 1.5
Nilotinib	3.9 ± 0.7
Nimesulide	24.0 ± 0.9
Olaparib	127.8 ± 3.2
Rivaroxaban	7.1 ± 0.5
Sertraline	168.4 ± 14.1
Sorafenib	33.9 ± 0.7
Tadalafil	7.0 ± 0.6
Thiabendazole	42.1 ± 0.9

10.1.2 Measured median particle sizes (D50) of drug powders

Table S2: Measured median particle sizes (D50) of drug powders before their use with standard deviations

Drug Compound	**D50 [µm] ± SD**
Albendazole	38.11 ± 2.55
Apixaban	212.4 ± 1.23
Apremilast	10.6 ± 0.71
Aripiprazole	185.98 ± 2.4
Candesartan Cilexetil	15.15 ± 0.38
Carbamazepine	15.87 ± 2.74
Celecoxib	8.24 ± 0.53
Ceritinib	72.51 ± 4.99
Cinnarizine	96.78 ± 0.36
Dasatinib	3.62 ± 0.03
Deferasirox	5.2 ± 0.14
Dipyridamole	64.35 ± 0.06
Enzalutamide	148.93 ± 1.26
Etoricoxib	10.89 ± 0.03
Ezetimibe	7.88 ± 0.63
Fenofibrate	255.26 ± 3.35
Gemfibrozil	23.35 ± 0.50
Glibenclamide	71.4 ± 0.57
Griseofulvin	14.96 ± 0.14
Indomethacin	32.01 ± 0.06
Mefenamic acid	50.93 ± 0.72
Nilotinib	83.61 ± 2.10
Nimesulide	15.1 ± 1.14
Olaparib	28.2 ± 2.01
Rivaroxaban	9.5 ± 1.54
Sertraline	49.05 ± 4.12
Sorafenib	37.46 ± 0.55
Tadalafil	15.89 ± 3.89
Thiabendazole	18.97 ± 0.89

10.1.3 Co-Milling Dissolution Ratios, 15 min timepoint

Table S3: Percentage of dissolved drug after 15 minutes dissolution in physical mixtures (PM) and co-milled mixtures (COM) with standard deviations and Co-Milling Dissolution Ratios ($COMDR_{15\ min}$).

Drug Compound	PM dissolved 15 min ± SD [%]	COM dissolved 15 min ± SD [%]	$COMDR_{15\ min}$
Albendazole	1.92 ± 0.16	3.46 ± 0.82	1.8
Apixaban	3.38 ± 0.22	27.18 ± 0.17	8.03
Apremilast	16.88 ± 0.53	27.05 ± 0.06	1.6
Aripiprazole	1.72 ± 0.12	12.00 ± 1.60	6.97
Candesartan Cilexetil	1.26 ± 1.11	5.72 ± 1.62	4.55
Carbamazepine	28.51 ± 0.08	31.75 ± 1.87	1.11
Celecoxib	8.40 ± 0.70	13.57 ± 1.39	1.61
Ceritinib	6.49 ± 0.22	18.5 ± 0.99	2.85
Cinnarizine	1.56 ± 0.18	10.90 ± 0.42	6.97
Dasatinib	18.78 ± 1.18	30.34 ± 0.60	1.63
Deferasirox	19.15 ± 1.14	26.44 ± 0.14	1.38
Dipyridamole	7.37 ± 0.09	29.17 ± 3.14	3.96
Enzalutamide	0.99 ± 0.01	20.30 ± 2.34	20.47
Etoricoxib	14.07 ± 0.47	32.43 ± 1.08	2.31
Ezetimibe	5.23 ± 0.31	15.95 ± 0.05	3.05
Fenofibrate	0.33 ± 0.12	8.66 ± 0.38	26.48
Gemfibrozil	23.66 ± 0.88	30.44 ± 0.69	1.29
Glibenclamide	2.30 ± 0.30	27.49 ± 0.70	11.94
Griseofulvin	22.30 ± 0.89	35.02 ± 0.33	1.57
Indomethacin	24.64 ± 0.45	28.39 ± 2.53	1.15
Mefenamic acid	17.24 ± 0.79	29.53 ± 0.86	1.71
Nilotinib	0.67 ± 0.08	4.50 ± 1.38	6.69
Nimesulide	22.22 ± 0.47	34.48 ± 0.92	1.55
Olaparib	21.64 ± 0.39	33.87 ± 0.31	1.56
Rivaroxaban	21.66 ± 3.69	30.92 ± 4.49	1.43
Sertraline	20.26 ± 0.31	31.36 ± 0.83	1.55
Sorafenib	2.30 ± 0.08	7.17 ± 0.91	3.12
Tadalafil	17.60 ± 2.16	22.39 ± 2.20	1.27
Thiabendazole	23.90 ± 0.26	35.87 ± 0.17	1.5

10.1.4 Co-Milling Dissolution Ratios, 60 min timepoint

Table S4: Percentage of dissolved drug after 60 minutes dissolution in physical mixtures (PM) and co-milled mixtures (COM) with standard deviations and Co-Milling Dissolution Ratios ($COMDR_{60\ min}$).

Drug Compound	PM dissolved 60 min ± SD [%]	COM dissolved 60 min ± SD [%]	$COMDR_{60\ min}$
Albendazole	2.32 ± 0.12	12.72 ± 0.50	5.49
Apixaban	5.69 ± 0.20	29.86 ± 0.22	5.24
Apremilast	19.43 ± 0.20	29.23 ± 0.35	1.5
Aripiprazole	3.09 ± 0.08	24.33 ± 2.00	7.88
Candesartan Cilexetil	5.40 ± 0.41	15.06 ± 1.09	2.79
Carbamazepine	30.08 ± 0.60	30.58 ± 0.87	1.02
Celecoxib	16.95 ± 0.20	23.99 ± 1.28	1.42
Ceritinib	8.70 ± 0.25	29.37 ± 0.91	3.38
Cinnarizine	3.31 ± 0.24	23.09 ± 0.47	6.98
Dasatinib	23.22 ± 0.42	35.97 ± 0.42	1.55
Deferasirox	26.57 ± 1.48	30.31 ± 0.10	1.14
Dipyridamole	10.85 ± 0.38	38.52 ± 1.09	3.55
Enzalutamide	2.67 ± 1.25	31.33 ± 2.69	11.73
Etoricoxib	16.47 ± 1.35	31.39 ± 0.72	1.91
Ezetimibe	15.11 ± 0.41	26.33 ± 0.13	1.74
Fenofibrate	1.18 ± 0.13	25.22 ± 0.35	21.41
Gemfibrozil	30.34 ± 0.34	31.89 ± 0.42	1.05
Glibenclamide	4.96 ± 2.62	30.13 ± 0.98	6.08
Griseofulvin	26.30 ± 0.61	36.01 ± 0.30	1.37
Indomethacin	30.42 ± 0.87	24.82 ± 1.45	0.82
Mefenamic acid	25.13 ± 0.60	33.12 ± 0.23	1.32
Nilotinib	0.97 ± 0.06	8.85 ± 1.61	9.12
Nimesulide	29.82 ± 0.78	34.61 ± 1.18	1.16
Olaparib	25.48 ± 0.40	36.59 ± 0.46	1.44
Rivaroxaban	26.10 ± 4.28	39.15 ± 4.19	1.5
Sertraline	18.76 ± 0.60	43.82 ± 2.60	2.34
Sorafenib	4.21 ± 0.34	22.02 ± 1.38	5.22
Tadalafil	25.48 ± 3.01	37.64 ± 3.27	1.47
Thiabendazole	27.89 ± 0.39	37.25 ± 0.29	1.34

10.1.5 Multicollinearity diagnosis of multiple linear regression equations

Table S5: Results of multicollinearity analysis. Following abbreviations are used: Variance inflation factor (VIF), Multiple linear regression (MLR), median drug particle size (D50), calculated partition coefficient at pH 6.5 ($clogD_{6.5}$)

Variable	**VIF**	**Conditions index**
MLR equation $logCOMDR_{15\ min}$		8.1
D50	1.3	
$clogD_{6.5}$	1.6	
Kappa 3	1.3	
MLR equation $logCOMDR_{60\ min}$		7.8
D50	1.3	
$clogD_{6.5}$	1.4	
Apparent solubility	1.1	

10.1.6 Powder X-ray diffractograms of screened drug compounds in co-milled and physical mixtures

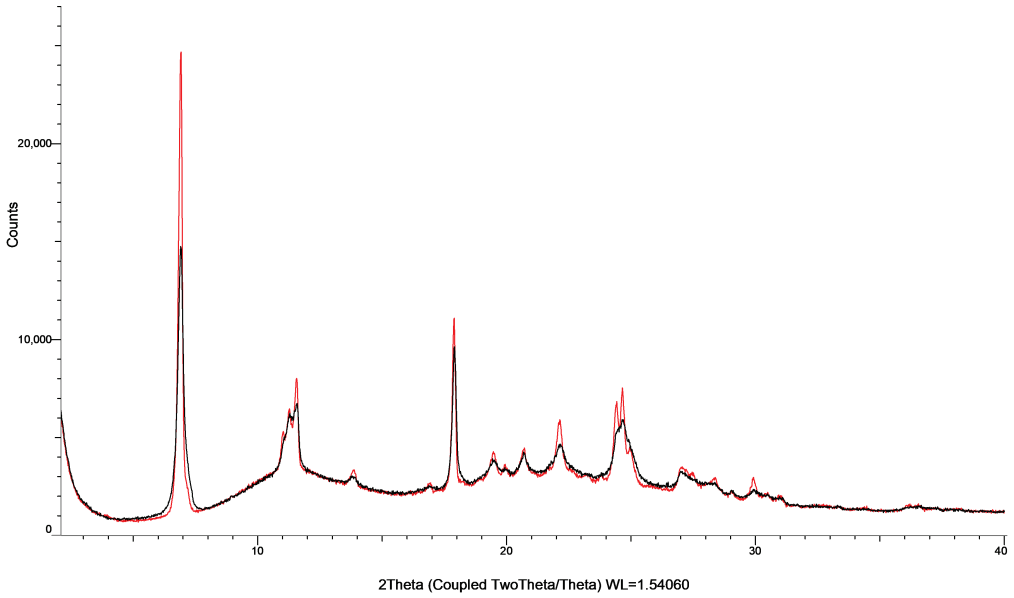


Figure S6: XRPD patterns of albendazole with PVP K25 in co-milled mixtures (black) and physical mixtures (red)

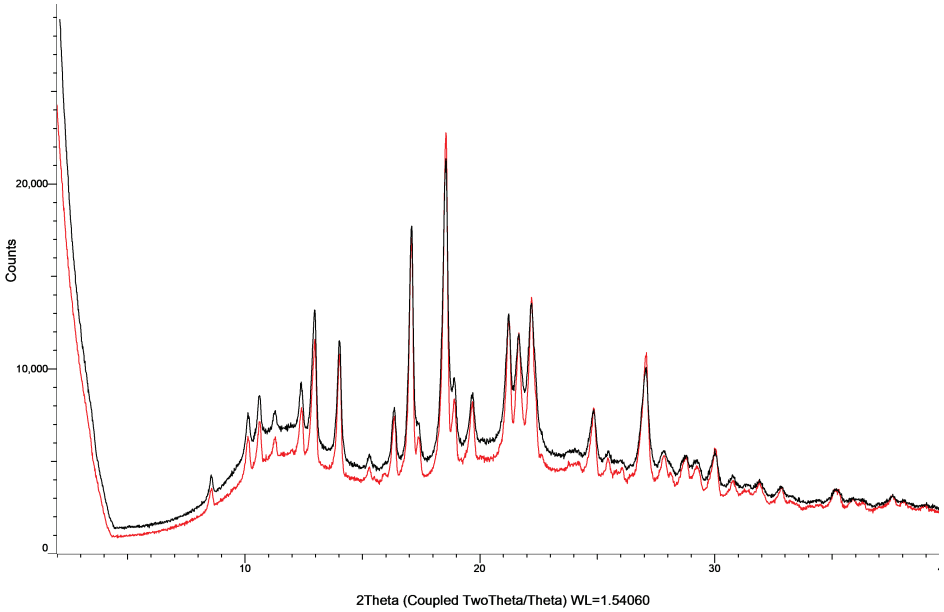


Figure S7: XRPD patterns of apixaban with PVP K25 in co-milled mixtures (black) and physical mixtures (red).

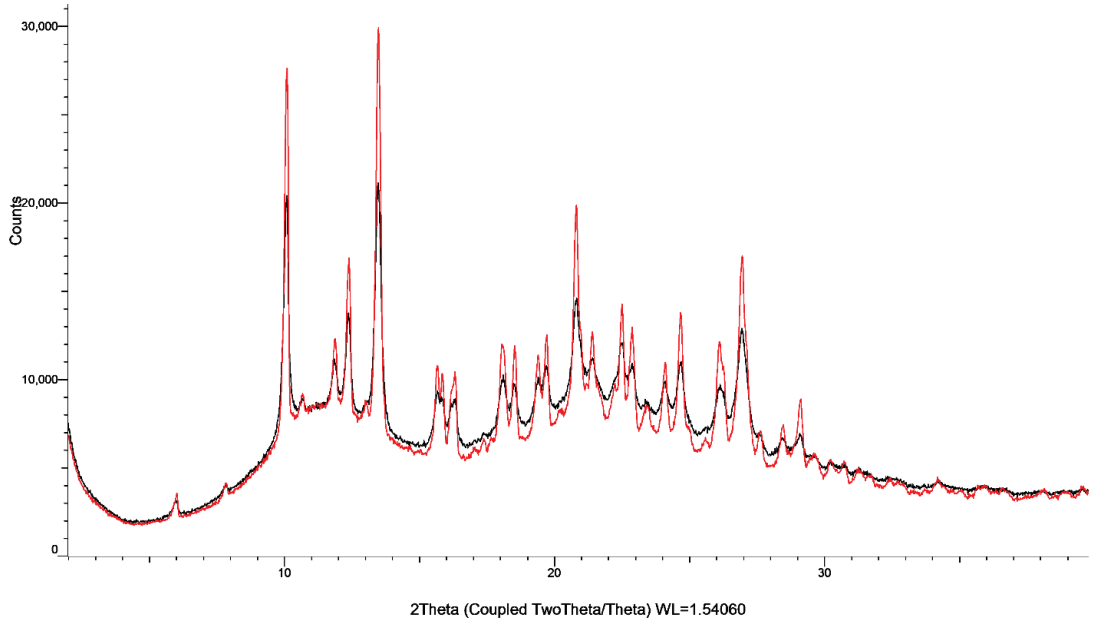


Figure S8: XRPD patterns of apremilast with PVP K25 in co-milled mixtures (black) and physical mixtures (red).

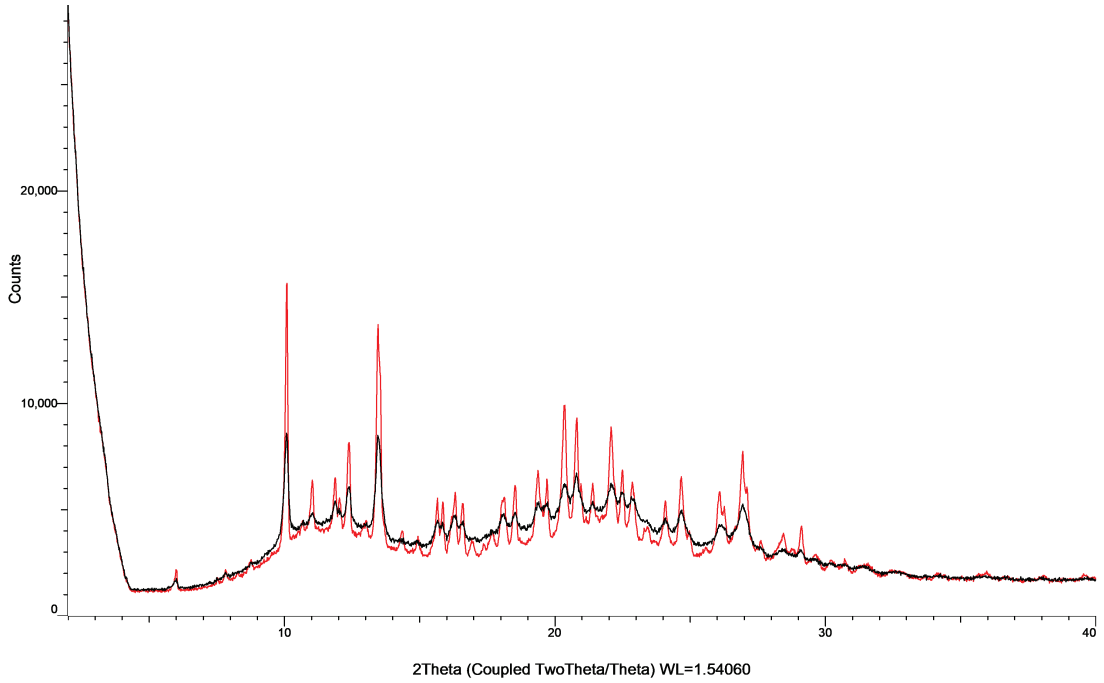


Figure S9: XRPD patterns of aripiprazole with PVP K25 in co-milled mixtures (black) and physical mixtures (red).

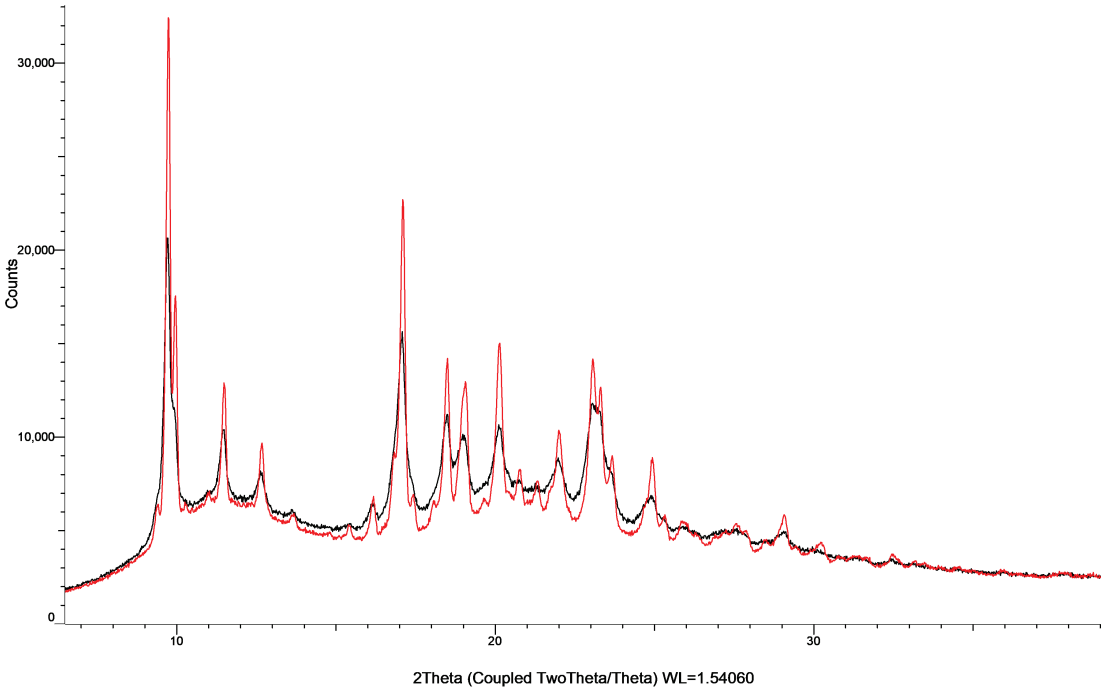


Figure S10: XRPD patterns of candesartan cilexetil with PVP K25 in co-milled mixtures (black) and physical mixtures (red).

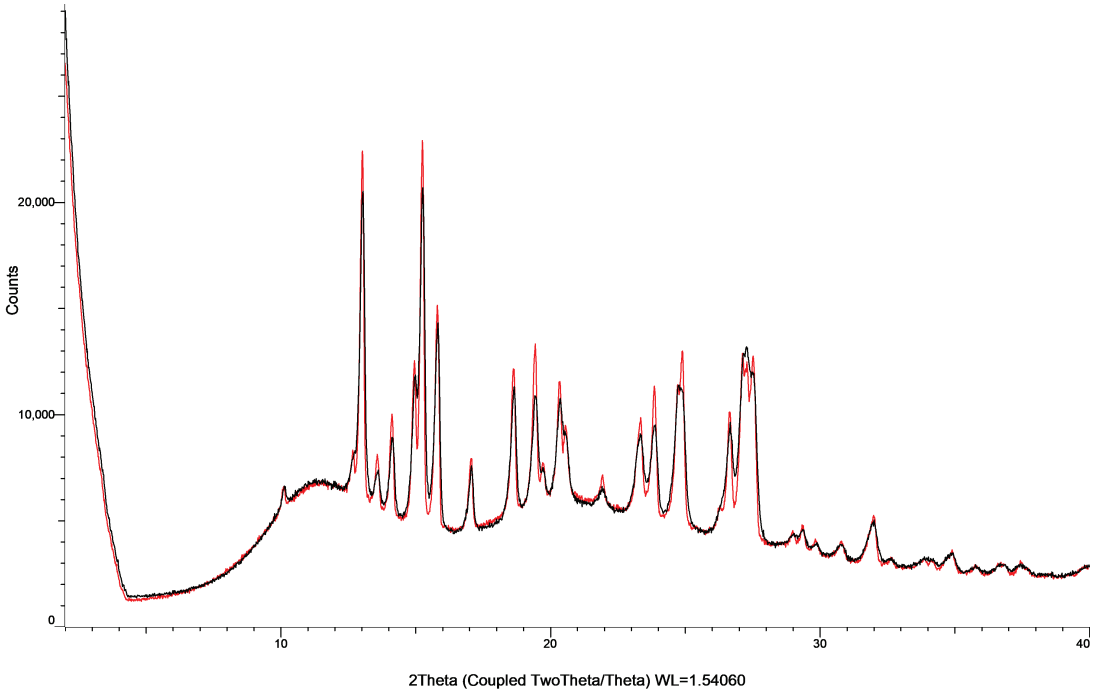


Figure S11: XRPD patterns of carbamazepine with PVP K25 in co-milled mixtures (black) and physical mixtures (red).

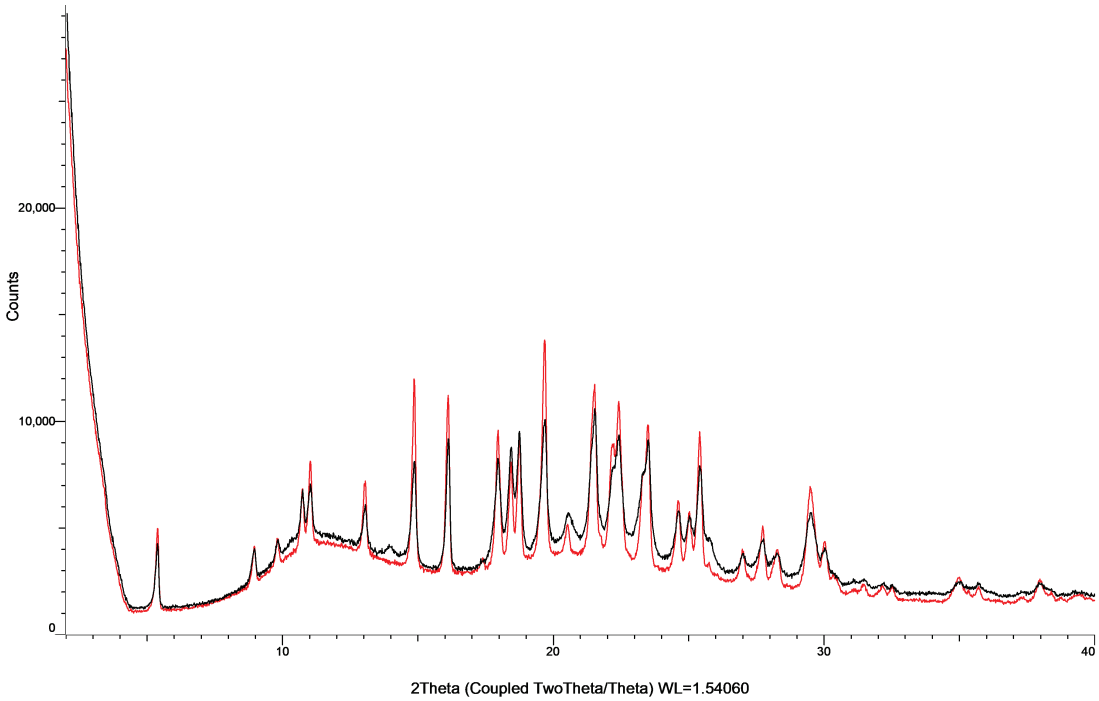


Figure S12: XRPD patterns of celecoxib with PVP K25 in co-milled mixtures (black) and physical mixtures (red).

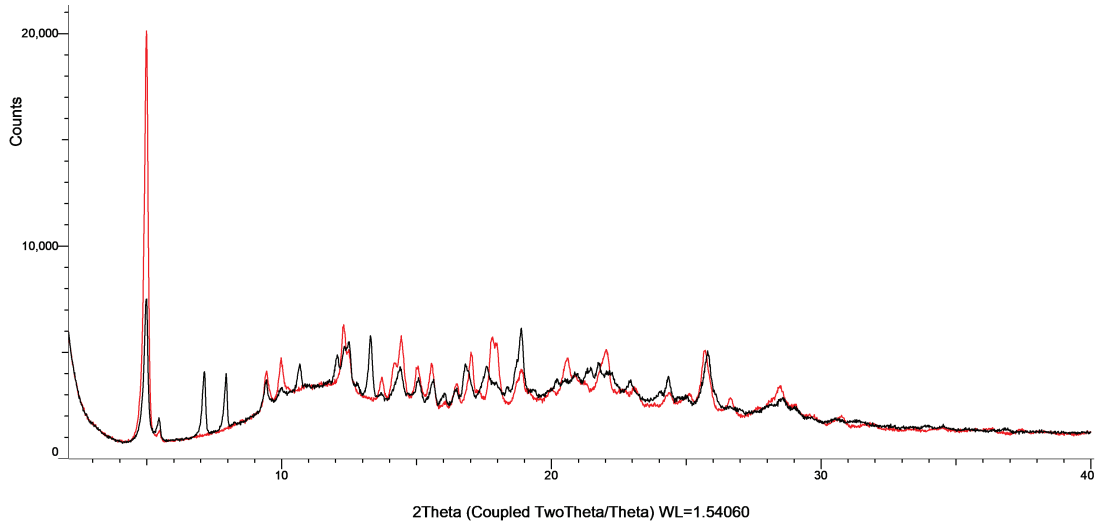


Figure S13: XRPD patterns of ceritinib with PVP K25 in co-milled mixtures (black) and physical mixtures (red).

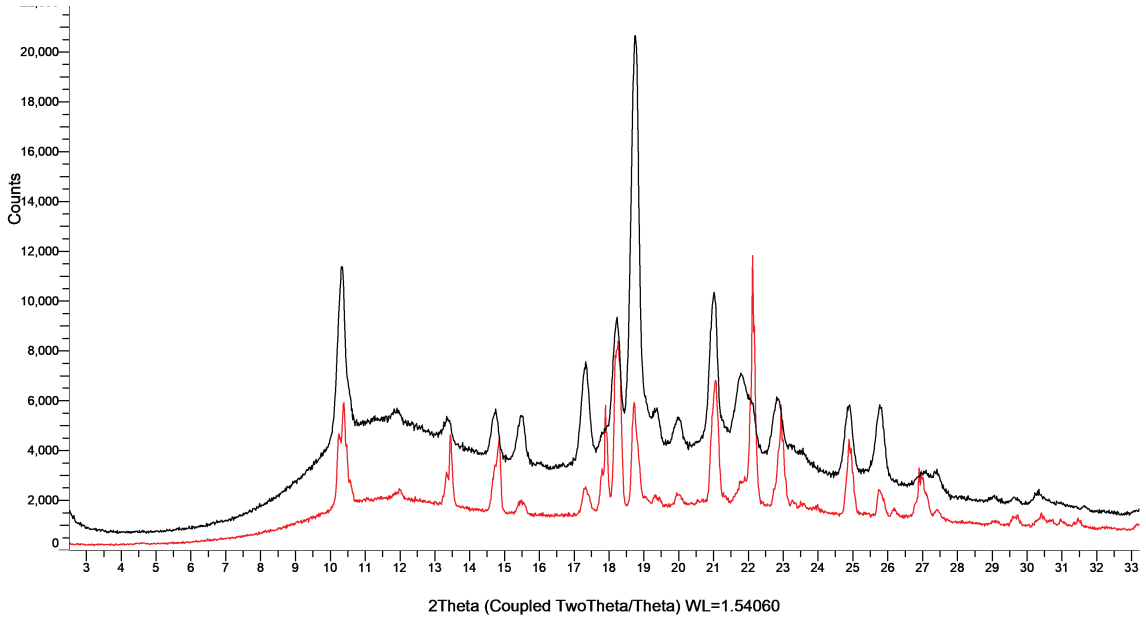


Figure S14: XRPD patterns of cinnarizine with PVP K25 in co-milled mixtures (black) and physical mixtures (red).

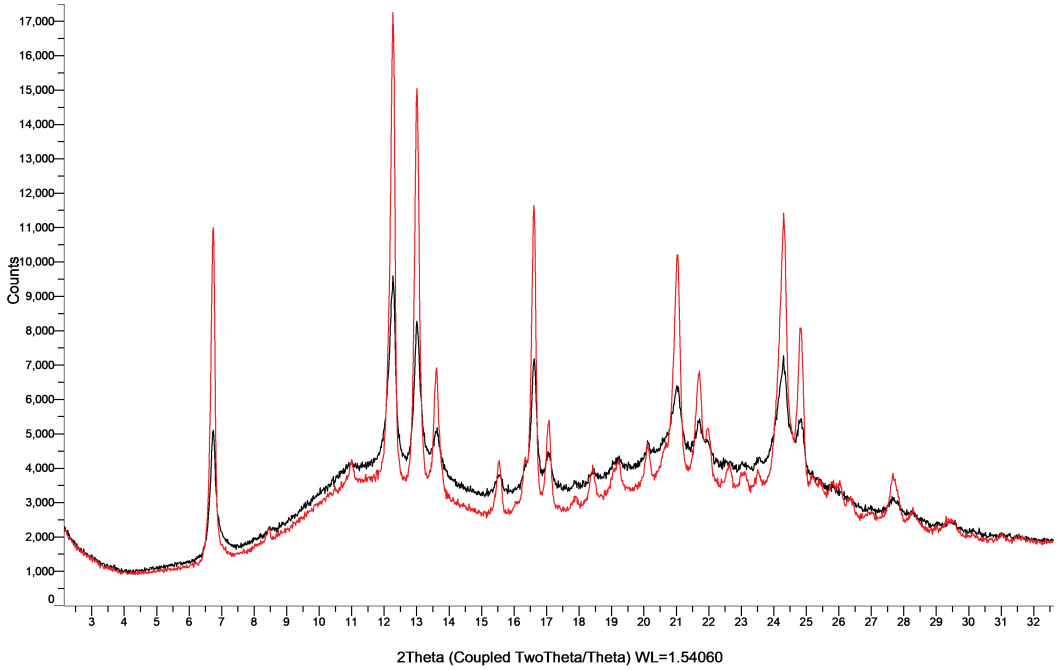


Figure S15: XRPD patterns of dasatinib with PVP K25 in co-milled mixtures (black) and physical mixtures (red).

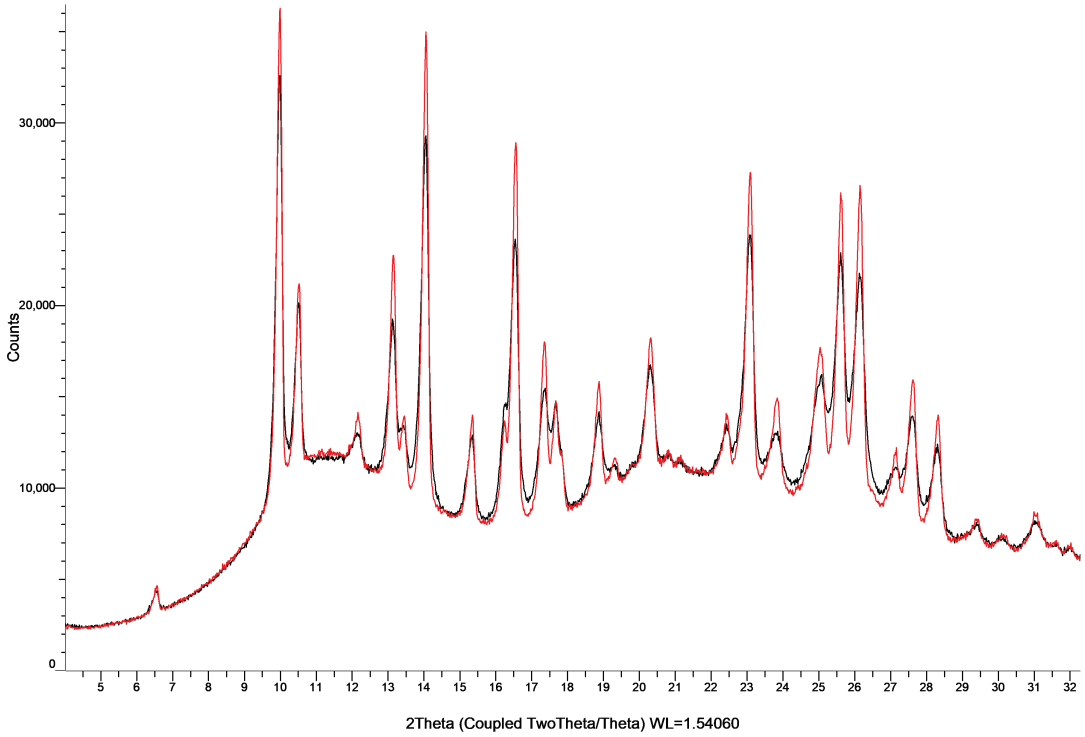


Figure S16: XRPD patterns of deferasirox with PVP K25 in co-milled mixtures (black) and physical mixtures (red).

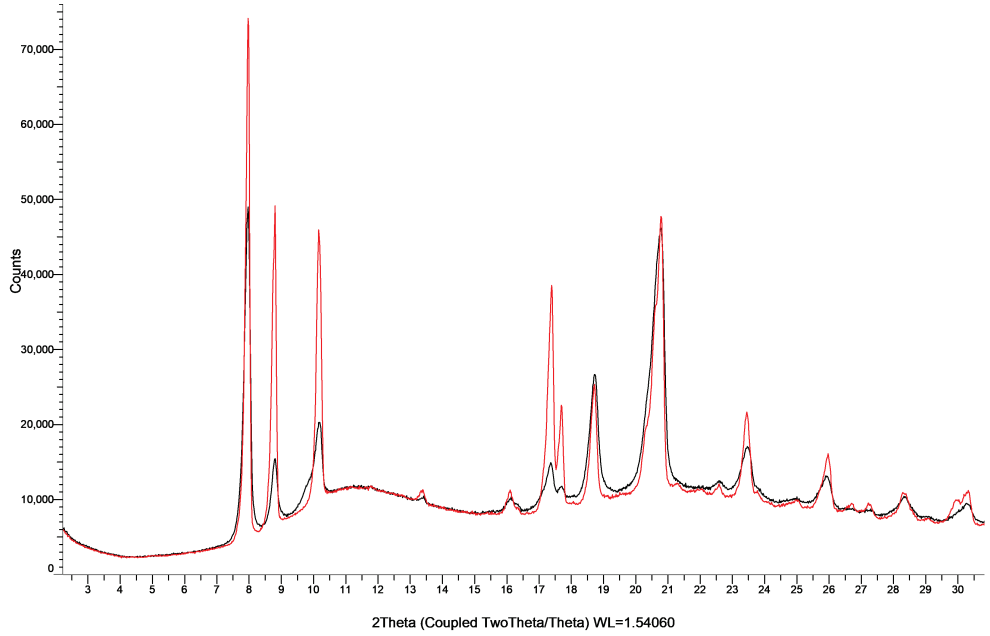


Figure S17: XRPD patterns of dipyridamole with PVP K25 in co-milled mixtures (black) and physical mixtures (red).

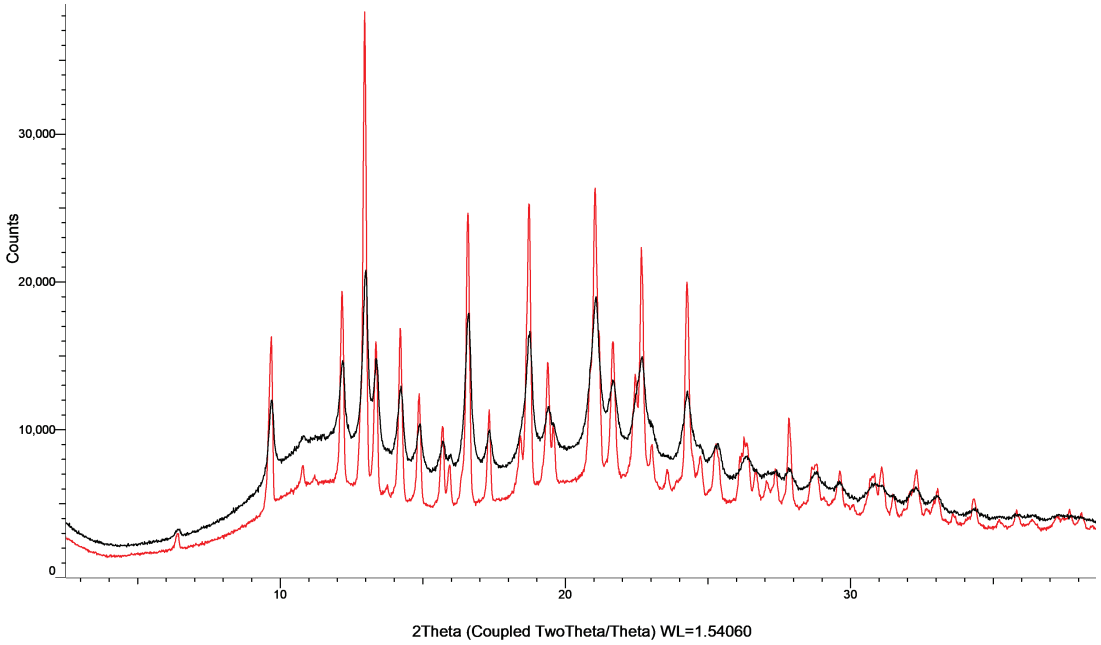


Figure S18: XRPD patterns of enzalutamide with PVP K25 in co-milled mixtures (black) and physical mixtures (red).

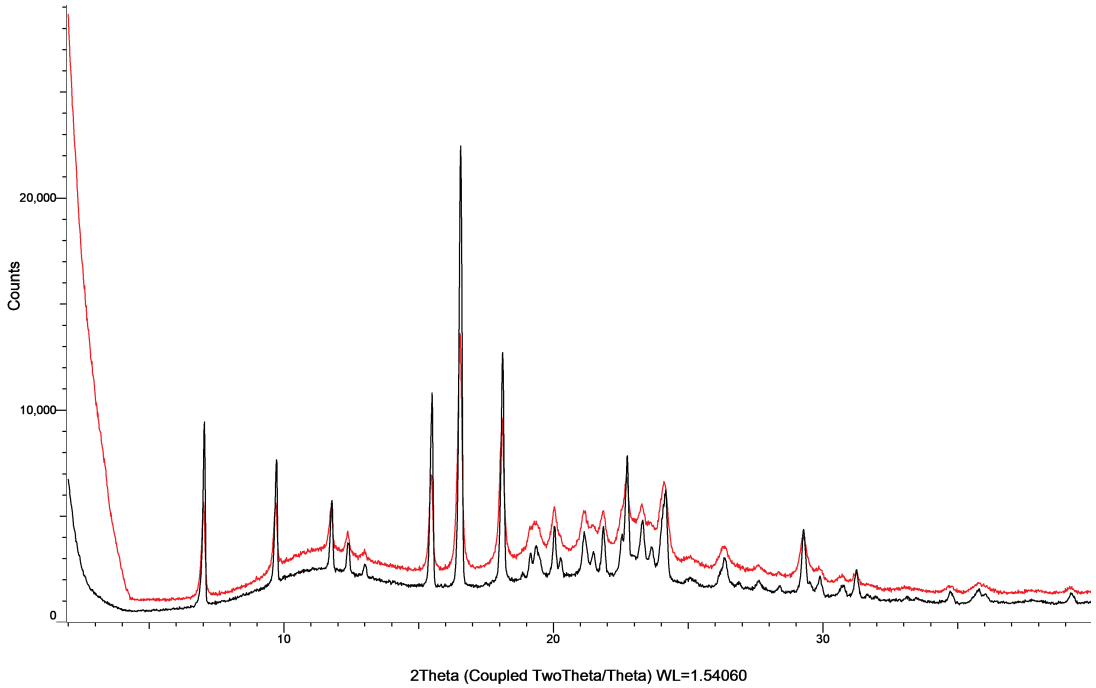


Figure S19: XRPD patterns of etoricoxib with PVP K25 in co-milled mixtures (black) and physical mixtures (red).

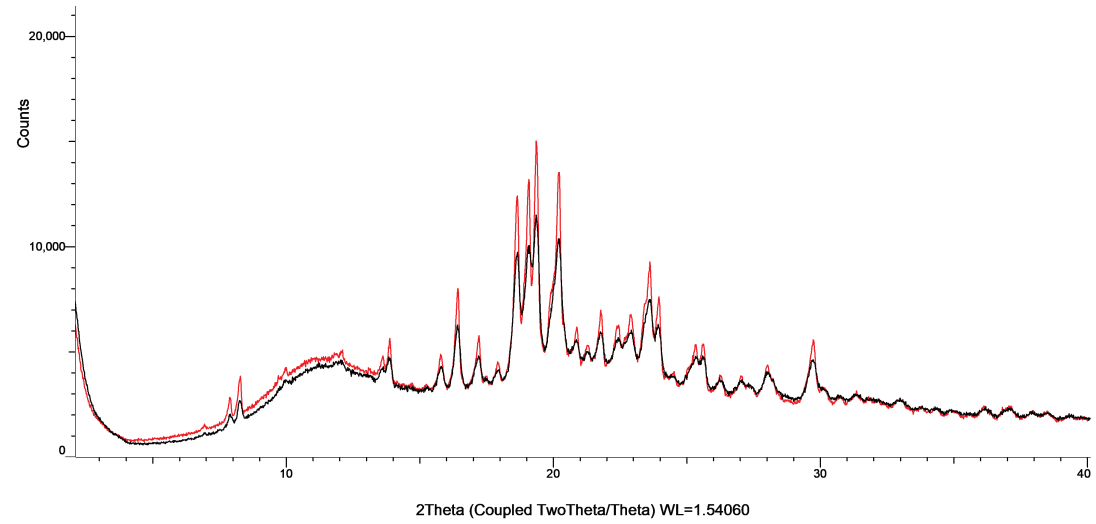


Figure S20: XRPD patterns of ezetimibe with PVP K25 in co-milled mixtures (black) and physical mixtures (red).

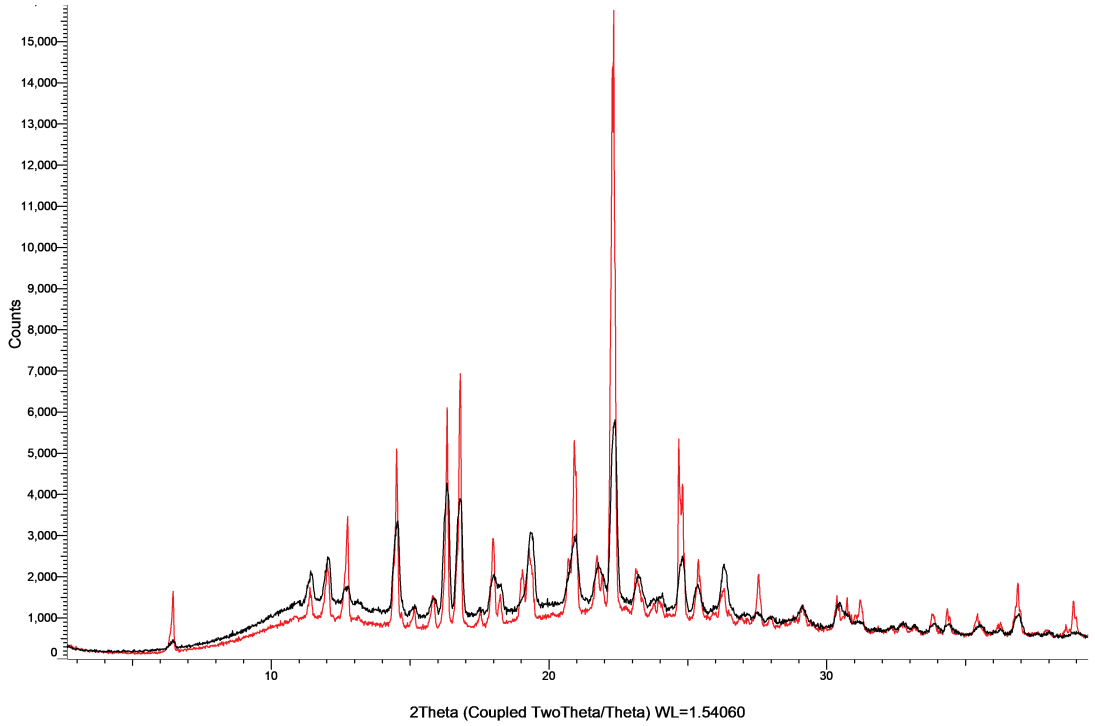


Figure S21: XRPD patterns of fenofibrate with PVP K25 in co-milled mixtures (black) and physical mixtures (red).

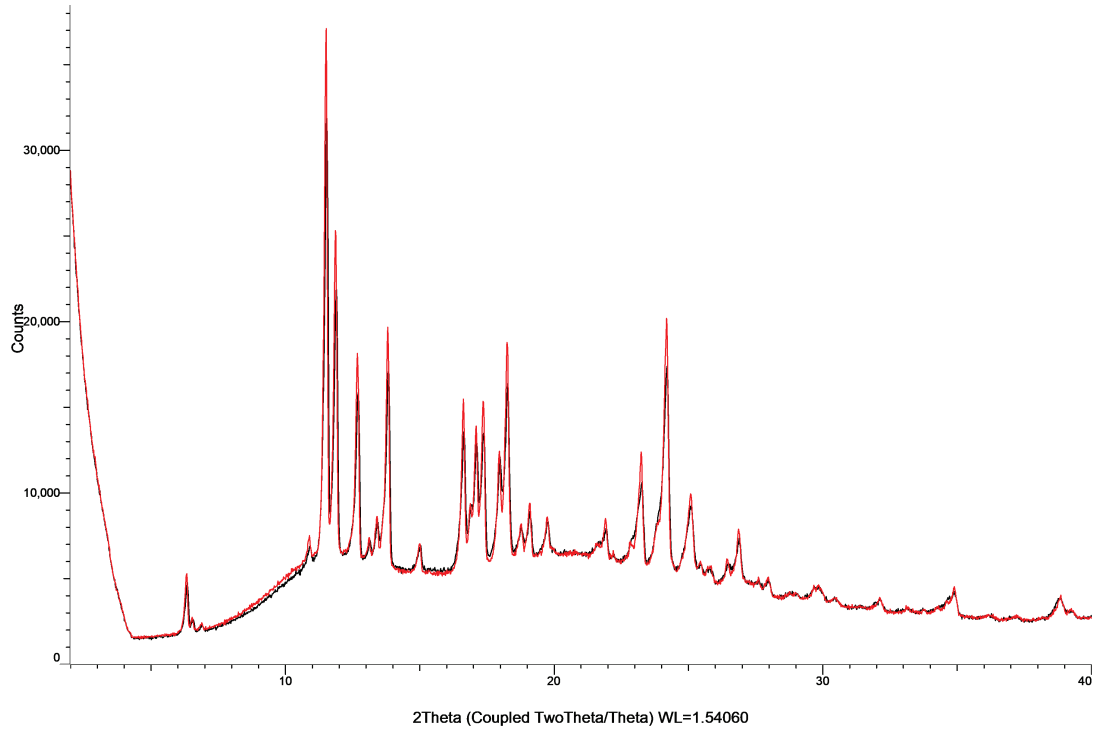


Figure S22: XRPD patterns of gemfibrozil with PVP K25 in co-milled mixtures (black) and physical mixtures (red).

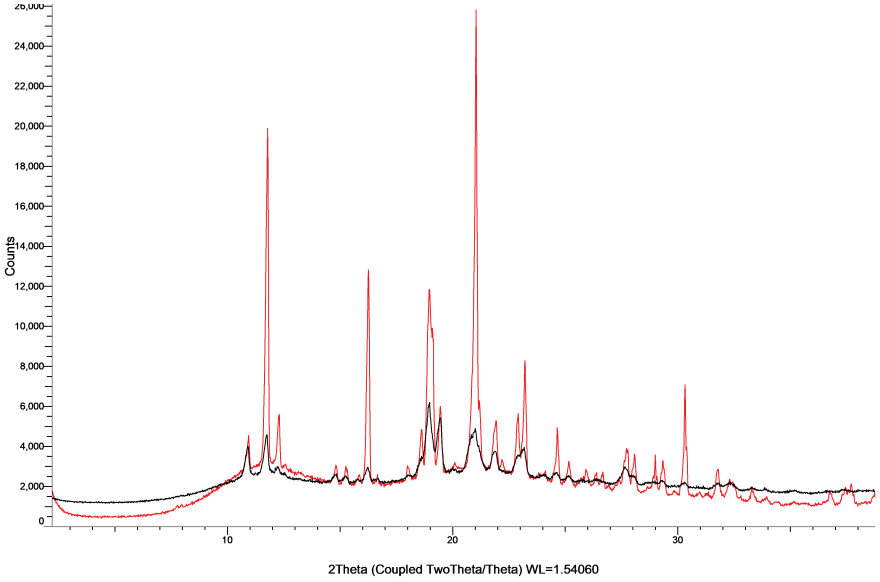


Figure S23: XRPD patterns of glibenclamide with PVP K25 in co-milled mixtures (black) and physical mixtures (red).

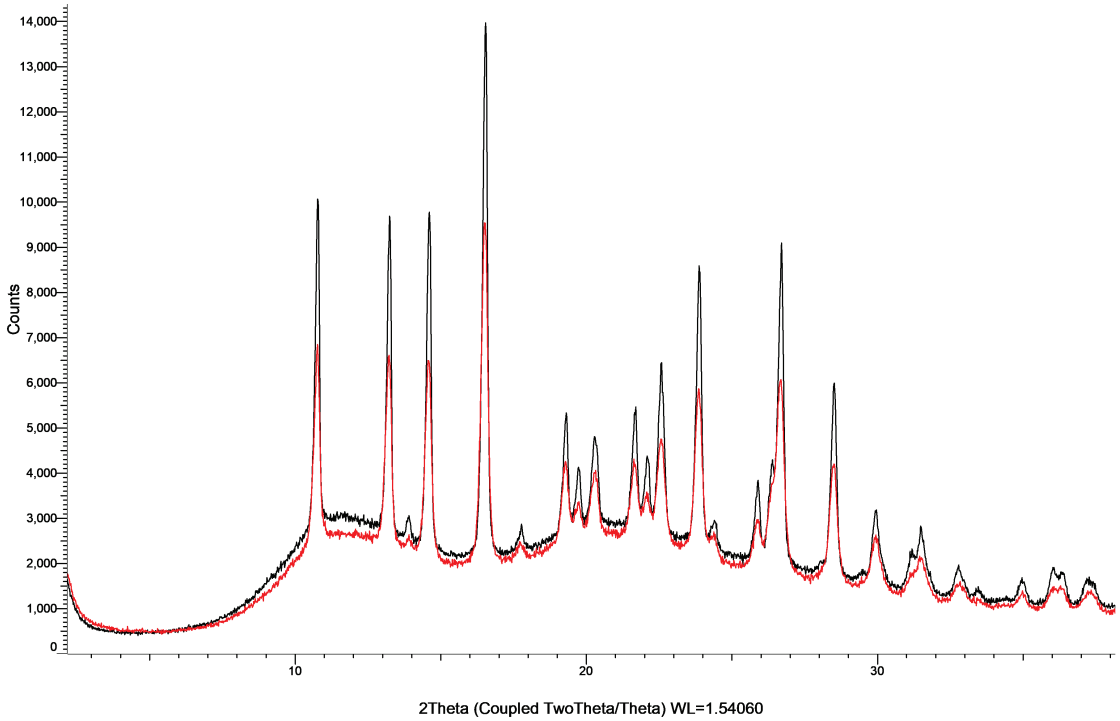


Figure S24: XRPD patterns of griseofulvin with PVP K25 in co-milled mixtures (black) and physical mixtures (red).

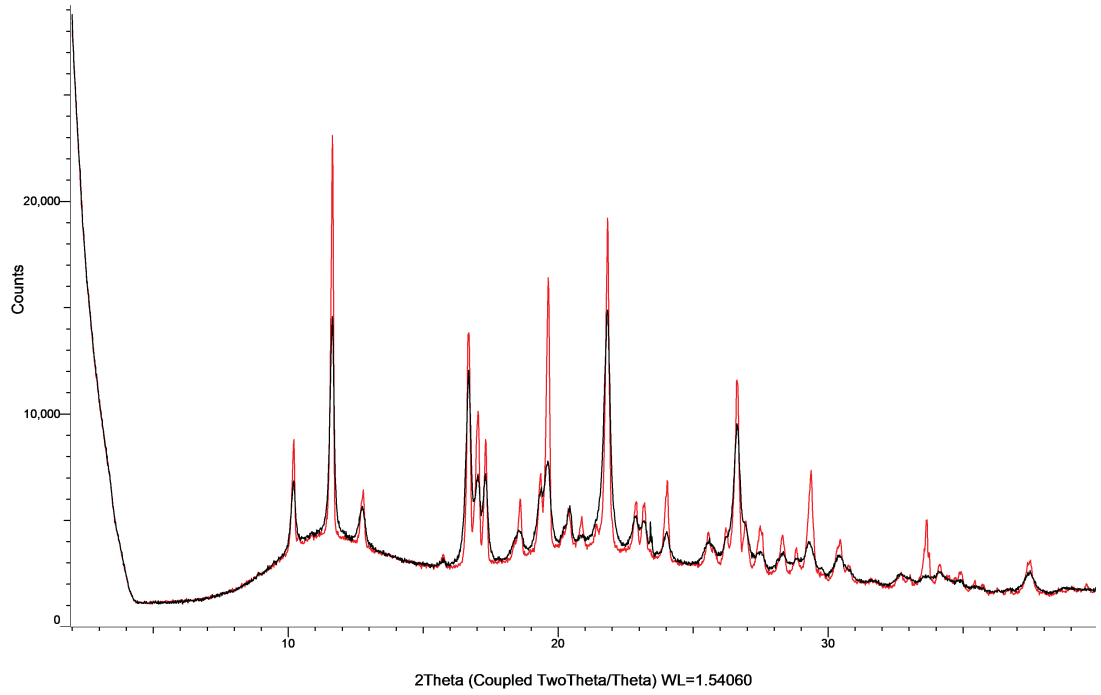


Figure S25: XRPD patterns of indomethacin with PVP K25 in co-milled mixtures (black) and physical mixtures (red).

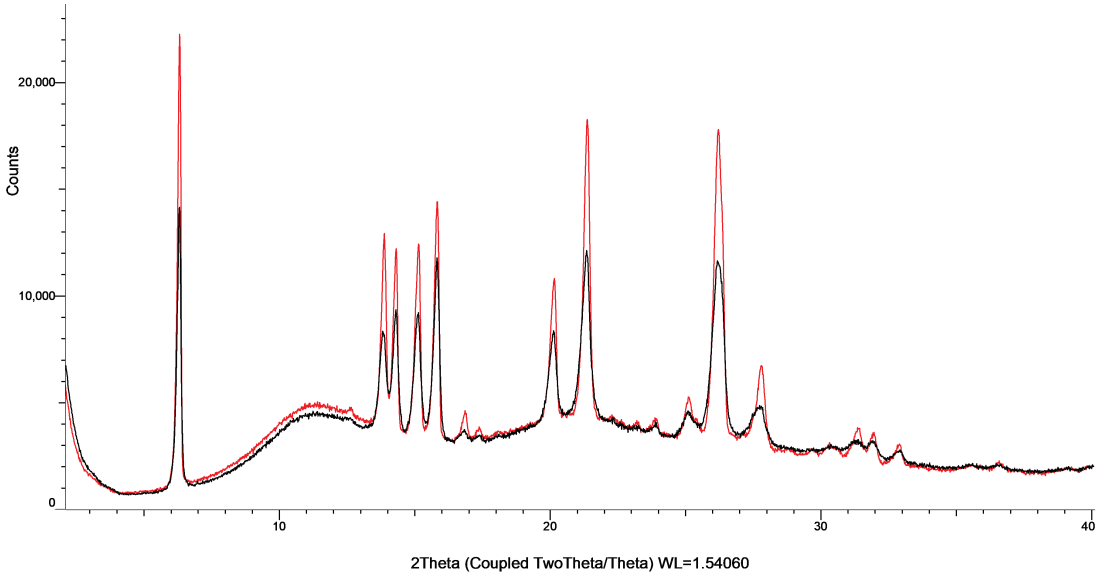


Figure S26: XRPD patterns of mefenamic acid with PVP K25 in co-milled mixtures (black) and physical mixtures (red).

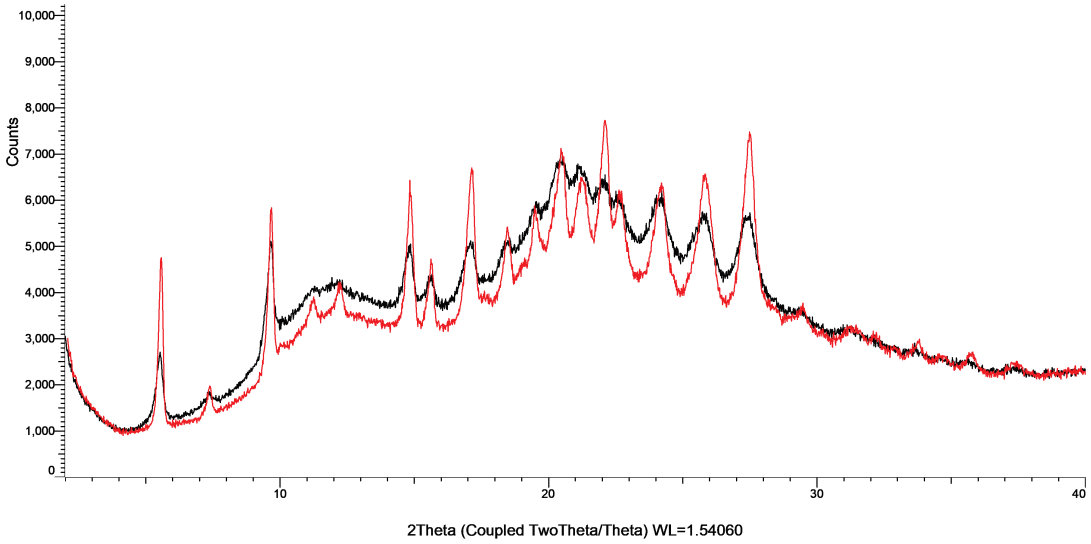


Figure S27: XRPD patterns of nilotinib with PVP K25 in co-milled mixtures (black) and physical mixtures (red).

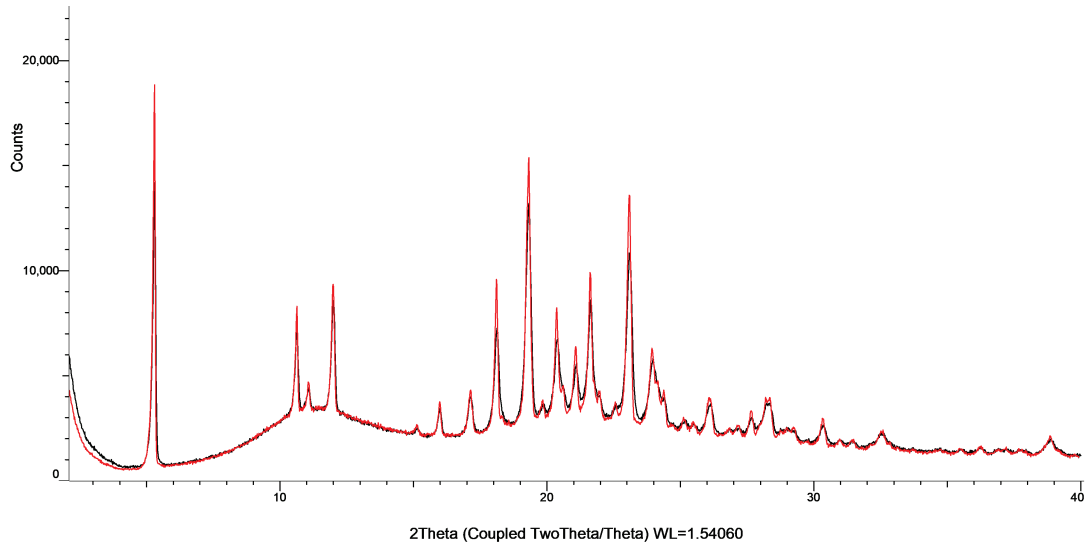


Figure S28: XRPD patterns of nimesulide with PVP K25 in co-milled mixtures (black) and physical mixtures (red).

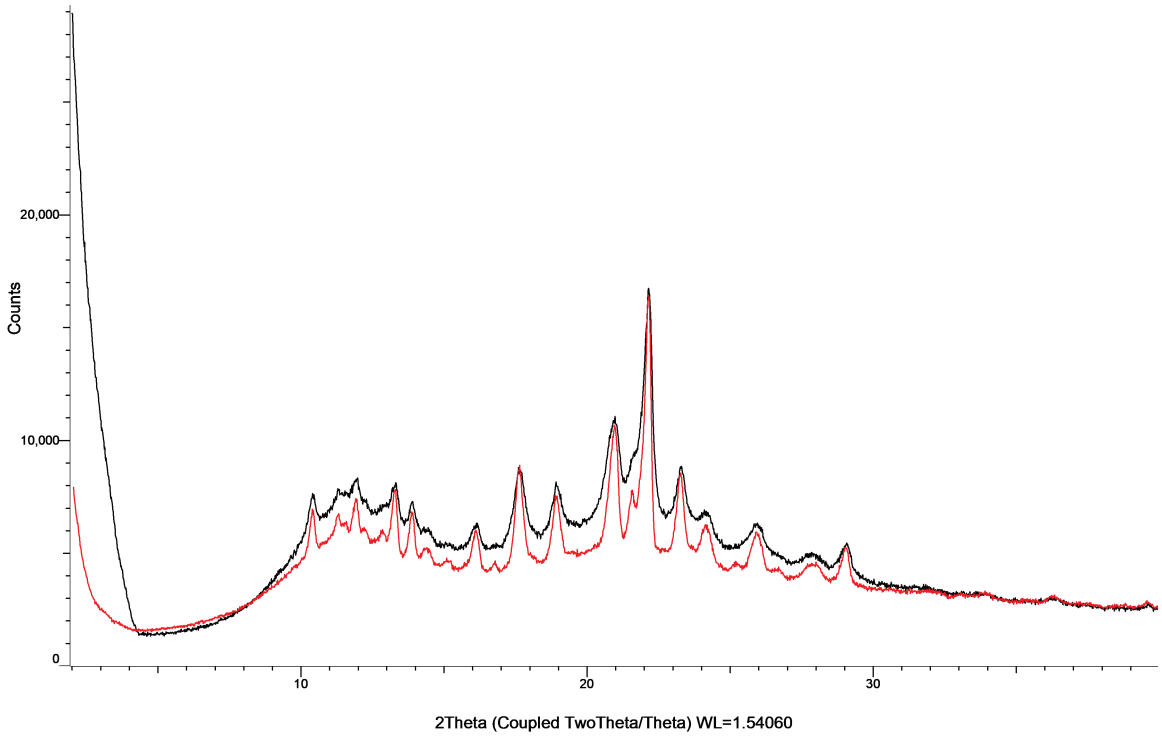


Figure S29: XRPD patterns of olaparib with PVP K25 in co-milled mixtures (black) and physical mixtures (red).

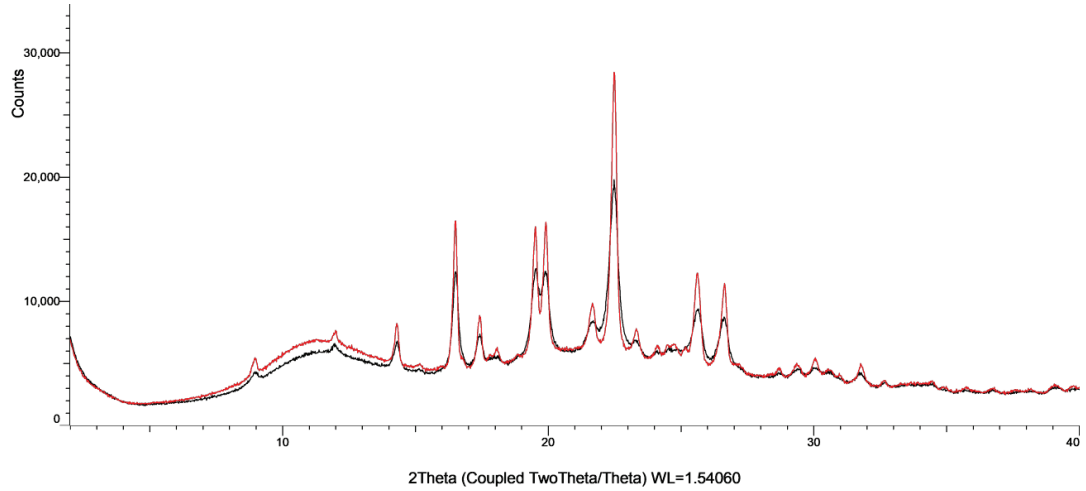


Figure S30: XRPD patterns of rivaroxaban with PVP K25 in co-milled mixtures (black) and physical mixtures (red).

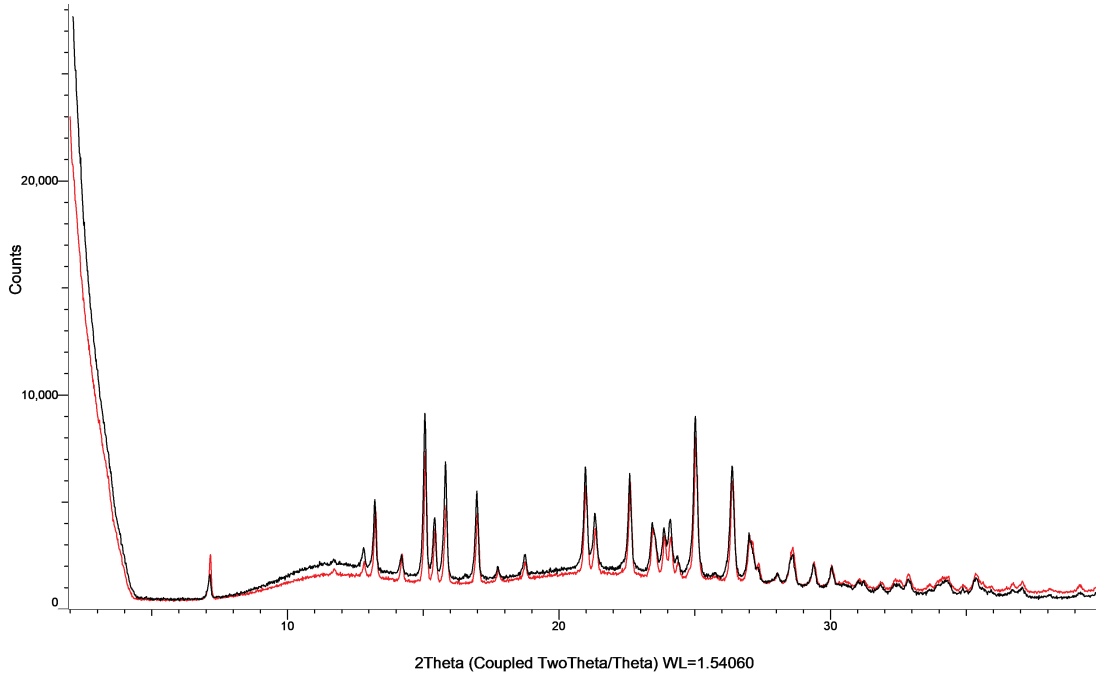


Figure S31: XRPD patterns of sertraline with PVP K25 in co-milled mixtures (black) and physical mixtures (red).

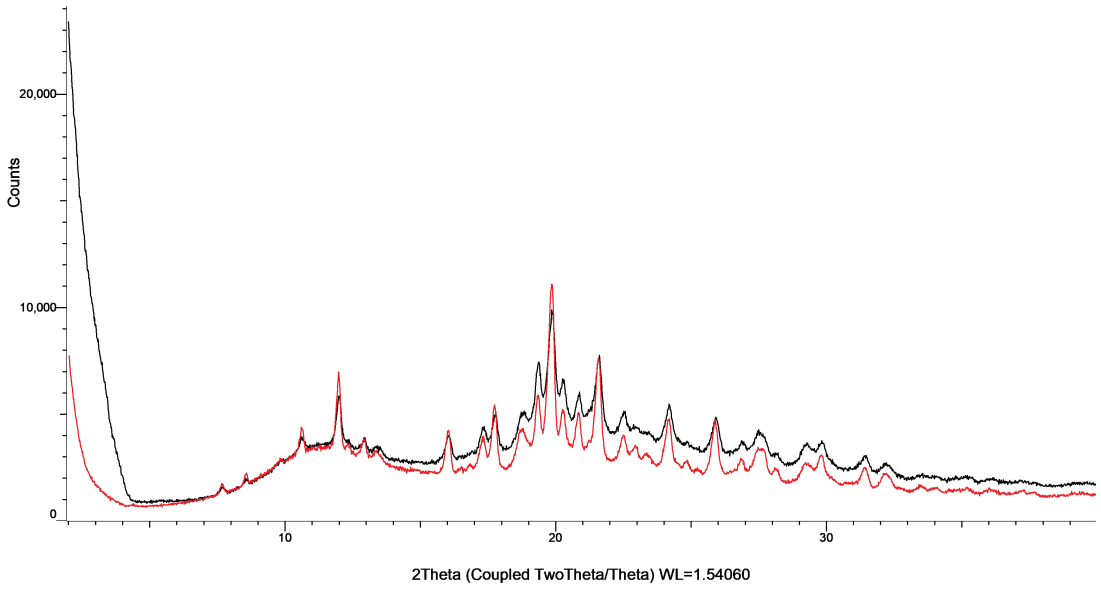


Figure S32: XRPD patterns of sorafenib with PVP K25 in co-milled mixtures (black) and physical mixtures (red).

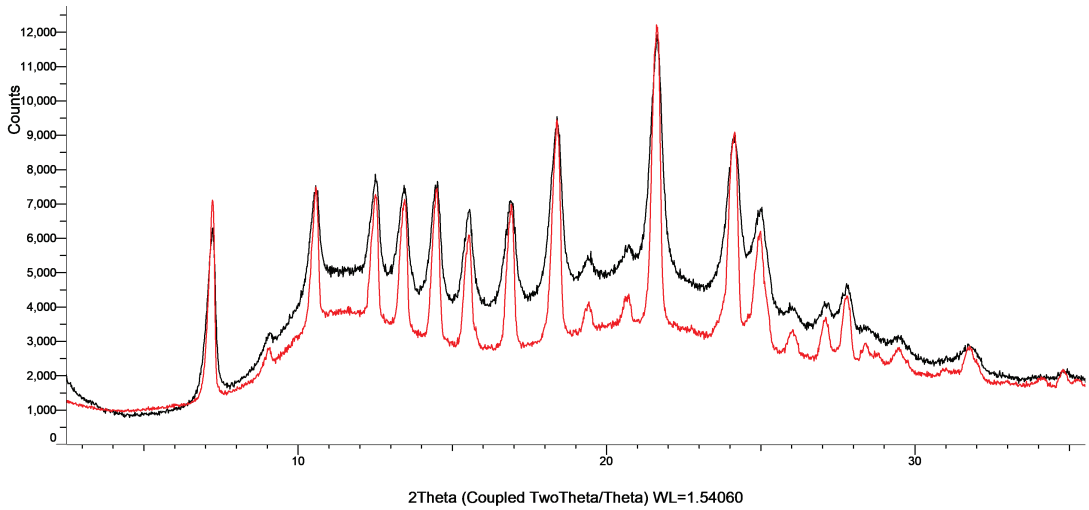


Figure S33: XRPD patterns of tadalafil with PVP K25 in co-milled mixtures (black) and physical mixtures (red).

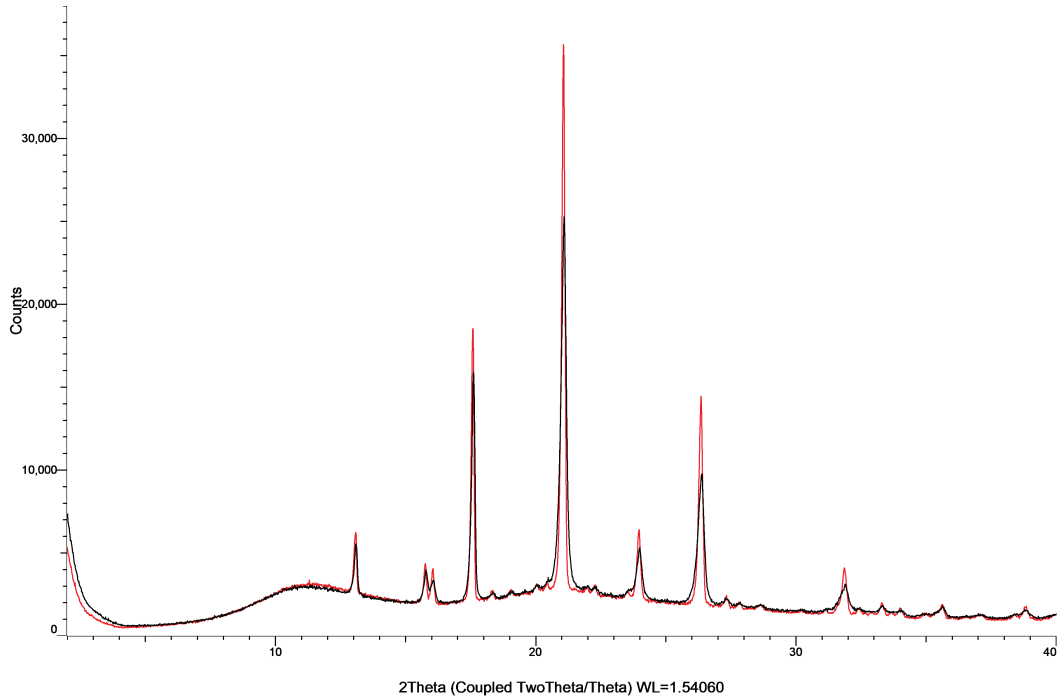


Figure S34: XRPD patterns of thiabendazole with PVP K25 in co-milled mixtures (black) and physical mixtures (red).

10.1.7 Powder X-ray diffractograms of unprocessed drug powder and milled drug powder

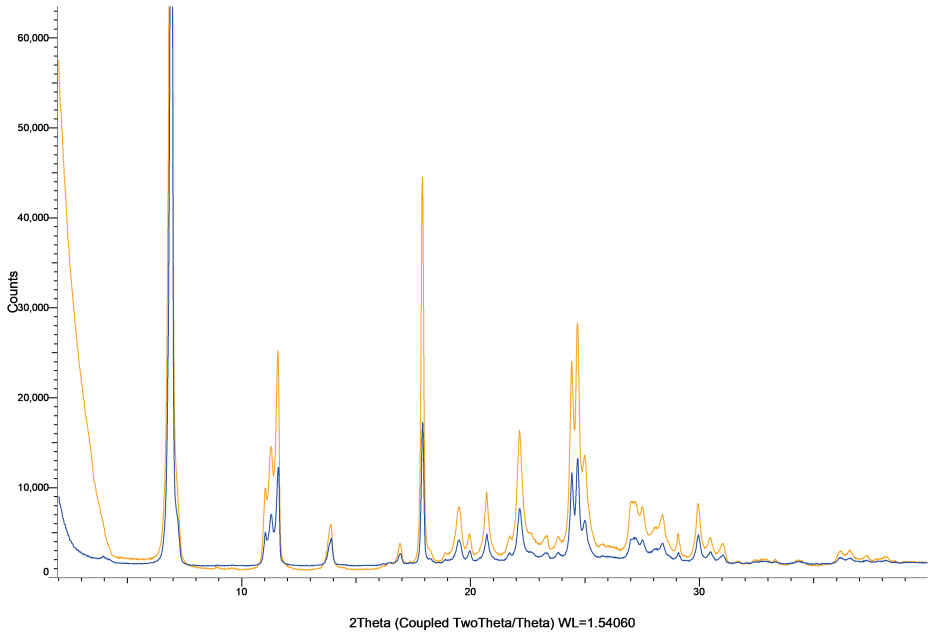


Figure S35: XRPD patterns of albendazole powder (blue) and milled albendazole powder (orange).

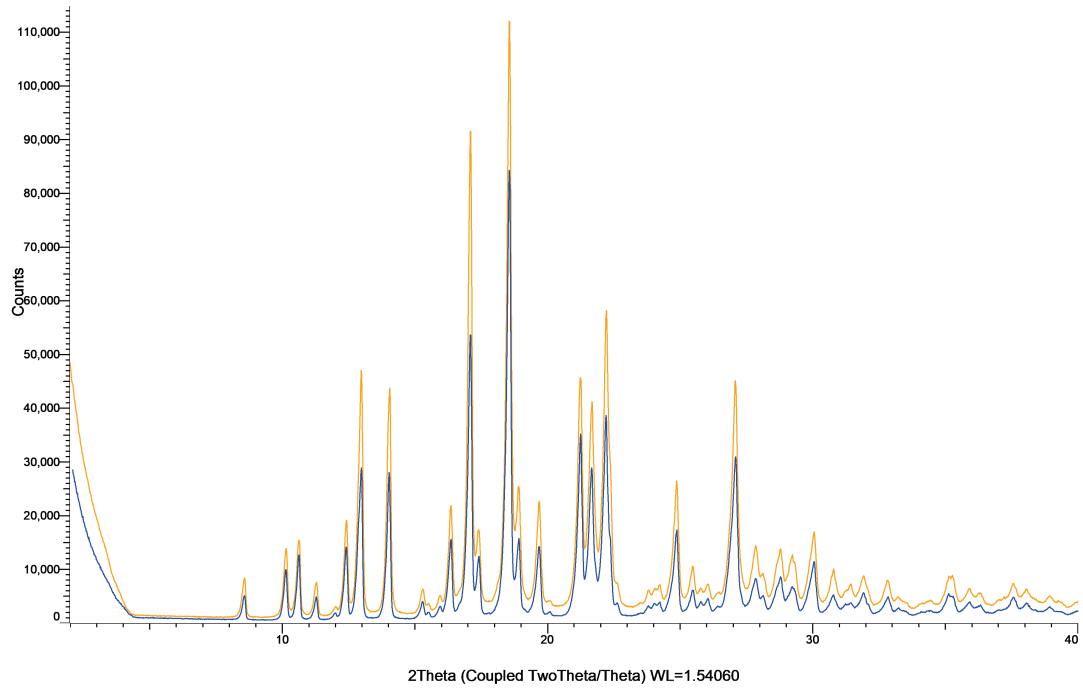


Figure S36: XRPD patterns of apixaban powder (blue) and milled apixaban powder (orange).

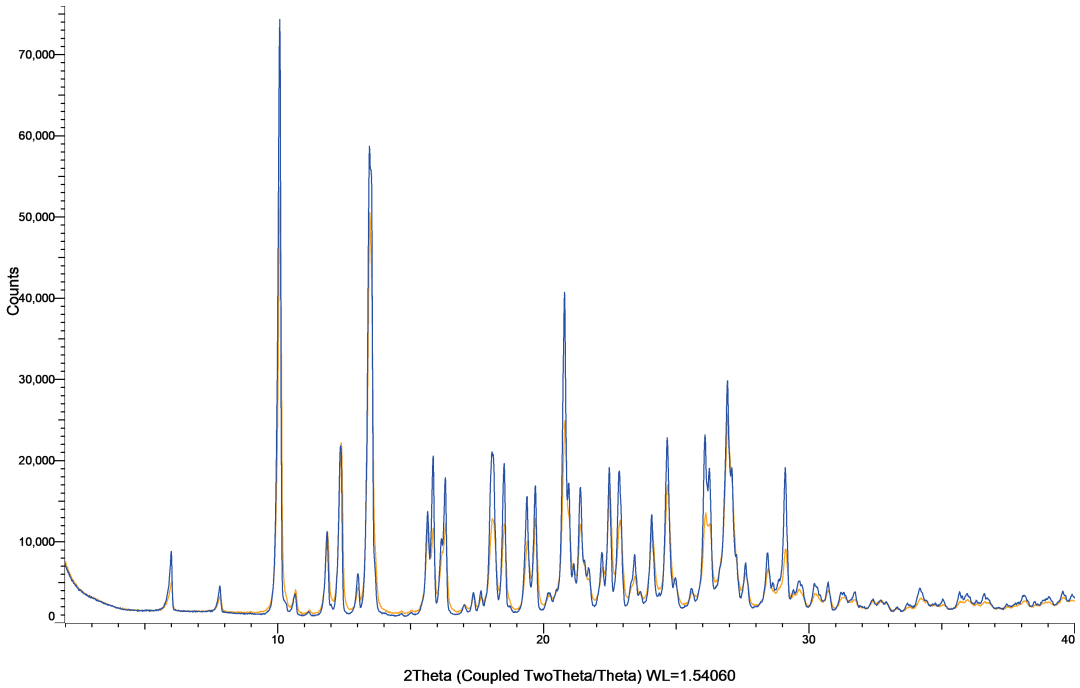


Figure S37: XRPD patterns of apremilast powder (blue) and milled apremilast powder (orange).

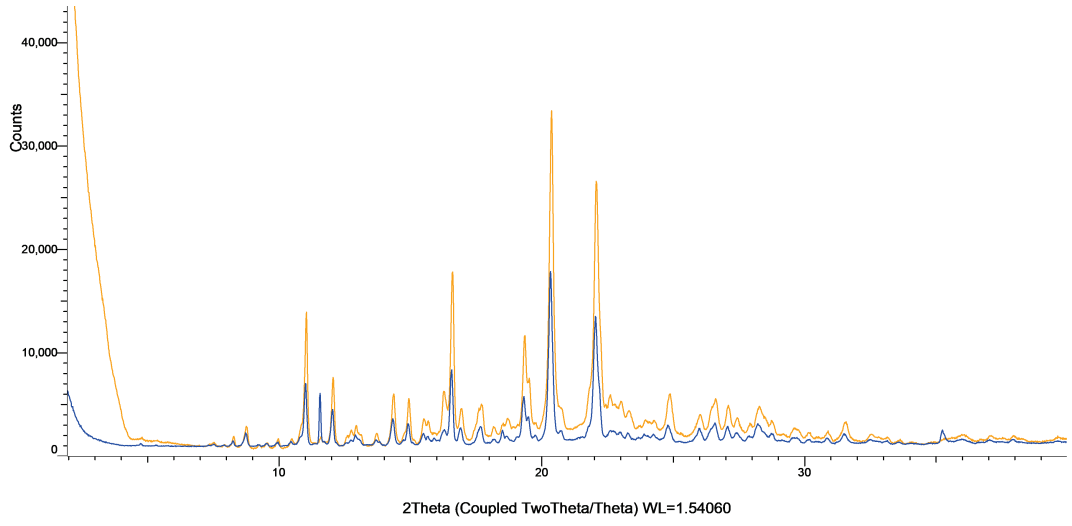


Figure S38: XRPD patterns of aripiprazole powder (blue) and milled aripiprazole powder (orange).

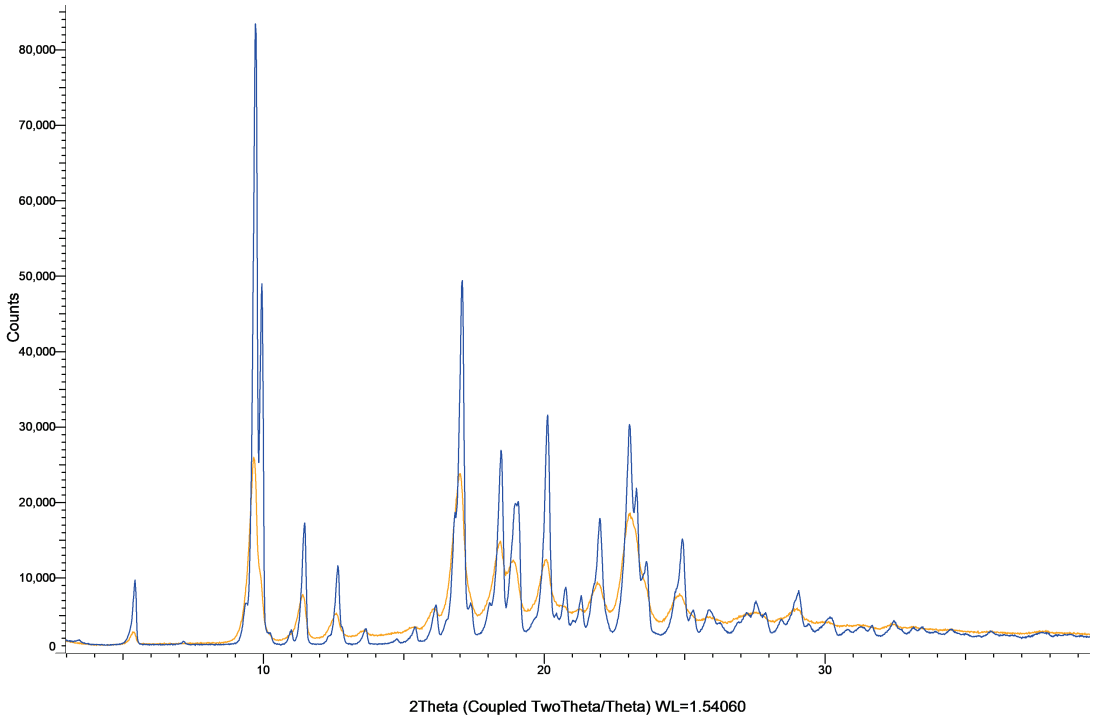


Figure S39: XRPD patterns of candesartan cilexetil powder (blue) and milled candesartan cilexetil powder (orange).

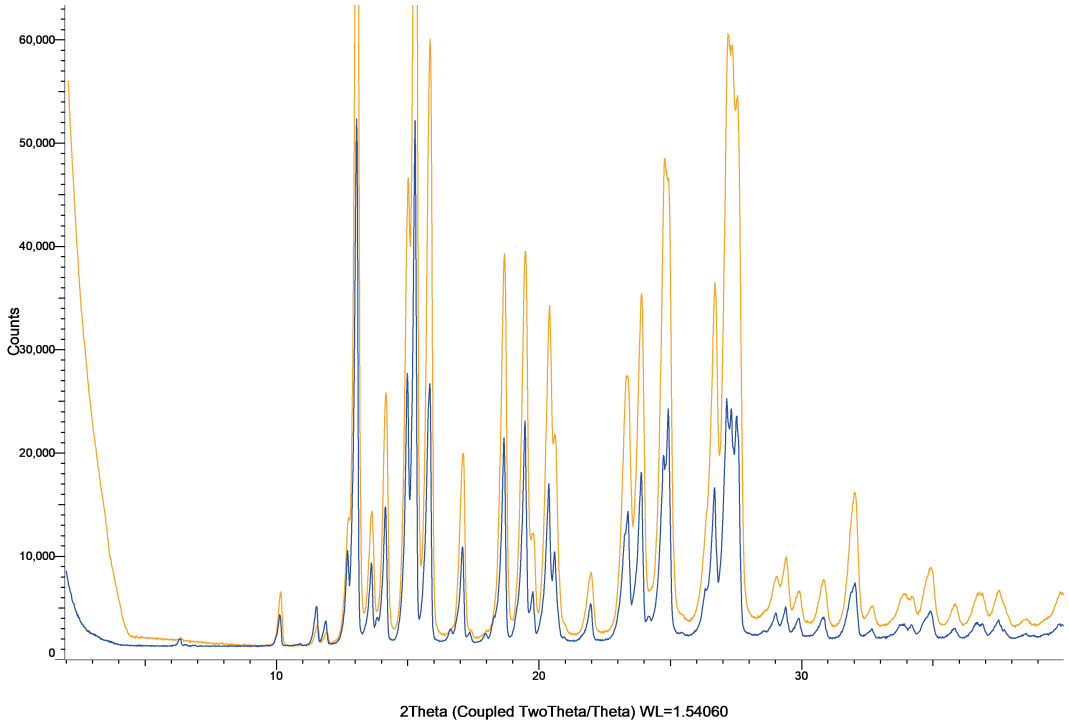


Figure S40: XRPD patterns of carbamazepine powder (blue) and milled carbamazepine powder (orange).

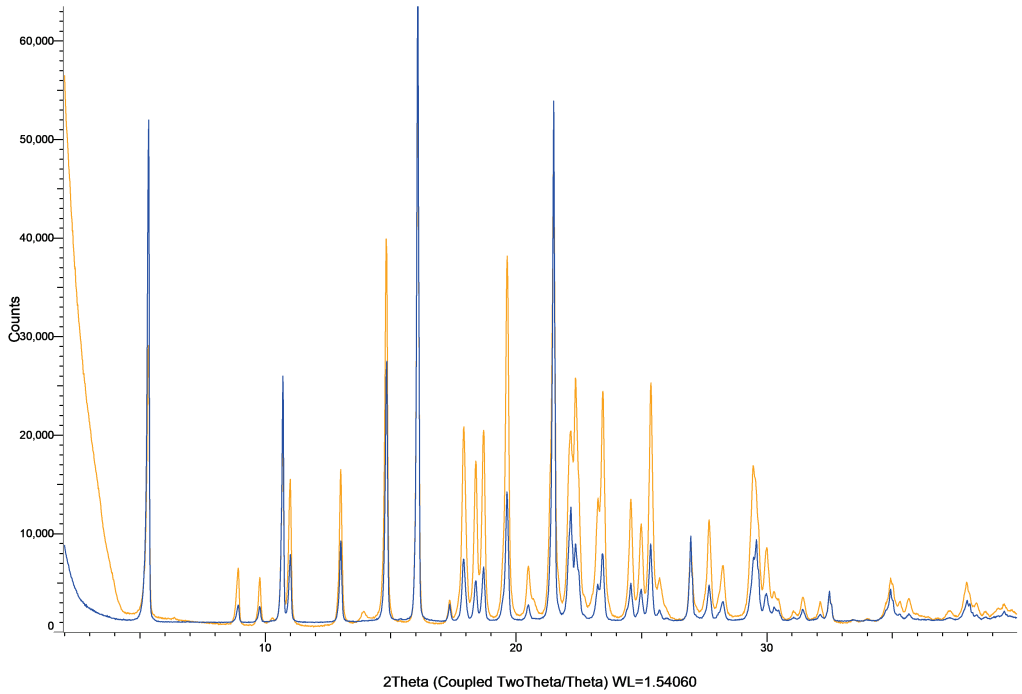


Figure S41: XRPD patterns of celecoxib powder (blue) and milled celecoxib powder (orange).

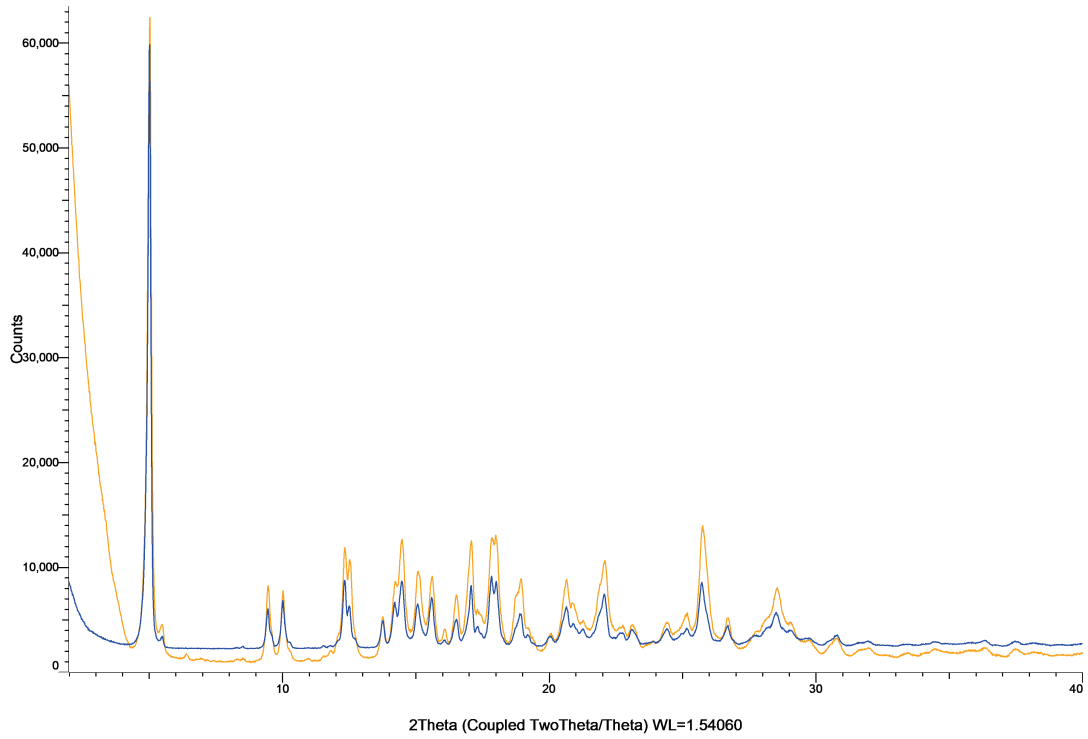


Figure S42: XRPD patterns of ceritinib powder (blue) and milled ceritinib powder (orange).

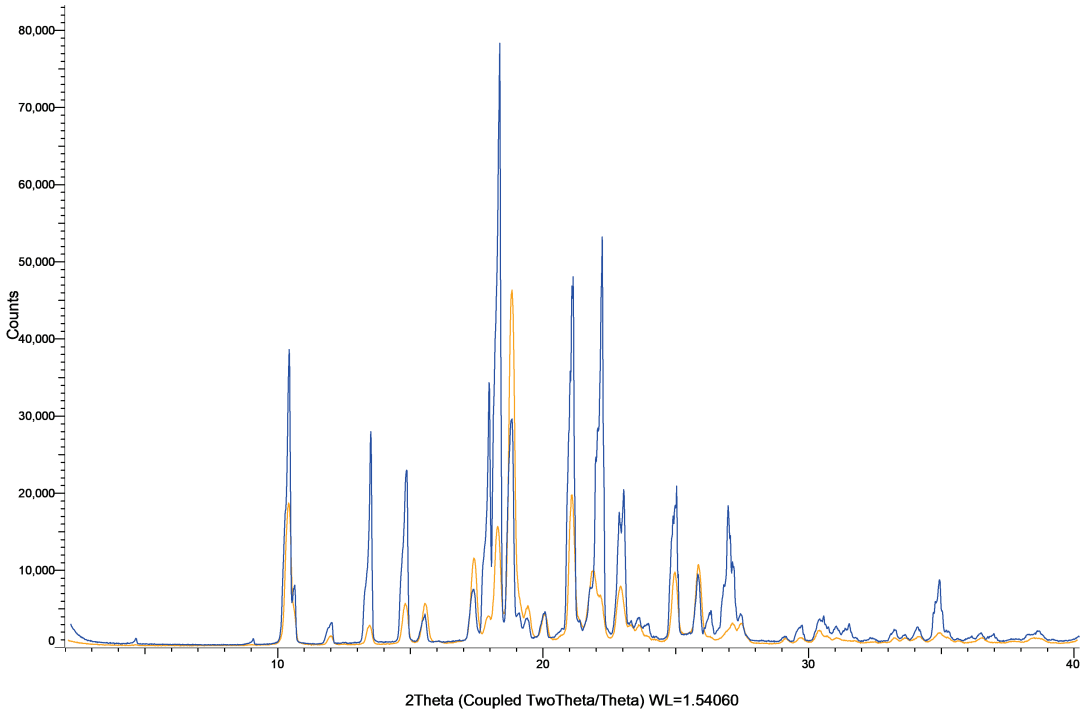


Figure S43: XRPD patterns of cinnarizine powder (blue) and milled cinnarizine powder (orange).

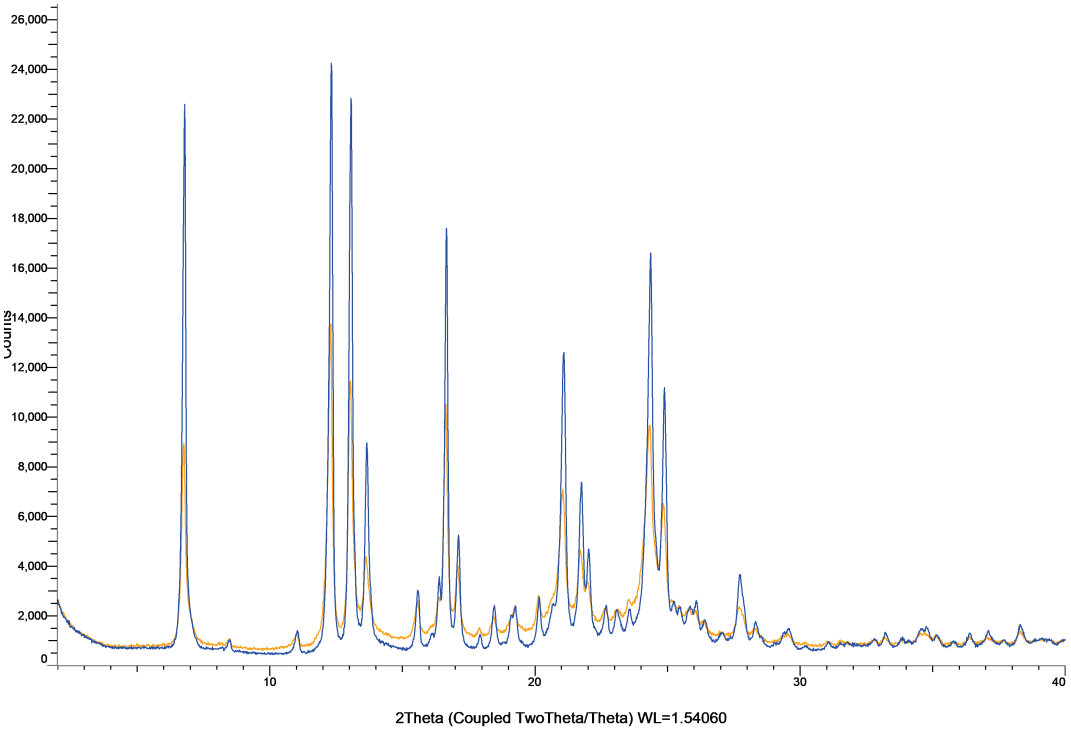


Figure S39: XRPD patterns of dasatinib powder (blue) and milled dasatinib powder (orange).

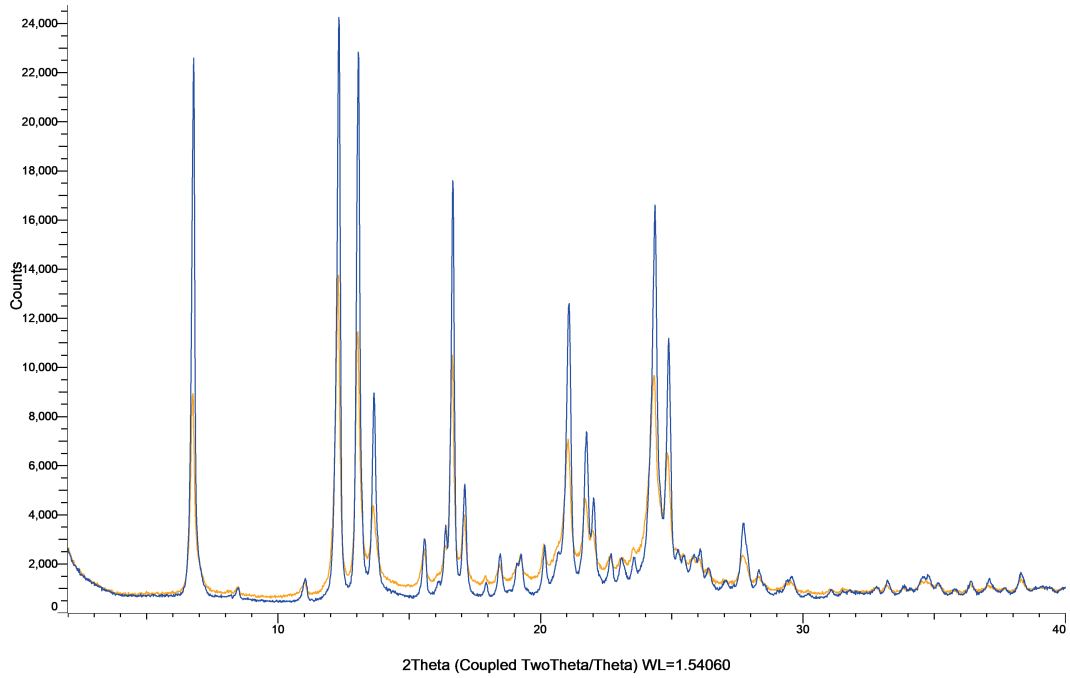


Figure S44: XRPD patterns of deferasirox powder (blue) and milled deferasirox powder (orange).

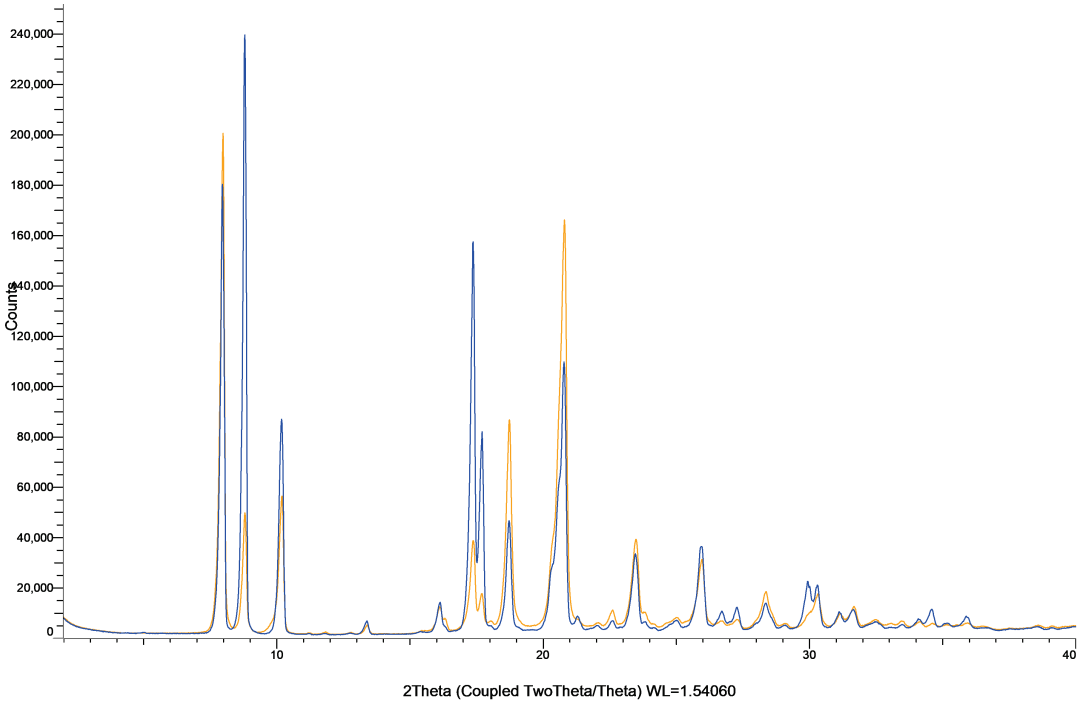


Figure S45: XRPD patterns of dipyridamole powder (blue) and milled dipyridamole powder (orange).

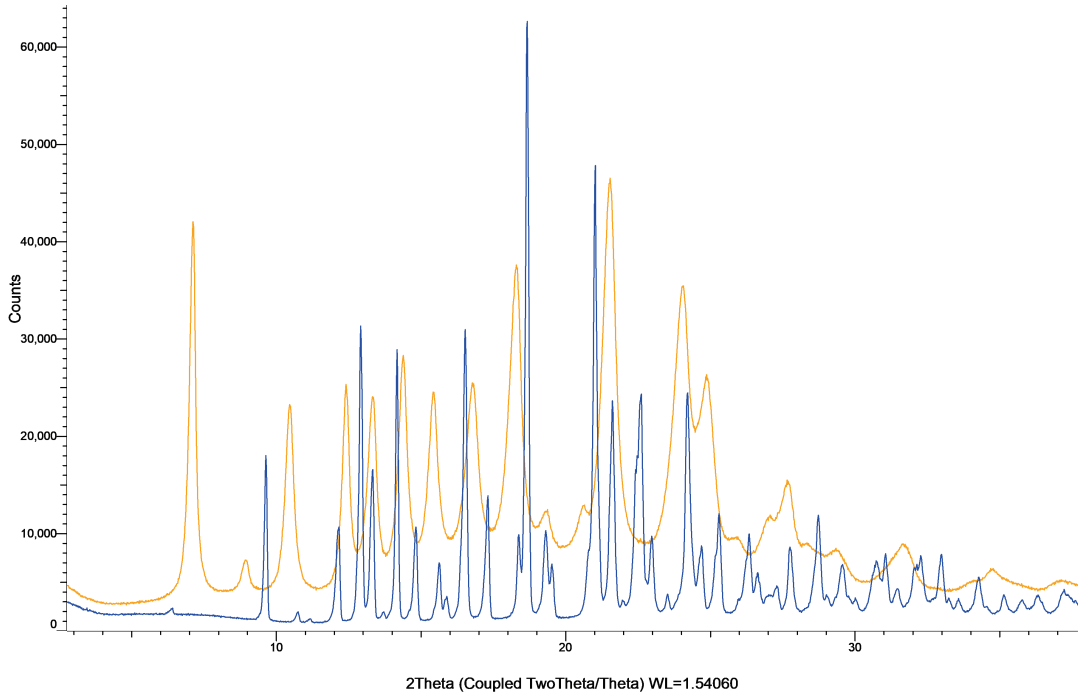


Figure S46: XRPD patterns of enzalutamide powder (blue) and milled enzalutamide powder (orange).

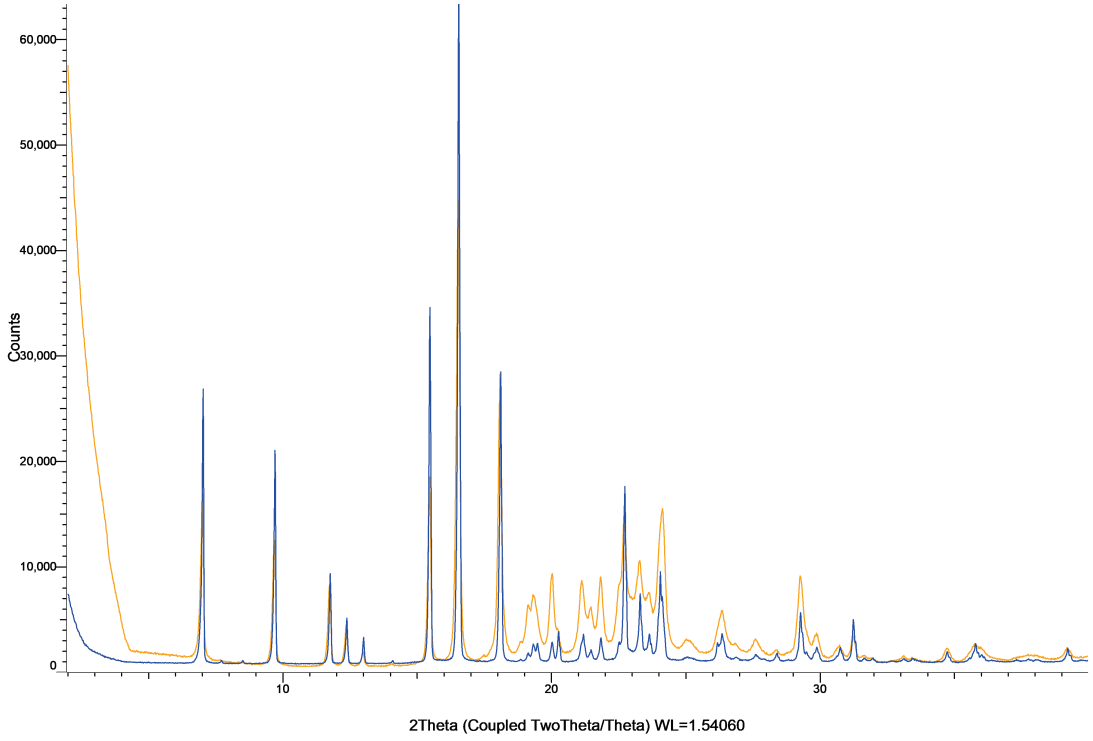


Figure S47: XRPD patterns of etorixcoxib powder (blue) and milled etoricoxib powder (orange).

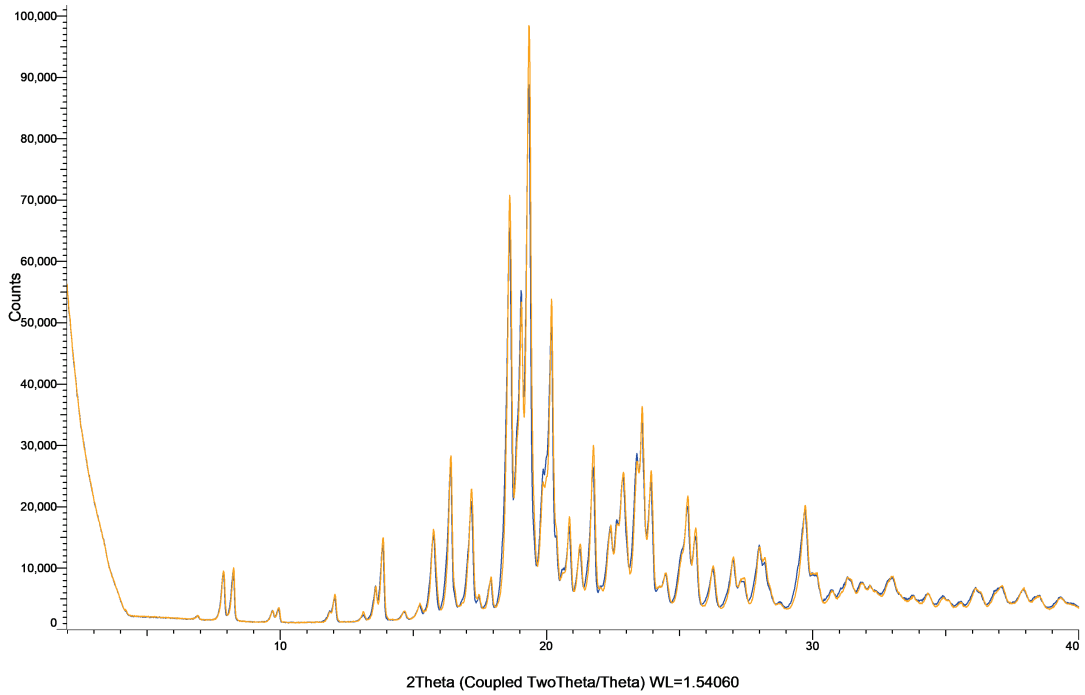


Figure S48: XRPD patterns of ezetimibe powder (blue) and milled ezetimibe powder (orange).

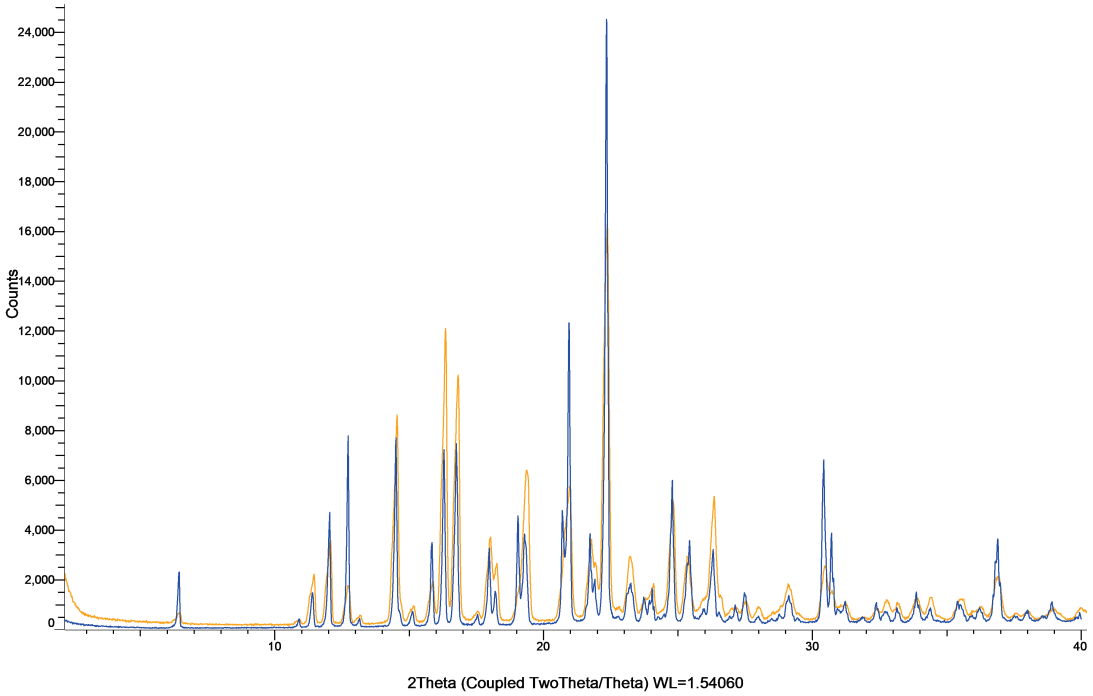


Figure S49: XRPD patterns of fenofibrate powder (blue) and milled fenofibrate powder (orange).

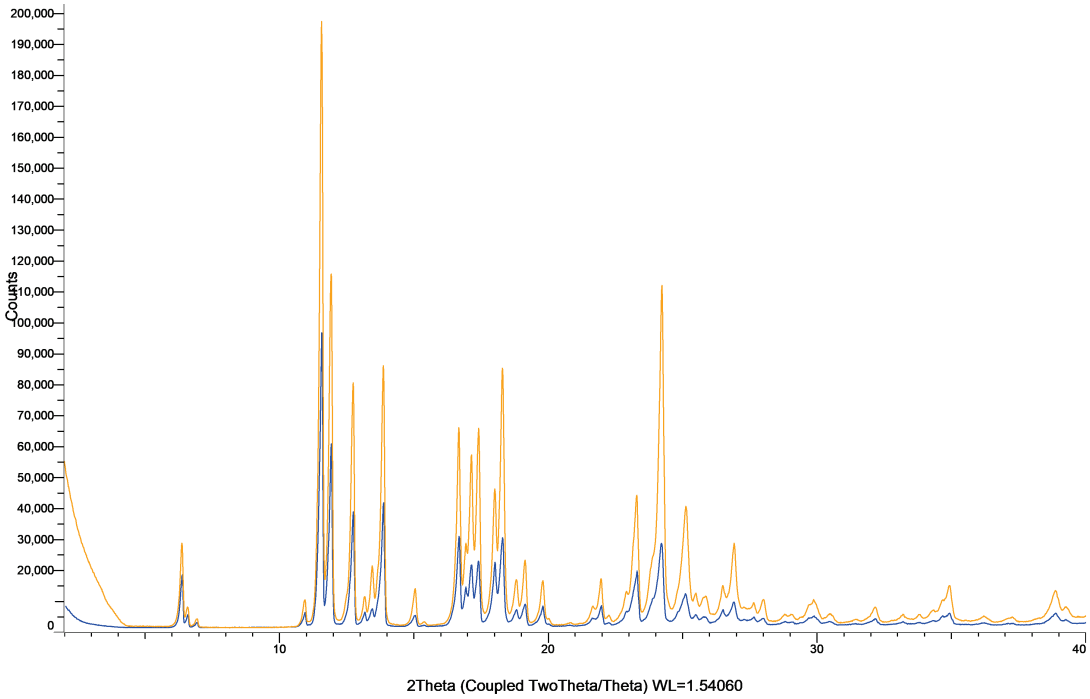


Figure S50: XRPD patterns of gemfibrozil powder (blue) and milled gemfibrozil powder (orange).

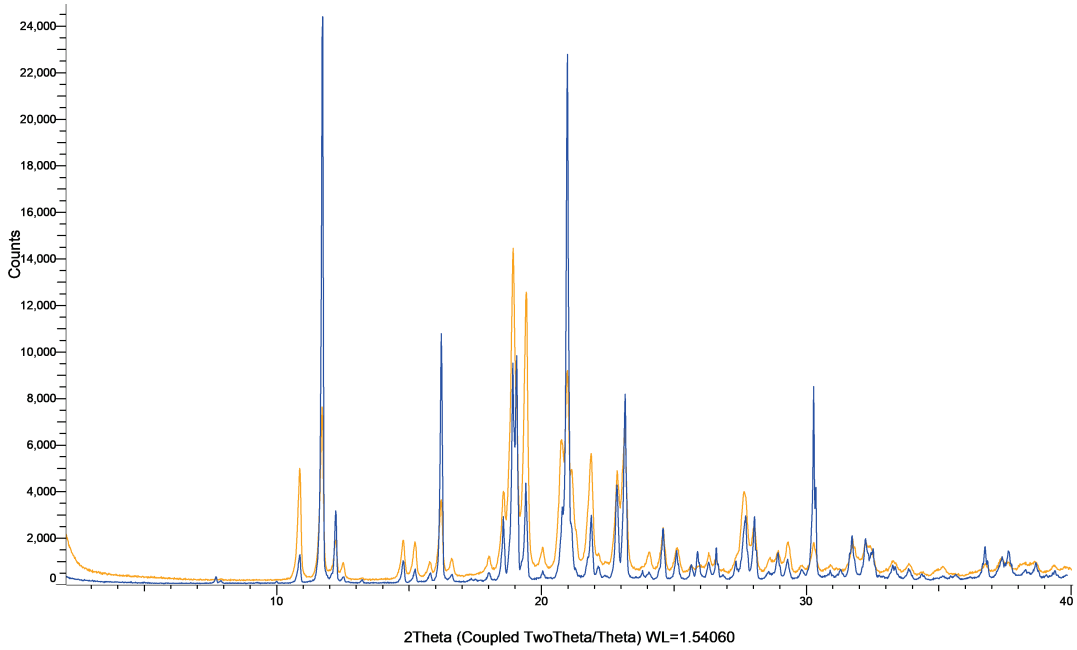


Figure S51: XRPD patterns of glibenclamide powder (blue) and milled glibenclamide powder (orange).

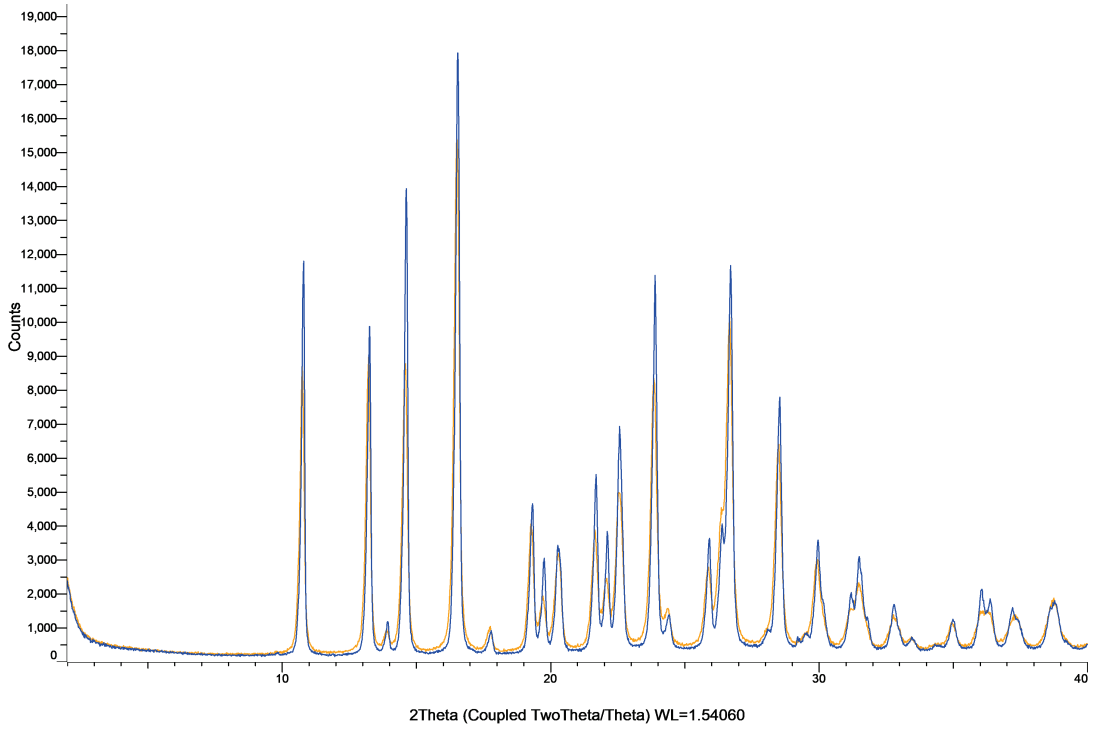


Figure S52: XRPD patterns of griseofulvin powder (blue) and milled griseofulvin powder (orange).

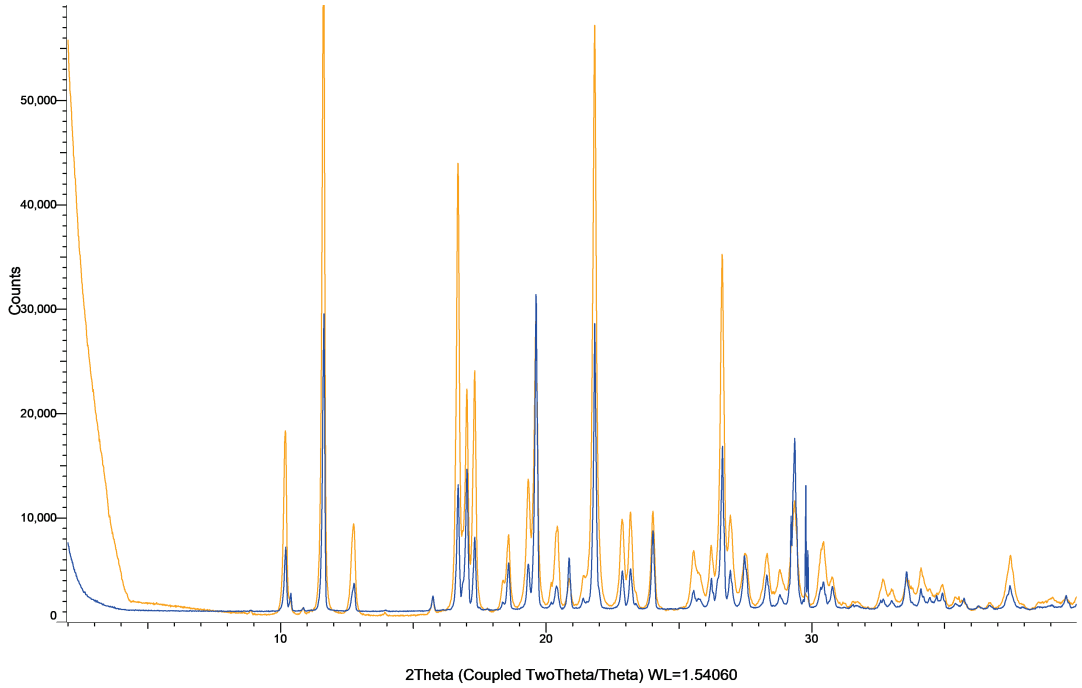


Figure S53: XRPD patterns of indomethacin powder (blue) and milled indomethacin powder (orange).

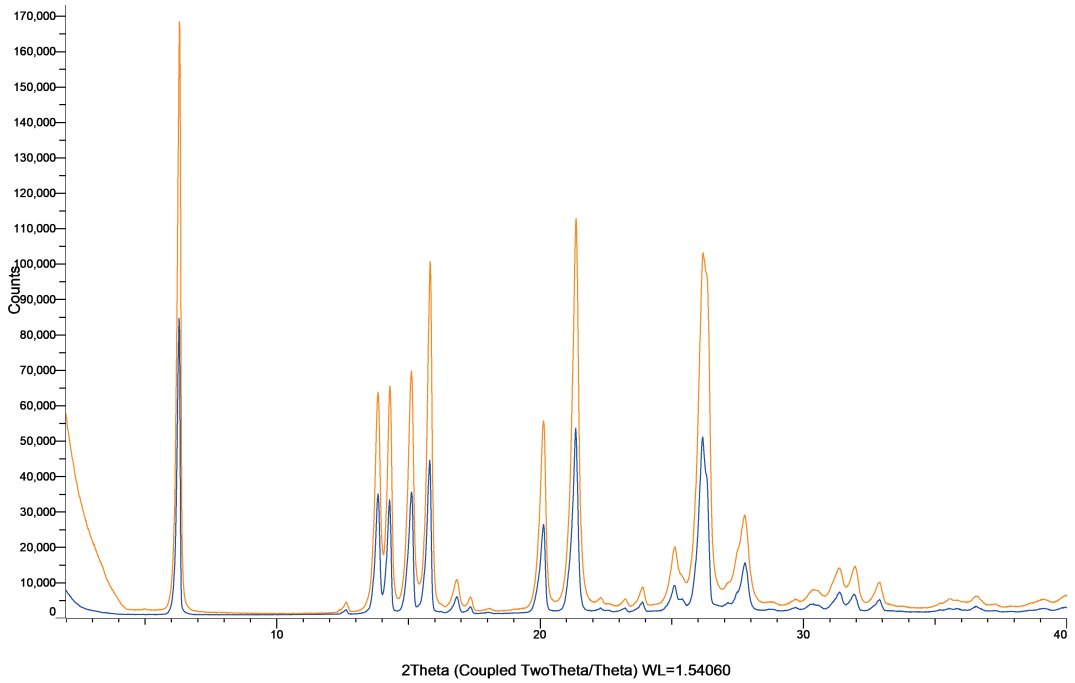


Figure S54: XRPD patterns of mefenamic acid powder (blue) and milled mefenamic acid powder (orange).

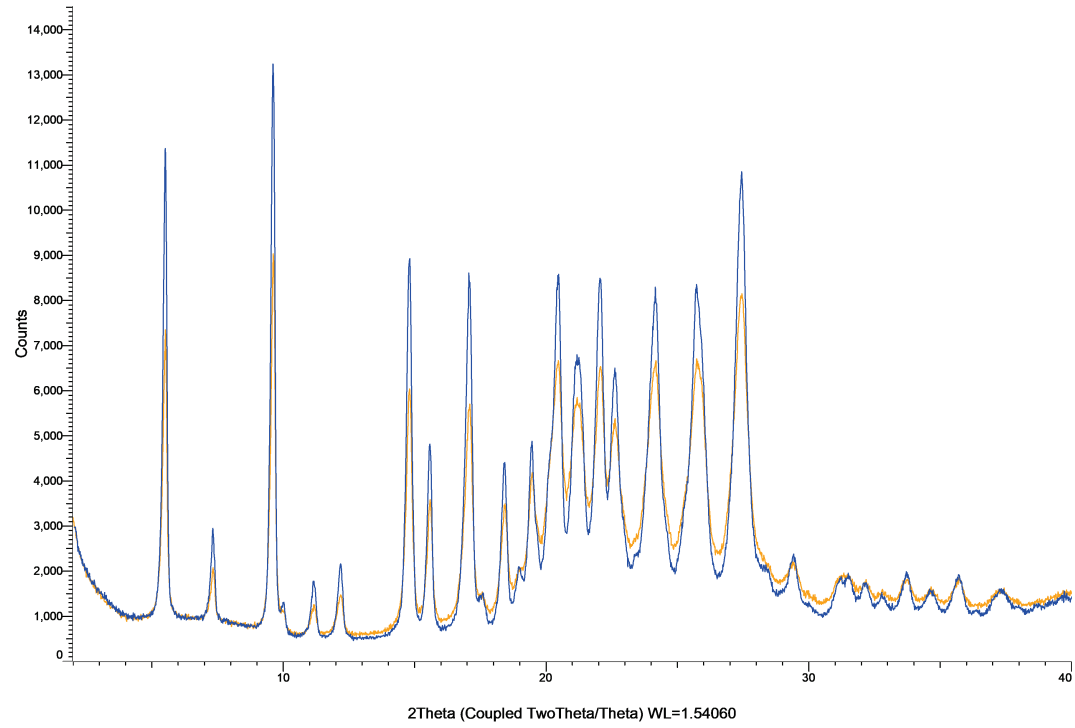


Figure S55: XRPD patterns of nilotinib powder (blue) and milled nilotinib powder (orange).

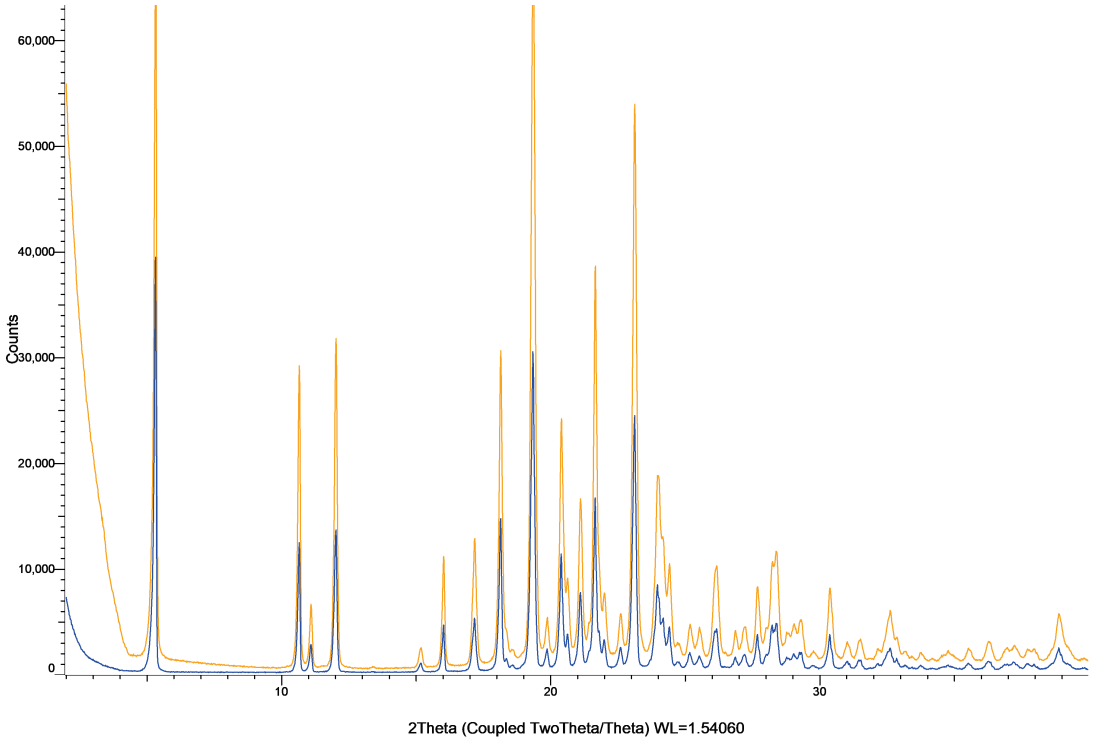


Figure S56: XRPD patterns of nimesulide powder (blue) and milled nimesulide powder (orange).

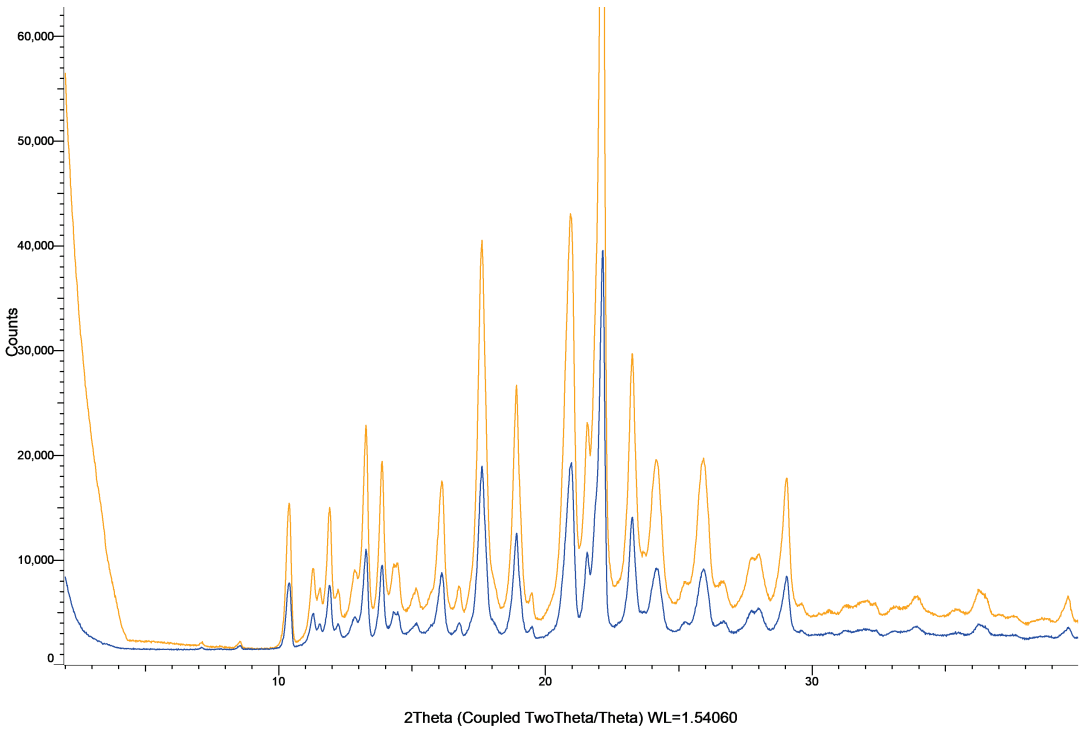


Figure S57: XRPD patterns of olaparib powder (blue) and milled olaparib powder (orange).

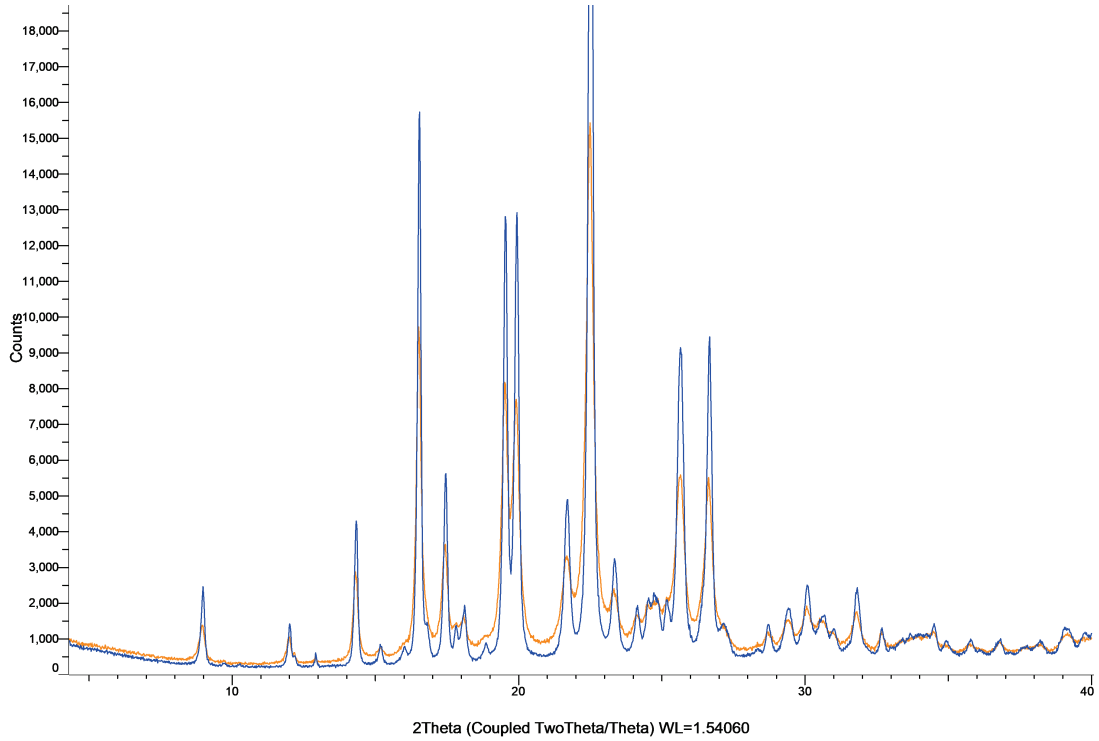


Figure S58: XRPD patterns of rivaroxaban powder (blue) and milled rivaroxaban powder (orange).

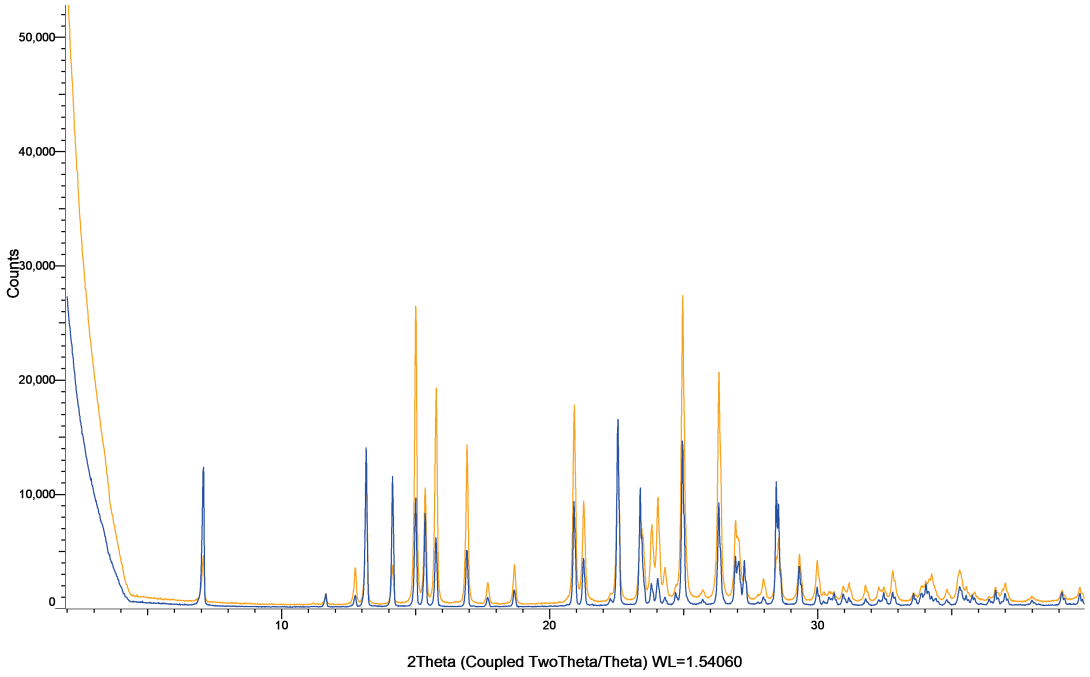


Figure S59: XRPD patterns of sertraline powder (blue) and milled sertraline powder (orange).

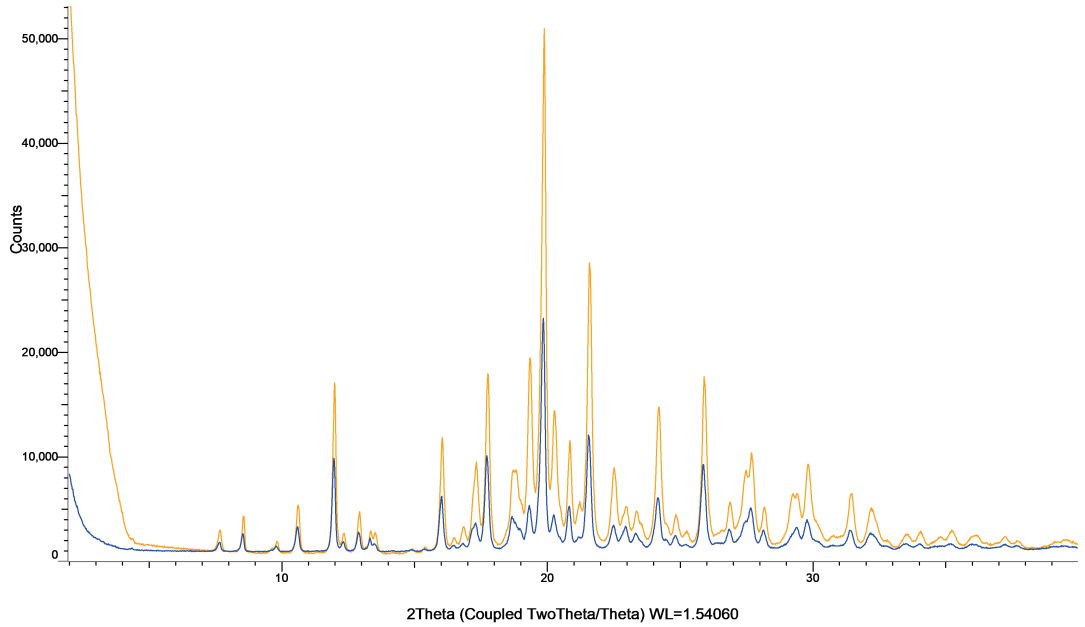


Figure S60: XRPD patterns of sorafenib powder (blue) and milled sorafenib powder (orange).

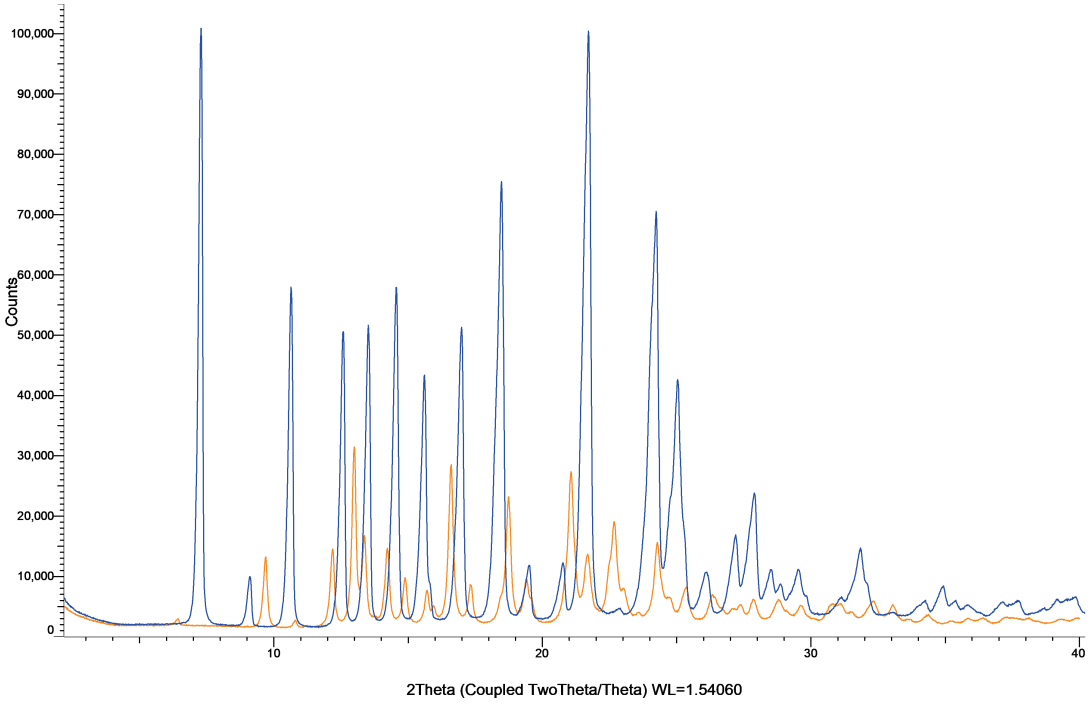


Figure S61: XRPD patterns of tadalafil powder (blue) and milled tadalafil powder (orange).

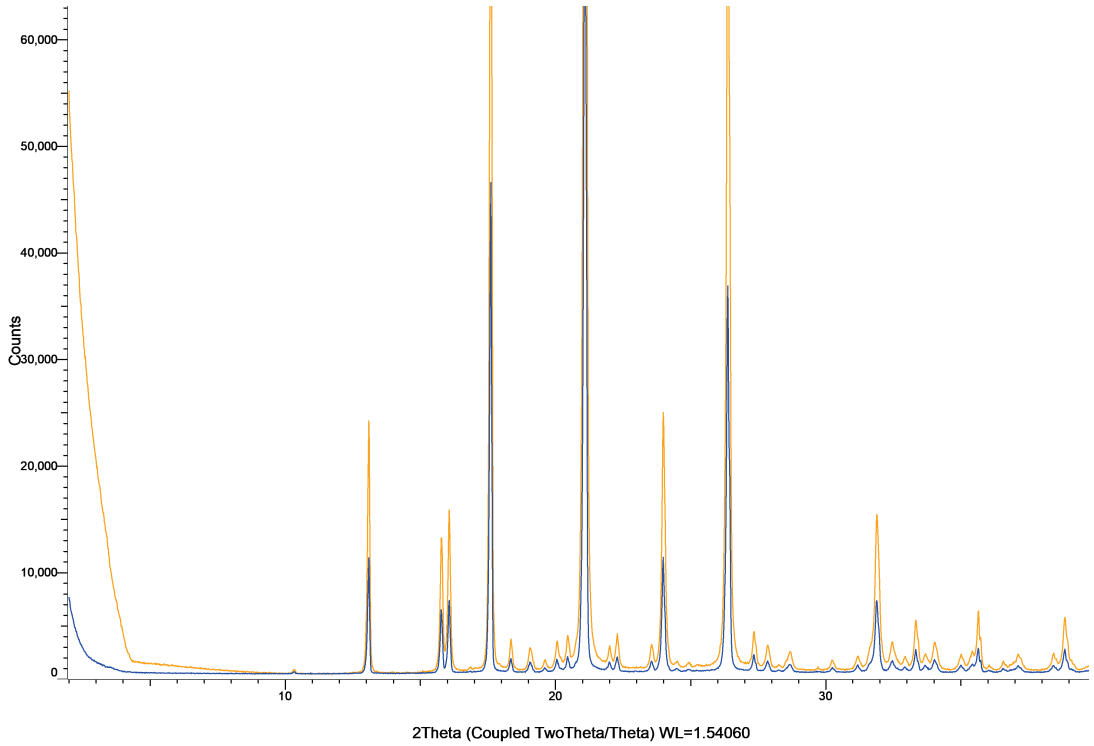


Figure S62: XRPD patterns of thiabendazole powder (blue) and milled thiabendazole powder (orange).

10.1.8 Polymorphs of investigated compounds

Table S6: List of polymorphs for all screened compounds.

Drug	Polymorph	Reference
Albendazole	Polymorphic form II	DOI: https://doi.org/10.1002/jps.22072
Apixaban	Polymorphic form I	DOI: https://doi.org/10.1021/acs.molpharmaceut.8b00060
Apremilast	Polymorphic form B	Patent No. US 9 , 850 , 205 B2
Aripiprazole	Polymorphic form III	DOI: https://doi.org/10.1016/B978-0-12-397220-0.00001-5
Candesartan Cilexetil	Polymorphic form I	DOI: https://doi.org/10.1021/ie2024855
Carbamazepine	Polymorphic form III	DOI: 10.1016/j.ejps.2017.05.013
Celecoxib	Polymorphic form III	Patent No. US 7476,744 B2
Ceritinib	Polymorphic form 2b	Patent No. WO 2017/016529 A1
Cinnarizine	no polymorphism reported in literature	
Dasatinib	Polymorphic form C	Patent No. US 2010/0256158 A1
Deferasirox	Polymorphic form A	Patent No. US 8,153,672 B2
Dipyridamole	Polymorphic form II	Patent No. US 8,092,785 B2
Enzalutamide	Polymorphic form R1, transition to polymorphic form R2 after milling without excipient	Patent No. US 9,701,641 B2
Etoricoxib	Polymorphic form XIII	Patent No. WO 2005/085199 A1
Ezetimibe	Polymorphic form II	Patent No. US 2005/0171080 A1
Fenofibrate	Polymorphic form I	DOI: 10.1039/C5CE01148E
Gemfibrozil	Polymorphic form I	DOI: https://doi.org/10.1016/j.tca.2019.03.026
Glibenclamide	Polymorphic form I	DOI: https://doi.org/10.1016/0378-5173(89)90134-8
Griseofulvin	Polymorphic form I	DOI: 10.1002/jps.23349
Indomethacin	Polymorphic form γ	DOI: 10.1021/acs.molpharmaceut.7b00930
Mefenamic acid	Polymorphic form I	DOI: 10.22159/ajpcr.2017.v10i5.15863
Nilotinib	Polymorphic form C	DOI: https://doi.org/10.1021/acs.cgd.2c00253
Nimesulide	Polymorphic form I	DOI: https://doi.org/10.1002/jps.22464
Olaparib	Polymorphic form A	Patent No. WO 2017/191562 A1
Rivaroxaban	Polymorphic form I	DOI: 10.1002/crat.201600379
Sertraline	Polymorphic form II	Patent No. US 6,872,853 B1
Sorafenib	Polymorphic form III	Patent No. US 8,217,061 B2
Tadalafil	Polymorphic form A. Milling without excipient induced a beginning polymorphic transition.	Patent No. WO 2006/049986 Al
Thiabendazole	no polymorphism reported in literature	

10.1.9 Variables importance in Projection plots

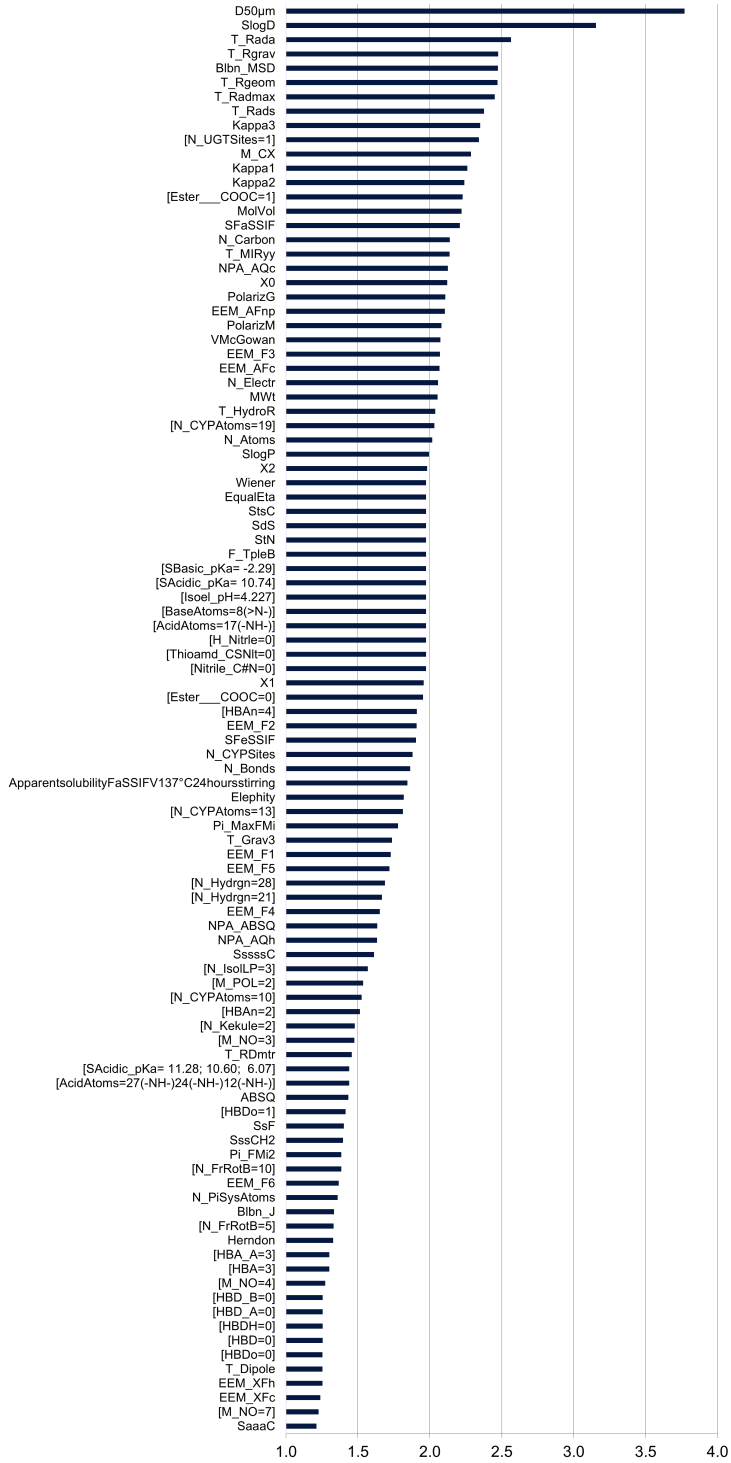


Figure S59: Variables Importance in Projection plots for COMDR$_{15min.}$

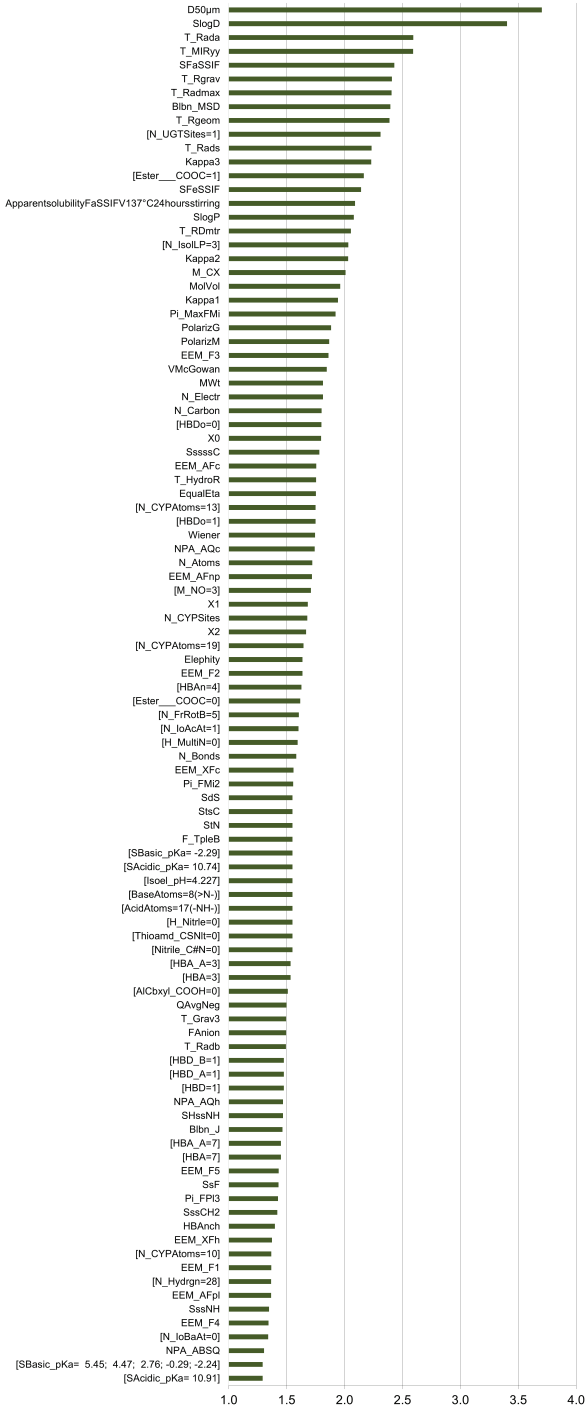


Figure S60: Variables Importance in Projection plots for COMDR$_{60min}$.

10.2 Appendix Chapter 3

10.21 Particle sizes of drug powders

Table S7: Particle sizes of drug powders before and after 15 min milling without the addition of an excipient.

Compound	Preparation	D10 [µm]	D50 [µm]	D90 [µm]
fenofibrate	Pre-milled	68.3	255.3	596.3
	Milled	10.0	40.4	168.4
apremilast	Pre-milled	3.3	10.2	37.2
	Milled	1.8	16.8	141.5

10.22 Specific surface areas of co-milled mixtures

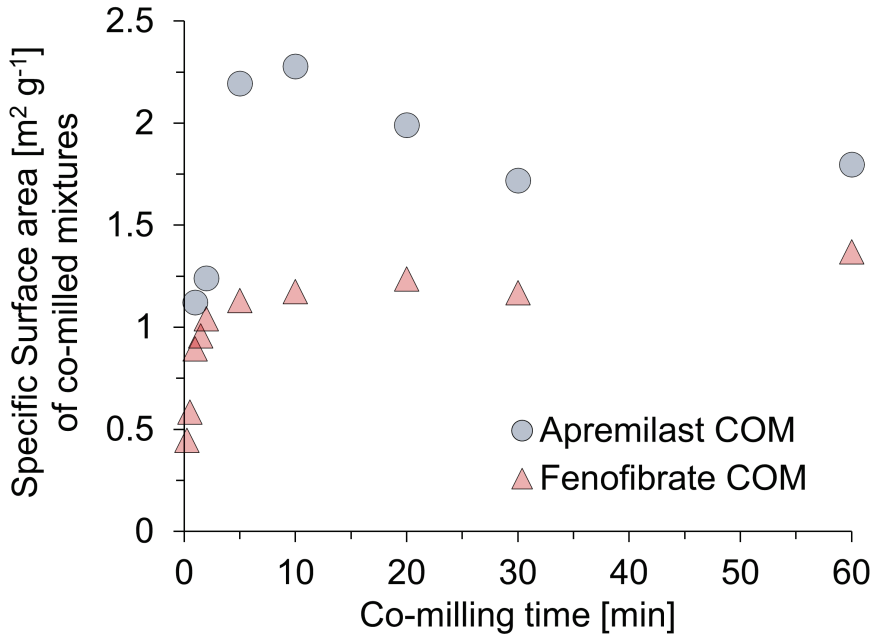


Figure S663: Relationship between Co-milling time and the specific surface area of co-milled mixtures.

10.23 Thermograms of apremilast mixtures freshly after preparation and 3 months stability testing

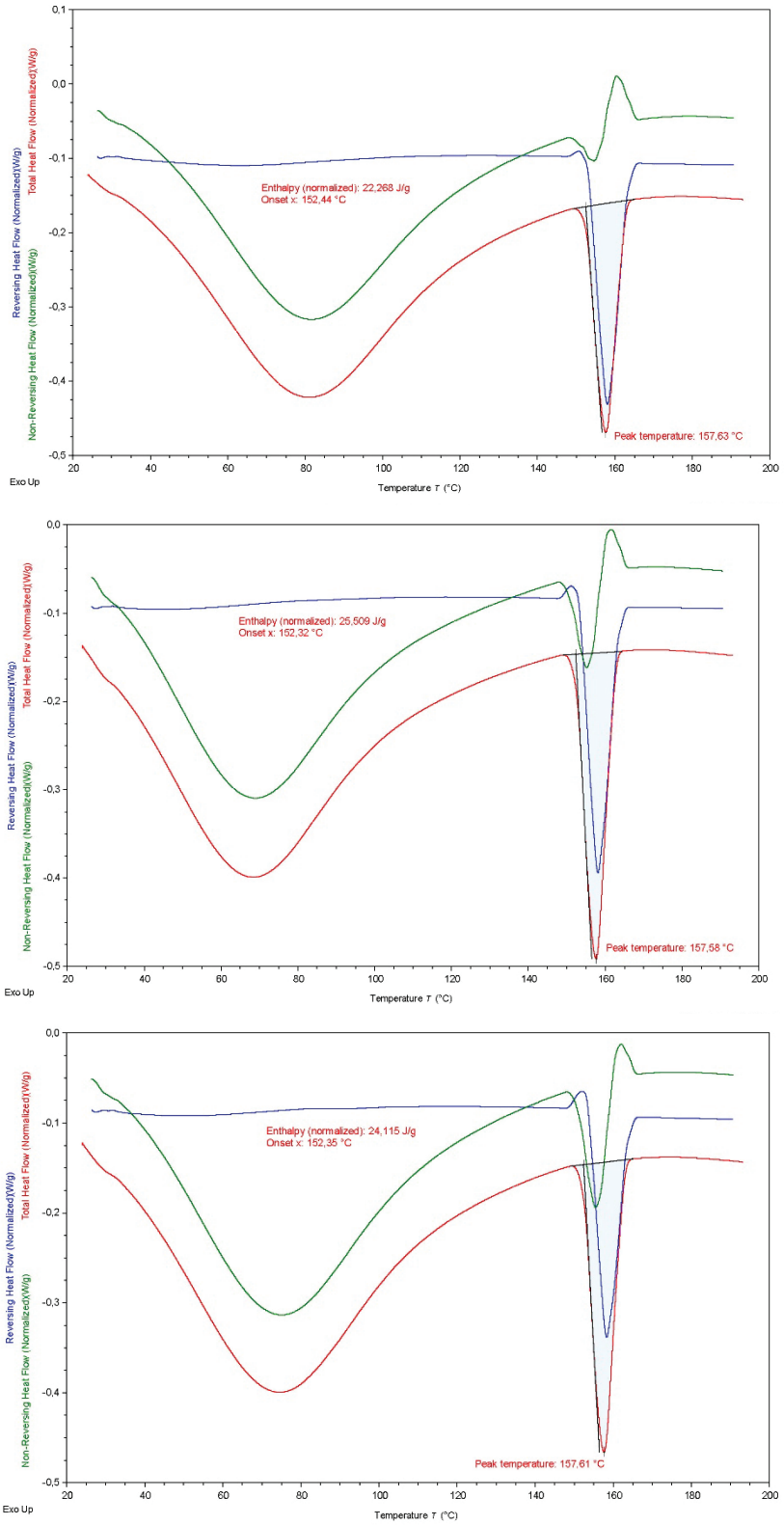


Figure S62:Thermograms illustrating the thermal behavior of apremilast blended (not milled) with croscarmellose sodium at a 1:2 (w/w), measured freshly after blending.

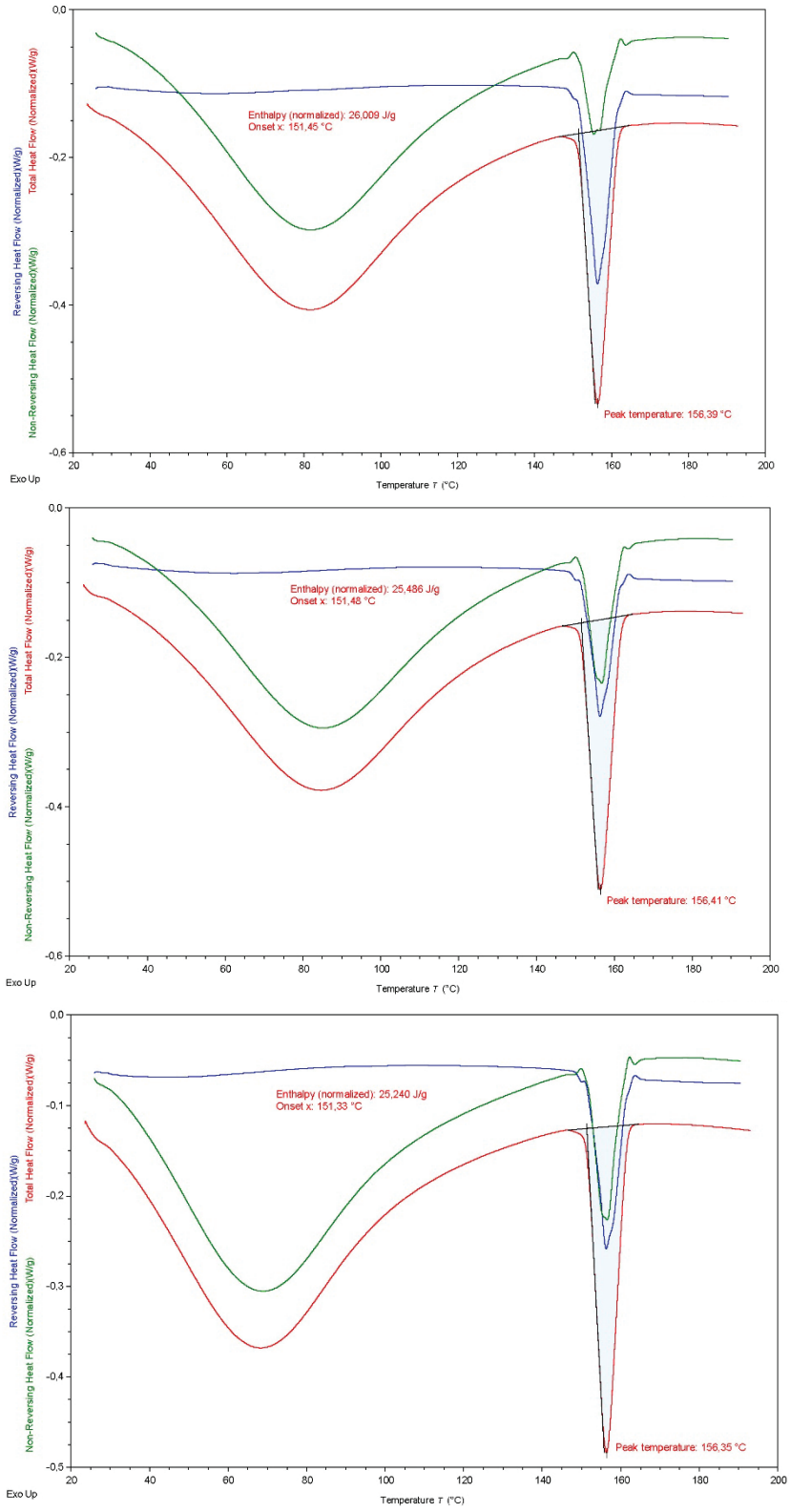


Figure S63: Thermograms illustrating the thermal behavior of apremilast co-milled with croscarmellose sodium at a 1:2 (w/w) ratio after 1 min of co-milling, measured freshly after preparation.

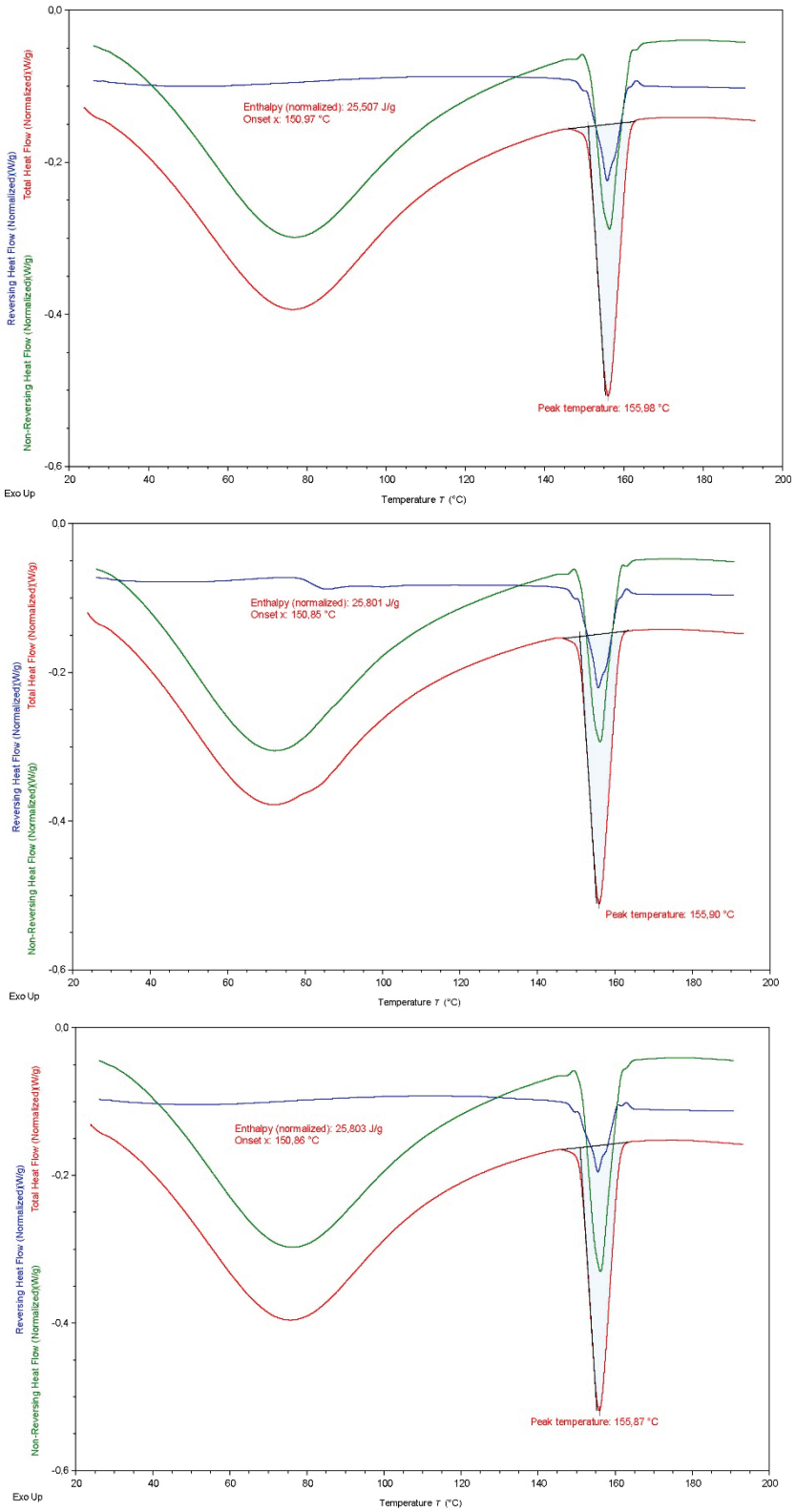


Figure S64: Thermograms illustrating the thermal behavior of apremilast co-milled with croscarmellose sodium at a 1:2 (w/w) ratio after 2 min of co-milling, measured freshly after preparation.

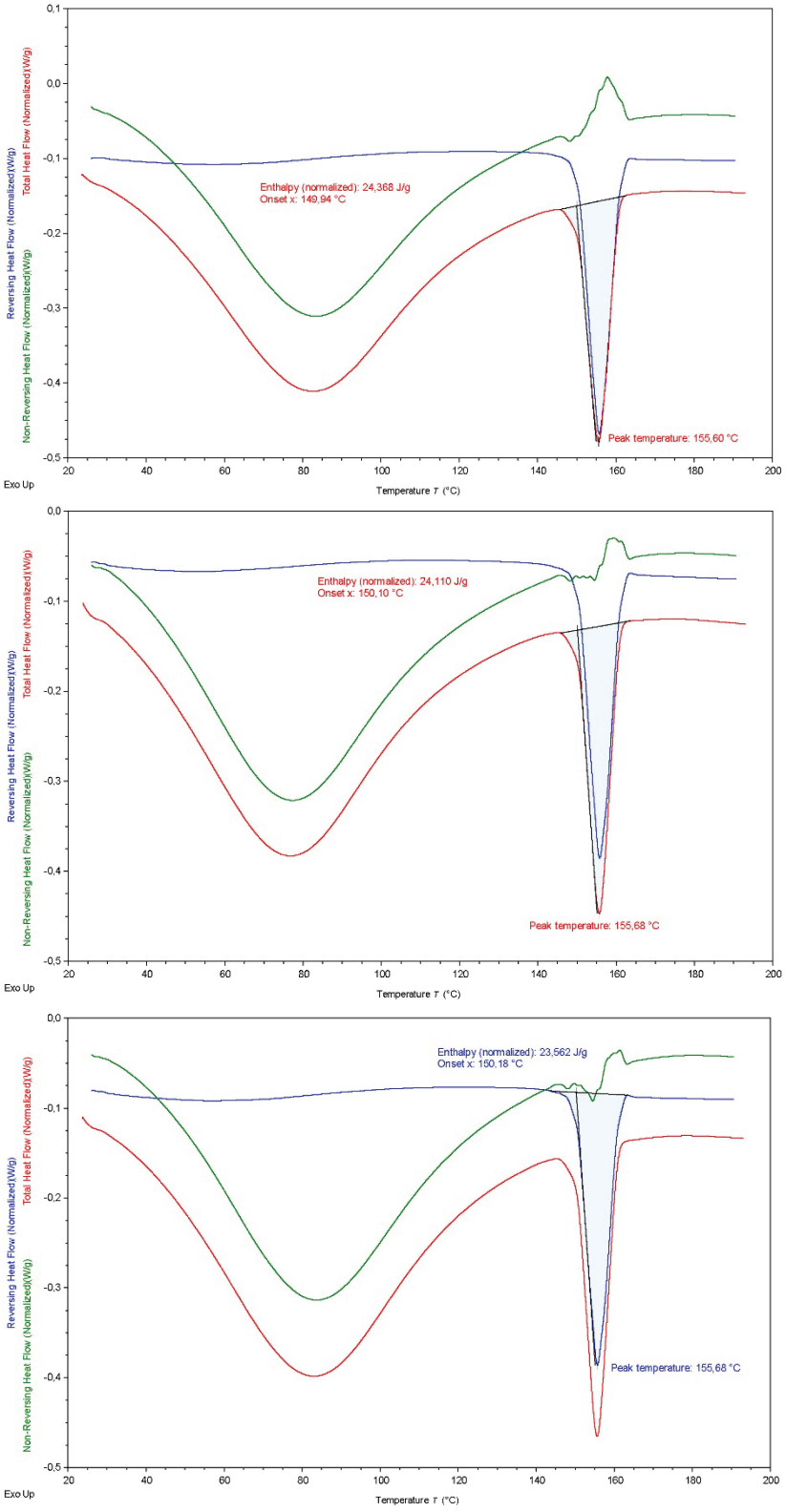


Figure S65: Thermograms illustrating the thermal behavior of apremilast co-milled with croscarmellose sodium at a 1:2 (w/w) ratio after 5 min of co-milling, measured freshly after preparation.

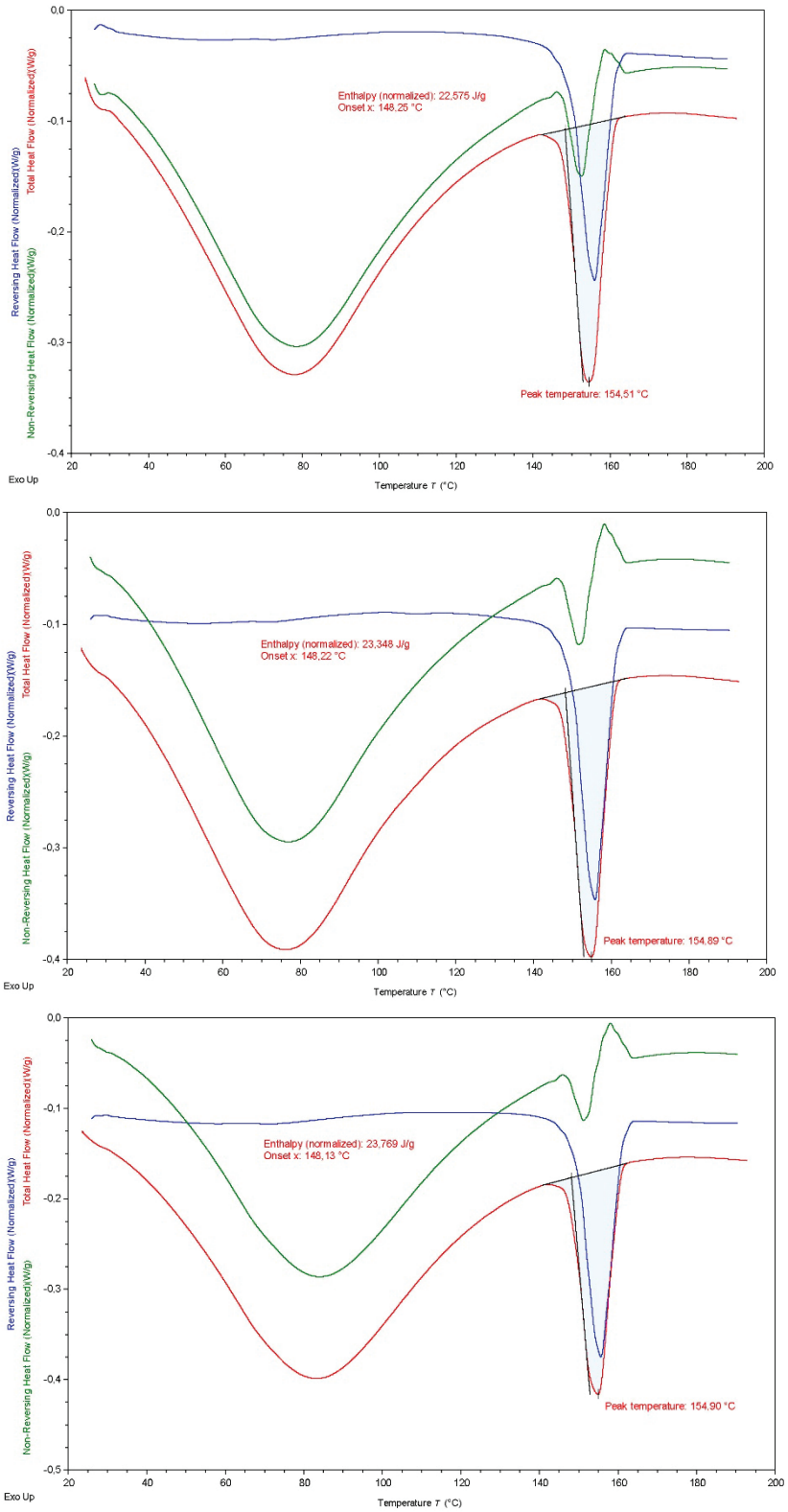


Figure S66: Thermograms illustrating the thermal behavior of apremilast co-milled with croscarmellose sodium at a 1:2 (w/w) ratio after 10 min of co-milling, measured freshly after preparation.

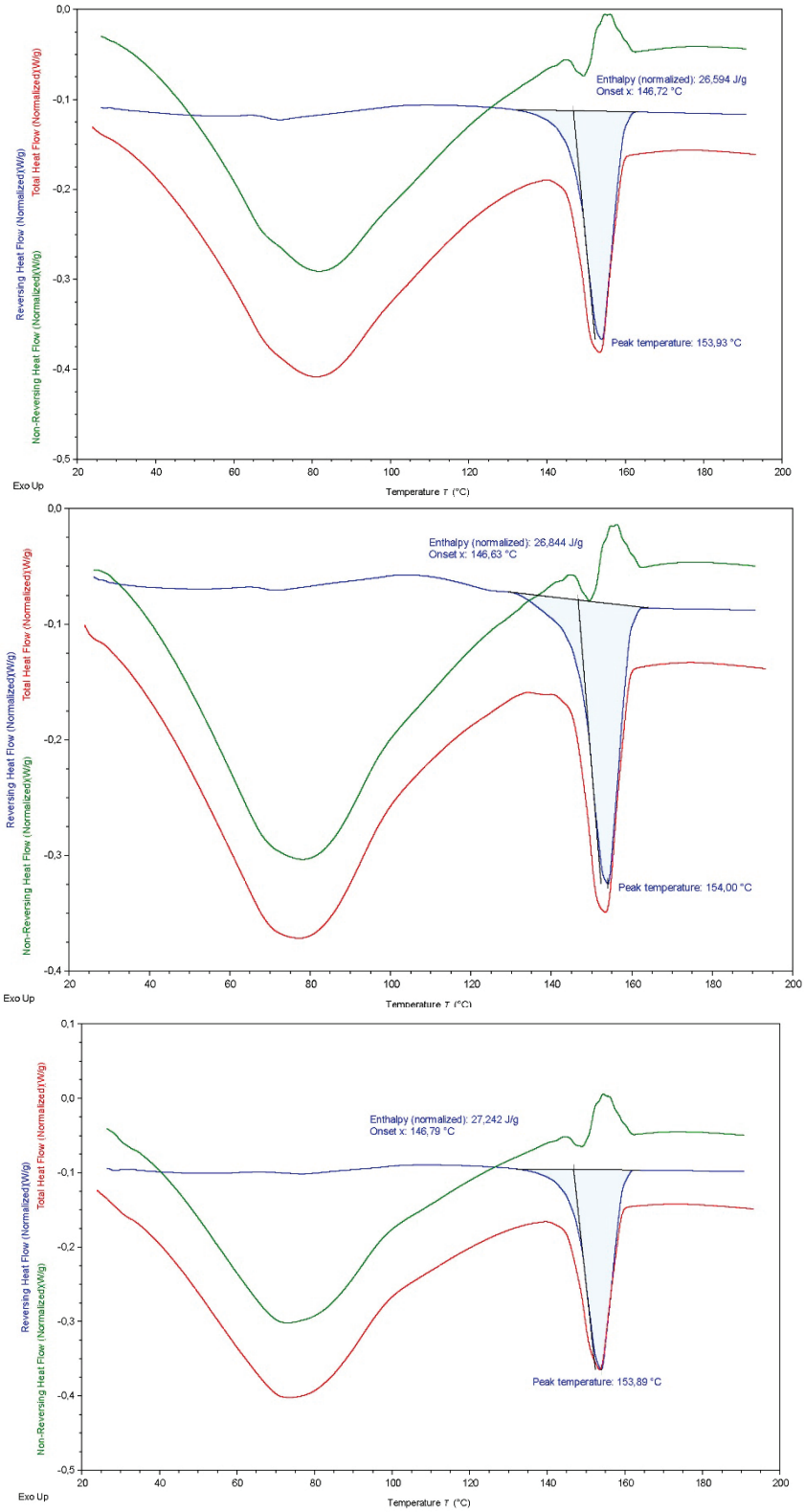


Figure S67: Thermograms illustrating the thermal behavior of apremilast co-milled with croscarmellose sodium at a 1:2 (w/w) ratio after 20 min of co-milling, measured freshly after preparation.

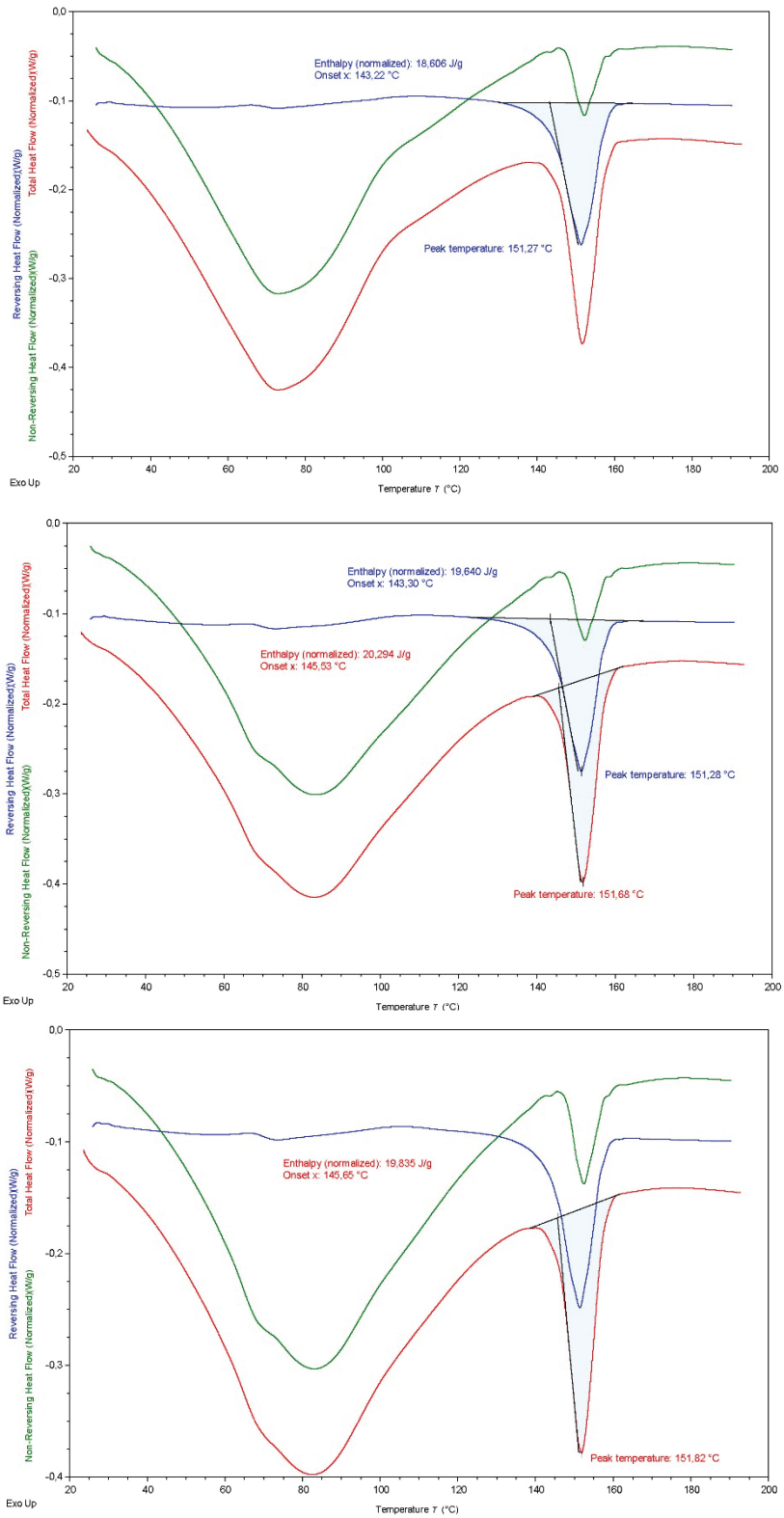


Figure S68: Thermograms illustrating the thermal behavior of apremilast co-milled with croscarmellose sodium at a 1:2 (w/w) ratio after 30 min of co-milling, measured freshly after preparation.

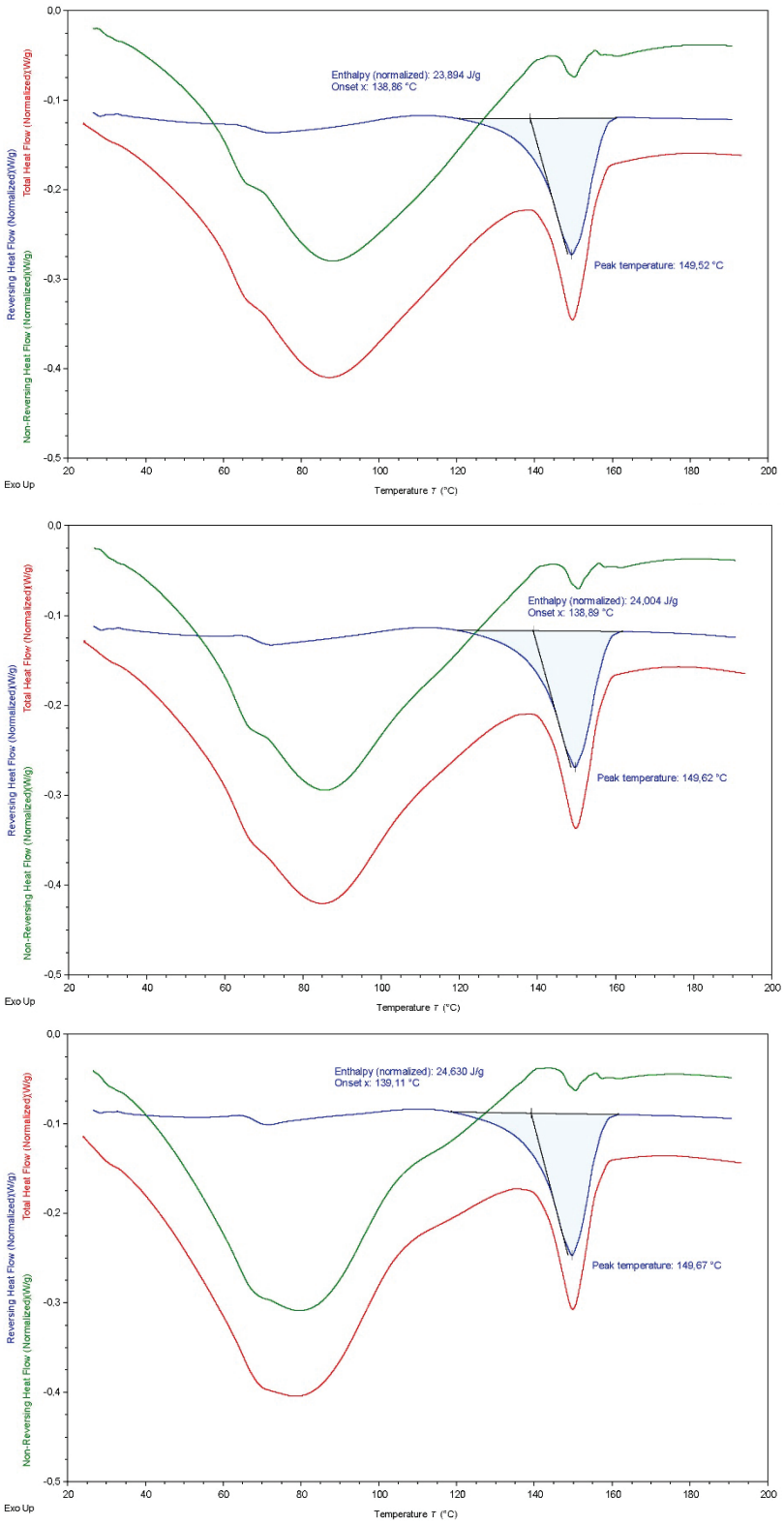


Figure S69: Thermograms illustrating the thermal behavior of apremilast co-milled with croscarmellose sodium at a 1:2 (w/w) ratio after 60 min of co-milling, measured freshly after preparation.

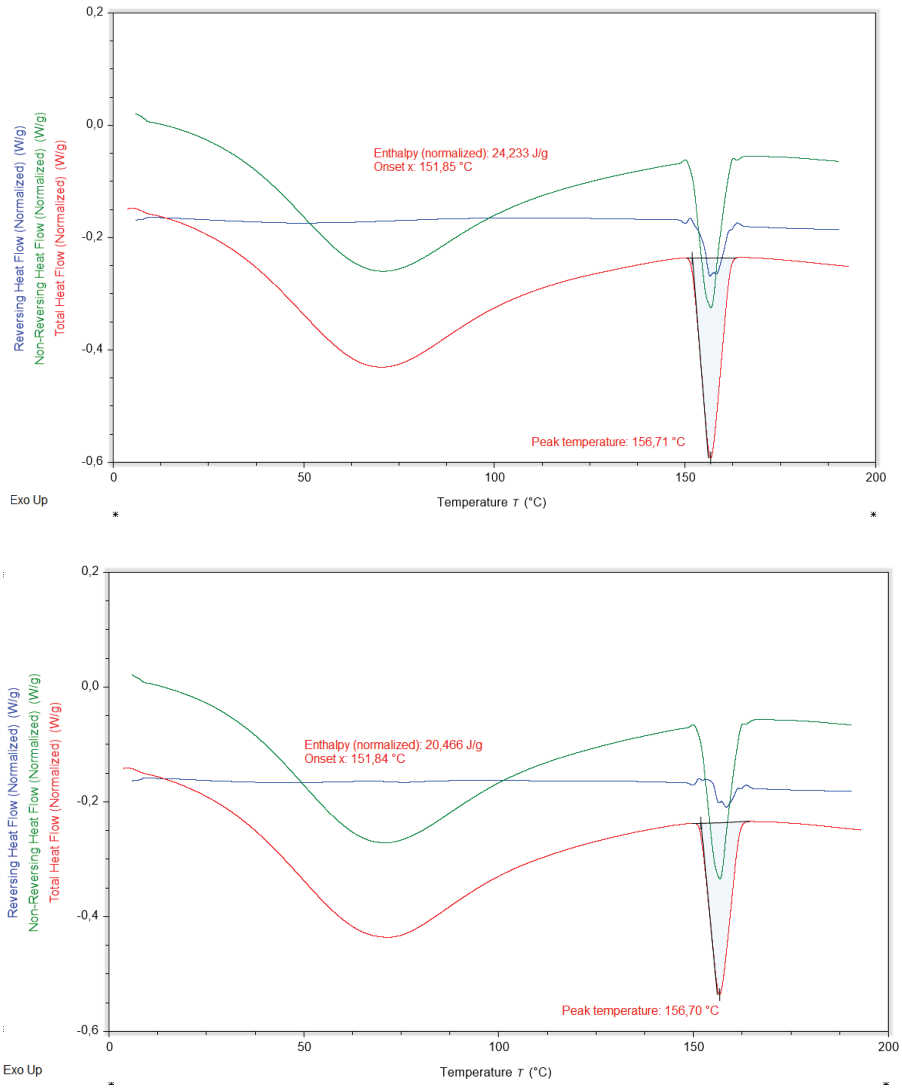


Figure S70: Thermograms illustrating the thermal behavior of apremilast blended (not milled) with croscarmellose sodium at a 1:2 (w/w), measured after 3 months of storage.

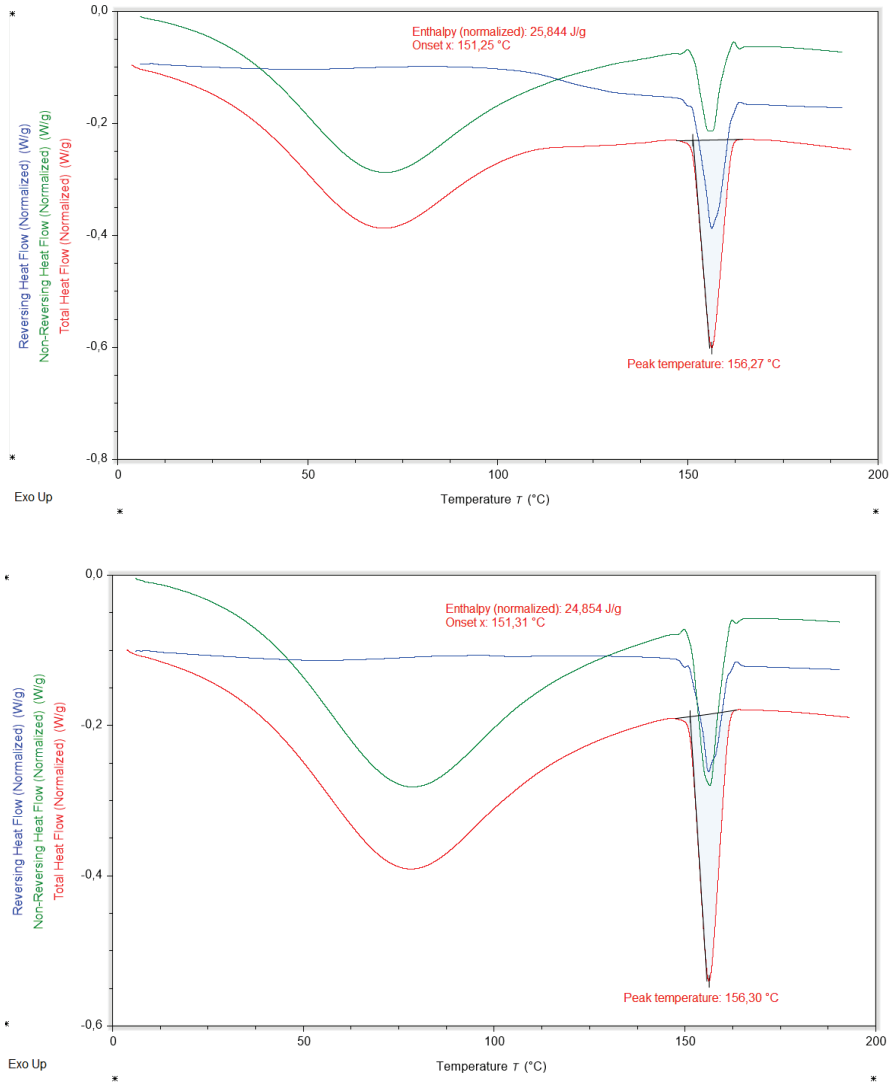


Figure S71: Thermograms illustrating the thermal behavior of apremilast co-milled with croscarmellose sodium at a 1:2 (w/w) ratio after 1 min of co-milling, measured after 3 months of storage.

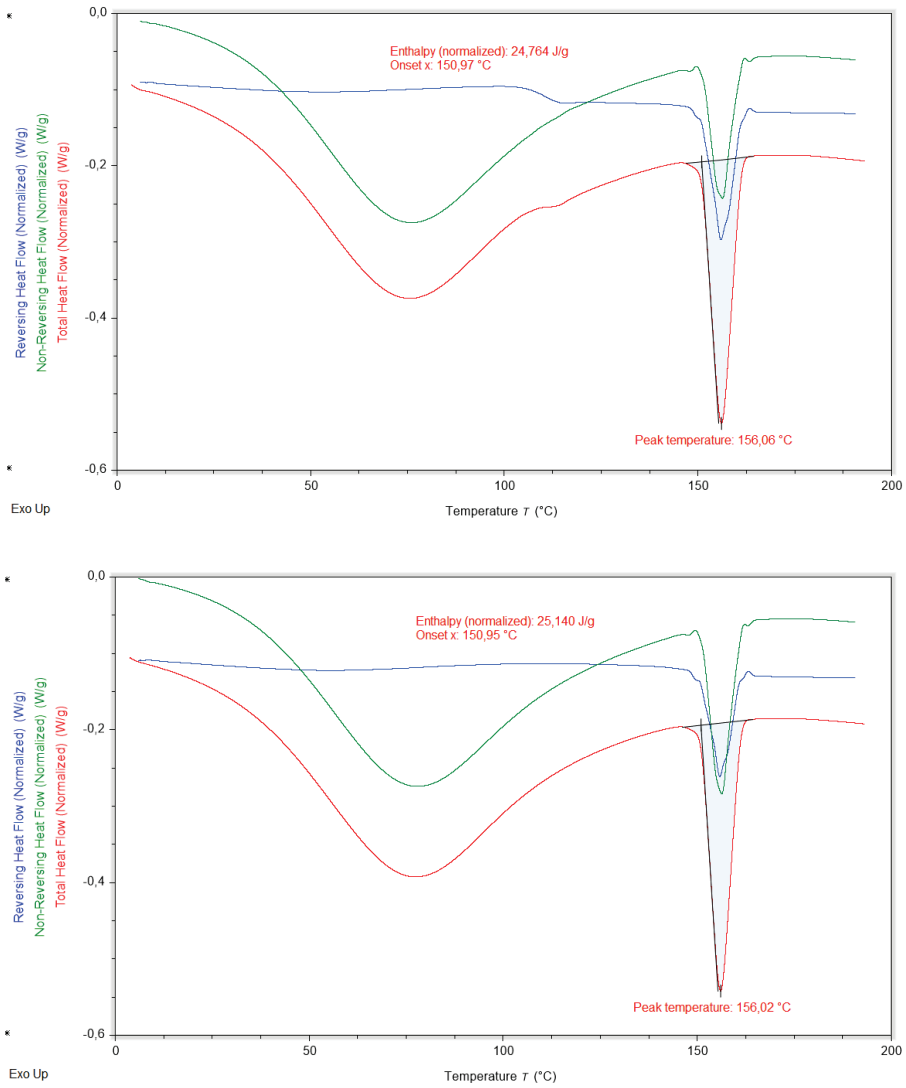


Figure S72: Thermograms illustrating the thermal behavior of apremilast co-milled with croscarmellose sodium at a 1:2 (w/w) ratio after 2 min of co-milling, measured after 3 months of storage.

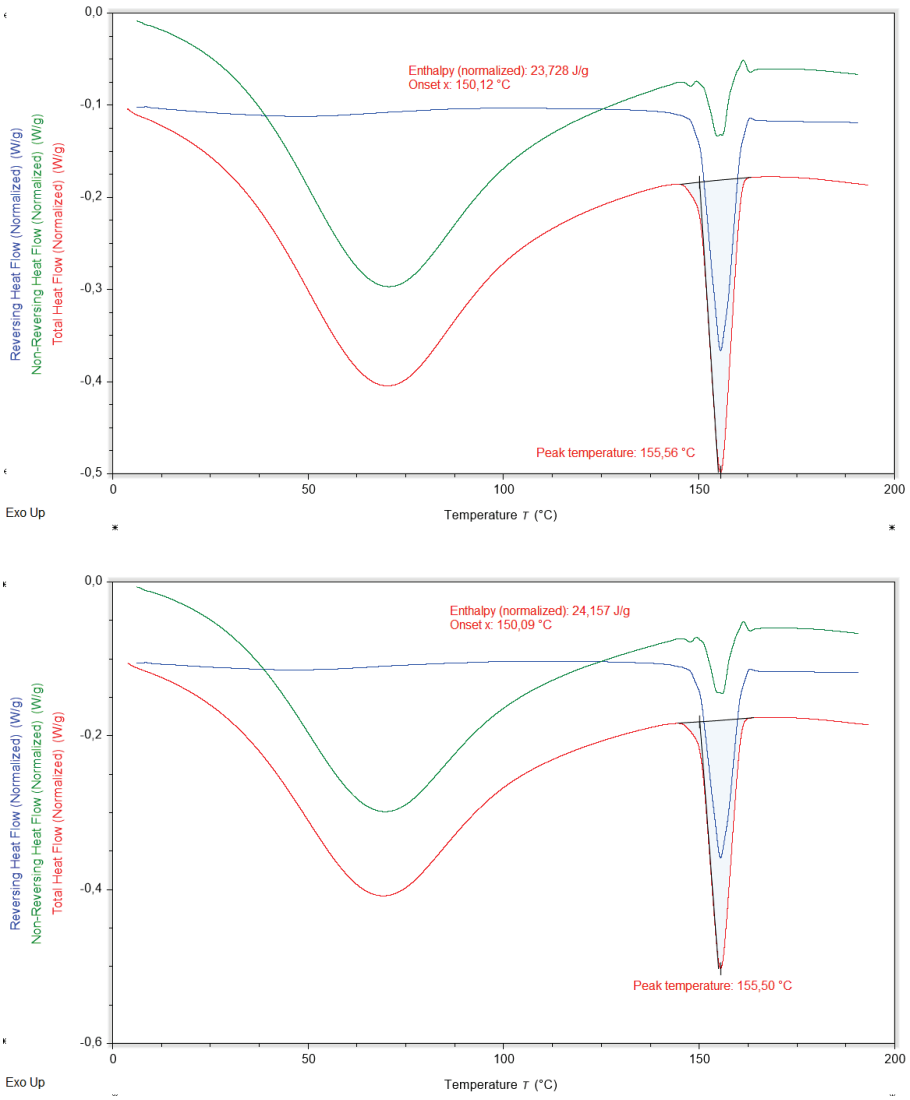


Figure S73: Thermograms illustrating the thermal behavior of apremilast co-milled with croscarmellose sodium at a 1:2 (w/w) ratio after 5 min of co-milling, measured after 3 months of storage.

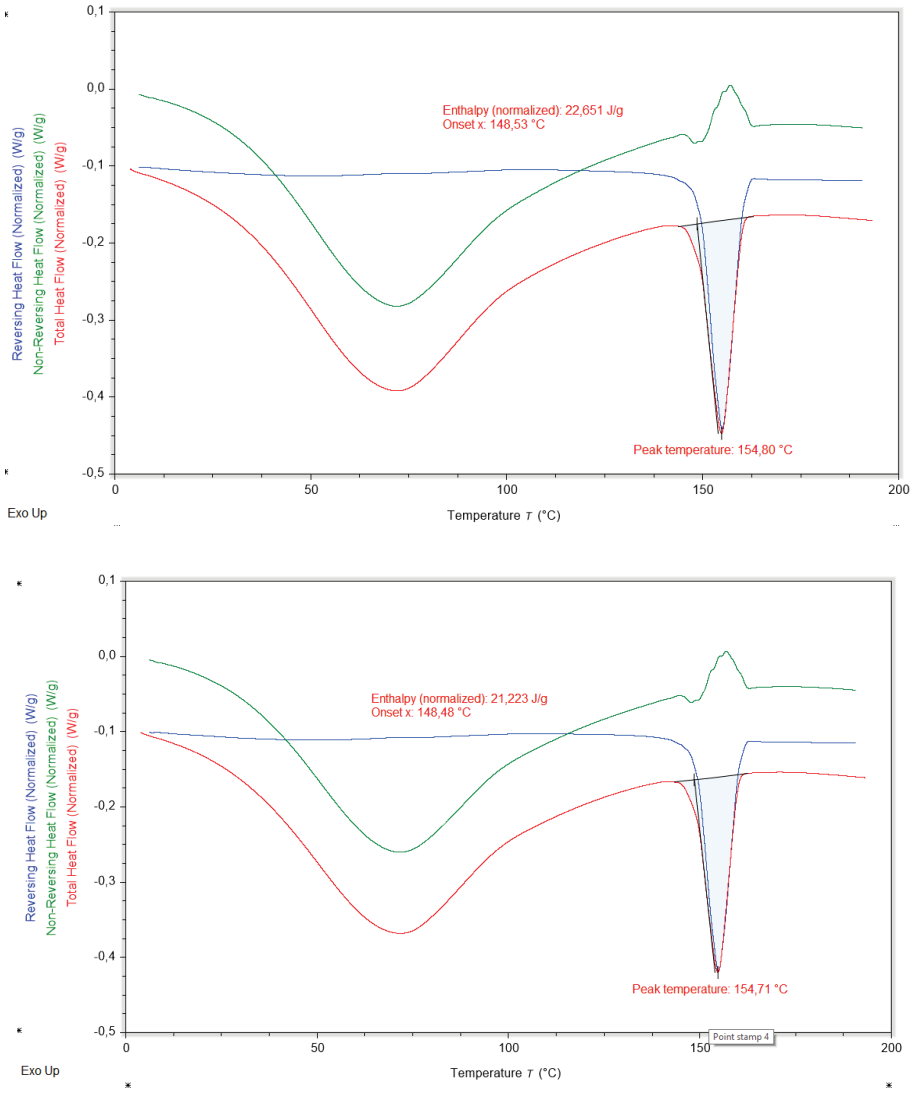


Figure S74: Thermograms illustrating the thermal behavior of apremilast co-milled with croscarmellose sodium at a 1:2 (w/w) ratio after 10 min of co-milling, measured after 3 months of storage.

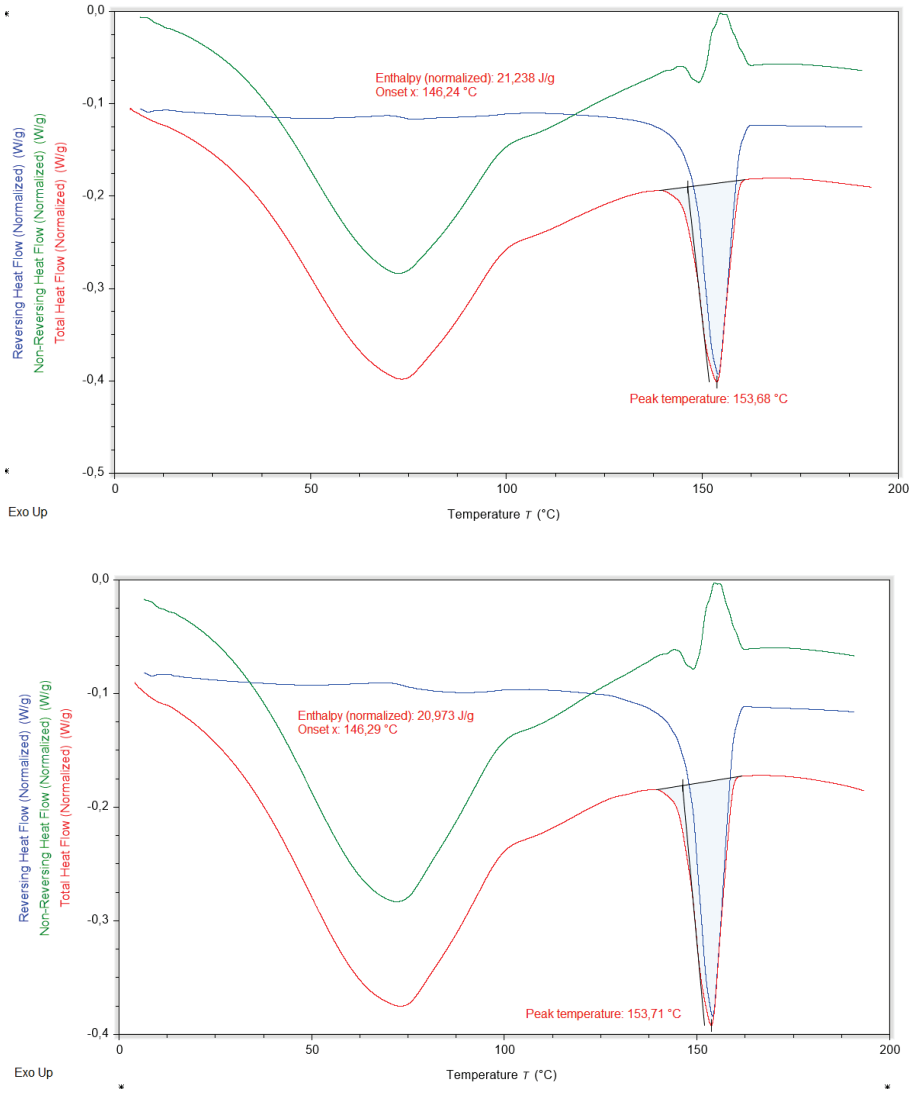


Figure S75: Thermograms illustrating the thermal behavior of apremilast co-milled with croscarmellose sodium at a 1:2 (w/w) ratio after 20 min of co-milling, measured after 3 months of storage.

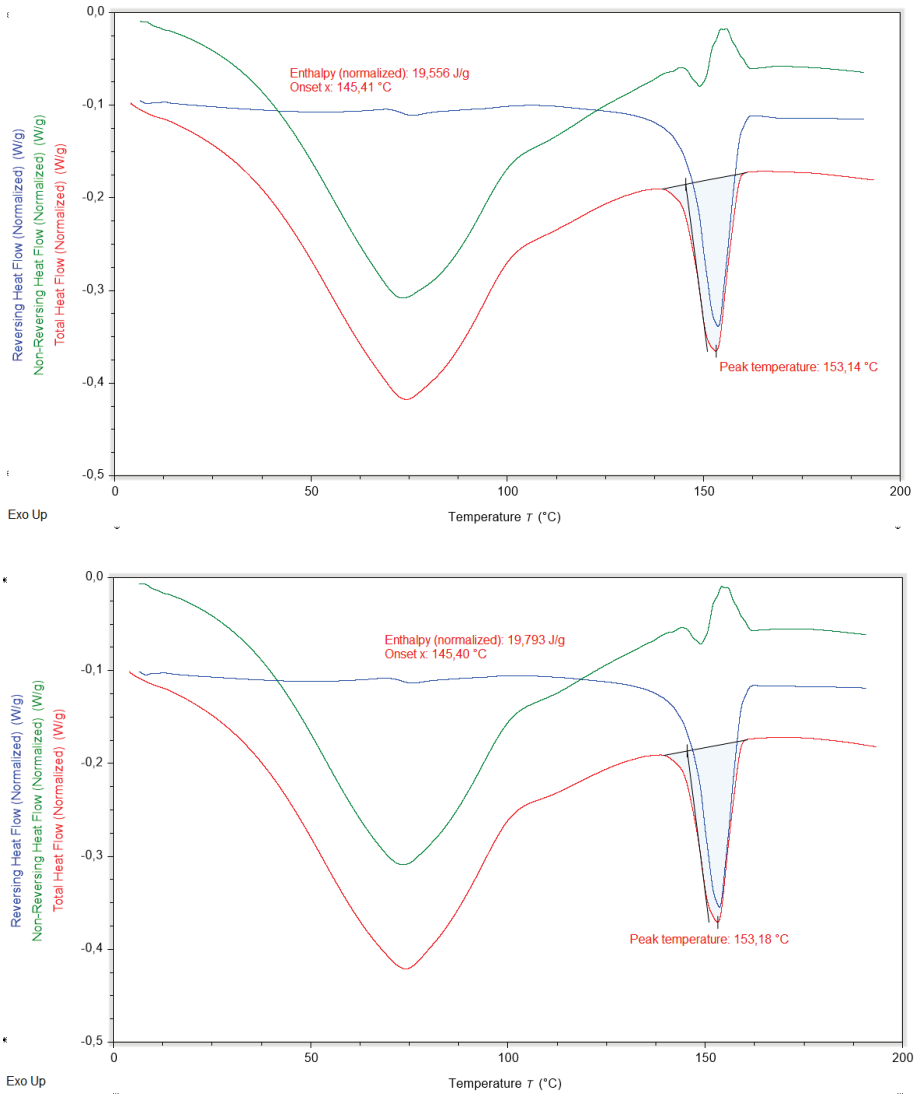


Figure S76: Thermograms illustrating the thermal behavior of apremilast co-milled with croscarmellose sodium at a 1:2 (w/w) ratio after 30 min of co-milling, measured after 3 months of storage.

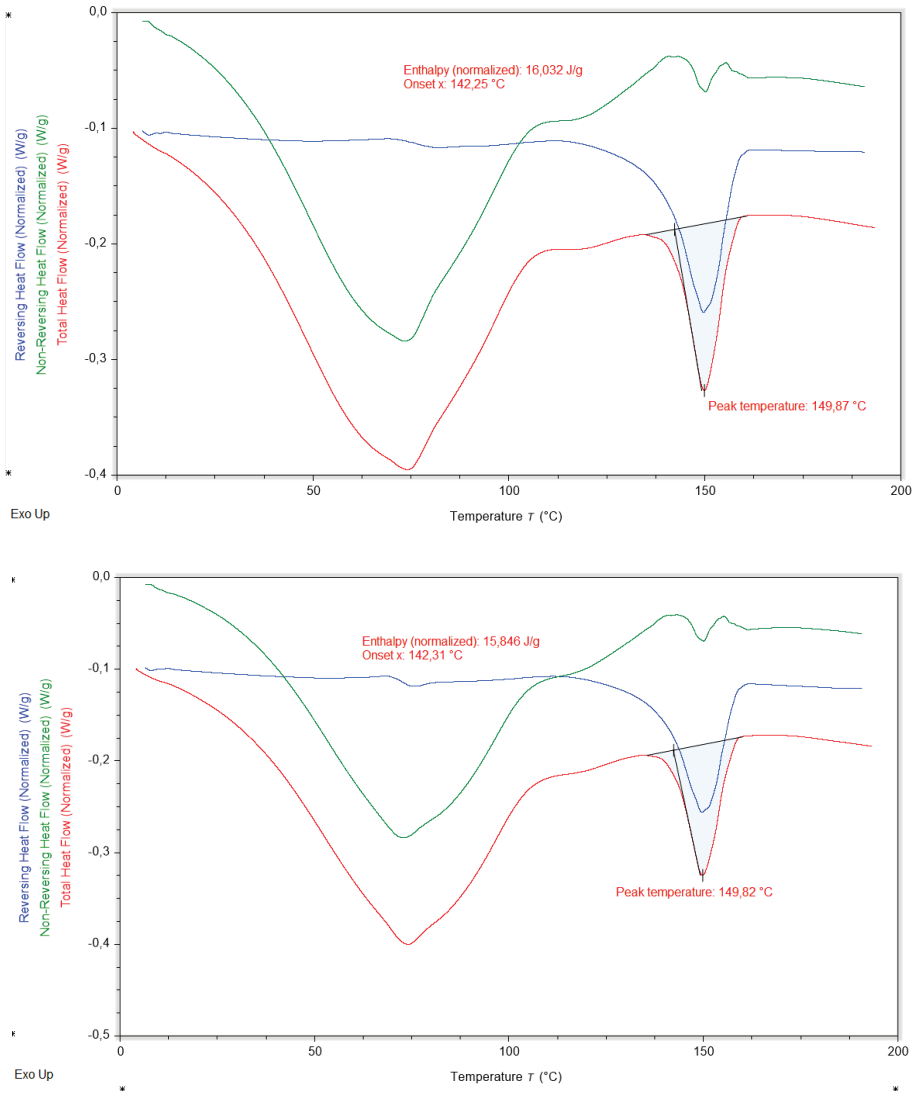


Figure S77: Thermograms illustrating the thermal behavior of apremilast co-milled with croscarmellose sodium at a 1:2 (w/w) ratio after 60 min of co-milling, measured after 3 months of storage.

10.24 Thermograms of fenofibrate mixtures freshly after preparation and 3 months stability testing

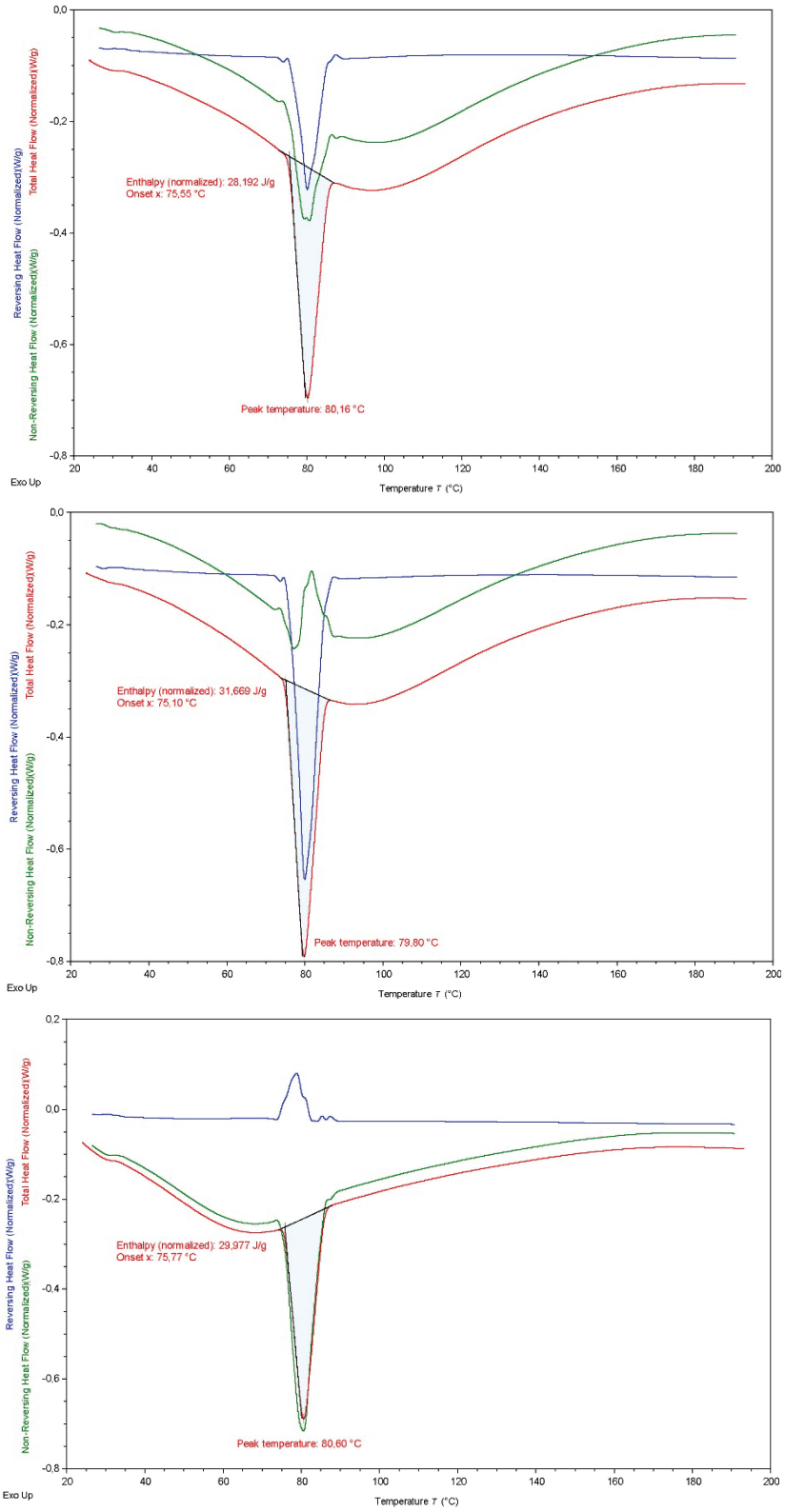


Figure S78: Thermograms illustrating the thermal behavior of fenofibrate blended (not milled) with croscarmellose sodium at a 1:2 (w/w), measured freshly after blending.

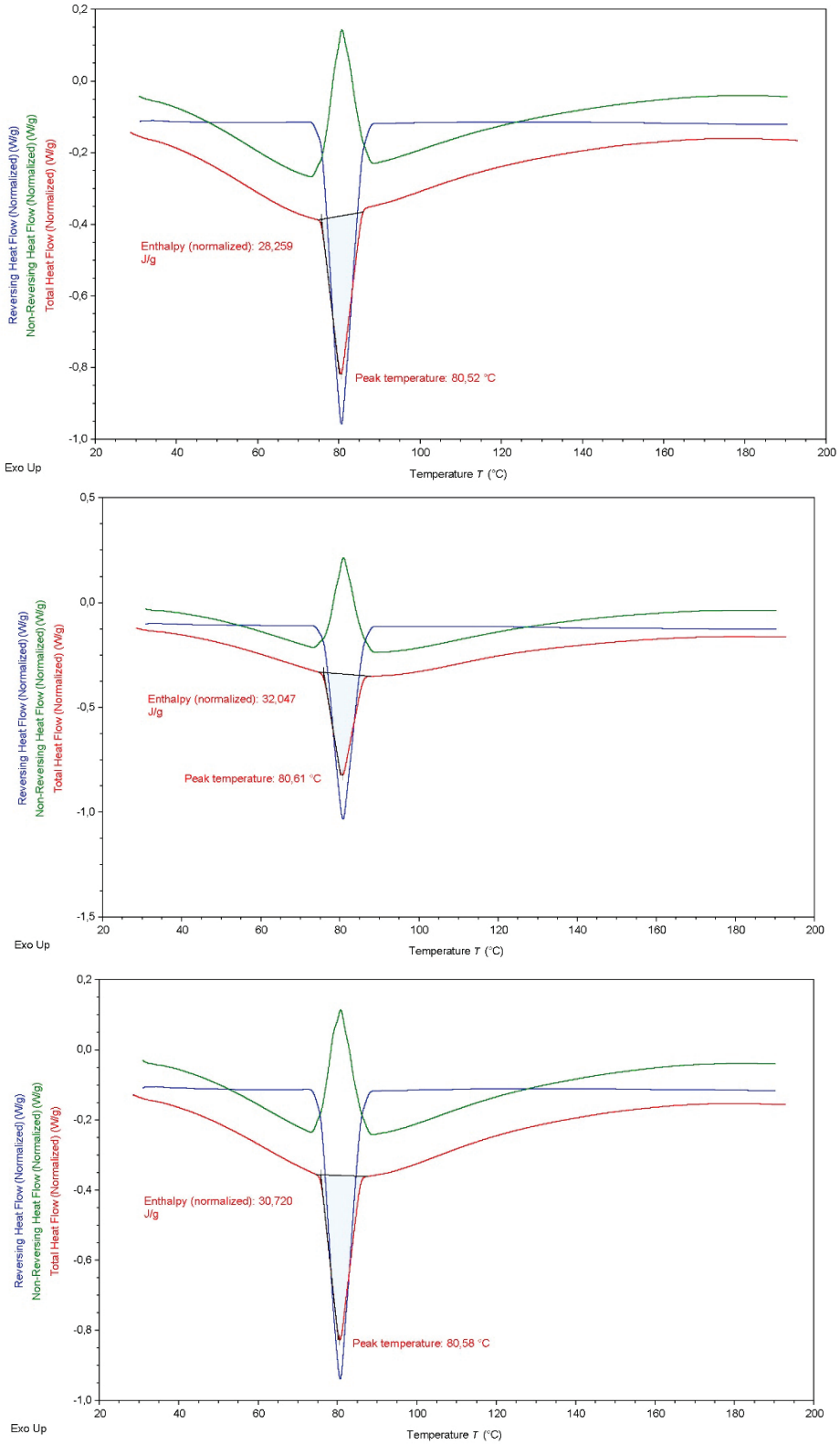


Figure S79: Thermograms illustrating the thermal behavior of fenofibrate co-milled with croscarmellose sodium at a 1:2 (w/w) ratio after 15 s of co-milling, measured freshly after preparation.

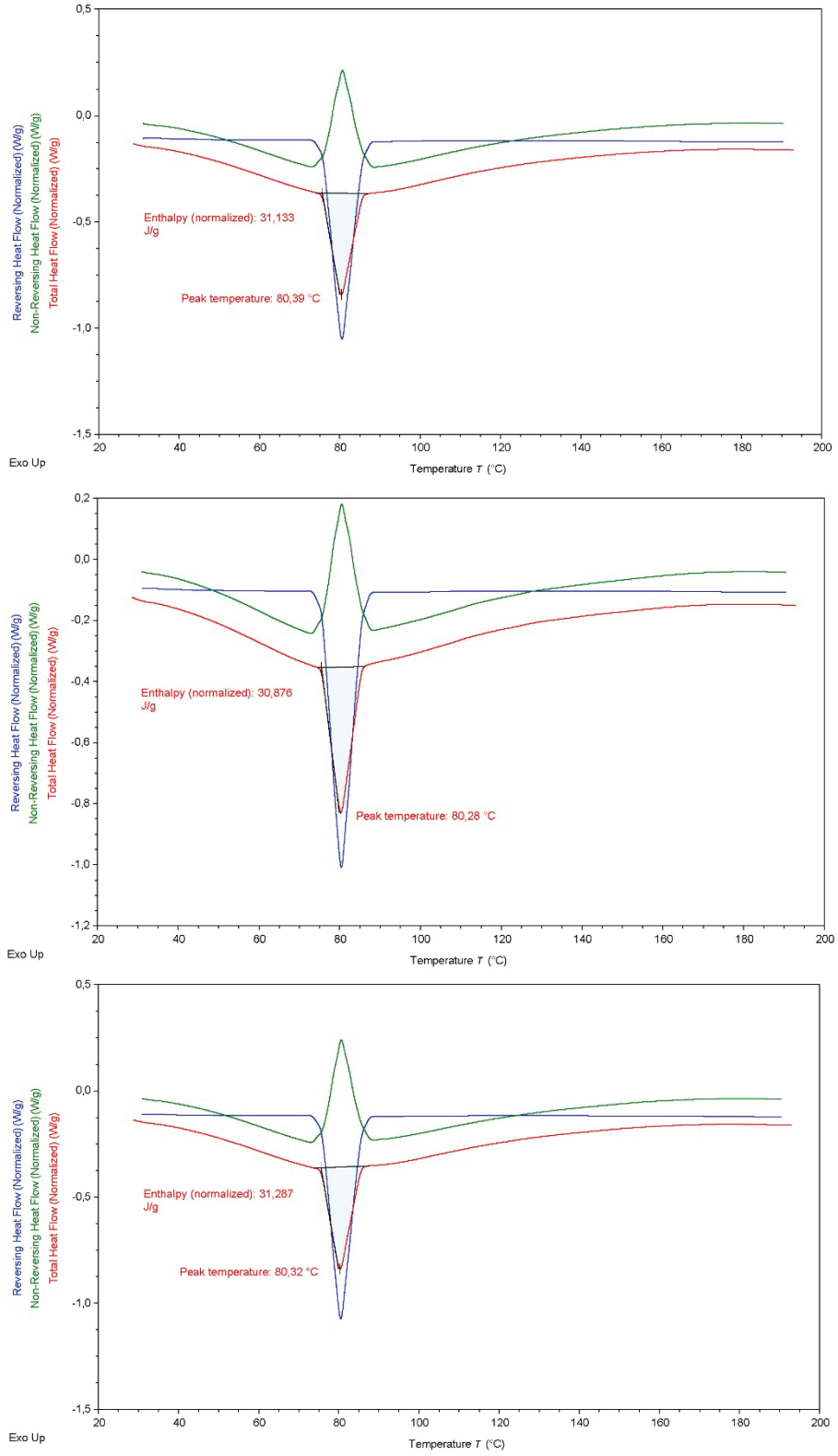


Figure S80: Thermograms illustrating the thermal behavior of fenofibrate co-milled with croscarmellose sodium at a 1:2 (w/w) ratio after 30 s of co-milling, measured freshly after preparation.

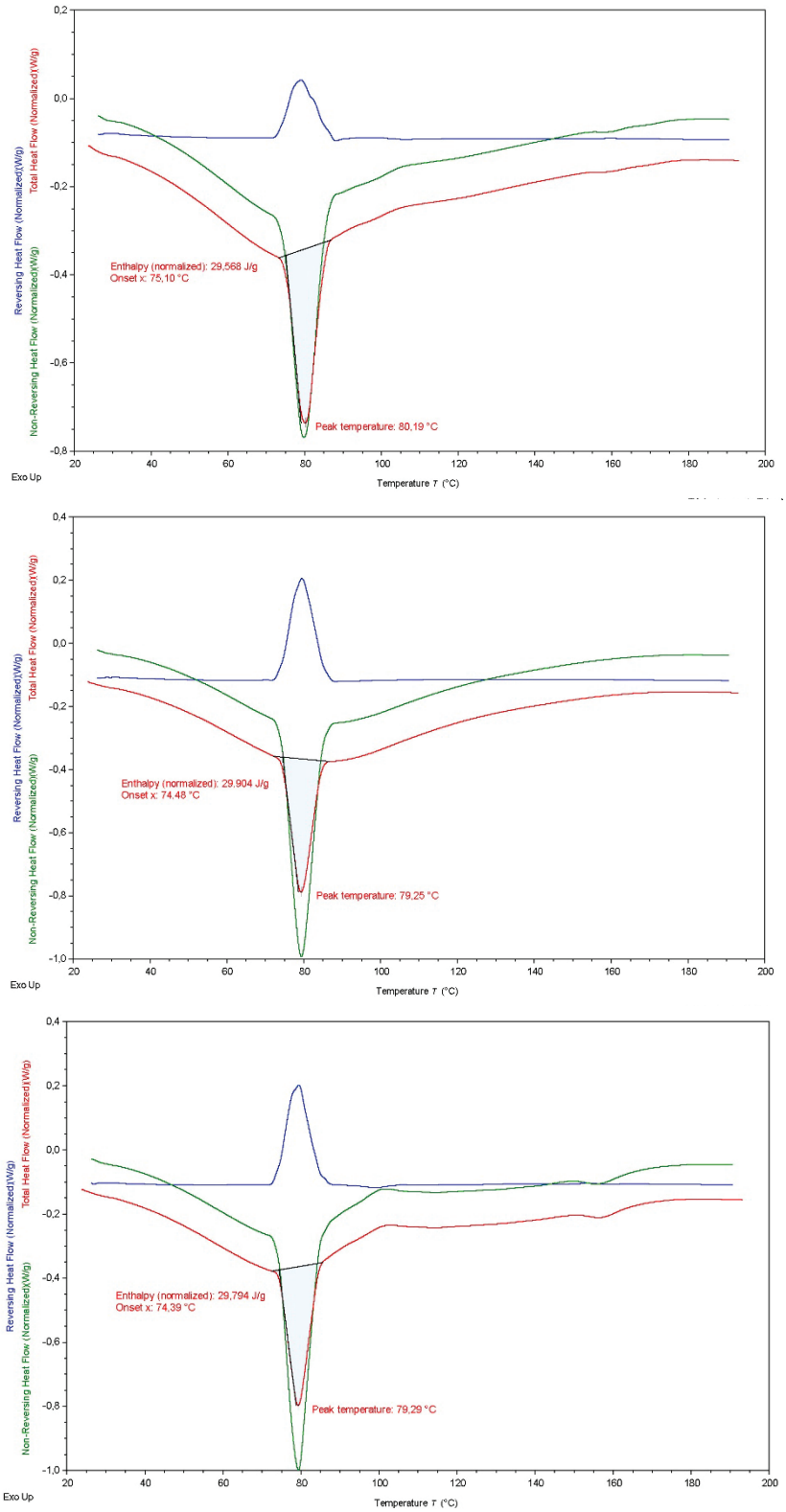


Figure S81: Thermograms illustrating the thermal behavior of fenofibrate co-milled with croscarmellose sodium at a 1:2 (w/w) ratio after 45 s of co-milling, measured freshly after preparation.

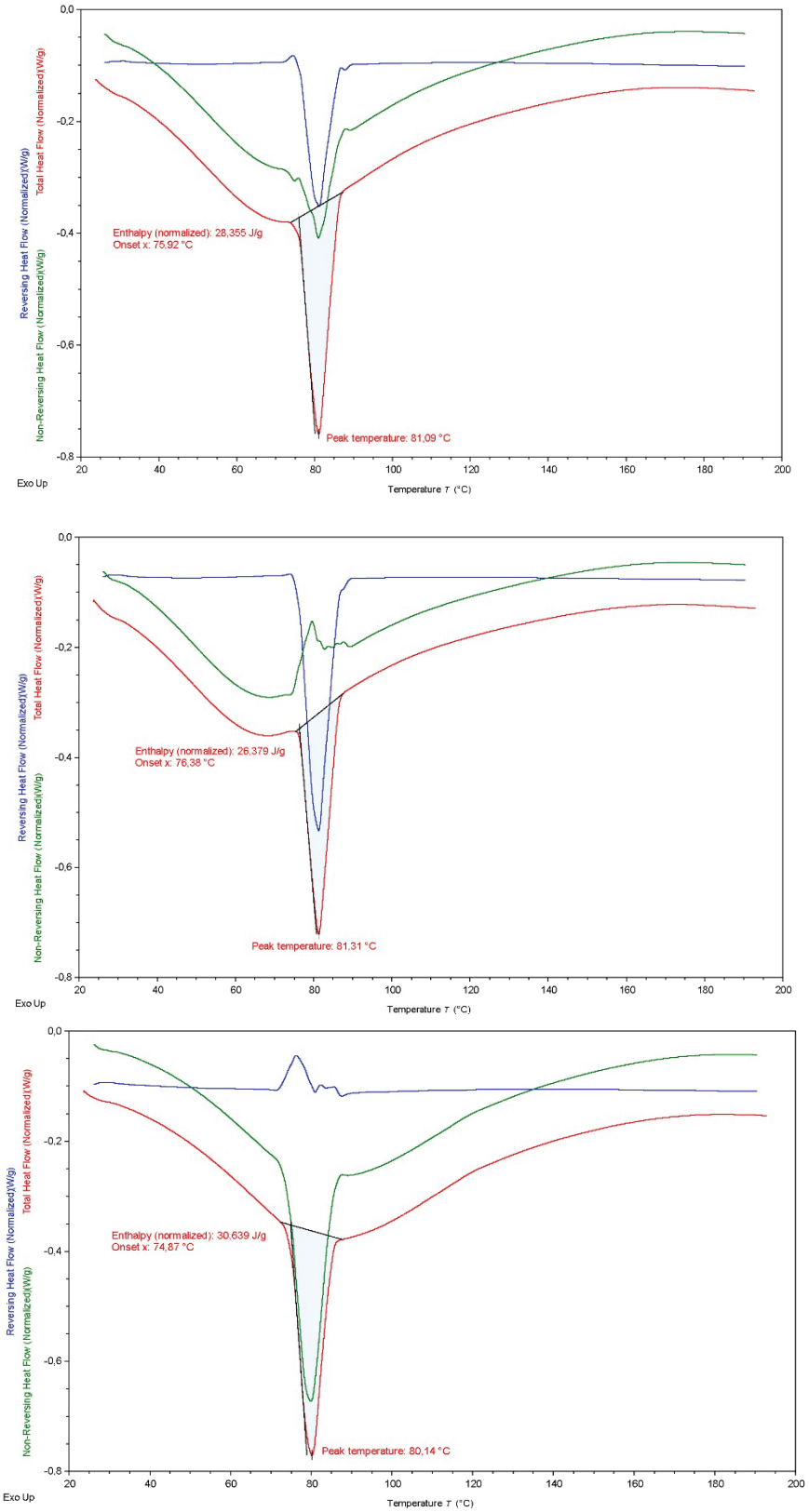


Figure S82: Thermograms illustrating the thermal behavior of fenofibrate co-milled with croscarmellose sodium at a 1:2 (w/w) ratio after 1 min of co-milling, measured freshly after preparation.

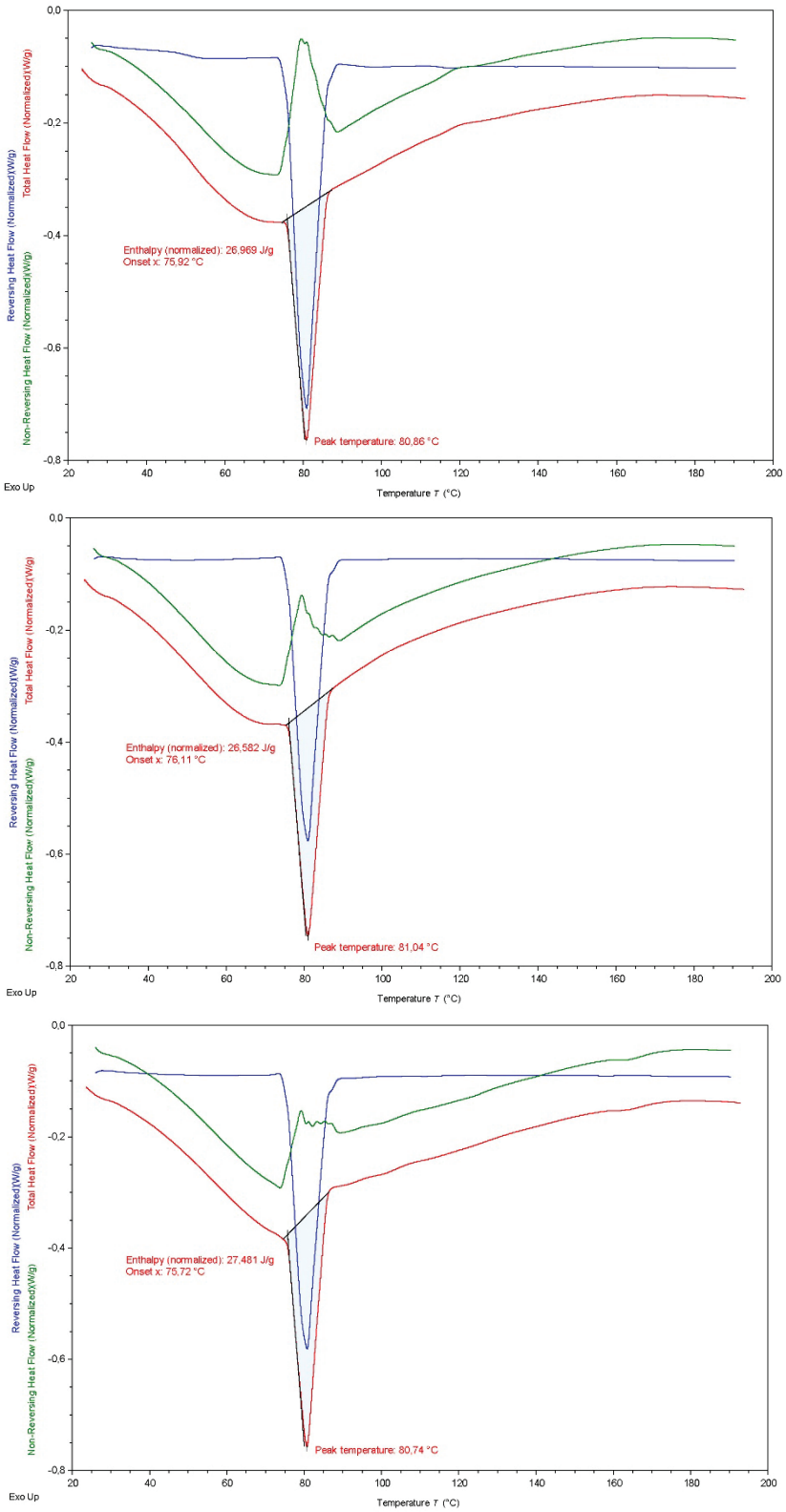


Figure S83: Thermograms illustrating the thermal behavior of fenofibratet co-milled with croscarmellose sodium at a 1:2 (w/w) ratio after 1.5 min of co-milling, measured freshly after preparation.

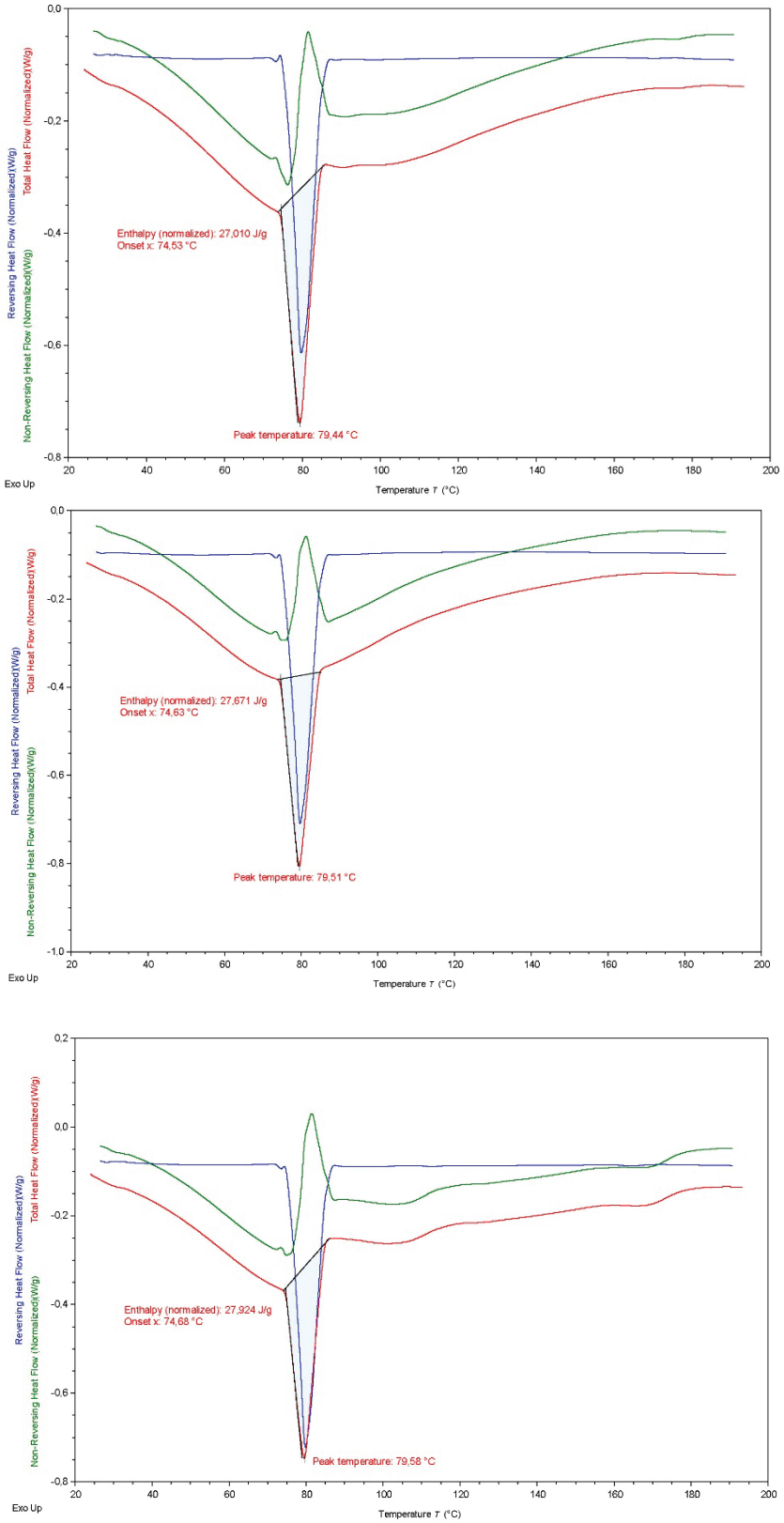


Figure S84: Thermograms illustrating the thermal behavior of fenofibrate co-milled with croscarmellose sodium at a 1:2 (w/w) ratio after 2 min of co-milling, measured freshly after preparation.

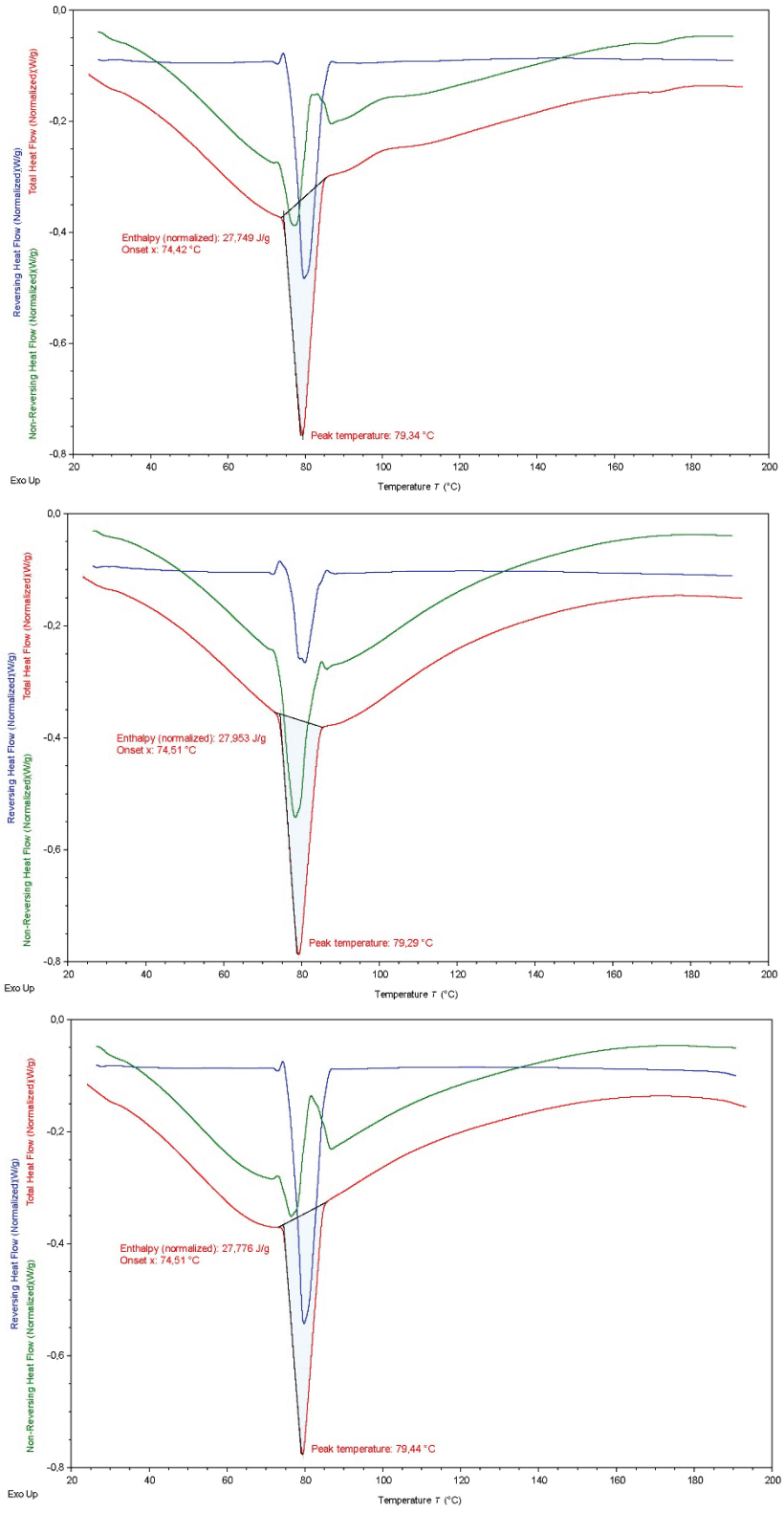


Figure S85: Thermograms illustrating the thermal behavior of fenofibrate co-milled with croscarmellose sodium at a 1:2 (w/w) ratio after 5 min of co-milling, measured freshly after preparation.

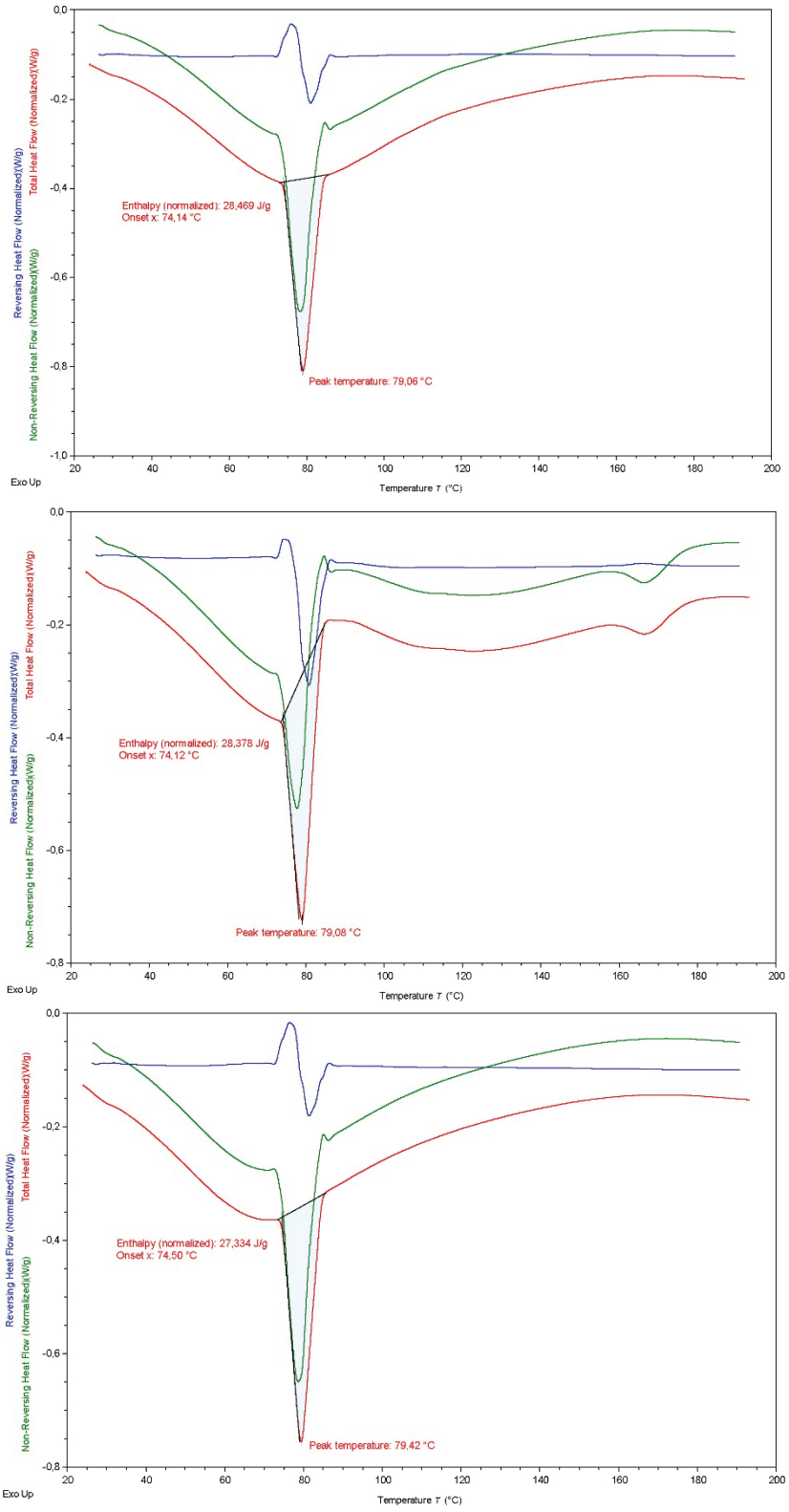


Figure S86: Thermograms illustrating the thermal behavior of fenofibrate co-milled with croscarmellose sodium at a 1:2 (w/w) ratio after 10 min of co-milling, measured freshly after preparation.

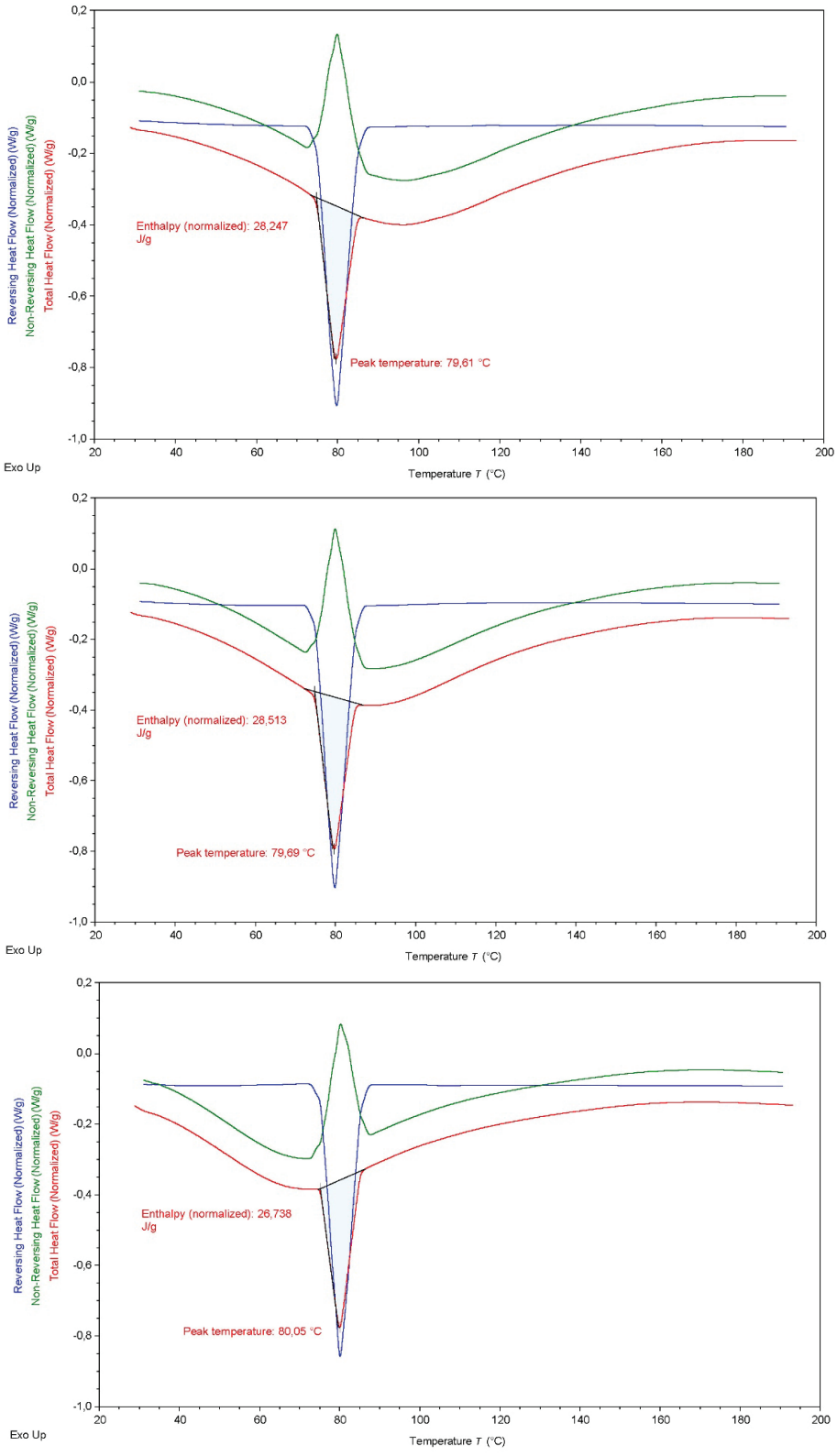


Figure S87: Thermograms illustrating the thermal behavior of fenofibrate co-milled with croscarmellose sodium at a 1:2 (w/w) ratio after 20 min of co-milling, measured freshly after preparation.

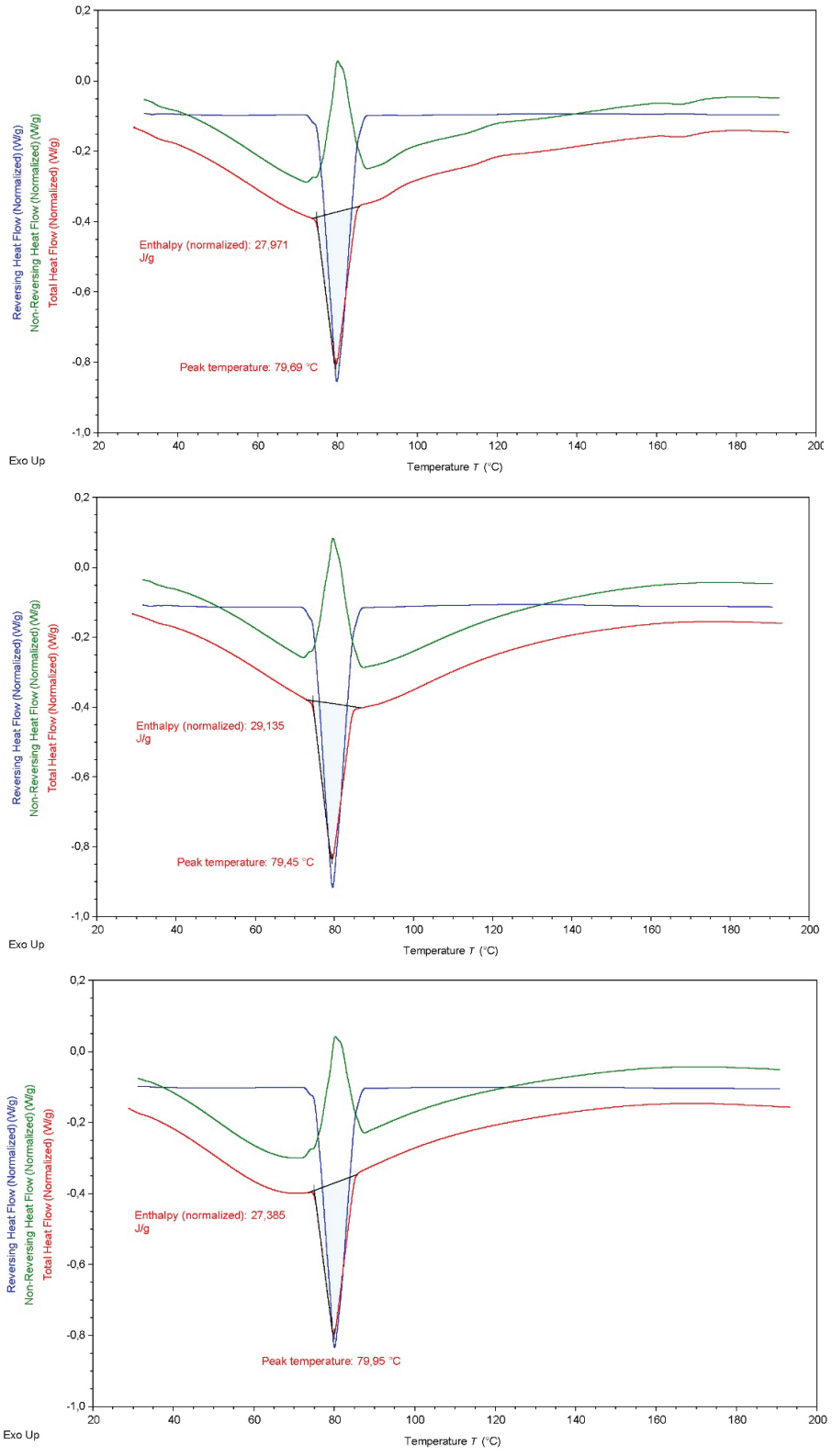


Figure S88: Thermograms illustrating the thermal behavior of fenofibrate co-milled with croscarmellose sodium at a 1:2 (w/w) ratio after 30 min of co-milling, measured freshly after preparation.

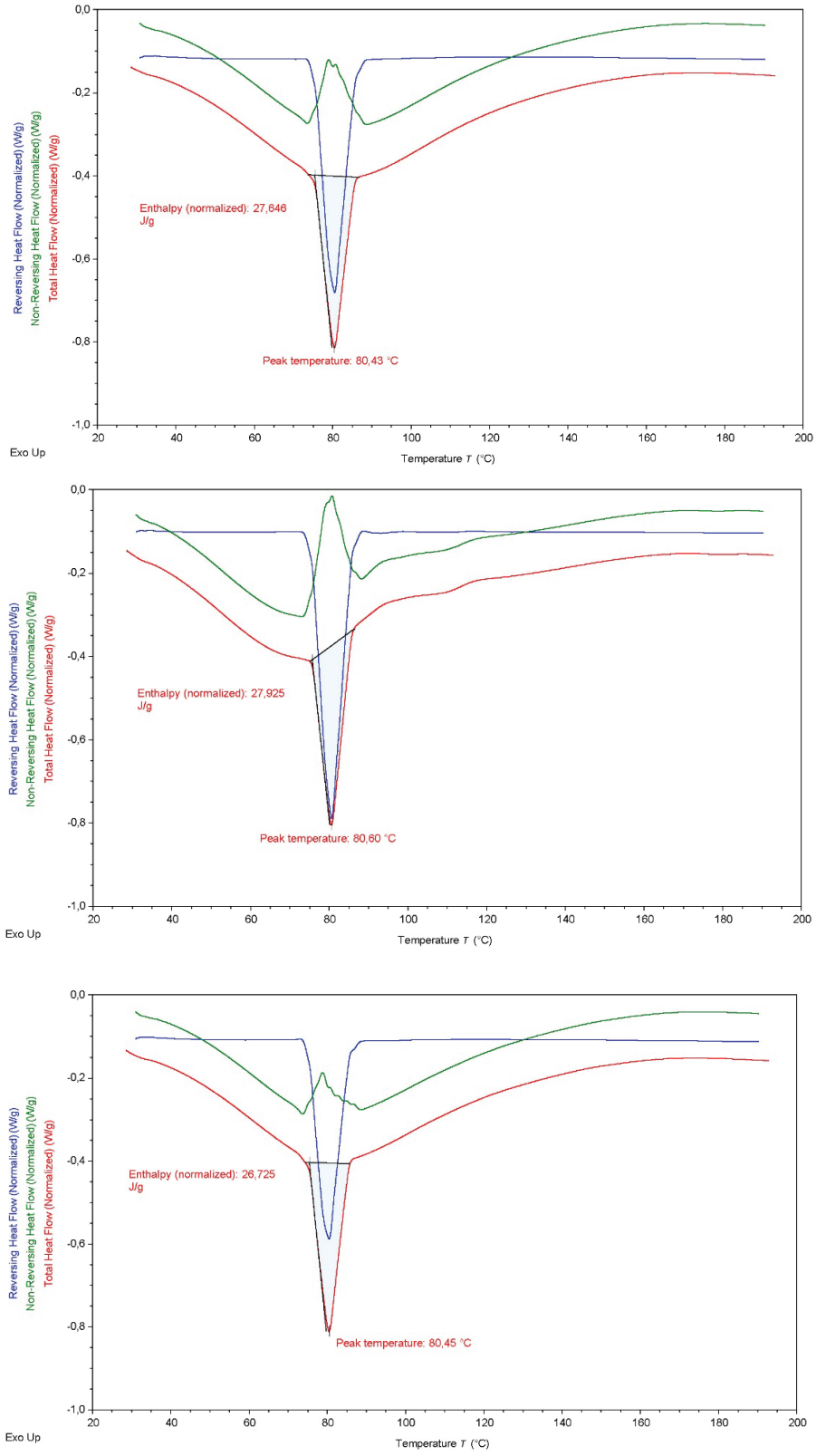


Figure S89: Thermograms illustrating the thermal behavior of fenofibrate co-milled with croscarmellose sodium at a 1:2 (w/w) ratio after 60 min of co-milling, measured freshly after preparation.

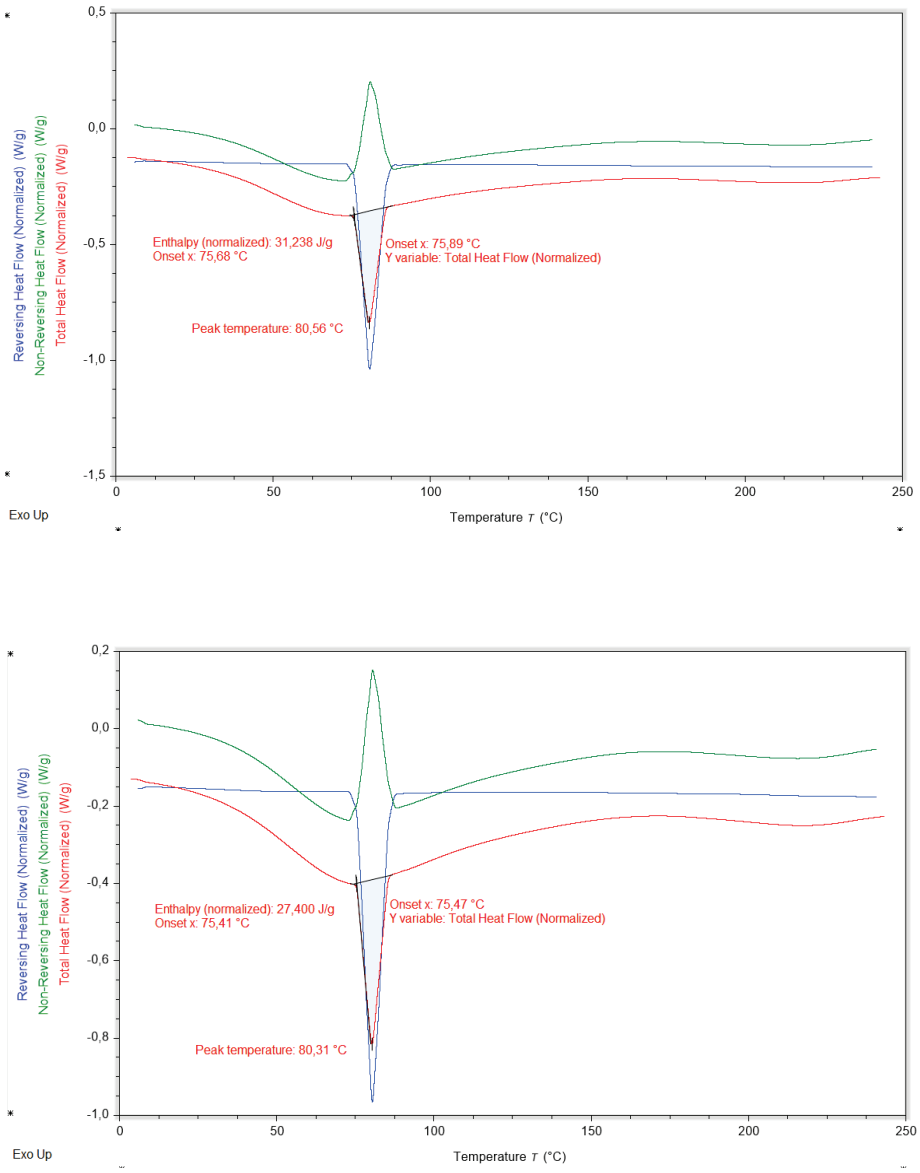
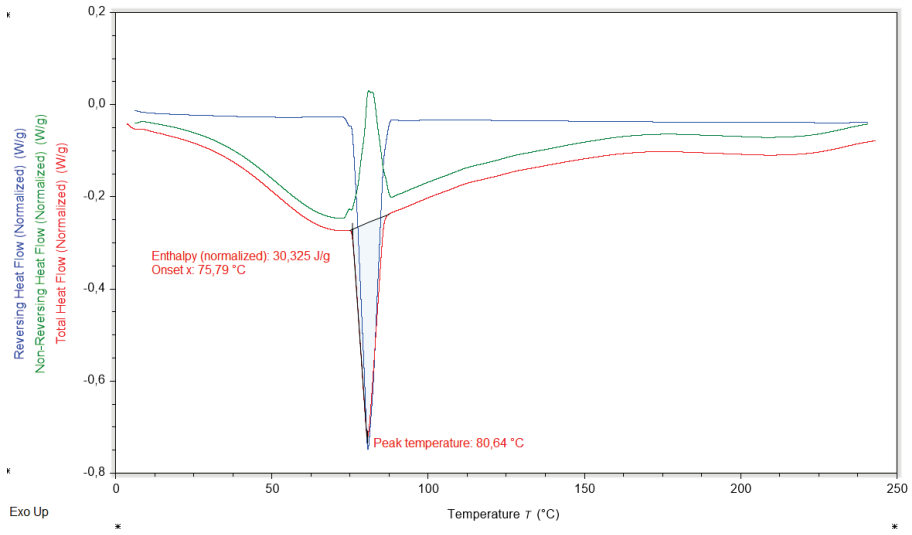


Figure S90: Thermograms illustrating the thermal behavior of fenofibrate co-milled with croscarmellose sodium at a 1:2 (w/w) ratio after 15 s of co-milling, measured after 3 months of storage.



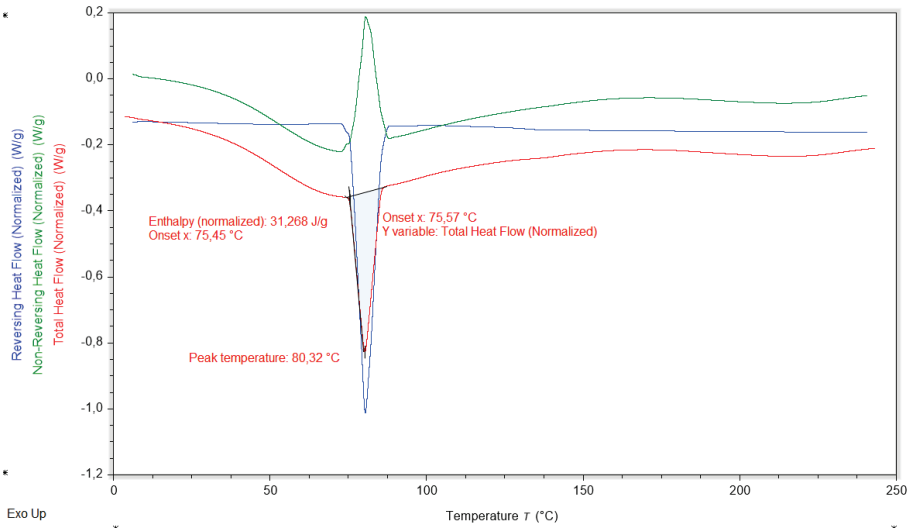
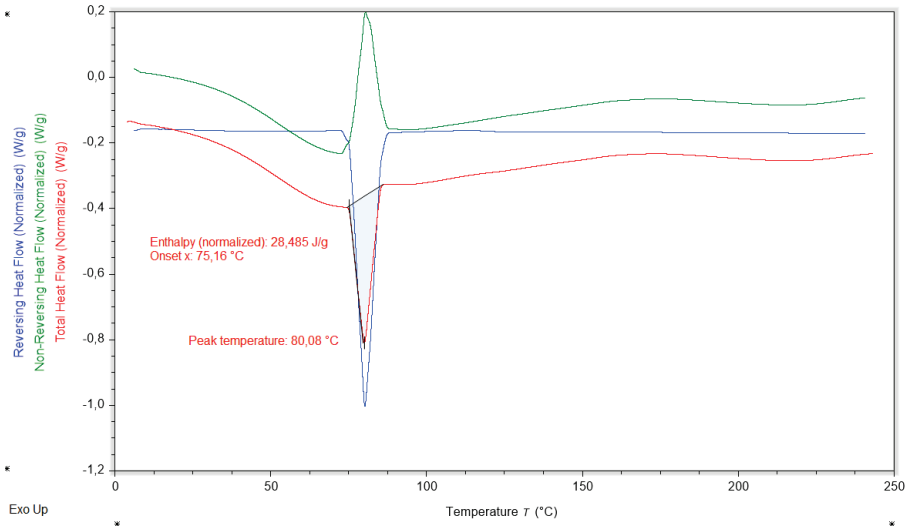


Figure S964: Thermograms illustrating the thermal behavior of fenofibrate co-milled with croscarmellose sodium at a 1:2 (w/w) ratio after 30 s of co-milling, measured after 3 months of storage.



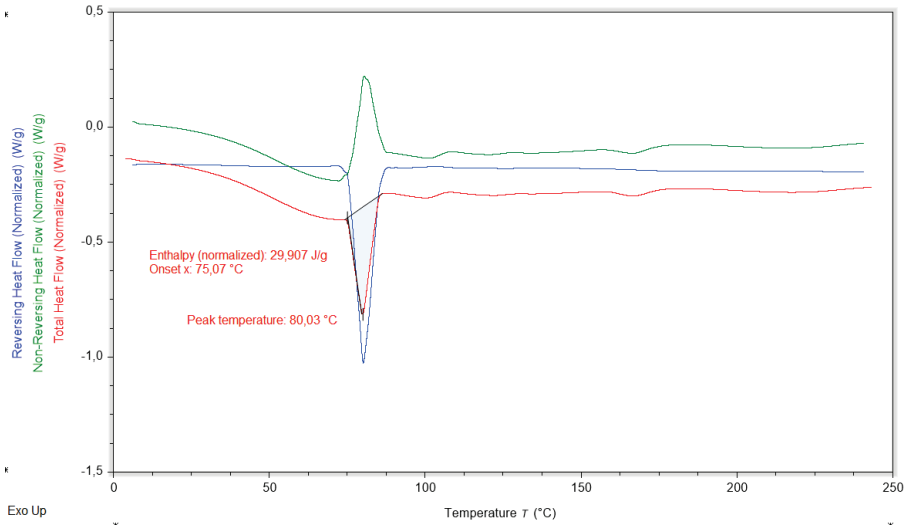


Figure S92: Thermograms illustrating the thermal behavior of fenofibrate co-milled with croscarmellose sodium at a 1:2 (w/w) ratio after 45 s of co-milling, measured after 3 months of storage.

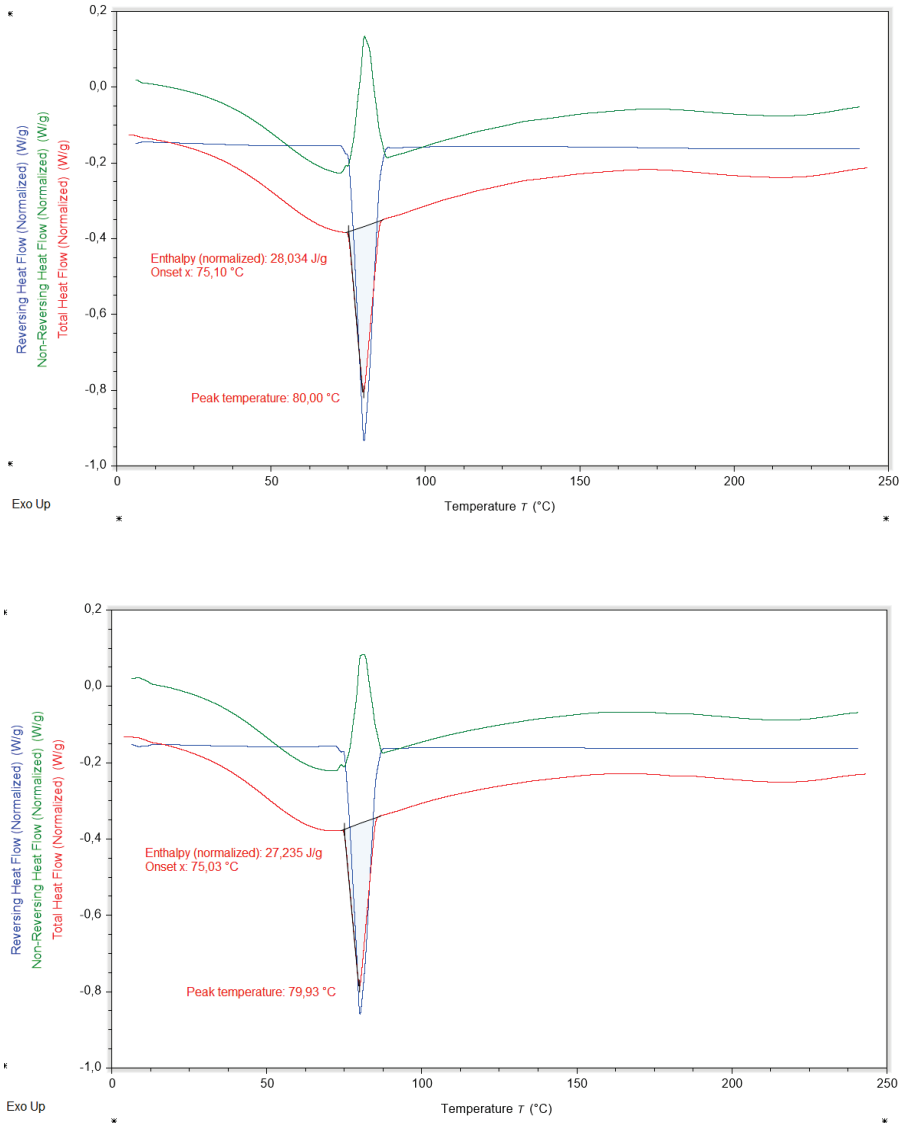


Figure S93: Thermograms illustrating the thermal behavior of fenofibrate co-milled with croscarmellose sodium at a 1:2 (w/w) ratio after 60 s of co-milling, measured after 3 months of storage.

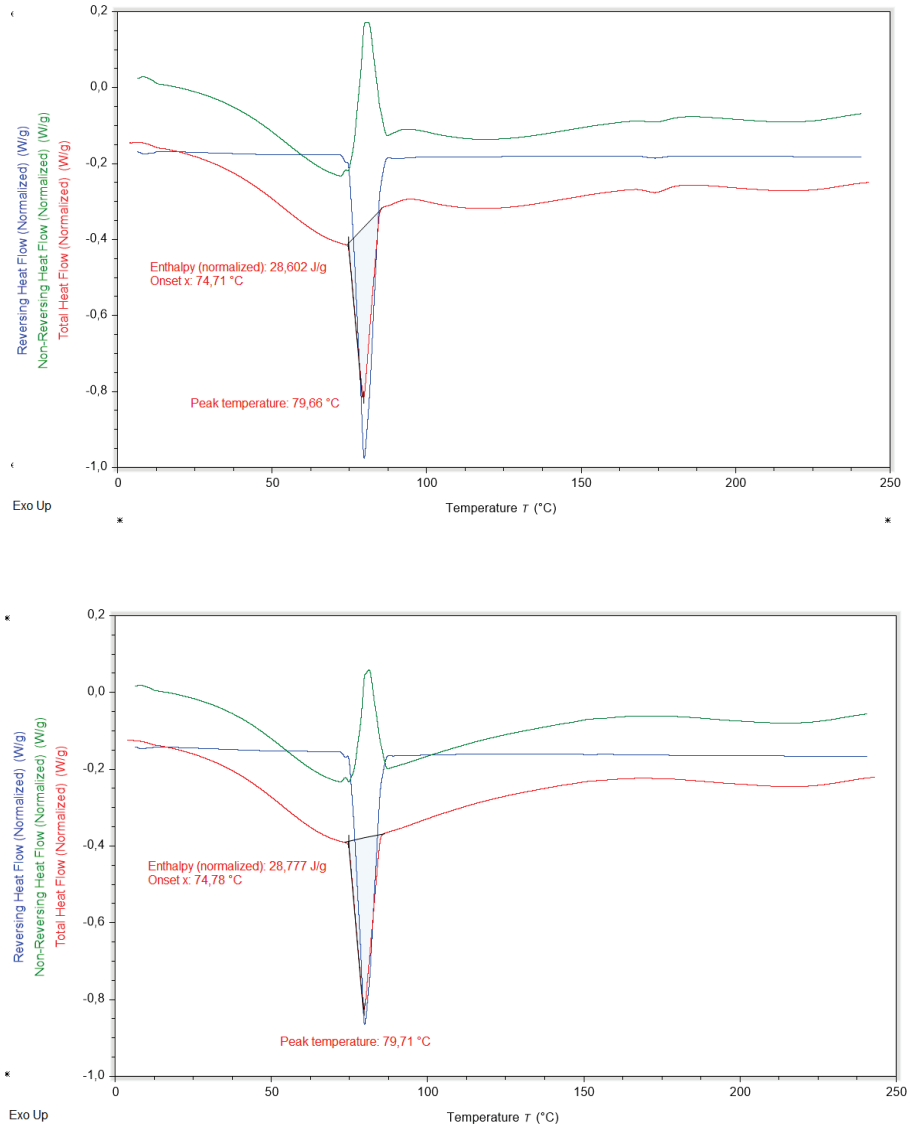
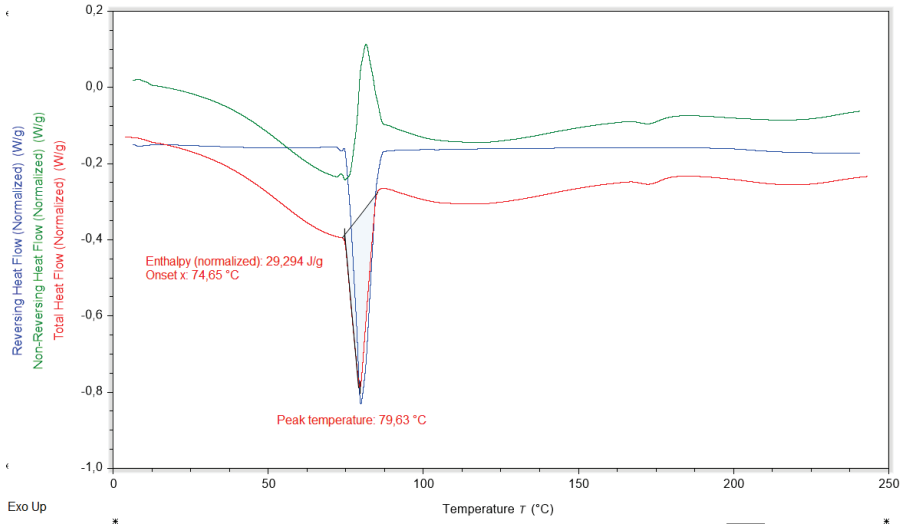


Figure S94: Thermograms illustrating the thermal behavior of fenofibrate co-milled with croscarmellose sodium at a 1:2 (w/w) ratio after 90 s of co-milling, measured after 3 months of storage.



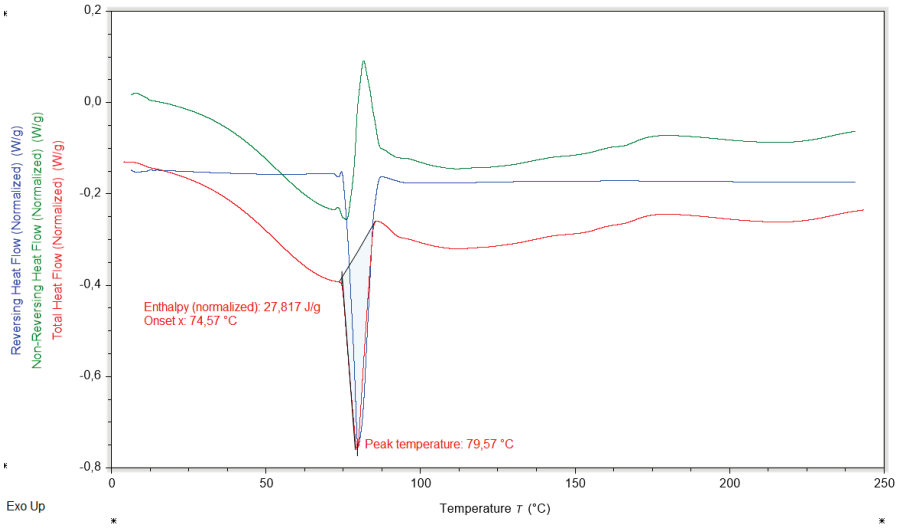


Figure S95: Thermograms illustrating the thermal behavior of fenofibrate co-milled with croscarmellose sodium at a 1:2 (w/w) ratio after 120 s of co-milling, measured after 3 months of storage.

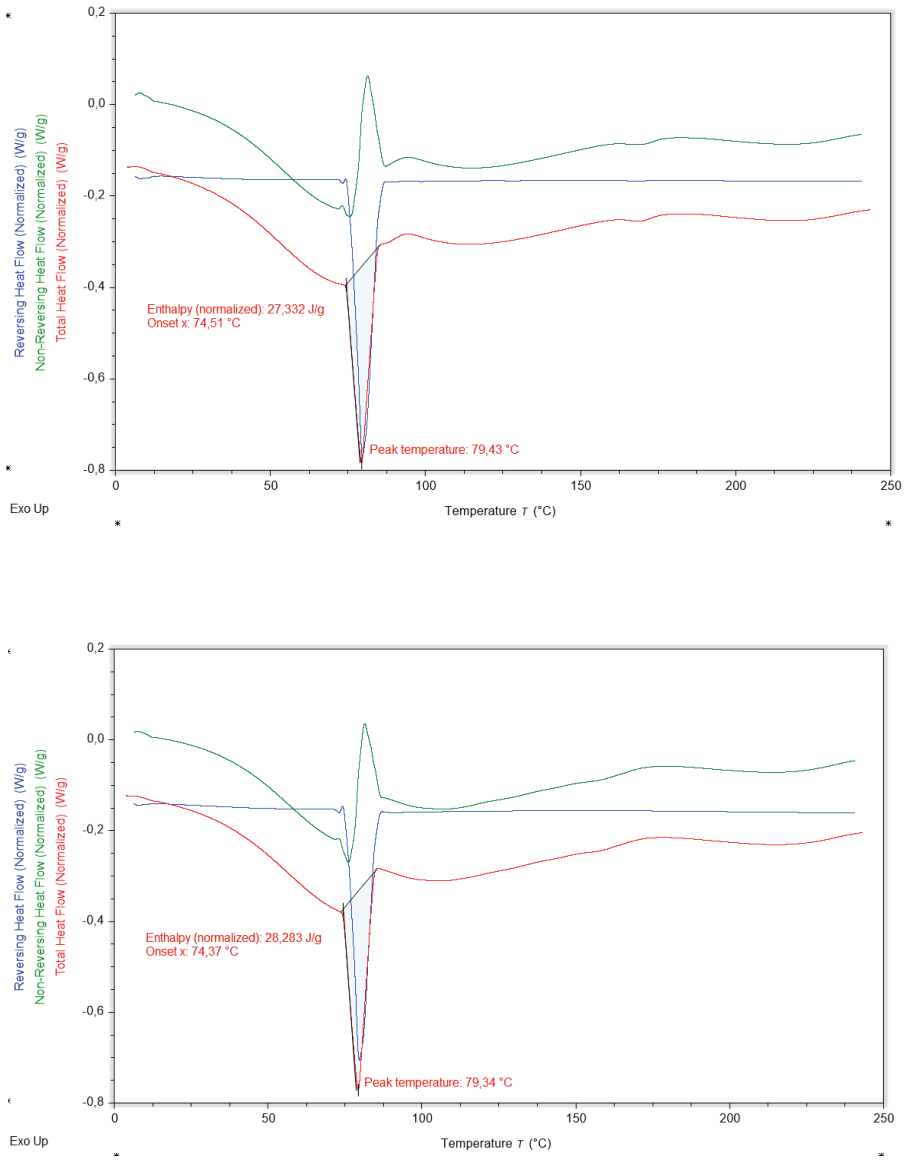


Figure S96: Thermograms illustrating the thermal behavior of fenofibrate co-milled with croscarmellose sodium at a 1:2 (w/w) ratio after 5 min of co-milling, measured after 3 months of storage.

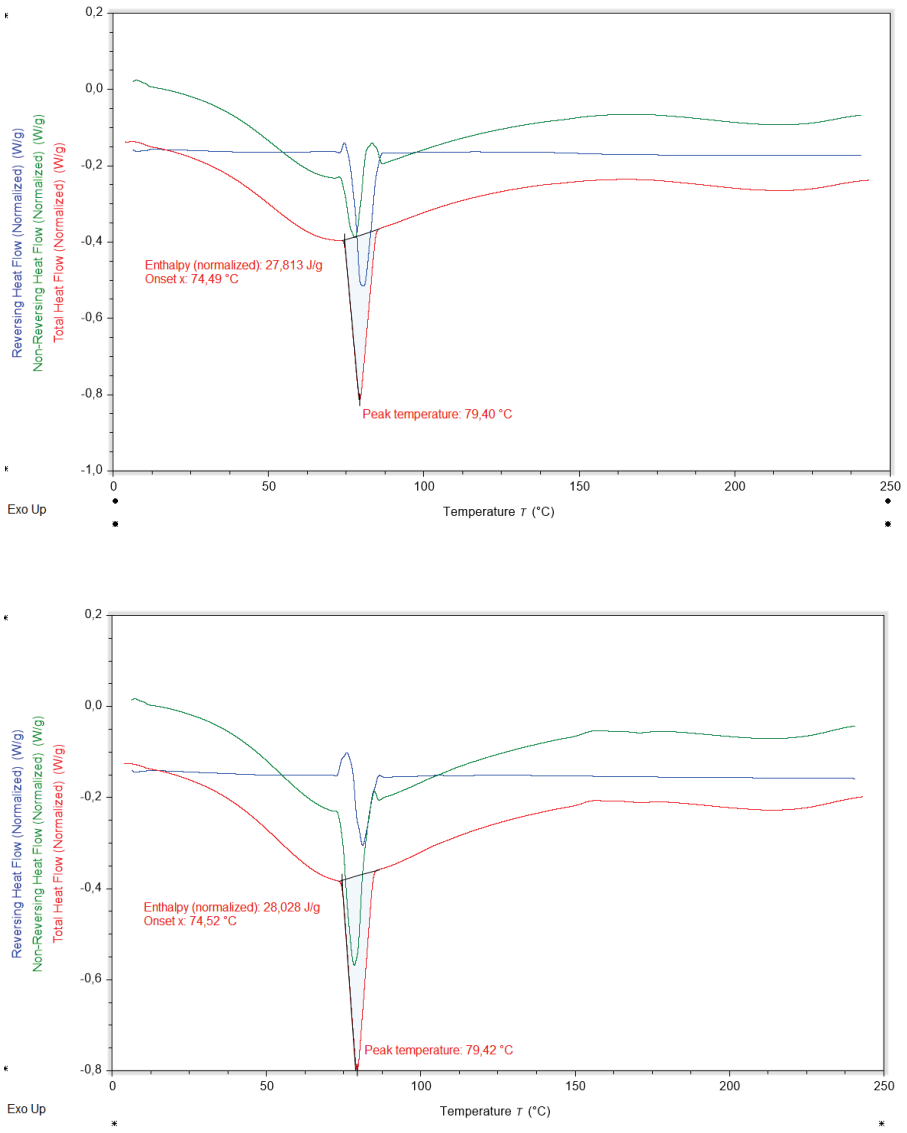


Figure S97: Thermograms illustrating the thermal behavior of fenofibrate co-milled with croscarmellose sodium at a 1:2 (w/w) ratio after 10 min of co-milling, measured after 3 months of storage.

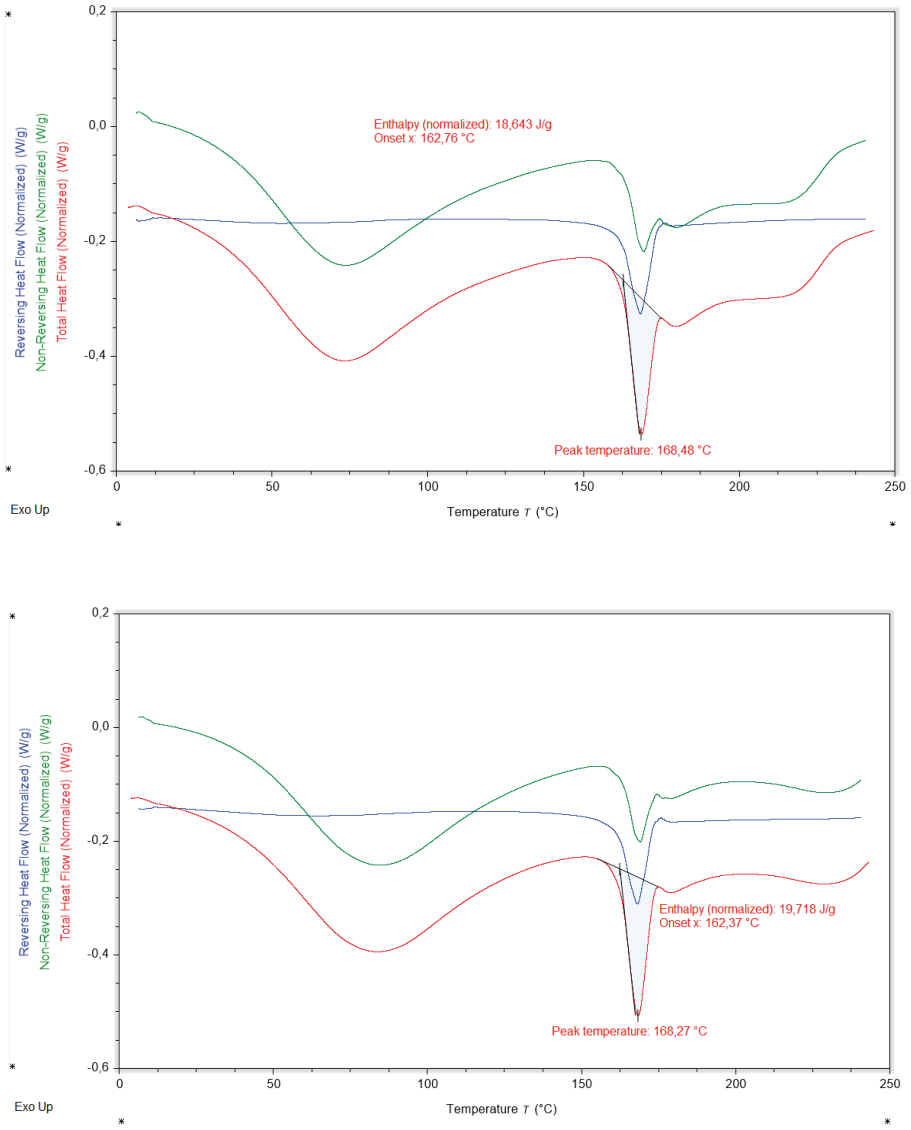


Figure S98: Thermograms illustrating the thermal behavior of fenofibrate co-milled with croscarmellose sodium at a 1:2 (w/w) ratio after 15 min of co-milling, measured after 3 months of storage.

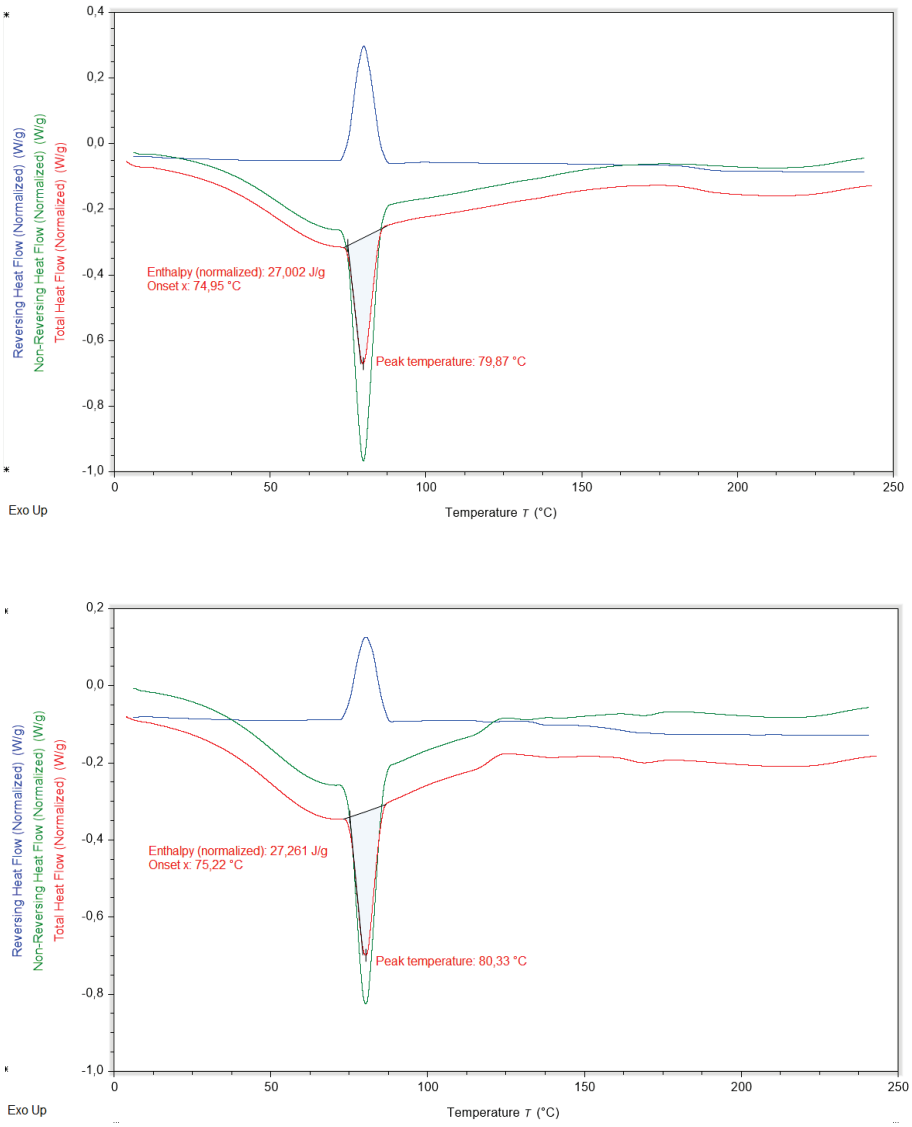


Figure S99: Thermograms illustrating the thermal behavior of fenofibrate co-milled with croscarmellose sodium at a 1:2 (w/w) ratio after 20 min of co-milling, measured after 3 months of storage.

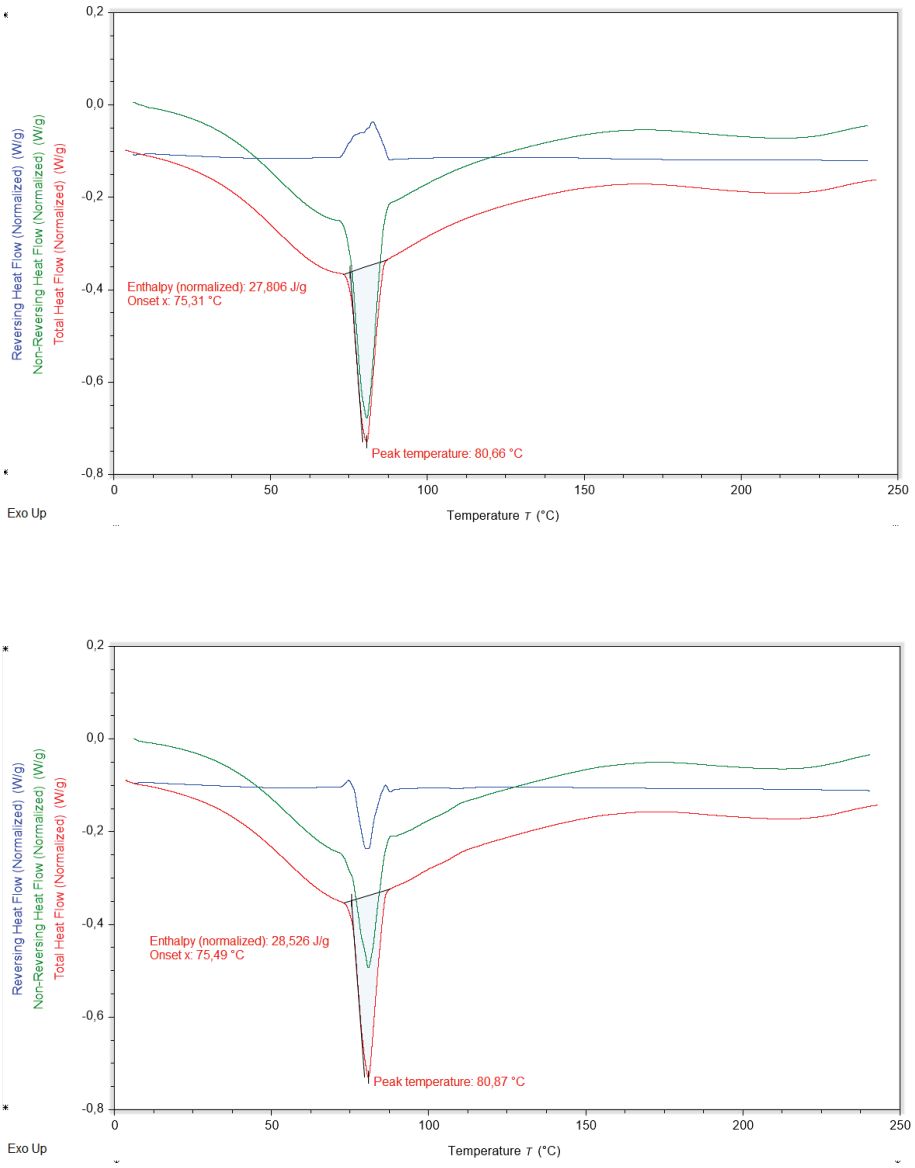
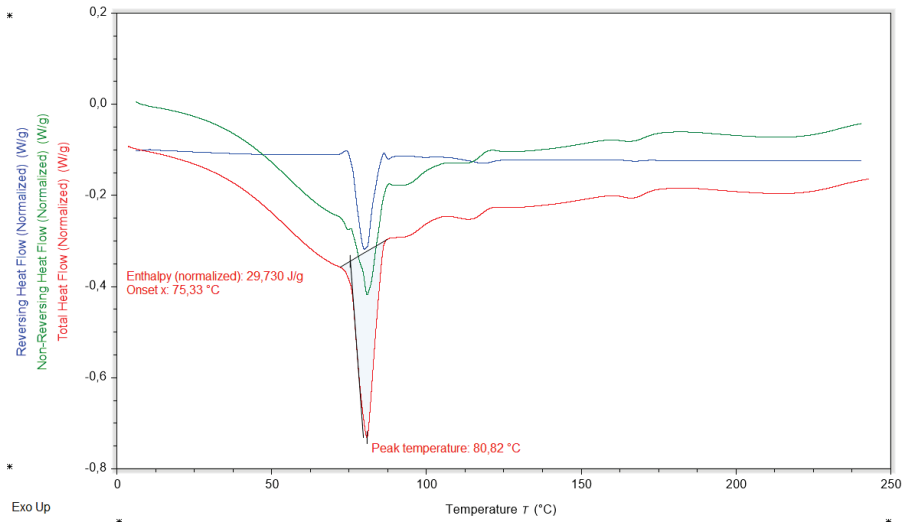


Figure S6500: Thermograms illustrating the thermal behavior of fenofibrate co-milled with croscarmellose sodium at a 1:2 (w/w) ratio after 30 min of co-milling, measured after 3 months of storage.



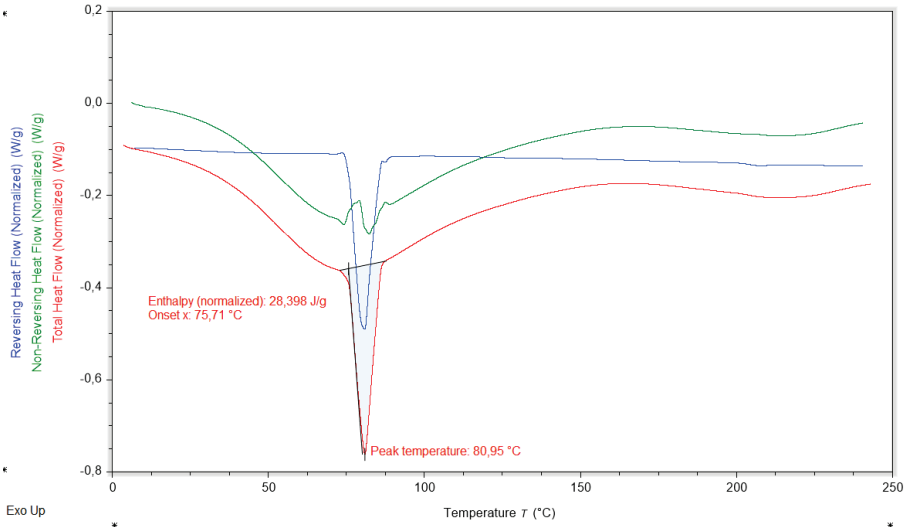


Figure S6601: Thermograms illustrating the thermal behavior of fenofibrate co-milled with croscarmellose sodium at a 1:2 (w/w) ratio after 60 min of co-milling, measured after 3 months of storage.

10.3 Appendix Chapter 5

10.3.1 Particle size measurement validation

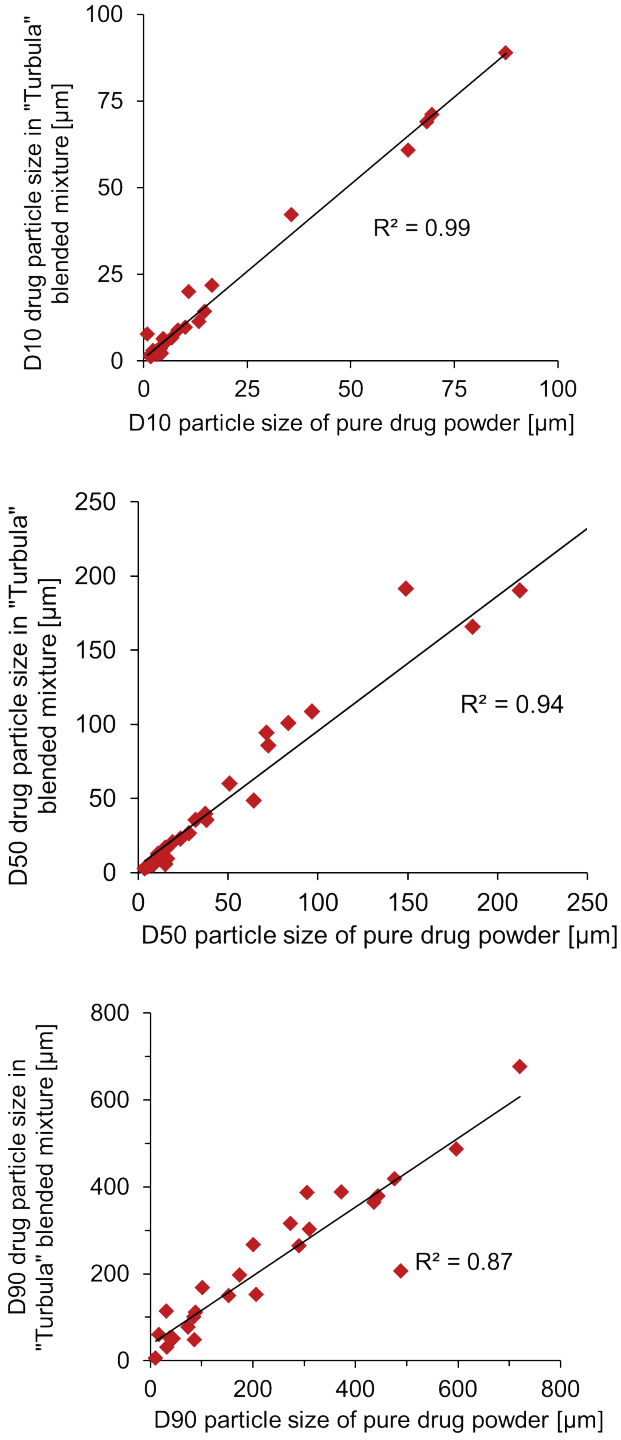


Figure S102: Validation of the water based drug particle size measurement in the presence of the water soluble excipient PVP. The particle size determination method was validated using the measured D10, D50 and D90 particle sizes of the pure drug compared with the determined drug particle sizes of physically blended mixtures with PVP.